The Dissertation Committee for Meilan Wu Certifies that this is the approved version of the following dissertation:

DNA Recognition and Mechanistic Investigation of Poly(ADP-ribose) Polymerase-1

Committee:

Hung-wen (Ben) Liu, Supervisor

Rick Russell

Kevin Dalby

David W. Hoffman

Christian P. Whitman

DNA Recognition and Mechanistic Investigation of Poly(ADP-ribose) Polymerase-1

by

Meilan Wu, B.S.

Dissertation

Presented to the Faculty of the Graduate School of

The University of Texas at Austin

in Partial Fulfillment

of the Requirements

for the Degree of

Doctor of Philosophy

The University of Texas at Austin

August, 2014

Dedication

I dedicate this work to my dearest parents, who are my life long motivation and giving me the courage to explore; to my sincere friends Xiaofei and Diming, who are always there for me these years even though they are miles away.

Acknowledgements

I would like to thank my research advisor Dr. Hung-wen (Ben) Liu, for accepting me to be a member of his great research team. I sincerely thank his valuable advice and support given all these years. I would also like to thank him for giving me the freedom and courage to explore in my scientific research, and at the same time, encouraging me to confront the difficulties as they come.

None of work presented here could be done with out collaborations. I feel so thankful for having the opportunities to meet and learn from different collaborators during different stages of my graduate study. I sincerely thank Dr. Yung-nan Liu, who teaches me different molecular cloning and protein expression skills. Many of the proteins being used in my experiments are generously provided by her. Being away from home for years, I truly feel touched for the care she gives in everyday life. I would also like to thank Dr. Mark W. Ruszczycky, who provides endless help during my graduate work, and being such a great mentor who always inspires me to think and be critical of my work. I also owe him a lot for his time in proofreading this dissertation. To Mark, I always think that saying “thank you” is never enough. I feel honored for having the opportunities to collaborate with Dr. Borries Demeler, Dr. Brian Cannon, Dr. Rick Russell and Dr. Steve O. Mansoorabadi in different research projects. I truly appreciate their time and patience in teaching me different research techniques. I earnestly thank them for their valuable discussion and encouragement for all these years.

Finally, I would like to thank the current and former Liu lab members. Besides research, they are the strongest motivation for me to stay in lab. This is a lovely group of people who provides endless care to their peers. They work hard, and they also play quite hard when getting together. Thank you, my dear friends!

DNA Recognition and Mechanistic Investigation of Poly(ADP-ribose) Polymerase-1

Meilan Wu, Ph.D

The University of Texas at Austin, 2014

Supervisor: Hung-wen Liu

Human PARP-1 is a nuclear protein containing six functional domains that catalyzes the poly(ADP-ribosyl)ation of a variety of protein substrates including itself. This process involves consumption of NAD+ as the ADP-ribose donor for forming the poly(ADP-ribose) (i.e., PAR). PARP-1 utilizes this polymerization reaction to effect its regulatory role in many important biological processes including transcription and DNA repair.

Activation of PARP-1 self-modification requires the presence of damaged DNA. Activity levels of PARP-1 differ depending on the type of DNA lesion. It is proposed that the differences in activity level of PARP-1 are related to the binding stoichiometry of PARP-1 to DNA. Using double and single stranded break DNA mimics, stoichiometric analyses of PARP-1 were performed using sedimentation velocity techniques. In both cases, PARP-1 forms both 1:1 and 2:1 protein:DNA complexes, consistent with protein dimer formation.

Correlation of PARP-1 activity with the DNA structure it encounters can also be explained by the utilization of different functional domains for DNA recognition. To

investigate this hypothesis, DNA-binding domain AB was labeled with the Cy3 fluorophore, and a Cy5-labeled DNA with a double stranded break, was used as its interaction counterpart. Protein-DNA interactions were monitored by single molecule fluorescence colocalization. It was observed that a 2:1 protein:DNA complex is formed. Furthermore, recognition of double stranded DNA breaks by domain AB involves two different binding steps with distinct dissociation kinetics. Finally, two FRET states were observed as domain AB interacted with DNA. This suggests that domain AB utilizes different regions to interact with DNA during the recognition process.

After activation, PARP-1 synthesizes poly(ADP-ribose) through three catalytic processes: initiation, elongation and branching. To study the domain requirements for polymer synthesis, truncated PARP-1 constructs ABC and DEF were tested. It was observed that initiation and elongation of short polymers requires the presence of DEF, ABC and DNA. As the polymer gets larger, DEF itself is capable of adding ADP-ribose onto the PAR polymers. Current data is consistent with a mechanistic proposal where automodification of PARP-1 happens intramolecularly and PAR elongation takes place at the distal end of the growing polymer.

Table of Contents

List of Tables

List of Figures

Chapter 1. Background and Significance

1.1. POLY (ADP-RIBOSE) (PAR): A NOVEL NUCLEIC ACID LIKE POLYMER

1.1.1. A short story of poly(ADP-ribose) discovery

The earliest discovery of poly(ADP-ribose) formation was reported in 1963 by Chambon et al. (1). It was observed that ^{14}C-labeled ATP was incorporated into the acid-insoluble fraction of prepared chicken liver nuclei upon the addition of nicotinamide mononucleotide (NMN). This reported activity was DNA-dependent, and the resulting product was insensitive to treatment with DNase, RNases or proteases. Therefore, it was suspected that the observed product was polyadenine (poly(A)) (1). This result was confirmed by a later study carried out by Fujimura et al. using nuclei from rat liver and hepatoma cells (2).

Further investigation performed by Chambon et al. showed that ^{32}P-NMN could also be incorporated into the polymer (3). Therefore, the previously observed stimulating effect of NMN could be ascribed to its capability to serve as either the substrate or the biosynthetic precursor of the substrate for polymer formation. Further investigation suggested that nicotinamide adenine dinucleotide (NAD^+), which is a known biosynthetic product of NMN and ATP, is the immediate substrate for polymerization (3).

The structure of the polymer residues was first studied by degrading the polymer using alkaline hydrolysis, snake venom pyrophosphatase and acid hydrolysis. This led to a mixture of adenine, ribose and phosphate with a ratio of 1:2:2, respectively, implying an isomer of ADP-ribose as the polymeric unit (3). This result was quickly confirmed by Nishizuka et al. (4), Reeder et al. (5) as well as other research groups (6, 7). The study carried out by Reeder et al. also suggested that the ADP-ribose unit is connected through ribose-ribose linkages to form a linear homopolymer (5).

1.1.2. Structural details of poly(ADP-ribose)

Extensive studies done in the 1970s provided more structural detail regarding the chemical nature of poly(ADP-ribose) (Fig.1-1). ^{13}C NMR studies carried out by Miwa et al. revealed that the ADP-ribose unit is connected through an α-(1''-2')-ribose-ribose glycosidic linkage (8). Upon enzymatic treatment with snake venom phosphodiesterase, the major unit released from the polymer is 2'-(5''-phosphoribosyl)-5'-AMP (PRAMP) as the elongation monomeric unit (9-10), along with a lesser amount of 5'-AMP, which is derived from the polymer termini (11). Thus, it was proposed that poly(ADP-ribose) is a linear polymer (10).

Polyacrylamide gel electrophoretic methods had been used to resolve poly(ADP-ribose) polymers with a size resolution of one residue. Enzymatic digestion was also used to provide additional information about the chain length of poly(ADP-ribose) polymers by comparing the number of elongation units (PRAMP) and the 5'-AMP terminal units (11). In 1978, Tanaka et al. reported an interesting observation: polymers with proximately 65 total residues have an average chain length of about 30 residues, indicative of a branched polymeric structure with multiple 5'-AMP termini (12). Further studies by the same group provided structural details of the branching unit, which is O-α-D-ribofuranosyl-(1'''→2')-*O*-α-D-ribofuranosyl-(1''→2')-adenosine-5',5'',5'''-tris(phosphate) (*13-14*), abbreviated as $(PR)_2AMP$, and presented direct evidence regarding the morphology of the branched poly(ADP-ribose) polymer using electron microscope (*15*) (Fig.1-1).

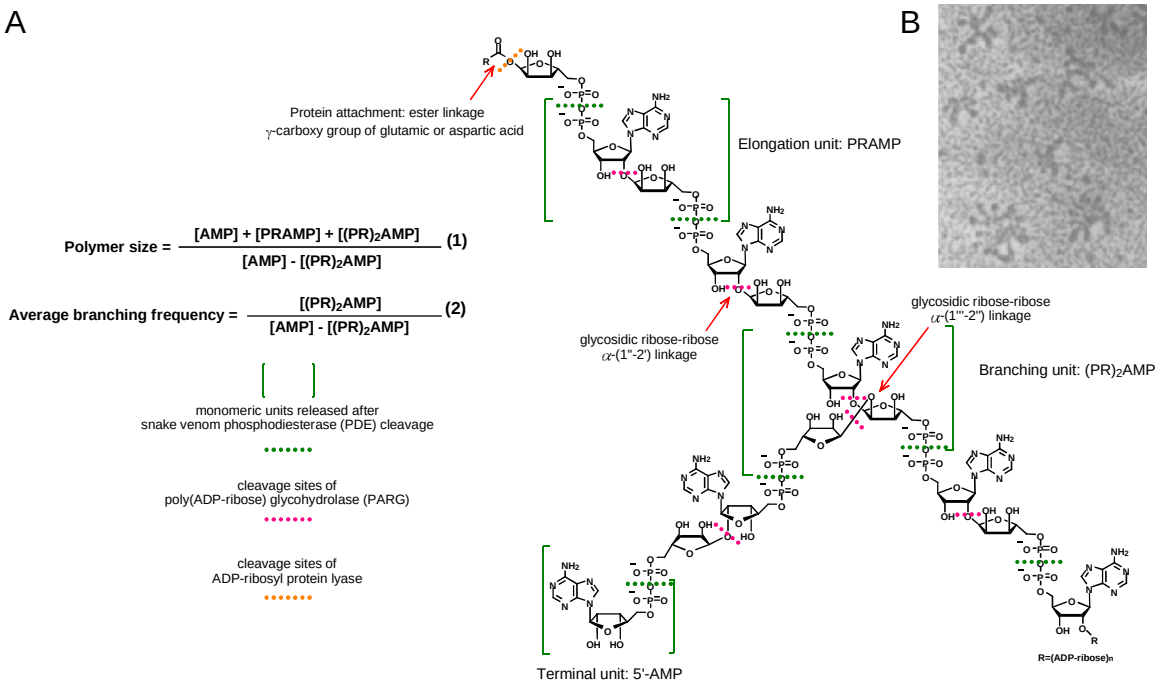

Figure 1-1. A. Basic structure of branched poly(ADP-ribose); B. An electron microscopic image of branched polymers (adapted from Hayashi et al., Biochem. Biophys. Res. Commun. 1983, 112: 101-107).

As shown in the electron micrograph in Figure 1-1, the polymers appear to be dendritic. But a defined versus random frequency of branching unit formation is difficult to discern. By quantitating the numbers of different monomeric units generated after phosphodiesterase treatment and using equations 1 and 2 (see Figure 1-1), it was reported that the average branching frequency is every 20 to 50 ADP-ribose units (16). Similarly, the size distribution of poly(ADP-ribose) polymers produced either in vivo or in vitro is highly heterogeneous judging from the polyacrylamide sequencing gel results (12,15-16).

Soon after the discovery of poly(ADP-ribose), Nishizuka et al. revealed that poly(ADP-ribose) was associated with histones in forms ranging from monomers to oligomers (17) and may be linked covalently as a result of a post-translational modification process. This finding was further confirmed and elaborated on by numerous investigations carried out both in vivo and in vitro (18-20). Since then, more and more functional proteins have been characterized as being poly(ADP-ribosyl)ated (21-23). The most salient covalent linkage between polymer and protein has been ester formation involving side chain carboxyl group of glutamic and aspartic acid residues as shown in Figure 1-1 (24). More recent studies have suggested that lysine can also serve as the acceptor residue for poly(ADP-ribosyl)ation (25).

1.1.3. Metabolism of poly(ADP-ribose)

Poly(ADP-ribosyl)ation is an important post-translation modification that results in the covalent attachment of ADP-ribose polymer to amino acid residues of a protein acceptor. This in turn changes its physico-chemical properties of the modified protein. This process appears to be highly dynamic and reversible in living cells. Long polymers have a half-life of less than 1 min, and short polymer has a half-life of 7.7 h in vivo (26). Furthermore, the substrate NAD^+, being consumed in this process, is an essential cofactor for energy metabolism as well as maintenance of cellular redox potentials (24). The interdependence between the cellular levels of NAD^+ and poly(ADP-ribose) is therefore a factor influencing cell survival. In order to maintain a physiological balance, metabolism of poly(ADP-ribose) is highly regulated in eukaryotes (24).

Poly(ADP-ribose) polymerase-1 (PARP-1) is an abundant nuclear protein capable of catalyzing initiation, elongation and branching reactions when synthesizing poly(ADP-ribose) polymer (PAR) conjugated with different acceptor proteins including itself (24). Its activity is responsible for more than 90% of PAR generated in living cells (26). Currently, 17 proteins have been identified belonging to the PARP family (27), but only PARP-1, PARP-2, and tankyrases have been shown to carry out poly- and oligo-(ADP-ribosyl)ation (28).

Degradation of poly(ADP-ribose) is catalyzed by two enzymes: poly(ADP-ribose) glycohydrolase (PARG) and ADP-ribosyl protein lyase (24) as shown in Figure 1-2. PARG has both exo- and endo-glycosidase activities (29-30). This results in the hydrolysis of the ribose-ribose bonds within PAR polymers leading to smaller oligomers and eventually the complete degradation to ADP-ribose monomers. The expected cleavage sites of PARG are shown in Figure 1-1. However, PARG cannot cleave the proximal ADP-ribose residues that are directly linked to the modified protein. ADP-ribosyl protein lyase is the enzyme responsible for catalyzing hydrolysis of the ester bond linking this most proximal ADP-ribose residual to the protein (Fig.1-1) (24). Not much is known about this enzyme until recently when Sharifi et al. identified a terminal ADP-ribose protein glycohydrolase (TARG1) that possesses such activity and is encoded by the c6orf130 gene (31).

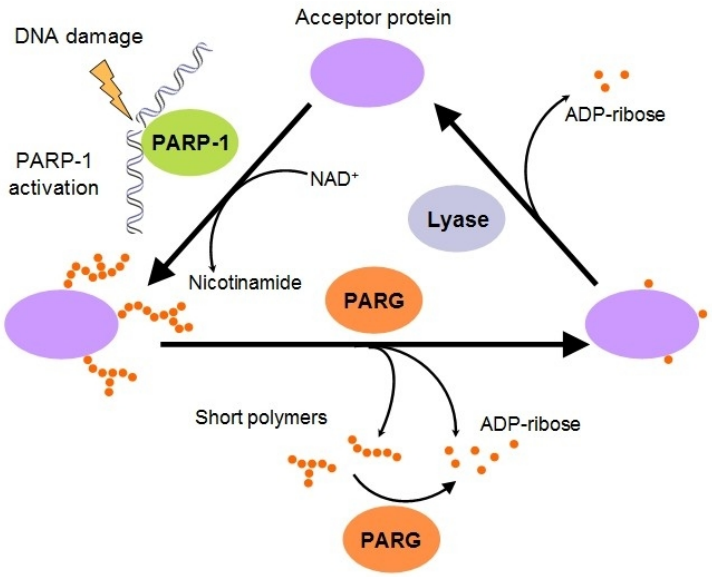

Figure 1-2. Metabolism of poly(ADP-ribose).

1.1.4. Biological importance of poly(ADP-ribosyl)ation

PARP-1 is a key factor for cell survival owing to its participation in different DNA repair machineries, such as the base excision repair (BER) pathway and double stranded break (DSB) repair pathways. When cells experience low to moderate levels of DNA damage, such as single or double stranded breaks, PARP-1 interacts with the DNA lesions and is activated. Upon activation, PARP-1 modifies a wide array of DNA repair proteins including itself with poly(ADP-ribose). The interactions between the highly negatively charged PAR polymers, histones and DNA relax chromosomal structure, which renders the lesion site accessible to repair proteins (32-33). Furthermore, PARP-1 associates with DNA repair proteins like XRCC1, DNA polymerase β and DNA ligase III through protein-protein interactions as well as protein-poly(ADP-ribose) interactions,

thereby contributing to the formation of base excision repair (BER) specific multi-protein complex (24,34-36). PARP-1 also acts in double stranded break DNA repair pathways. It does so by interacting with DNA protein kinase (DNA-PK), which is involved in double stranded break repair via non-homologous end joining (NHEJ) (37-38).

Activation of PARP-1 facilitates the assembly of repair machinery at the site of a DNA lesion. At the same time, PARP-1 itself is also modified with negatively charged PAR polymers through the process of automodification (24). This eventually makes PARP-1 lose its affinity for DNA (24). As a result, PARP-1 dissociates from DNA and its activity returns to basal level (33). It is also believed that this dissociation process allows access of the DNA repair proteins (24). As a key contributor to the DNA repair machinery, inhibition of PARP-1 can further potentiate the therapeutic effect of DNA-damaging agents used in cancer therapy. Therefore, identification of new PARP-1 inhibitors is an active area of research for better cancer drugs (28, 40).

When the level of DNA damage is moderate, which may be caused by UV radiation or reactive species generated from metabolism (39), PARP-1 serves as a safeguard against genomic aberrations; however, when the level of DNA damage is excessive, high levels of poly(ADP-ribosyl)ation become a hallmark for DNA damage-induced cell death. It has been shown that poly(ADP-ribosyl)ation is a critical event affecting the NAD^+ level in cells. Wielckens et al. observed that the Ehrlich ascites cell line is capable of converting 10 nmol of NAD^+ to ADP-ribose per minute per 10^8 cells (41). This rapid consumption is sufficient to deplete the entire cellular NAD^+ pool within 10 minutes (24). Depending on the biosynthetic route one considers, one molecule of NAD^+ would require an input of at least two molecules of ATP (42-43). Furthermore, exhaustion of the cellular pool of NAD^+ would shut down glycolysis pathway (44), which in turn would slow down the regeneration of ATP. Taken together, NAD^+ depletion

would cause a dramatic drop in the cellular level of ATP. While depletion of NAD^+ caused by extensive poly(ADP-ribosyl)ation would cause cell apoptosis soon after excessive DNA damage (44-45), subsequent depletion of ATP could lead to necrotic cell death (24).

It should be noted that there are distinct biochemical and morphological differences between apoptotic and necrotic cell death. Apoptotic cells tend to become more compact and can be rapidly cleared from body tissues by macrophages. In the case of necrosis, the plasma membrane of the necrotic cells disintegrates, and the cellular contents are released into the surroundings, which may cause further tissue injury (28). Established evidence suggests that PARP-1 is hyperactivated during various pathophysiological conditions such as stroke, myocardial infarction, heart transplantation, hemorrhagic shock and acute respiratory distress syndrome (28). These observations have spurred the development of PARP-1 inhibitors in drug discovery as part of protective medicines: inhibition of PARP-1 would help to maintain the NAD^+ and ATP pool within cells under the aforementioned disease conditions, thereby attenuating the progress of necrosis which may cause further organ dysfunction (28).

In addition to the biological roles of poly(ADP-ribosyl)ation discussed above, accumulating evidence now suggests that poly(ADP-ribosyl)ation is also involved in the modulation of chromatin structure and controlling DNA replication, transcription, cell division and development, as well as maintaining genomic stability (24, 46-47). As poly(ADP-ribose) is also present in mitochondria, its participation in mitochondrial function and metabolic regulation is currently under active investigation (48-49). As poly(ADP-ribosyl)ation related research continues to advance at a fast pace, new functions of PARP-1 are expected to emerge. Therefore, it is important to fully understand how PARP-1 contributes to various biological pathways in terms of nucleic

acid and protein substrate recognition. Learning how these different interactions may translate into the observed activity level, as well as their effects on the size and branching patterns of poly(ADP-ribose) synthesized by PARP-1 in specific biological contexts may provide fundamental insight as to how regulation of PARP-1 is achieved.

1.2. Functional Aspects of PARP-1

1.2.1. The domain architecture of human PARP-1

PARP-1 is the first and the best characterized enzyme for poly(ADP-ribose) formation in eukaryotes. It is a 113 kDa nuclear protein composed of six domains identified based on homology with reported functional modules (Figure 1-3) (50).

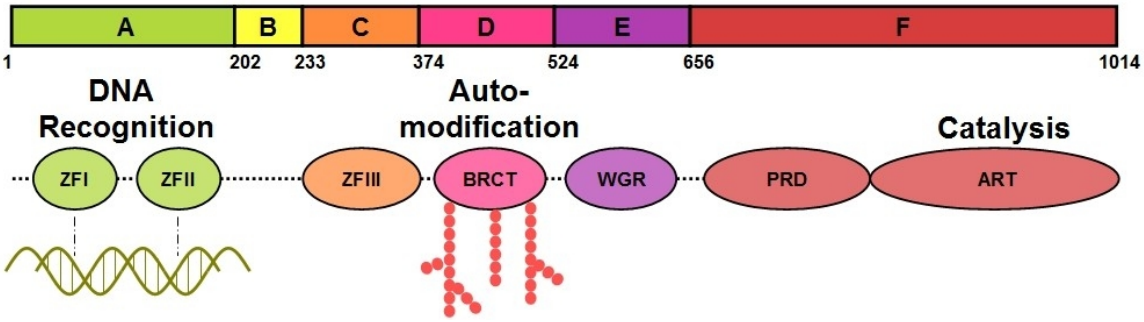

Figure 1-3. Functional domains of PARP-1.

Beginning at the N-terminus of PARP-1, domain A contains two unique zinc finger motifs ($CX_2CX_{28/30}HX_2C$), zinc finger I (FI) and zinc finger (FII), that recognize different structural DNA lesions with high binding affinity as opposed to specific nucleotide sequences (51-52). This protein-DNA interaction subsequently triggers PARP-1 activation. In addition to its DNA binding ability, zinc finger I has also been established

to be important for PARP-1 activation, whereas zinc finger II is the main segment participate in DNA recognition (24, 53).

The domain B region contains a bipartite nuclear localization signal (NLS) encoded in the form of KRK-X(11)-KKKSKK (amino acids 207-226). This short sequence is essential for targeting PARP-1 to the nucleus (54). The X(11) linker region between two basic amino acid clusters in NLS harbors a caspase-3 cleavage site ($D_{211}EVD_{214}$). After cleavage of PARP-1 by caspase-3, only a basal level of PARP-1 activity is retained, and the truncated enzyme can no longer be activated by nicked DNA (55). The proteolytic processing of PARP-1 is an early event for apoptosis, which helps to maintain the cellular energy pool by preventing rapid NAD^+ consumption (55).

Domain C contains a zinc-binding motif ($CX_2CX_{12}CX_9C$) with a structurally novel zinc-ribbon fold (56). Unlike the previously discussed zinc fingers I and II in domain A, zinc finger III (FIII) within domain C does not bind to DNA. Instead, it was demonstrated to interact with poly(ADP-ribose) (56). Studies of a domain C deletion mutant and several PARP-1 mutants with point mutations within domain C region revealed that domain C is essential for DNA-dependent PARP-1 activation (56-68). The importance of domain C in PARP-1 activation may be due to its involvement in interdomain interactions as well as stabilizing the active conformation of the PARP-1/DNA complex (56, 58). An NMR study indicated that domain C exists in monomeric form in free solution (56), whereas a dimeric structure was demonstrated by X-ray crystallography (58). The disparity may be due to the slight differences in the protein constructs used as well as the effects of crystal packing. During activation, whether PARP-1 functions as a dimer or a monomer remains an unresolved question awaiting additional investigation by the PARP community.

When poly(ADP-ribosyl)ation takes place, PARP-1 itself is actually the major acceptor of the PAR polymer. Domain D was first named as the automodification domain due to the high abundance of glutamic acid residues within this region which can potentially be ADP-ribosylated (59-61). Recently, a number of automodification sites within this region have been confirmed by MS studies. These include D387, E488 and E491 (62), as well as D461 and E456 (63). However, the acceptor sites of PARP-1 for ADP-ribosylation are not limited to domain D, as they can also be found in domains A, E and F (63). In addition, domain D contains a BRCT motif which is critical for mediating protein-protein interactions in the case of heteromodification as well as cellular signaling (64).

Domain E contains a WGR motif, which is an abbreviation for the conserved amino acid sequence Trp-Gly-Arg (65). Huambachano et al. has demonstrated that the WGR region can interact with poly(ADP-ribose) and short RNAs (66). The same research group also identified a loop between the BRCT and the WGR regions that functions as the double stranded DNA binding domain (DsDB) and may also be involved in DNA-dependent PARP-1 activation (66).

The active site for poly(ADP-ribosyl)ation is located at the C-terminal region of PARP-1 (domain F) and is responsible for the initiation, elongation and branching reactions of poly(ADP-ribose) formation (Figure 1-4). In human PARP-1, the region spans amino acid residues 859 to 908, and is phylogenetically well conserved (67), which constitutes part of the so-called “PARP signature” (50). The signature region harbors the NAD^+ binding site as a β-α-loop-β-α structural fold as well as the essential residues involved in the three reactions of PAR polymer formation (67). At the N-terminal region of domain F, there is a so-called PARP regulatory domain (68-69). However, the function of this region has not been fully established.

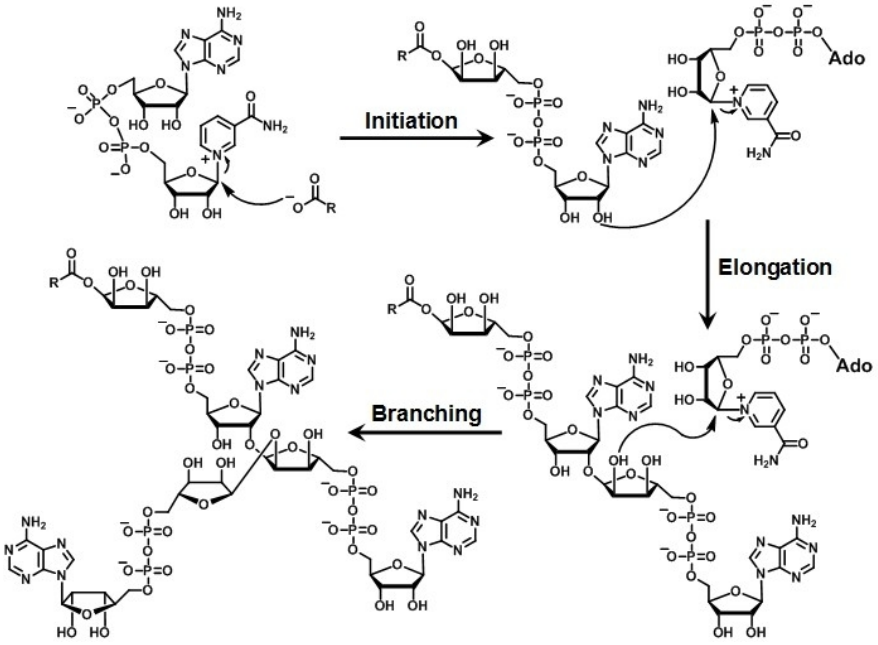

Figure 1-4. Initiation, elongation and branching reactions carried out by PARP-1.

1.2.2. The PARP superfamily

While structural and functional studies of PARP-1 are still ongoing, 16 genes in the human genome have been assigned to encode protein members of the PARP family based upon sequence homology to the "PARP signature" in the catalytic site of PARP-1 (Figure 1-5) (40,71). However, when more stringent criteria are applied based on the definition of poly(ADP-ribose) polymerase (i.e., the ability to form poly(ADP-ribose) chains), only four proteins can be characterized as true poly(ADP-ribose) polymerases: PARP-1, PARP-2, tankyrase 1 and tankyrase 2 (71). Studies have shown that PARP-1 and PARP-2 are capable of forming long branched polymers (16, 72); whereas tankyrase-1 can form linear polymers (73). Tankyrase-2 is also capable of forming long polymers, but its ability to introduce branching units has not been established (74). Currently, not

much mechanistic information is available with respect to how the single active site of PARP coordinates and regulates the three different reactions of initiation, elongation and branching required for polymer formation. Detailed biochemical and structural investigation of these four enzymes, which appear to generate polymer with different structural patterns, together with the mono-ADP-ribosyltransferases will be discussed later, and have shed some light on the mechanism of poly(ADP-ribose) biosynthesis.

Based on mutagenesis and structural studies of the PARP-1 catalytic domain, it has been suggested that the so-called H-Y-E triad is important for substrate binding and polymer elongation (75). This triad is well-conserved within the PARP family. The histidine and tyrosine residues are essential for NAD^+ binding, and the glutamic acid residue (E988 in human PARP-1) has been shown to be important for polymer formation (76). PARP-6 to PARP-16 do not have the conserved glutamic acid residue, which is instead replaced with an isoleucine, leucine or tyrosine residue. For this reason, these latter members of the PARP family are believed to be mono(ADP-ribosyl)transferases (40).

Nevertheless, whether the presence of an active site glutamate is the sole determinant for polymer formation is still arguable and worthy of further investigation. It is likely that determinants of polymer formation are not relegated solely to features of the active site, but may also be dependent on adjacent domains within the protein architecture. Consistent with this hypothesis is the fact that the catalytic domains of PARP-1 and PARP-2 show structural homology to the active site of the bacterial ADP-ribosylating Corynebacterium diphtheriae toxin (Figure 1-6), where the H-Y-E triad is present, but the toxin is not capable of forming poly(ADP-ribose) (71). Likewise, PARP-3 also contains the conserved triad, whereas its ability to catalyze polymer formation has yet to be established (40).

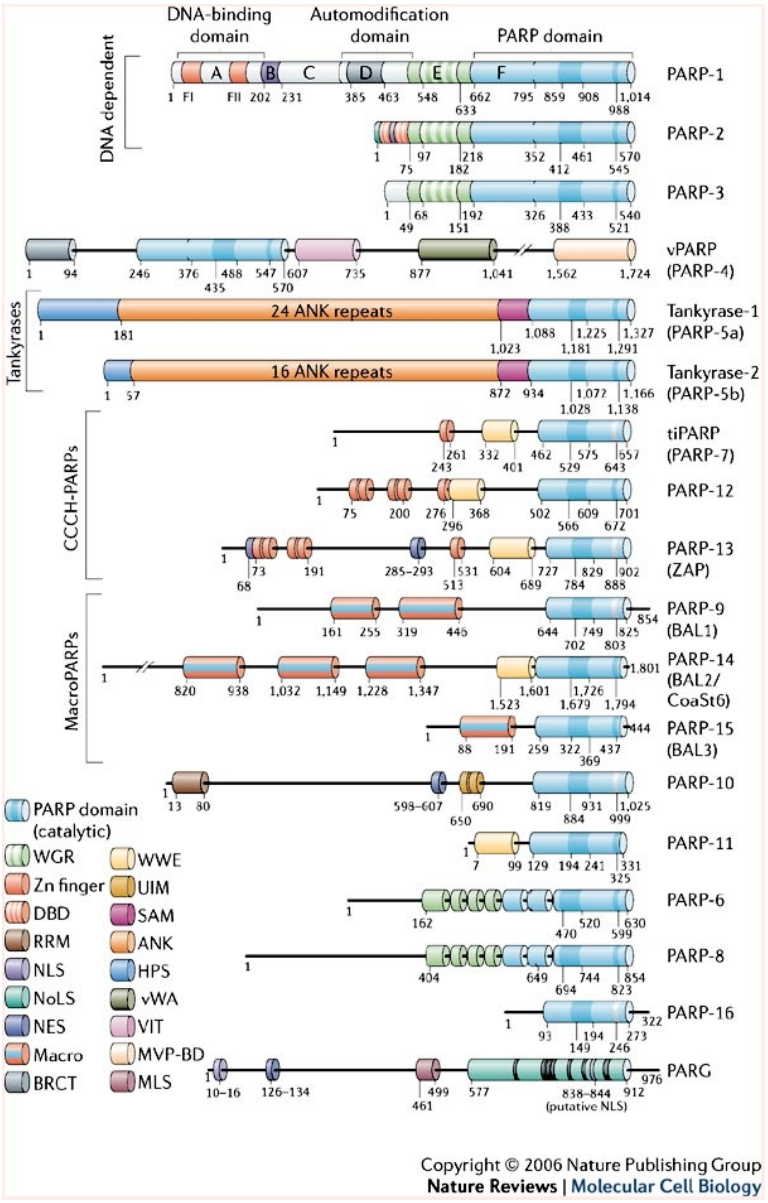

Figure 1-5. Members of PARP superfamily (adapted from Schreiber et al., Nat. Rev. Mol. Cell. Biol. 2006, 7: 517-528).

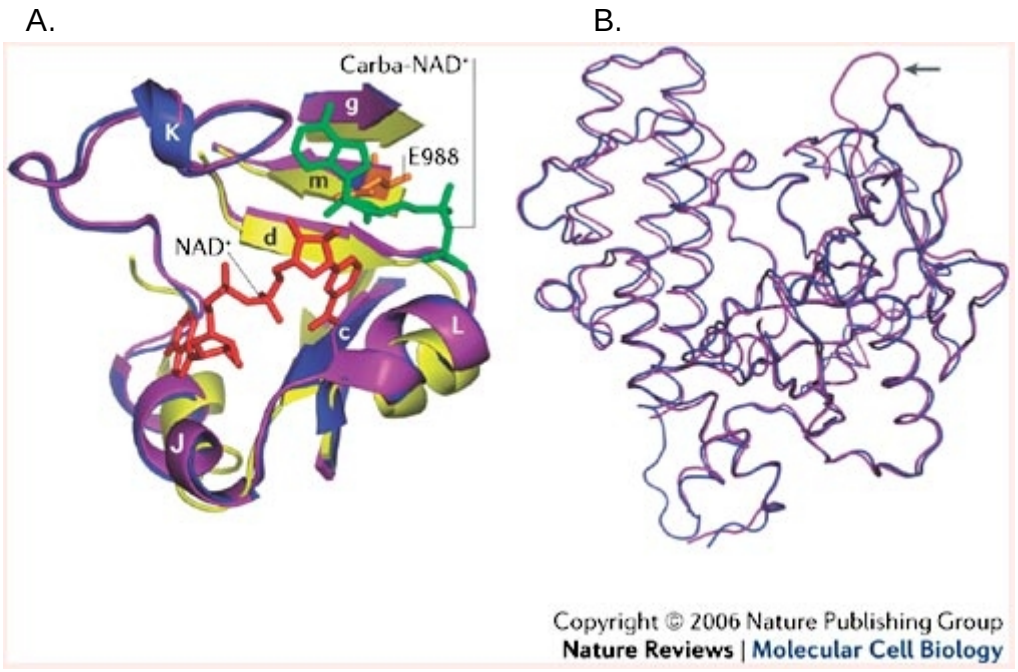

Figure 1-6. A. Structural alignment of chicken PARP-1 (2PAW, blue), mouse PARP-2 (1GS0, magenta) and Corynebacterium diphtheriae toxin (1TOX, yellow) catalytic domains. NAD^+ binding site was identified from co-crystallization of NAD^+ (red) with diphtheria toxin. Poly(ADP-ribose) acceptor site was deduced based on the ADP-moiety from bound carba-NAD^+ (1A26, green), with the 2'-OH group from the ribose staying close to the catalytic residue E988 (orange). B. The overlayed carbon α-backbone of chicken PARP-1 (2PAW, blue) and mouse PARP-2 (1GS0, magenta) catalytic domains. Two structures are highly conserved, except the extend loop region of PARP-2, as indicated by the arrow. Adapted from Schreiber et al., Nat. Rev. Mol. Cell. Biol. 2006, 7: 517-528.

1.3. DNA BINDING PROPERTIES OF PARP-1

1.3.1. Differential recognition by DNA-binding motifs of PARP-1

Interaction with damaged DNA can stimulate PARP-1 activity over 500-fold than its basal activity (26). This robust response toward DNA damage is mediated in large part by the two unique zinc fingers FI and FII within domain A. In addition to the rich contents of basic amino acid residues, which are likely to contribute to the DNA

interaction, this region also displays novel features that are only observed in the case of DNA ligase III (77) and 3'-DNA phosphodiesterase from Arabidopsis thaliana (AtZDP) (78). First, the zinc ion is coordinated with a Cys-Cys-His-Cys motif; second, the zinc fingers have 28 and 30 residues, which can facilitate larger surface contact when compared with typical zinc fingers having 12-13 amino acid residues. Furthermore, they recognize special structural features of DNA instead of specific nucleotide sequences (24).

The two zinc fingers exhibit differential roles when recognizing different DNA lesions. Using full-length PARP-1 protein, Ikejima et al. demonstrated that when PARP-1 encounters a single stranded break within plasmid DNA, both FI and FII are required for full activity; however, in the case of a double stranded break, only zinc finger I is required for PARP-1 activation (79). In contrast to this result, Gradwohl and colleagues used a truncated PARP-1 construct containing two zinc fingers to show that mutations in FII dramatically affect the recognition of nicked DNA, which mimics single stranded breaks, whereas FI mutations are much less important (51). Using DNA foot-printing, they also demonstrated that the site of interaction is at the nicked region of the DNA construct (51).

The inconsistency between the above two studies may be due to the different proteins and DNA constructs used. However, the two studies may not be as inconsistent as they seem, because each research group was looking at a different aspect of PARP-1 activity: PARP-1 enzymatic activity versus DNA binding ability. It is possible that in the case of single stranded breaks, zinc finger II is required for protein-DNA interactions, whereas the N-terminal zinc finger I is important for activation of the PARP-1 activity, possibly through conformational changes. This hypothesis can explain why both zinc fingers are required for activity, though only zinc finger II is the main contributor to

DNA recognition. Currently, detailed studies on how the two zinc fingers cooperate and contribute to DNA-dependent activation of PARP-1 remain few in number. Crystal structures of the two zinc fingers may provide additional insight to this matter and will be discussed in a later section. DNA recognition studies described in Chapter 3 address the hypothesis discussed here.

A double-stranded DNA binding domain (DsDB) located between the BRCT and the WGR domains was recently identified by Huambachano et al. (80). The authors also suggested that the DsDB domain may regulate the size of poly(ADP-ribose) being synthesized, because a protein construct possessing the WGR and catalytic domains preferentially forms long PAR polymers in the presence of double stranded DNA, whereas a protein construct containing the DsDB, WGR and catalytic domains leads to shorter polymer formation (80). Even though the DsDB domain can interact with double stranded DNA, the interaction appears to be relatively weak when compared that with the zinc fingers (80). In the case of full-length PARP-1, it is possible that the DsDB domain helps to stabilize binding to DNA that is distant from the lesion site, while the two zinc fingers directly interact with the DNA at the lesion site. It would be interesting to investigate the role of the DsDB domain within the context of full-length protein in terms of DNA binding versus polymer formation, which has yet to be done.

1.3.2. Interaction with different DNA structures

PARP-1 can interact with different DNA lesions, but the binding affinities toward different DNA structures can vary significantly. Being a DNA-damage “sensor,” PARP-1 shows strong affinities toward nicked DNA (81), 3'-single base overhangs as well as blunt end DNAs. The interaction is much weaker when considering DNAs with long 5'-

or 3'-overhangs (82). However, polymerase activity seems to be inversely correlated with the DNA binding affinities: DNAs with long overhangs typically have larger apparent V_{max} values (reported as unit per mg protein) when compared with those of blunt DNA and single base 3'-overhangs (82). In a more systematic study carried out by Pion et al., DNA constructs with 3'-overhangs exhibited higher PARP-1 activities when compared with 5'- overhangs and blunt end DNAs (*83*). Therefore, the 5'- recessed end of the damaged DNA may be the specific recognition site for PARP-1 activation. Based on fluorescence anisotropy measurements, higher activities may be attributable to the dimerization of PARP-1 at lesions involving a 5'-recessed end, whereas in the case of a 3'-recessed end and double stranded DNAs, PARP-1 binds to DNA in a 1:1 stoichiometry (*83*). Again, these results suggest that PARP-1 may adapt different recognition modes based on the DNA structures it encounters.

In addition to DNA damage, the presence of certain DNA sequences, such as the palindromic sequence of a *Not I* restriction site or a telomeric repeat, can further enhance the PARP-1 activity (*83*). Palindromic sequences like the *Not I* restriction site can form hairpin structures (*84*). This may explain the observed interaction between PARP-1 and a specific DNA sequence. Consistent with this hypothesis, PARP-1 has been shown to interact with numerous other non-B DNA structures in the absence of DNA breaks such as hairpins, three or four-way junctions, as well as bent and looped DNAs (*52*). It was also observed that PARP-1 interacts with DNA-adducts formed by crosslinking with DNA-alkylating agents such as cisplatin (*85*).

1.3.3. Structural evidence for DNA interaction with zinc fingers

As discussed above, studies of PARP-1/DNA interactions are complicated by the different domains involved and the variable binding stoichiometries depending on the nature of the DNA. Therefore, structural snapshots of PARP-1 interacting with DNAs have been valuable for investigating the matter, despite being a challenging task for the PARP community.

In 2011, the crystal structures of blunt end DNA complexed with each individual zinc fingers, FI and FII, were first reported by Langelier et al. (86). Using short, blunt end DNA as the mimic for a double stranded break, FI and FII were observed to exhibit similar binding modes when interacting with the duplex DNA (Figure 1-7). The mode of interaction can be characterized in terms of two distinct features, which are similar for both zinc fingers: 1. a conserved “base stacking loop” caps the 3'-end of the DNA lesion site, and 2. a “phosphate backbone grip” is in contact with the minor groove of the DNA (86).

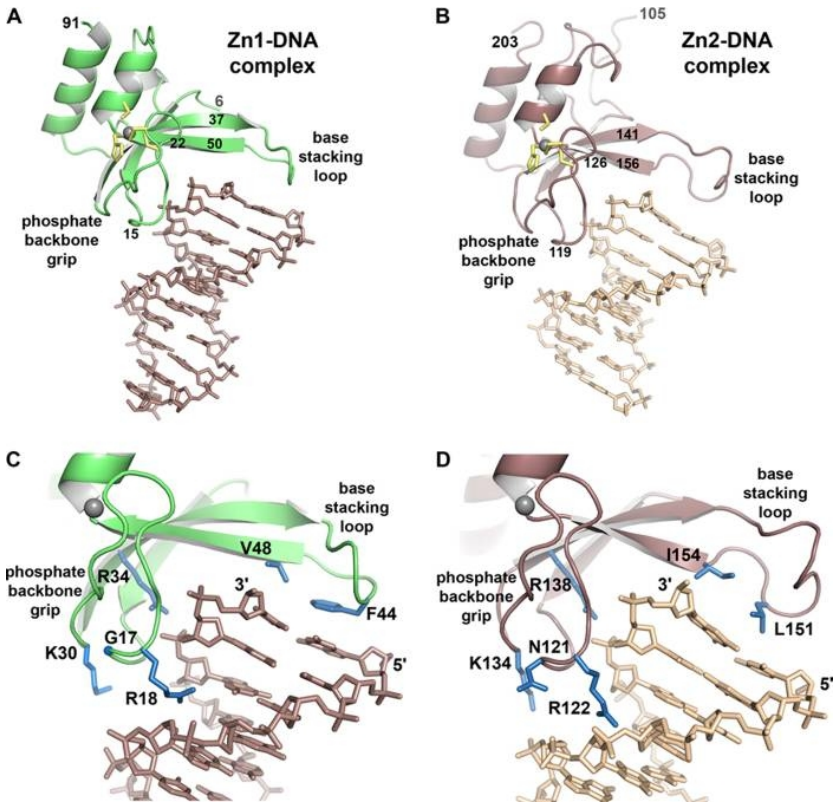

Figure 1-7. Crystal structures of PARP-1 zinc fingers complexed with a DNA duplex. A. Zinc finger I complexed with 10-bp DNA (PDB ID: 3OD8); B. Zinc finger II complexed with 8-bp DNA (PDB ID: 3ODC); C. Structural details of the base stacking loop and phosphate backbone grip of the zinc finger I/DNA complex; D. Structural details of the base stacking loop and phosphate backbone grip of the zinc finger II/DNA complex. Adapted from Langelier, J. Biol. Chem. 2011, 286: 10690-106701.

Based on the crystal structures shown in Figure 1-7, the interactions between DNA and the two zinc fingers appear similar. However, as discussed previously, their functional roles are significantly different in the context of full-length PARP-1. While FII has strong affinity toward blunt end DNA, an FII deletion mutant of PARP-1 can be activated by DNA to a similar extent as wild-type protein whether in vitro or in vivo (86). In contrast, when FI is deleted, the automodification activity is completely abolished even though DNA binding affinity is not significantly affected (86).

Later on, Ali and colleagues solved the crystal structure of a single peptide containing both zinc fingers complexed with an 11 base pair DNA duplex containing a single-base 5' overhang on each end (87). This structural complex was intended to mimic a single strand break and provide some insight as to how the two zinc fingers cooperate in recognizing DNA lesions. It was observed that FII interacts with DNA in a fashion similar to that when FI is absent (Figure 1-8, B and C). In contrast, the binding behavior of FI is different in the presence versus absence of FII. When in isolation, FI interacts with the same DNA lesion site as FII by capping the 3'- end (Figure 1-7C and 1-8A). Unlike its isolated form, however, the phosphate backbone grip of FI in the presence of FII is in contact with the major groove of the DNA while the base stacking loop is placed on top of the overhanging 5'-end (Figure 1-8 C) (70, 87). It was also observed that the two zinc fingers interacting at the same lesion site are not part of the same peptides, suggesting an intermolecular dimerization at the damage site of DNA.

Furthermore, the authors established that both zinc fingers are needed for PARP-1 localization at the site of DNA damage in vivo (87). Together with the observations reported by Langelier et al. (86), it is clear that FI is important for both DNA recognition and activation of PARP-1, whereas FII is mainly involved in recognizing DNA damage but not stimulating polymerase activity. When FII is mutated, its DNA binding ability can be partially substituted by FI, due to the similar interaction interfaces between the two zinc fingers (Figure 1-7). This substitution is not very efficient since the FII mutant of PARP-1 experiences a delay in localization to sites of DNA damage (70). Nevertheless, FI alone is still able to mediate DNA-dependent activation of PRAP-1 though at a suboptimal level.

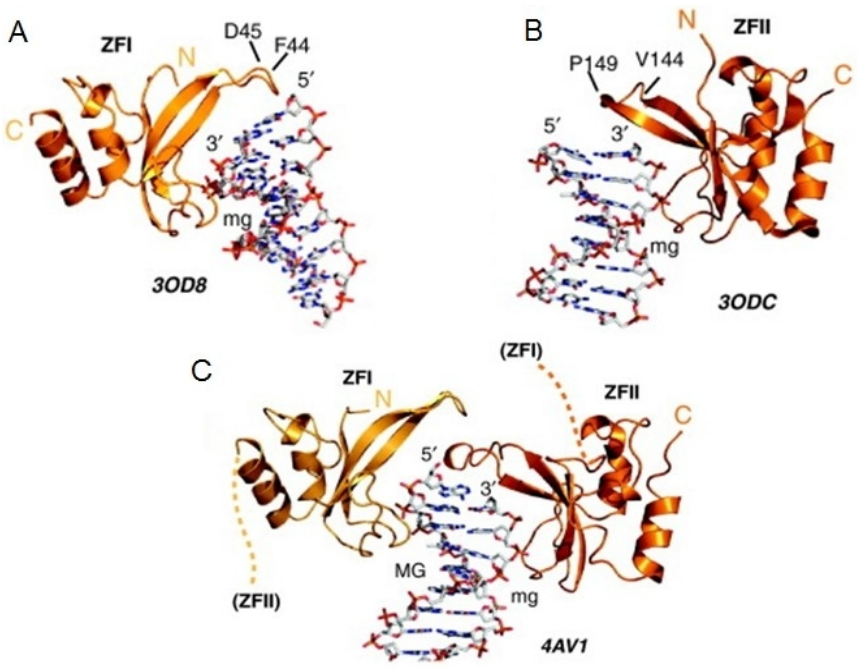

Figure 1-8. Crystallographic snapshots of PARP-1 zinc fingers complexed with a DNA duplex. A. Zinc finger I complexed with 10-bp blunt end DNA (PDB ID: 3OD8) solved by Langilier et al. (86); B. Zinc finger II complexed with 8-bp blunt end DNA (PDB ID: 3ODC) solved by Langilier et al. (86); C. Two zinc fingers complexed with 11-bp 5' overhang DNA (PDB ID: 4AV1) solved by Ali et al. (87). Adapted from Hassler et al., Curr. Opin. Struct. Biol. 2012, 22: 721-729.

1.4. ACTIVATION OF PARP-1

1.4.1. DNA-dependent activation of PARP-1

The best studied mode of activation for PARP-1 is the DNA-dependent pathway. Crystallographic studies of PARP-1 domains complexed with DNA have provided valuable structural information that allows investigators to envision how activation can be achieved in this manner. As shown in Figure 1-8, the observed dimerization of two zinc fingers with a single base 5'-overhang DNA led Ali et al. to propose an intermolecular model for the activation of PARP-1 in the presence of DNA lesions (Figure 1-9) (87).

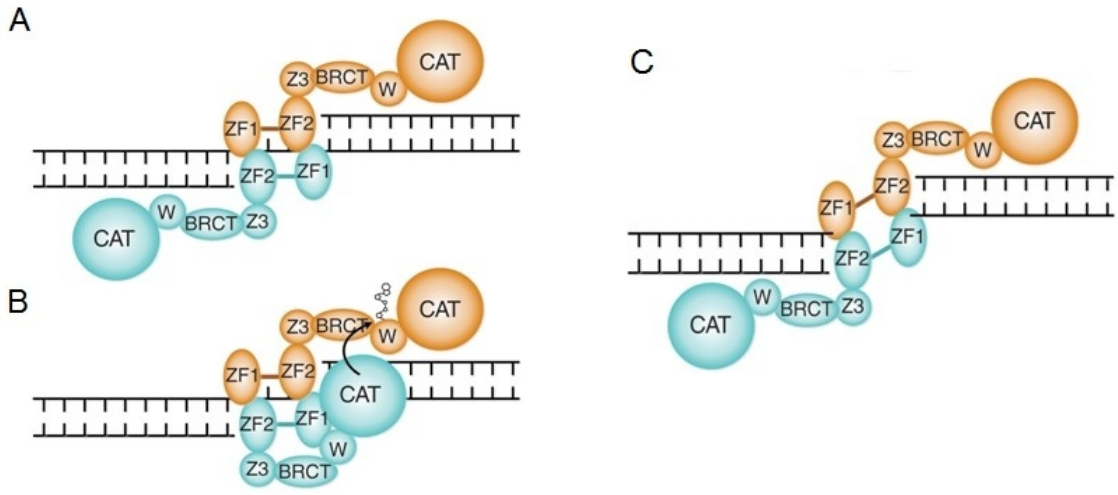

Figure 1-9. Proposed mechanism of trans-activation of PARP-1 by damaged DNA. A. and B. Model for single stranded DNA break; C. Model for double stranded DNA break. Adapted from Ali et al., Nat. Struct. Mol. Biol. 2012, 19: 685-692.

The model suggests that two PARP-1 molecules interact at the lesion site via the N-terminal zinc fingers. This dimerization is stabilized by protein-protein interactions between zinc finger I of one protein molecule and zinc finger II from the second PARP-1

molecule. This DNA induced dimerization then activates PARP-1 by inducing conformational changes in the adjacent domains. This also allows the catalytic domain of one PARP-1 protein to access the polymer acceptor sites at the BRCT domain in the second PARP-1 molecule resulting in intermolecular modification. Therefore, the proposed model requires PARP-1 dimer formation and intermolecular automodification.

Due to its large size and structural flexibility, it is difficult to crystallize full-length PARP-1 with DNA. The first successful attempt in crystallizing near full-length PARP-1 with DNA was accomplished by Langelier et al. in 2012, and the result is shown in Figure 1-10. The crystal structure was obtained using a 26 bp DNA duplex and three protein peptides: zinc finger I (FI), zinc finger III (FIII) and the WGR-CAT domain. These three components represent the minimal functional requirements for reconstituting DNA-dependent activation of PARP-1 (88). As shown in Figure 1-10, the WGR domain is in contact with FI, FIII, the CAT domain and DNA, which serves as the coordinating component for the domain-domain interactions as well as protein-DNA interactions. Thus, FI binds to the DNA in a fashion similar to its isolated form (see Figure 1-7), while FIII and the WGR domain also interact with the DNA duplex: FIII contacts the DNA backbone, and the WGR domain interacts with the 5' end of the DNA. It is worth noting that FIII in isolation does not interact with DNA (56). Upon binding to DNA, both FI and FIII interact with only one face of the WGR domain, whereas the regulatory HD domain of the CAT fragment is in contact with the opposite face of the WGR domain. Overall, this crystal structure implies that PARP-1 interacts with the DNA lesion only in a monomeric form.

A. B.

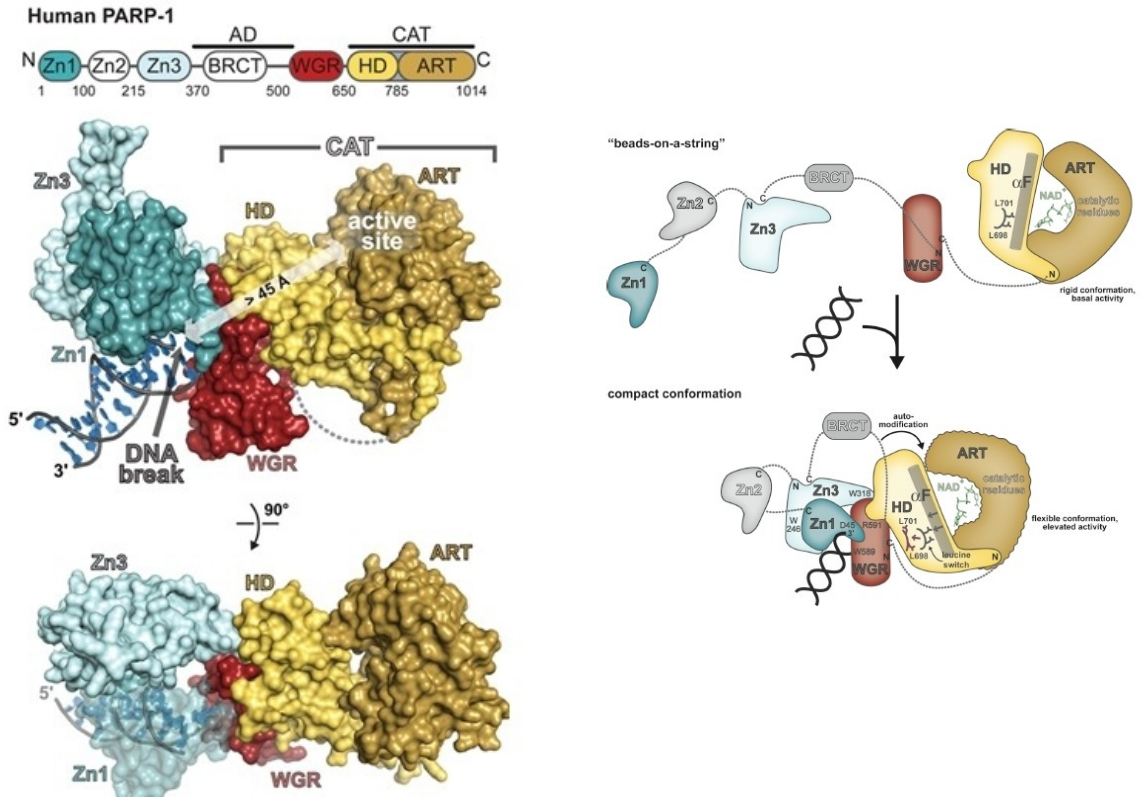

Figure 1-10. A. The crystal structure of PARP-1 domains/DNA complex. B. A proposed model for DNA-dependent activation of PARP-1. Adapted from Langelier et al., Science 2012, 336: 728-732.

Based on the structural evidence (Figure 1-10A) in combination with a series of mutational studies, Langelier et al. proposed an intramolecular DNA-dependent activation model for PARP-1 automodification (see Figure 1-10B). In the absence of DNA, PARP-1 exists in an elongated, “beads-on-a-string” conformation, and the catalytic ART domain is in a closed and rigid conformation that is regulated by the adjacent HD domain. This results in a low basal level of PARP-1 activity. When PARP-1 encounters a DNA lesion, FI, FIII and the WGR domain aggregate together into close contact about the DNA to form a compact complex at the site of the lesion. The interdomain

interactions perturb the interaction between the HD and ART domains thereby destabilizing the closed conformation of the ART domain. The result is a more flexible catalytic domain, which allows the BRCT domain to approach closer to the active site. This leads to stimulation of PARP-1 activity and automodification at the BRCT domain (88-89).

As discussed, the two mechanisms proposed for DNA-dependent activation of PARP-1 differ in terms of protein stoichiometry and intra- versus intermolecular automodification. Therefore, these opposing models serve as interesting hypotheses that are worthy of further testing. Studies to be described in Chapter 2 and Chapter 3 of this dissertation are intended to provide information for addressing the issues of stoichiometry and DNA-protein interaction dynamics.

1.4.2. DNA-independent activation of PARP-1

In addition to the DNA-dependent activation pathway of PARP-1, accumulating evidence suggests that PARP-1 can also be activated through alternative pathways that do not involve DNA. As demonstrated by Huambachano et al., single stranded RNAs such as poly(rA), poly(U) and poly(rC) alone can activate the WGR-CAT domain for automodification in the absence of DNA (66). Furthermore, PARP-3, which is a mono-ADP-ribosylase within the PARP family, can interact with PARP-1 and act as an activator for PARP-1 automodification (90). Interestingly, the WGR domain seems to play an essential role in both scenarios. In the case of PARP-1, the WGR domain is important for facilitating interactions with RNA (66), while the WGR domain of PARP-3 is important for activating PARP-1 in the absence of DNA (90).

Another interesting discovery is that PARP-1 can also be activated by the phosphorylated-ERK2 kinase in the absence of DNA. DNA competition assays performed by Cohen-Armon et al. suggested that phosphorylated-ERK2 (p-ERK2) may interact with PARP-1 in the same region as where DNA binds, with p-ERK2 being a stronger activator in comparison with DNA (91). This result has raised the question as to whether there is any similarity in the modes of interaction between PARP-1 and p-ERK2 versus DNA. Both activating species contain phosphate groups that may serve as the key component for PARP-1 activation upon binding. Furthermore, PARP-1 can be phosphorylated by free ERK2, and this results in enhanced automodification activity in the presence of DNA; however, phosphorylation alone is not strong enough to activate PARP-1 in the absence of DNA (92). Phosphorylation of PARP-1 may, therefore, be a potentiating switch that still requires the participation of DNA.

1.5. Reaction Mechanism of PARP-1

In contrast to the extensive studies of PARP-1 activation, information regarding the PARP-1 reaction mechanism is still quite limited. This may be ascribed to the heterogeneity of poly(ADP-ribose) products generated during catalysis, and the uncertain number of automodification sites within PARP-1. Few details are known regarding how PARP-1 utilizes a single active site to catalyze the separate reactions of initiation, elongation and branching during poly(ADP-ribose) formation.

1.5.1. Catalytic mechanism of PARP-1

PARP-1 catalyzes poly(ADP-ribosyl)ation using NAD^+ as the donor of polymer residues. PARP-1 itself can also serve as the substrate for modification with polymer.

PAR polymer formation occurs via three different reaction processes: initiation, elongation and branching (see Figure 1-4). Initiation involves the formation of a covalent linkage between ADP-ribose and the carboxyl group of a glutamic or aspartic acid residue on the protein substrate via displacement of nicotinamide from NAD^+ (*93*). Based on a QM/MM computations carried out by *Bellocchi et al.*, PARP-1 is believed to catalyze cleavage of the nicotinamide-ribosyl bond through a S_N2 mechanism *(94*). The initiation reaction can also utilize lysine as the acceptor residue in the protein substrate, though this appears to be less common (*25*).

The distinction between initiation, elongation and branching essentially depends on the identity of the acceptor unit. Whereas a protein residue serves as the acceptor for initiation, the 2'-OH of the adenine-ribose moiety of the terminal unit serves as the acceptor during elongation reactions. In branching reactions, however, the 2"-OH of a nicotinamide-ribose moiety in the polymer becomes the acceptor site for the incoming ADP-ribose moiety (*93*). The majority of the PARP family members are mono-ADP-ribosylases (71), which effectively only catalyze initiation reactions. The mechanistic question of PARP-1 catalysis is how PARP-1 can utilize three different acceptor substrates and catalyze polymer synthesis with a single active site.

Before crystal structures of the PARP-1 catalytic domain became available, mutagenesis studies carried out by Marisischky et al. identified E988 as an important amino acid residue involved in poly(ADP-ribose) elongation (76). E988Q and E988A mutants could carry out initiation, but polymer formation was reduced by more than 2000- fold when compared with the wild type enzyme. Likewise, the E988D mutation decreases polymer formation by about 20-fold. These observations led to the proposal that E988 acts as a general base to activate the 2'-OH group of the terminal adenine-ribose of the nascent poly(ADP-ribose) during the elongation (Figure 1-11B).

Furthermore, by co-crystallizing the catalytic domain of PARP-1 with a carba-NAD substrate analog, Ruf et al. observed that E988 forms a hydrogen bond with the 2'-OH group of the adenine-ribose moiety (95). The role of E988 in initiation is apparently less significant because E988 mutants have relatively little effect on chain initiation. Nevertheless, it could still serve in initiation by positioning the acceptor nucleophile of the protein substrate through hydrogen bonding (Figure1-11A) (76). Experiments described in Chapter 4 address the regulatory elements of polymer synthesis by considering the involvement of different domains of PARP-1.

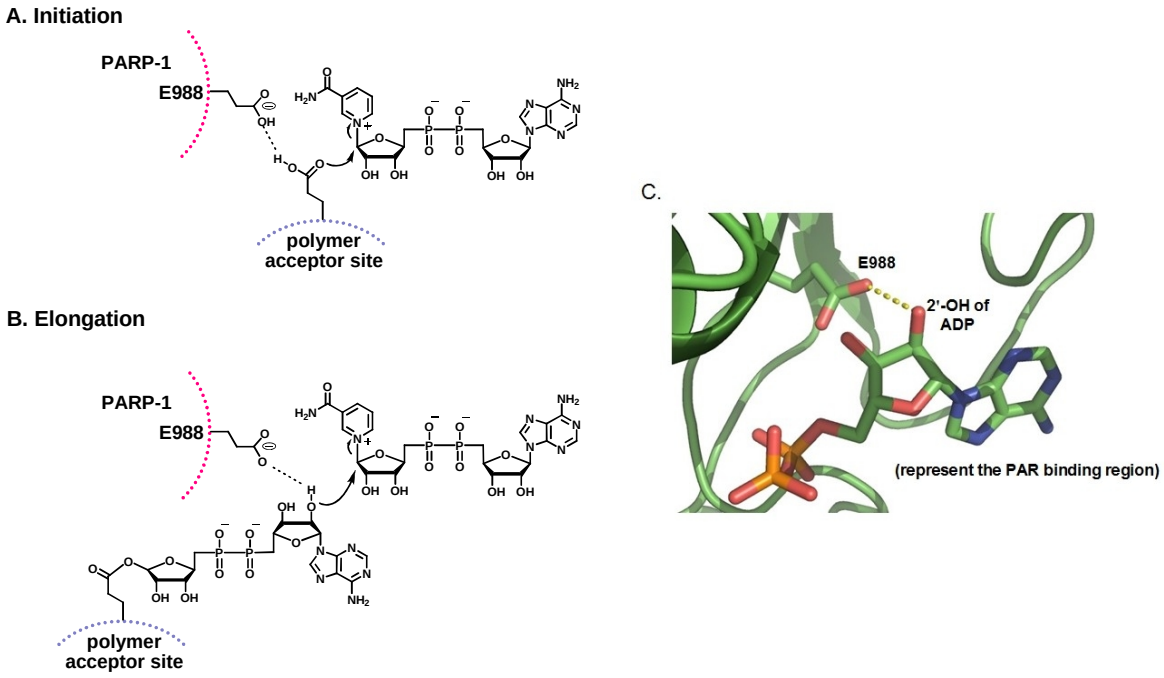

Figure 1-11. The role of Glu988 in initiation and elongation of poly(ADP-ribose) synthesis. A. Initiation. B. Elongation. C. Crystal structure of PARP-1 catalytic domain in complex with carba-NAD (PDB ID: 1A26). Adapted from Marsischky et al., J. Biol. Chem. 1995, 270: 3247-3254 and Ruf et al., J. Mol. Biol. 1998, 278: 57-65.

Study of the branching reaction is hampered due to the relatively low abundance of branching units, which amounts to approximately 2 to 5% of polymerized residues

(24). Furthermore, branching unit formation is irregular and depends on the size of the polymers (15), which is hard to control based on current techniques. Nevertheless, the crystal structure described previously in Figure 1-12 A and B revealed that position of the pyrophosphate group of ADP is fixed by an extensive hydrogen bonding network, whereas the adenine-ribose moiety is more flexible and lying at the open end of the active site. The presumably weak interactions between the adenine-ribose region of the polymer and the exposed surface groove of PARP-1 have led researchers to propose the model in Figure 1-12 C to explain how branching takes place.

According to this model, the bound NAD^+ is fixed within the catalytic domain. It is the recognition of the pyrophosphate moieties of the polymer rather than the terminal adenine-ribose that renders the nascent polymer be more flexible and be able to orient differently within the active site. Catalysis proceeds through elongation or branching reactions depending on whether the terminal adenine-ribose or the internal nicotinamide-ribose moiety is closer to the NAD^+ binding site (95). Consistent with this hypothesis, early random mutation studies carried out by Rolli et al. identified the Y986 residue as an important residue for modulating the branching frequency. Y986 is in close proximity to both E988 and the pyrophosphate moiety of an ADP-ribose in the crystal structure (PDB ID: 1A26). While a Y986H mutant retained about 10% of the enzymatic activity as the wild-type, the branching frequency was about 15-fold higher (96). It is possible that Y986 may interact with the adenine ribose moiety of the incoming polymer and thereby position the nicotinamide ribose close to E988, which would thus be activated for a branching reaction (Figure 1-12).

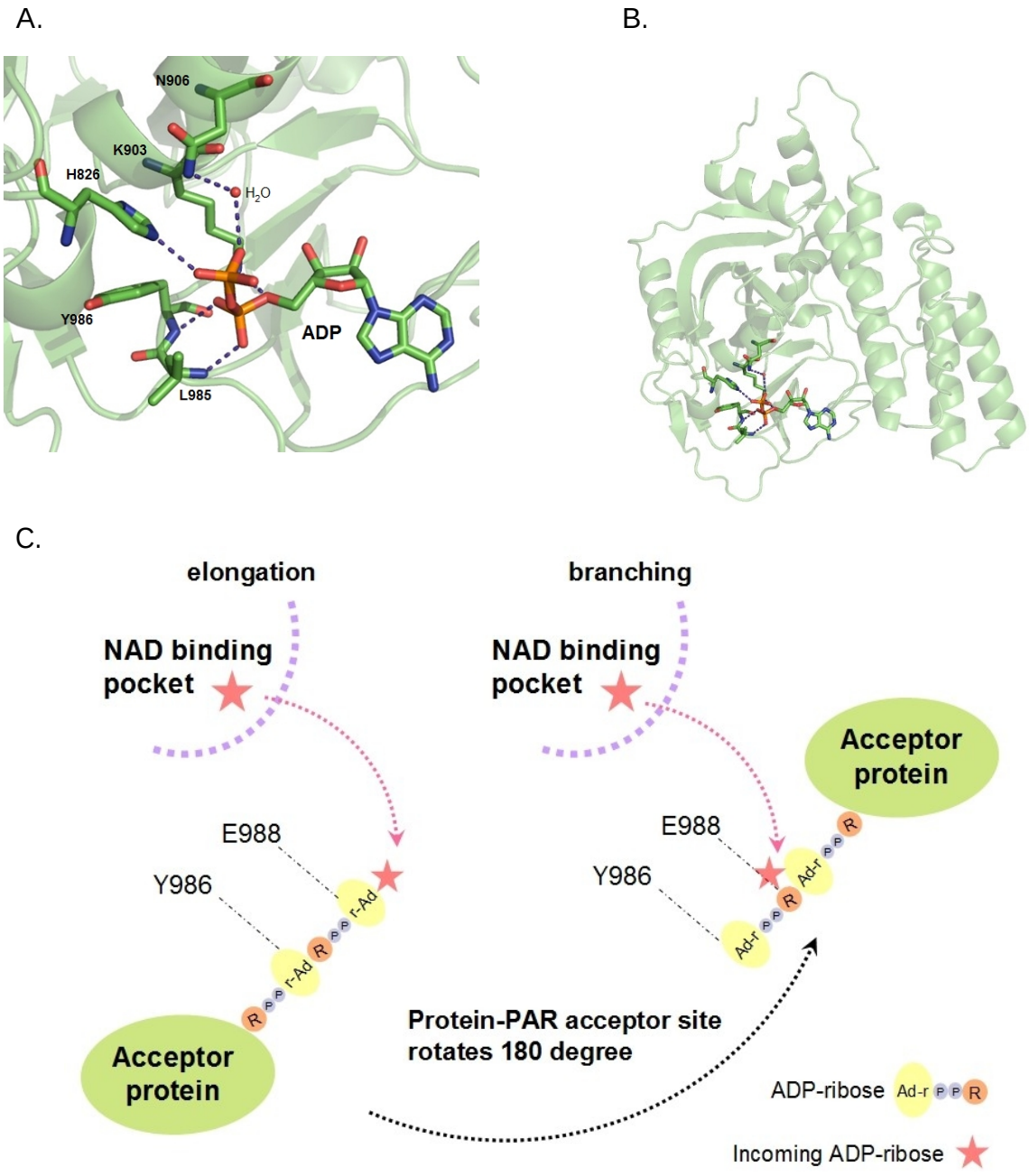

Figure 1-12. A. Residues involved in hydrogen bonding with the pyrophophosphate moiety (PDB ID: 1A26). B. The binding pocket of the ADP moiety of carba-NAD^+ is relatively open. C. Proposed mechanism for elongation and branching reactions of PARP-1 (modified based on Ruf, J. Mol. Biol. 1998, 278: 57-65).

1.5.2. Automodification of PARP-1

The intriguing aspects of PARP-1 catalysis are not limited to the three reaction steps discussed above. As PARP-1 itself is the major acceptor during poly(ADP-ribose) synthesis, there are several questions regarding how PARP-1 automodification takes place. One question is the role of each individual PARP-1 molecule in the automodification process. As discussed previously, it is possible that automodification takes place after dimerization of PARP-1, such that one protein molecule serves as the catalytic enzyme, with the other being the acceptor substrate (Figure 1-9). In such a scenario, automodification would be an intermolecular process. Alternatively, a single PARP-1 protein could serve as both catalyst and substrate in an intramolecular mechanism as shown in Figure 1-10.

In attempting to address this question, Mendoza-Alvarez et al. reported the observation of the second order kinetics when the initial rate of PARP-1 automodification was measured as a function of PARP-1 concentration. This is consistent with the formation of activated dimers during intermolecular PARP-1 automodification (97). However, the above conclusion is questionable because the kinetic measurements were based on total NAD^+ incorporation. Furthermore, it was generally believed that automodification of PARP-1 must be an intermolecular process if PARP-1 forms a dimer. However, this is not necessarily true, since activation and automodification steps are two separate processes. While not much information is available, one can image that activation may require dimer formation at the DNA lesion site (Figure 1-9), but the subsequent automodification reaction can be either an intra- or intermolecular process. If the later hypothesis is true, then it would be hard to distinguish whether automodification takes place intra- versus intermolecularly based on a simple kinetic analysis alone.

Another interesting question regarding PARP-1 automodification pertains to the topology of poly(ADP-ribose) extension. For example, the incoming ADP-ribose may be added to the terminal end of the growing polymer, which is termed distal addition, or it could be added to the site where the polymer linked to the protein substrate, which is termed as proximal addition (Figure 1-13). Several research groups have tried to answer this question by carrying out pulse-chase experiments. Despite the same fundamental designs, different conclusions were reached (98-101). With data interpreted as support for both proximal and distal elongation in the literature, this question clearly remains unresolved. Therefore, a modified version of pulse-chase experiment described in Chapter 4 is aimed to provide additional insight into this question.

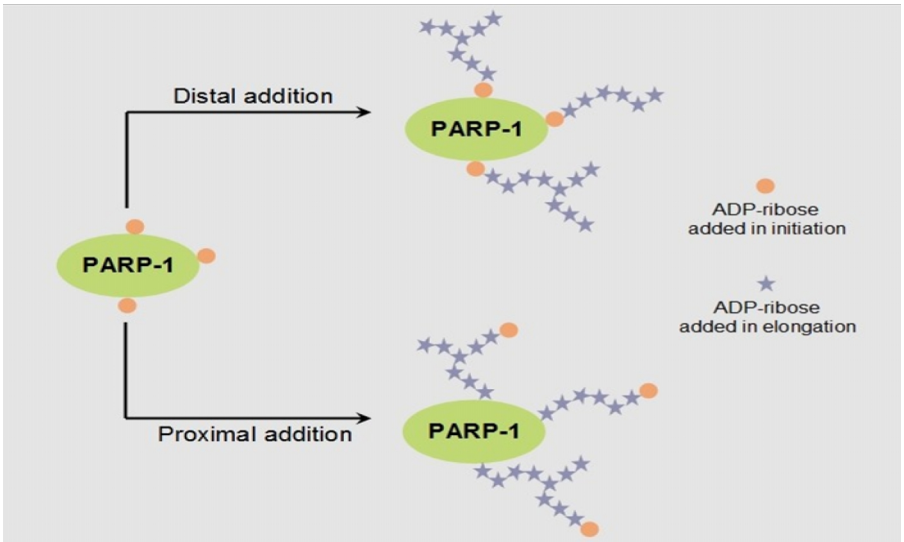

Figure 1-13. Schematic diagram of two possible mechanisms of polymer elongation.

1.5.3. Heteromodification of PARP-1

Poly(ADP-ribosyl)ation of acceptor substrates other than PARP-1 itself is called heteromodification. The best studied substrate for heteromodification is histone H1,

which is one of the first identified PARP-1 substrates. Since PARP-1 itself is the major acceptor substrate for poly(ADP-ribose)ation, it is of interest to learn how PARP-1 selects and modifies heterosubstrates. One possibility is that PARP-1 transfers polymers synthesized via automodification en masse to an acceptor residue of a heterosubstrate. Alternatively, PARP-1 may initiate polymer formation directly onto a heterosubstrate in a manner analogous to automodification. Using histone H1, it has been shown that pre-established polymers are unlikely to be transferred from PARP-1 to histone H1 (61,102). This is consistent with the hypothesis that modification of heterosubstrates by PARP-1 follows a process of initiation, elongation and branching much like automodification.

Heteromodification requires a mechanism for substrate recognition by PARP-1, and the pre-established polymer of automodified PARP-1 may play a role. Heterosubstrates such as histone H1 can bind with PAR polymers (103). This leads to the hypothesis that automodification may be a pre-requisite for heteromodification: the pre-established PAR polymers on automodified PARP-1 may function as a locus of interaction for histone H1 thereby increasing its effective concentration near the PARP-1 active site. Furthermore, a specific size of the polymer may be required for optimal heteromodification activity. For example, if the polymer is too large, it may prevent the heterosubstrate to bind close to the catalytic domain of PARP-1 for effective initiation and elongation. Under typical in vitro conditions, levels of histone H1 modification are relatively low when compared with levels of PARP-1 automodification. However, it has been reported that when a small amount of PARG is added to the reaction, the observed level of histone modification increases (104). This is consistent with the hypothesis that there is an optimal size of the pre-established PAR polymer required for efficient heteromodification.

1.5.4. Inactivation of PARP-1

While DNA stimulates PARP-1 activity over 500-fold from its basal level (24), the net negative charges on PARP-1 are rapidly increased due to the subsequent automodification. Zaharadka et al. monitored the sedimentation patterns of DNA with PARP-1 and found that after automodification of PARP-1, the pre-bound DNA was released (105). When PARG is also present during automodification, however, the DNA remained bound with PARP-1 (105). These results indicate that polymer formation leads to a decrease in the affinity between DNA and PARP-1 and support an inactivation model called "PARP shuttling" (24). This model predicts that the level of modification will eventually reach to a "point of repulsion", the interaction between PARP-1 and DNA becomes destabilized due to the negative charges on both DNA and PAR polymer, and at which point, leading to the dissociation of DNA from PARP-1. As a result, PARP-1 activity is returned to its basal level (24). While large PAR polymers can cause PARP-1 inactivation, under physiological condition, another factor which could affect the size of PAR polymer in PARP-1 automodification is the presence of PARG, which can hydrolyze the polymers to smaller size. When PARG is present, automdofication activity of PARP-1 can be sustained without inactivation (106). Therefore, PARG has an essential role in maintaining PARP-1 activity in vivo, and how this process being regulated is currently unknown.

1.6. THESIS STATEMENT

Work presented in this dissertation provides additional insight into the mechanisms of DNA-dependent activation of PARP-1 and poly(ADP-ribose) biosynthesis. Chapter 2 describes analytical ultracentrifugation as a technique to investigate the oligomerization states of PARP-1 proteins bound to different DNA

constructs. The results obtained from sedimentation velocity experiments indicate that PARP-1 as well as the DNA binding domains AB associate with DNA lesions as dimers. In addition, a secondary DNA binding site within the WGR motif is characterized. In Chapter 3, single molecule fluorescence colocalization experiments were performed to investigate the interaction dynamics of DNA recognition by domain AB. It was observed that recognition of double strand breaks by domains AB includes two different steps that exhibit distinct dissociation kinetic behaviors and involve different regions of the domains AB based on FRET efficiency analyses. Consistent with the results obtained from sedimentation velocity experiments, total intensity analyses indicate dimer formation with the double stranded break. In Chapter 4, the domain requirements for initiation and elongation processes of poly(ADP-ribose) synthesis were investigated using the truncated PARP-1 constructs ABC and DEF. Data support the requirement of both ABC and DEF for both initiation and short polymer formation. When protein-conjugated polymers become longer, the DEF construct alone is capable of incorporating NAD^+ in the absence of ABC. Based on results from a series of biochemical studies together with the available crystal structure of PARP-1 domains in complex with DNA (see Figure 1-10), an automodification model of PARP-1 has been proposed. One aspect of the proposed model is that polymer elongation happens through distal addition. In Chapter 4, pulse-chase experiments as well as polymer transfer assays are described as intended to test this proposed model. These results are consistent with distal elongation.

1.7. REFERENCES

1. Chambon, P., Weill, J. D., and Mandel, P. (1963) Nicotinamide mononucleotide activation of new DNA-dependent polyadenylic acid synthesizing nuclear enzyme, Biochem. Biophys. Commun. 11, 39-43.

2. Fujimura, S., Sugimura, T., Okabe, K., and Yoshida, T. (1965) NMN-activated poly(A) polymerase in nuclei from rat liver and hepatoma cells. Proc. Annu. Meeting Jpn. Biochem. Soc. 38, 591 (In Japanese).

3. Chambon, P., Weill J. D., Strosser, M. T., and Mandel, P. (1966) On the formation of a novel adenylic compound by enzymatic extracts of liver nuclei, Biochem. Biophys. Commun. 25, 638-643.

4. Nishizuka, Y., Ueda, K., Nakazawa, K., and Hayaishi, O. (1967) Studies on the polymer of adenosine diphosphate ribose. I. Enzymatic formation from nicotinamide adenine dinucleotide in mammalian Nuclei. J. Biol. Chem. 242, 3164-3171.

5. Reeder R. H., Ueda K., Honjo, T., Nishizuka Y., and Hayaishi, O. (1967) Studies on the polymer of adenosine diphosphate ribose. II. Characterization of the polymer. J. Biol. Chem. 242, 3172-3179.

6. Fujimura, S., Hasegawa, S., Shimizu, Y., and Sugimura, T. (1967) Polymerization of the adenosine 5'-diphosphate-ribose moiety of nicotinamide-adenine dinucleotide by nuclear enzyme. I. Enzymatic reactions, Biochim. Biophys. Acta. 145, 247-259.

7. Futai, M., Mizuno, D., and Sugimura, T. (1967) Hydrolysis of the polymer formed from NAD with rat liver phosphodiesterase yielding nucleoside 5'-monophosphate, Biochem. Biophys. Res. Commun. 28, 395-399.

8. Miwa M., Saitô H., Sakura H., Saikawa N., Watanabe F., Matsushima T., and Sugimura T. (1977) A ^{13}C NMR study of poly(adenosine diphosphate ribose) and its monomers: evidence of alpha-(1'' leads to 2') ribofuranosy1 ribofuranoside residue, Nucleic Acid Res. 4, 3997-4005.

9. Ferro, A. M., and Oppenheimer N. J. (1978) Structure of a poly (adenosine diphosphoribose) monomer: 2'-(5"-hosphoribosyl)-5'-adenosine monophosphate, Proc. Natl. Acad. Sci. U.S.A. 75, 809-813.

10. Hayaishi, O., and Ueda, K. (1977) Poly(ADP-ribose) and ADP-ribosylation of proteins, Ann. Rev. Biochem. 46, 95-116.

11. Tanaka, M., Miwa, M., Hayashi, K., Kubota, K., and Matsushima, T. (1977) Separation of oligo(adenosine diphosphate ribose) fractions with various chain lengths and terminal structures, Biochemistry 16, 1485-1489.

12. Tanaka, M., Hayashi, K., Sakura, H., Miwa, M., Matsushima, T., and Sugimura, T. (1978) Demonstration of high molecular weight poly (adenosine diphosphate ribose), Nucleic Acid Res. 5, 3183-3194.

13. Miwa, M., Saikawa, N., Yamaizumi, Z., Nishimura, S., and Sugimura ,T. (1979) Structure of poly(adenosine diphosphate ribose): identification of 2'-[1''-ribosyl-

2''-(or 3''-)(1'''-ribosyl)]adenosine-5',5'',5'''-tris(phosphate) as a branch linkage, Proc. Natl. Acad. Sci. U.S.A. 76, 595-599.

14. Miwa, M., Ishihara, M., Takishima, S., Takasuka, N., Maeda, M., Yamaizumi, Z., Sugimura, T., Yokoyama, S., and Miyazawa T. (1981) The branching and linear portions of poly(adenosine diphosphate ribose) have the same alpha(1 leads to 2) ribose-ribose linkage, J. Biol. Chem. 256, 2916-2921.

15. Hayashi, K., Tanaka, M., Shimada, T., Miwa, M., and Sugimura, T. (1983) Size and shape of poly(ADP-ribose): examination by gel filtration, gel electrophoresis and electron microscopy, Biochem. Biophys. Res. Commun. 112, 102-107.

16. Alvarez-Gonzalez, R., and Jacobson, M. K. (1987) Characterization of polymers of adenosine diphosphate ribose generated in vitro and in vivo, Biochemistry 26, 3218-3224.

17. Nishizuka, Y., Ueda, K., Honjo, T., and Hayaishi, O. (1968) Enzymic adenosine diphosphate ribosylation of histone and poly adenosine diphosphate ribose synthesis in rat liver nuclei, J. Biol. Chem. 243, 3765-3767.

18. Nishizuka, Y., Ueda, K., Yoshihara, K., Yamamura, H., Takeda, M., and Hayaishi, O. (1969) Enzymic adenosine diphosphoribosylation of nuclear proteins, Cold Spring Harb. Symp. Quant. Biol. 34, 781-786.

19. Otake, H., Miwa, M., Fujimura, S., and Sugimura, T. (1969) Binding of ADP-ribose polymer with histone, J. Biochem. 65, 145-146.

20. Ueda, K., Omachi, A., Kawaichi, M., and Hayaishi, O. (1975) Natural occurrence of poly(ADP-ribosyl) histones in rat liver, Proc. Natl. Acad. Sci. U.S.A. 72, 205-209.

21. Tao, Z., Gao, P., and Liu, H.W. (2009) Studies of the expression of human poly(ADP-ribose) polymerase-1 in Saccharomyces cerevisiae and identification of PARP-1 substrates by yeast proteome microarray screening, Biochemistry 48, 11745-11754.

22. Davidovic, L., Vodenicharov, M., Affar, E.B., and Poirier, G.G. (2001) Importance of poly(ADP-ribose) glycohydrolase in the control of poly(ADP-ribose) metabolism, Exp. Cell. Res. 268, 7-13.

23. Nguewa, P.A., Fuertes, M.A., Valladares, B., Alonso, C., and Pérez, J.M. (2005) Poly(ADP-ribose) polymerases: homology, structural domains and functions. Novel therapeutical applications, Prog. Biophys. Mol. Biol. 88, 143-72.

24. D'Amours ,D., Desnoyers, S., D'Silva, I., and Poirier, G.G. (1999) Poly(ADP-ribosyl)ation reactions in the regulation of nuclear functions, Biochem. J. 342, 249-268.

25. Messner, S., Altmeyer, M., Zhao, H., Pozivil, A., Roschitzki, B., Gehrig, P., Rutishauser, D., Huang, D., Caflisch, A., Hottiger, M.O. (2010) PARP1 ADP-

ribosylates lysine residues of the core histone tails, Nucleic Acids Res. 38,6350-6362.

26. Alvarez-Gonzalez, R., and Althaus, F.R. (1989) Poly(ADP-ribose) catabolism in mammalian cells exposed to DNA-damaging agents, Mutat. Res. 218, 67-74.

27. Gibson, B.A., and Kraus, W.L. (2012) New insights into the molecular and cellular functions of poly(ADP-ribose) and PARPs, Nat. Rev. Mol. Cell Biol. 13, 411-424.

28. Nguewa, P.A., Fuertes, M.A., Valladares, B., Alonso, C., Pérez, J.M. (2005) Poly(ADP-ribose) polymerases: homology, structural domains and functions. Novel therapeutical applications, Prog. Biophys. Mol. Biol. 88, 143-172.

29. Miwa, M., Tanaka, M., Matsushima, T., and Sugimura, T. (1974) Purification and properties of glycohydrolase from calf thymus splitting ribose-ribose linkages of poly(adenosine diphosphate ribose), J. Biol. Chem. 249, 3475-3482.

30. Ikejima, M., and Gill, D.M. (1988) Poly(ADP-ribose) degradation by glycol-hydrolase starts with an endonucleolytic incision, J. Biol. Chem. 263, 11037-11040.

31. Sharifi, R., Morra, R., Appel, C.D., Tallis, M., Chioza, B., Jankevicius, G., Simpson, M.A., Matic, I., Ozkan, E., Golia, B., Schellenberg, M.J., Weston, R., Williams, J.G., Rossi, M.N., Galehdari, H., Krahn, J., Wan, A., Trembath, R.C., Crosby, A.H., Ahel, D., Hay, R., Ladurner, A.G., Timinszky, G., Williams, R.S., and Ahel I. (2013) Deficiency of terminal ADP-ribose protein glycohydrolase TARG1/C6orf130 in neurodegenerative disease, EMBO J. 32, 1225-1237.

32. Poirier, G. G., de Murcia, G., Jongstra-Bilen, J., Niedergang, C., and Mandel, P. (1982) Poly(ADP-ribosyl)ation of polynucleosomes causes relaxation of chromatin structure, Proc. Natl. Acad. Sci. U.S.A. 79, 3423-3427.

33. Realini, C. A., and Althaus, F. R. (1992) Histone shuttling by poly(ADP-ribosylation), J. Biol. Chem. 267, 18858-18865.

34. Masson, M., Niedergang, C., Schreiber, V., Muller, S., Menissier-de Murcia, J., and de Murcia, G. (1998) XRCC1 is specifically associated with poly(ADP-ribose) polymerase and negatively regulates its activity following DNA damage, Mol. Cell. Biol. 18, 3563-3571.

35. Audebert, M., Salles, B. and Calsou, P. (2004) Involvement of poly(ADP-ribose) polymerase-1 and XRCC1/DNA ligase III in an alternative route for DNA double-strand breaks rejoining, J. Biol. Chem. 279, 55117-55126.

36. Caldecott, K.W., Aoufouchi, S., Johnson, P., and Shall, S. (1996) XRCC1 polypeptide interacts with DNA polymerase beta and possibly poly (ADP-ribose) polymerase, and DNA ligase III is a novel molecular 'nick-sensor' in vitro, Nucleic Acids Res.,24, 4387-4394.

37. Weinfeld, M., Chaudhry, M.A., D'Amours, D., Pelletier, J.D,, Poirier, G.G., Povirk, L.F., and Lees-Miller, S.P. (1997) Interaction of DNA-dependent protein kinase and poly(ADP-ribose) polymerase with radiation-induced DNA strand breaks, Radiat. Res. 148, 22-28.

38. D'Silva, I., Pelletier, J.D., Lagueux, J., D'Amours, D., Chaudhry, M.A., Weinfeld, M., Lees-Miller, S.P., and Poirier, G.G. (1999) Relative affinities of poly(ADP-ribose) polymerase and DNA-dependent protein kinase for DNA strand interruptions, Biochim. Biophys. Acta. 1430, 119-126.

39. Clancy, S. (2008) DNA Damage & Repair: Mechanisms for Maintaining DNA Integrity, Nature Education 1, 103

40. Rouleau, M., Patel, A., Hendzel, M.J., Kaufmann, S.H., and Poirier, G.G. (2010) PARP inhibition: PARP1 and beyond, Nat. Rev. Cancer 10, 293-301.

41. Wielckens, K., Schmidt, A., George, E., Bredehorst, R., and Hilz, H. (1982) DNA fragmentation and NAD depletion. Their relation to the turnover of endogenous mono(ADP-ribosyl) and poly(ADP-ribosyl) proteins, J. Biol. Chem. 257, 12872–12877.

42. Jacobson, E.L., Lange, R.A., and Jacobson, M.K. (1979) Pyridine nucleotide synthesis in 3T3 cells, J. Cell Physiol. 99, 417-425.

43. Bernofsky, C. (1980) Physiology aspects of pyridine nucleotide regulation in mammals, Mol. Cell. Biochem. 33, 135-143.

44. Goodwin, P.M., Lewis, P.J., Davies, M.I., Skidmore, C.J., and Shall, S. (1978) The effect of gamma radiation and neocarzinostatin on NAD and ATP levels in mouse leukaemia cells, Biochim. Biophys. Acta. 543, 576-582.

45. Skidmore, C.J., Davies, M.I., Goodwin, P.M., Halldorsson, H., Lewis, P.J., Shall, S., and Zia'ee, A.A. (1979) The involvement of poly(ADP-ribose) polymerase in the degradation of NAD caused by gamma-radiation and N-methyl-N-nitrosourea, Eur. J. Biochem. 101, 135-142.

46. Rouleau, M., Aubin, R.A., and Poirier, G.G. (2004) Poly(ADP-ribosyl)ated chromatin domains: access granted, J. Cell. Sci. 117, 815-825.

47. Oei, S.L., Keil, C., and Ziegler, M. (2005) Poly(ADP-ribosylation) and genomic stability, Biochem. Cell Biol. 83, 263-269.

48. Bürkle, A., and Virág, L. (2013) Poly(ADP-ribose): PARadigms and PARadoxes, Mol. Aspects Med. 34, 1046-1065.

49. Bai, P., and Cantó, C. (2012) The role of PARP-1 and PARP-2 enzymes in metabolic regulation and disease, Cell Metab. 16, 290-295

50. de Murcia, G., and Ménissier-de Murcia, J. (1994) Poly(ADP-ribose) polymerase: a molecular nick-sensor, Trends Biochem. Sci. 19, 172-176.

51. Gradwohl, G., Menissier de Murcia, J. M., Molinete, M., Simonin, F., Koken, M., Hoeijmakers, J. H., and de Murcia, G. (1990) The second zinc-finger domain of poly(ADP-ribose) polymerase determines specificity for single-stranded breaks in DNA, Proc. Natl. Acad. Sci. U.S.A. 87, 2990-2994.

52. Lonskaya, I., Potaman, V.N., Shlyakhtenko, L.S., Oussatcheva, E.A., Lyubchenko, Y,L,, and Soldatenkov, V.A. (2005) Regulation of poly(ADP-ribose) polymerase-1 by DNA structure-specific binding, J. Biol. Chem. 280, 17076-17083.

53. Altmeyer, M., Messner, S., Hassa, P.O., Fey, M, and Hottiger, M,O. (2009) Molecular mechanism of poly(ADP-ribosyl)ation by PARP1 and identification of lysine residues as ADP-ribose acceptor sites, Nucleic Acids Res. 37, 3723-3738.

54. Schreiber, V., Molinete, M,, Boeuf, H,, de Murcia, G,, and Ménissier-de Murcia, J. (1992) The human poly(ADP-ribose) polymerase nuclear localization signal is a bipartite element functionally separate from DNA binding and catalytic activity, EMBO J. 11, 3263-3269.

55. Kaufmann, S.H., Desnoyers, S., Ottaviano, Y., Davidson, N.E., and Poirier, G.G. Specific proteolytic cleavage of poly(ADP-ribose) polymerase: an early marker of chemotherapy-induced apoptosis, Cancer Res. 53, 3976-3985.

56. Tao, Z., Gao, P., Hoffman, D.W., and Liu, H.W. (2008) Domain C of human poly(ADP-ribose) polymerase-1 is important for enzyme activity and contains a novel zinc-ribbon motif, Biochemistry 47, 5804-5813.

57. Trucco, C., Flatter, E., Fribourg, S., de Murcia, G., and Ménissier-de Murcia J. (1996) Mutations in the amino-terminal domain of the human poly(ADP-ribose) polymerase that affect its catalytic activity but not its DNA binding capacity, FEBS Lett. 399, 313-316.

58. Langelier, M.F., Servent, K.M., Rogers, E.E., and Pascal, J.M. (2008) A third zinc-binding domain of human poly(ADP-ribose) polymerase-1 coordinates DNA-dependent enzyme activation, J. Biol. Chem., 283, 4105-4114.

59. Cherney, B.W., McBride, O.W., Chen, D.F., Alkhatib, H., Bhatia, K., Hensley, P., and Smulson, M.E. (1987) cDNA sequence, protein structure, and chromosomal location of the human gene for poly(ADP-ribose) polymerase, Proc. Natl. Acad. Sci. U.S.A. 84, 8370-8374.

60. Uchida, K., Morita, T., Sato,T., Ogura, T., Yamashita, R., Noguchi, S., Suzuki, H., Nyunoya, H., Miwa, M., and Sugimura, T. (1987) Nucleotide sequence of a full-length cDNA for human fibroblast poly(ADP-ribose) polymerase, Biochem. Biophys. Res. Commun. 148,617-622.

61. Kawaichi, M., Ueda, K., and Hayaishi, O. (1981) Multiple autopoly(ADP-ribosyl)ation of rat liver poly(ADP-ribose) synthetase. Mode of modification and properties of automodified synthetase, J. Biol. Chem. 256, 9483-9489.

62. Tao, Z., Gao, P., and Liu, H,W. (2009) Identification of the ADP-ribosylation sites in the PARP-1 automodification domain: analysis and implications, J. Am. Chem. Soc. 131, 14258-14260.

63. Chapman ,J.D., Gagné, J.P., Poirier, G.G., and Goodlett, D.R. (2013) Mapping PARP-1 auto-ADP-ribosylation sites by liquid chromatography-tandem mass spectrometry, J. Proteome Res. 12, 1868-1880.

64. Bork, P., Hofmann, K., Bucher, P., Neuwald, A. F., Altschul, S. F., and Koonin, E. V. (1997) A superfamily of conserved domains in DNA damage-responsive cell cycle checkpoint proteins, FASEB J. 11, 68-76.

65. Hassa, P.O., Haenni, S.S., Elser, M., and Hottiger, M.O. (2006) Nuclear ADP-ribosylation reactions in mammalian cells: where are we today and where are we going, Microbiol. Mol. Biol. Rev. 70, 789-829.

66. Huambachano, O., Herrera, F., Rancourt, A., and Satoh, M. S. (2011) Double-stranded DNA binding domain of poly(ADP-ribose) polymerase-1 and molecular insight into the regulation of its activity, J. Biol. Chem. 286, 7149-7160.

67. Ruf, A., Mennissier-de Murcia, J., de Murcia, G., and Schulz, G.E. (1996) Structure of the catalytic fragment of poly(AD-ribose) polymerase from chicken, Proc. Natl. Acad. Sci. U.S.A. 93, 7481-7485.

68. Simonin, F., Höfferer, L., Panzeter, P. L., Muller, S., de Murcia, G., and Althaus, F. R. (1993) The carboxyl-terminal domain of human poly(ADP-ribose) polymerase. Overproduction in Escherichia coli, large scale purification, and characterization, J. Biol. Chem. 268, 13454-13461.

69. Ruf, A., de Murcia, G., and Schulz, G. E. (1998) Inhibitor and NAD^+ binding to poly(ADP-ribose) polymerase as derived from crystal structures and homology modeling, Biochemistry 37, 3893-3900.

70. Hassler, M., and Ladurner, A.G. (2012) Towards a structural understanding of PARP1 activation and related signalling ADP-ribosyl-transferases, Curr. Opin. Struct. Biol. 22, 721-729.

71. Schreiber, V., Dantzer, F., Ame, J.C., and de Murcia, G. (2006) Poly(ADP-ribose): novel functions for an old molecule, Nat. Rev. Mol. Cell Biol. 7, 517-528.

72. Amé, J.C., Rolli, V., Schreiber, V., Niedergang, C., Apiou, F., Decker, P., Muller, S., Höger, T., Ménissier-de Murcia, J., and de Murcia, G. (1999) PARP-2, A novel mammalian DNA damage-dependent poly(ADP-ribose) polymerase, J. Biol. Chem. 274, 17860-17868.

73. Rippmann, J.F., Damm, K., and Schnapp, A. (2002) Functional characterization of the poly(ADP-ribose) polymerase activity of tankyrase 1, a potential regulator of telomere length, J. Mol. Biol. 323, 217-224.

74. Sbodio, J.I., Lodish, H.F., and Chi, N.W. (2002) Tankyrase-2 oligomerizes with tankyrase-1 and binds to both TRF1 (telomere-repeat-binding factor 1) and IRAP (insulin-responsive aminopeptidase), Biochem. J. 361, 451-459.

75. Hottiger, M.O., Hassa, P.O., Lüscher, B., Schüler, H., and Koch-Nolte, F. (2010) Toward a unified nomenclature for mammalian ADP-ribosyltransferases, Trends Biochem. Sci. 35, 208-219.

76. Marsischky, G.T., Wilson, B.A., and Collier, R.J. (1995) Role of glutamic acid 988 of human poly-ADP-ribose polymerase in polymer formation. Evidence for active site similarities to the ADP-ribosylating toxins, J. Biol. Chem. 270, 3247-3254.

77. Caldecott, K.W., Aoufouchi, S., Johnson, P., and Shall, S. (1996) XRCC1 polypeptide interacts with DNA polymerase beta and possibly poly (ADP-ribose) polymerase, and DNA ligase III is a novel molecular 'nick-sensor' in vitro, Nucleic Acids Res. 24, 4387-4394.

78. Petrucco, S. (2003) Sensing DNA damage by PARP-like fingers, Nucleic Acids Res. 31, 6689-6699.

79. Ikejima, M., Noguchi, S., Yamashita, R., Ogura, T., Sugimura, T., Gill, D.M., and Miwa, M. (1990) The zinc fingers of human poly(ADP-ribose) polymerase are differentially required for the recognition of DNA breaks and nicks and the consequent enzyme activation. Other structures recognize intact DNA, J. Biol. Chem. 265, 21907-21913.

80. Huambachano, O., Herrera, F., Rancourt, A., and Satoh, M.S. (2010) Double-stranded DNA binding domain of poly(ADP-ribose) polymerase-1 and molecular insight into the regulation of its activity, J. Biol. Chem. 286, 7149-7160.

81. Clark, N.J., Kramer, M., Muthurajan, U.M., and Luger K. (2012) Alternative modes of binding of poly(ADP-ribose) polymerase 1 to free DNA and nucleosomes, J. Biol. Chem. 287, 32430-32439.

82. D'Silva, I., Pelletier, J.D., Lagueux, J., D'Amours, D., Chaudhry, M.A., Weinfeld, M., Lees-Miller, S.P., and Poirier, G.G. (1999) Relative affinities of poly(ADP-ribose) polymerase and DNA-dependent protein kinase for DNA strand interruptions, Biochim. Biophys. Acta. 1430, 119-126.

83. Pion, E., Ullmann, G.M., Amé, J.C., Gérard, D., de Murcia, G., and Bombarda, E. (2005) DNA-induced dimerization of poly(ADP-ribose) polymerase-1 triggers its activation, Biochemistry 44, 14670-14681.

84. Sambrook, J., Fritsch, E. F., and Maniatis, T. (1989) Molecular Cloning, Vol. 2, Cold Spring Harbor Laboratory Press, Cold Spring Harbor, NY.

85. Zhang, C.X., Chang, P.V., and Lippard, S.J. (2004) Identification of nuclear proteins that interact with platinum-modified DNA by photoaffinity labeling, J. Am. Chem. Soc. 126, 6536-6537.

86. Langelier, M.F., Planck, J.L., Roy, S., and Pascal, J.M. (2011) Crystal structures of poly(ADP-ribose) polymerase-1 (PARP-1) zinc fingers bound to DNA: structural and functional insights into DNA-dependent PARP-1 activity, J. Biol. Chem. 286, 10690-106701.

87. Ali, A.A., Timinszky, G., Arribas-Bosacoma, R., Kozlowski, M., Hassa, P.O., Hassler, M., Ladurner, A.G., Pearl, L.H., and Oliver, A.W. (2012) The zinc-finger domains of PARP1 cooperate to recognize DNA strand breaks, Nat. Struct. Mol. Biol. 19, 685-692.

88. Langelier, M.F., Planck, J.L., Roy, S., and Pascal, J.M. (2012) Structural basis for DNA damage-dependent poly(ADP-ribosyl)ation by human PARP-1, Science 336, 728-732.

89. Langelier, M.F., and Pascal, J.M. (2013) PARP-1 mechanism for coupling DNA damage detection to poly(ADP-ribose) synthesis, Curr. Opin. Struct. Biol. 23, 134-143.

90. Loseva, O., Jemth, A.S., Bryant, H.E., Schüler, H., Lehtiö, L., Karlberg, T., and Helleday, T. (2010) PARP-3 is a mono-ADP-ribosylase that activates PARP-1 in the absence of DNA, J. Biol. Chem. 285, 8054-8060.

91. Cohen-Armon, M., Visochek, L., Rozensal, D., Kalal, A., Geistrikh, I., Klein, R., Bendetz-Nezer, S., Yao, Z., and Seger, R. (2007) DNA-independent PARP-1 activation by phosphorylated ERK2 increases Elk1 activity: a link to histone acetylation, Mol. Cell 25, 297-308.

92. Kauppinen, T.M., Chan, W.Y., Suh, S.W., Wiggins, A.K., Huang, E.J., Swanson, R.A. (2006) Direct phosphorylation and regulation of poly(ADP-ribose) polymerase-1 by extracellular signal-regulated kinases 1/2, Proc. Natl. Acad. Sci. U.S.A 103, 7136-7141.

93. Alvarez-Gonzalez, R., Pacheco-Rodriguez, G., and Mendoza-Alvarez, H. (1994) Enzymology of ADP-ribose polymer synthesis, Mol. Cell. Biochem. 138, 33-37.

94. Bellocchi, D., Costantino, G., Pellicciari, R., Re, N., Marrone, A., and Coletti, C. (2006) Poly(ADP-ribose)-polymerase-catalyzed hydrolysis of NAD+: QM/MM simulation of the enzyme reaction, ChemMedChem 1, 533-539.

95. Ruf, A., Rolli,V., de Murcia, G., and Schulz, G.E. (1998) The mechanism of the elongation and branching reaction of poly(ADP-ribose) polymerase as derived from crystal structures and mutagenesis, J. Mol. Biol. 278, 57-65.

96. Rolli, V., O'Farrell, M., Ménissier-de Murcia, J., and de Murcia, G. (1997) Random mutagenesis of the poly(ADP-ribose) polymerase catalytic domain

reveals amino acids involved in polymer branching, Biochemistry 36, 12147-12154.

97. Mendoza-Alvarez, H., and Alvarez-Gonzalez, R. (1993) Poly(ADP-ribose) polymerase is a catalytic dimer and the automodification reaction is intermolecular, J. Biol. Chem. 268, 22575-22580.

98. Ueda, K., Kawaichi, M., Okayama, H., and Hayaishi, O. (1979) Poly(ADP-ribosy)ation of nuclear proteins. Enzymatic elongation of chemically synthesized ADP-ribose-histone adducts, J. Biol. Chem. 254, 679-687.

99. Taniguchi, T. (1987) Reaction mechanism for automodification of poly(ADP-ribose) synthetase, Biochem. Biophys. Res. Commun. 147, 1008-1012.

100. Ikejima, M., Marsischky, G., and Gill, D.M. (1987) Direction of elongation of poly(ADP-ribose) chains. Addition of residues at the polymerase-proximal terminus, J. Biol. Chem. 262, 17641-17650.

101. Alvarez-Gonzalez, R. (1988) 3'-Deoxy-NAD^+ as a substrate for poly(ADP-ribose)polymerase and the reaction mechanism of poly(ADP-ribose) elongation, J. Biol. Chem. 263, 17690-17696.

102. Naegeli, H., and Althaus, F.R. (1991) Regulation of poly(ADP-ribose) polymerase. Histone-specific adaptations of reaction products, J. Biol. Chem. 266, 10596-105601.

103. Panzeter, P.L., Realini, C.A., and Althaus, F.R. (1992) Noncovalent interactions of poly(adenosine diphosphate ribose) with histones, Biochemistry 31, 1379-1385.

104. Ménard, L., Thibault, L., and Poirier, G.G. (1990) Reconstitution of an in vitro poly(ADP-ribose) turnover system, Biochim. Biophys. Acta. 1049, 45-58.

105. Zahradka, P., and Ebisuzaki, K. (1982) A shuttle mechanism for DNA-protein interactions. The regulation of poly(ADP-ribose) polymerase, Eur. J. Biochem. 127, 579-585.

Chapter 2. DNA Recognition of Human PARP-1

Part I: Investigation of Binding Stoichiometry and Characterization of the Secondary DNA Interaction Site

2.1. INTRODUCTION

As discussed in Section 1.2, human PARP-1 is a multi-modular protein which exerts its biological function through protein-protein and protein-DNA interactions. With regards to PARP-1 automodification, it was believed that the activation process requires dimer formation based on kinetic studies carried out by Mendoza-Alvarez et al. (1). The proposed dimerization process allows two PARP-1 protein molecules to modify each other intermolecularly. Therefore, it is of interest to understand the oligomeric states of human PARP-1. Furthermore, it has been well-established that interaction with damaged DNA is one of the prerequisites for PARP-1 activation (2). This leads to the question of whether this proposed dimerization process requires the presence of activating molecules such as DNA.

The requirement of dimer formation for PARP-1 activity still remains controversial despite more than 35 years of research efforts. An early study of native PARP-1 purified from Ehrlich ascites tumor cells indicated a molecular weight greater than 500 kDa suggesting the formation of oligomers (3). Later on, PARP-1 purified from bovine thymus was shown to be a monomer in solution as demonstrated by gel filtration chromatography and analytical ultracentrifugation (4). In the 1990s, studies done by Prof. Ernest Kun's research group suggested that PARP-1 purified from calf thymus existed in a monomer-dimer equilibrium using gel filtration, cross-linking and native gel electrophoretic analysis (5,6). They also found that the DNA-binding domain and the automodification domain were important for the self-association process (5-6). In 2004,

Mendoza-Alvarez et al. heterologously expressed the catalytic domain of human PARP-1 and used ultrafiltration studies to demonstrate the ability the catalytic domain to self-associate in the absence of DNA (7). While the studies discussed here suggested that different functional domains are involved in the self-association process, it should be noted that all of these functional domains were observed using NMR structural experiments to be present in solution as monomers (8).

To further test the hypothesis that PARP-1 undergoes self-association, sedimentation velocity (SV) experiments were carried using human full-length PARP-1 and its DNA-binding domain AB. SV data analyses demonstrated no self-association under the tested conditions and thus suggest that both domain AB and full-length PARP-1 remain monomeric in solution in the absence of DNA.

Whether the presence of DNA would induce PARP-1 dimerization is another interesting hypothesis that remains to be fully tested. Known as a "nick sensor," PARP-1 has been shown to produce a symmetric pattern of protection at sites of nicked DNA during DNAse footprinting experiments (9). Intrinsic tryptophan fluorescence studies carried out by Pion et al. have indicated that the PARP-1 DNA-binding domain AB interacts with DNA at 5'-recessed ends in a dimeric form, whereas in the case of 3'-recessed ends and double stranded DNA, domain AB forms a 1:1 protein-DNA complex (10). In agreement with the biochemical studies of blunt end DNA, crystal structures reported by Langelier et al. showed that the individual zinc fingers I and II interact with the blunt end region of double stranded DNA as a monomer, as shown in Chapter 1, Figure 1-7 (11). In contrast, when two zinc fingers are present in a single protein and are co-crystallized with a DNA construct with a single base 5'-overhang, then dimer formation could be observed as shown in Chapter 1, Figure 1-8 (12). The cause of the observed differences between the biochemical and crystallographic data is still unclear.

To further investigate the putative dimerization process of PARP-1, stoichiometric analyses of PARP-1 and domain AB in the presence of DNA were conducted using sedimentation velocity techniques. When a 66bp double stranded DNA (66DS) was used, both 1:1 and 2:1 protein-DNA complexes were observed in the case of PARP-1. Both protein-DNA complexes were also observed when a 66bp DNA construct with a single base gap (66G1) was used. Interestingly, in the case of domain AB, higher oligomeric states of 3:1 and 4:1 protein-DNA complexes were observed with the 66DS and 66G1 DNA constructs, respectively. The results presented in this section may provide additional information for the DNA recognition mechanism of PARP-1.

While PARP-1 is a relatively large protein composed of six functional domains, data obtained from SV experiments indicated that PARP-1 alone has an elongated conformation in solution. Questions arise as to how DNA binding at the N-terminal domain leads to activation of the catalytic domain F at the C-terminus. It is possible that upon DNA binding, the PARP-1 structure may undergo conformational change and leads to activation. Consistent with this notion, based on the frictional ratio obtained from SV experiments, PARP-1/DNA complexes have more compact shapes when compared with PARP-1 alone in solution. Since there is no crystal structure of full-length PARP-1 complexed with DNA currently available, our previous group member Dr. Steven Mansoorabadi was interested in understanding changes in PARP-1 conformation during DNA-dependent activation. Utilizing small-angle X-ray scattering and molecular dynamics simulations, a structural model of PARP-1 complexed with 8-mer DNA was constructed (13). In addition to the N-terminal DNA-binding zinc fingers, another DNA interaction site within the WGR domain was proposed. In the present study, the DNA binding ability of the PARP-1 C-terminal domains (i.e., DEF) was investigated, and the involvement of the WGR domain in DNA binding was confirmed using a deletion mutant

DEFΔ. Compared with domain ABC, DEF demonstrated a weaker DNA binding ability, and its influence in DNA binding was less substantial when it was investigated in the context of full-length PARP-1. However, deletion of the proposed DNA-contact region within the WGR domain caused a dramatic drop in PARP-1 activity, indicating an important role in the DNA-dependent activation of PARP-1 (13).

2.2. Materials and Methods

2.2.1. Cloning, expression and purification of human PARP-1 protein constructs AB, ABC and DEF

DNAs encoding amino acid residues 1–232 [domains A and B (AB)], 1–373 [domains A-C (ABC)] and 374–1014 [domains D-F (DEF)] of the human PARP-1 protein were each cloned into the MalE-pET vector generated in house by Dr. Peng Gao at the NdeI and XhoI restriction sites (14). Construction of MalE-pET was accomplished by modifying a pET-24b(+) vector (Novagen) so that the cloned protein constructs would be expressed as a fusion proteins with a decahistidine tagged maltose-binding protein (MBP) at the N-terminus. A TEV protease cleavage site was also engineered into the constructs to allow removal of the MBP.

The MalE-pET vectors with the cloned protein constructs were used to transform Escherichia coli BL21 Codon-Plus (DE3)-RP competent cells (Stratagene). Cells were grown at 37 °C in 6 L Luria-Bertani (LB) broth containing 50 μg/mL of kanamycin and 35 μg/mL of chloramphenicol. IPTG was added to 0.2 mM when the OD_{600} reached 0.6, and the culture was grown at 18 °C for another 20 h. Cells were harvested by centrifugation at 4500 x g for 15 min, and stored at –80 °C until purification.

Cells were thawed and re-suspended in lysis buffer containing 20 mM HEPES, 300 mM NaCl, 10 mM imidazole, 1 mM β-mercaptoethanol and 10% glycerol at pH 7.5, and ruptured by sonication. Cell debris was then removed by centrifugation at 20000 x g for 30 min, and the resulting supernatant was incubated at 4 °C for 1 hr with 10 mL of Ni-NTA agarose resin (Qiagen), which had been pre-equilibrated with the lysis buffer. The mixture was then loaded onto a column, drained and washed with the wash buffer containing 20 mM imidazole and 1 M NaCl. The MBP fusion protein was eluted with buffer containing 250 mM imidazole and 300 mM NaCl. The fractions containing eluted protein were pooled and dialyzed against the lysis buffer. After 2 h of dialysis, the dialyzed MBP-protein was incubated with 5% (w/w) His_6-tagged TEV protease for 24 hr at 4 °C to cleave the His_{10}-MBP tag. The protein mixture was then slowly passed through a column containing 10 mL of Ni-NTA agarose resin. The protein recovered in the flow through was concentrated using an Amicon ultra-15 centrifugal filter unit with a 10000 Da cut off (Millipore). Due to the TEV protease digestion site, the cleaved protein constructs contained two additional amino acids residues, GH, at the N-terminus. Further purification was achieved by size-exclusion chromatography using a Superdex 200 column and an AKTA FPLC system (GE Healthcare). The elution buffer included 10 mM sodium phosphate, 100 mM NaCl and 10% glycerol at pH 7.5. Protein was flash-frozen with liquid nitrogen and stored at –80°C.

2.2.2. Cloning, expression and purification of human full-length PARP-1 using baculovirus expression system

Because cDNA for full-length PARP-1 contains an NcoI restriction site, it can not be directly cloned into the donor vector. Instead, an intermediate pFastbac™HT B/MBP-Tev vector was first generated. To do so, pFastbac™HT B vector (Invitrogen) was linearized by double digestion with NcoI and XhoI restriction enzymes, and the same was

done with recombinant MBP-TEV-ABC/pET vector. Both the linearized pFastbac™HT B vector and the DNA fragment encoding MBP-TEV-ABC were purified using 0.8% agarose gel and ligated using T4 ligase. The ligated recombinant DNA was used to transform Escherichia coli DH5α competent cells (Novagen), and the resulting pFastbac™HT B/MBP-Tev-ABC plasmid was amplified and recovered from the bacteria. To generate the pFastbac™HT B/MBP-Tev vector, the ABC fragment was removed by digestion using NdeI and XhoI restriction enzymes followed by treatment with CIP (calf intestinal alkaline phosphatase). The resulting pFastbac™HT B/MBP-Tev fragment was agarose gel purified and used for subsequent steps.

To generate pFastbac™HT B/MBP-Tev-PARP recombinant plasmid, the recombinant PARP-1/pET28(b+) plasmid was digested with NdeI and XhoI restriction enzymes. The DNA fragment encoding the PARP-1 gene was agarose-gel purified and ligated with the linearized pFastbac™HT B/MBP-Tev fragment using T4 ligase. The ligated product was then transferred DH5α Escherichia coli competent cells for plasmid amplification and purification.

To generate the recombinant bacmid, which is the baculovirus shuttle vector for the MBP-Tev-PARP-1 construct, the pFastbac™HT B/MBP-Tev-PARP recombinant plasmid was used to transform the MAX Efficiency® DH10Bac™ Escherichia coli competent cells according to instructions in the manual for the Bac-to-Bac® Baculovirus Expression System (Invitrogen). Transformant was plated on LB agar containing with 50 μg/mL kanamycin, 7 μg/mL gentamicin, 10 μg/mL tetracycline, 100 μg/mL Bluo-gal, and 40 μg/mL IPTG for blue/white colony selection. The plates were incubated at 37 °C for 48 h. Following the incubation, white colonies were selected, re-streaked on a fresh LB plate containing the same additives as before, and incubated at 37 °C overnight to confirm the white colony phenotypes. A single white colony was then selected and used

to inoculate a liquid culture containing 50 μg/mL kanamycin, 7 μg/mL gentamicin and 10 μg/mL tetracycline. The culture was subsequently incubated at 37 °C overnight with shaking at 250 rpm. The resulting recombinant bacmid DNA was isolated using the Purelink™ HiPure Plasmid DNA Miniprep Kit (Invitrogen) and analyzed using PCR based on the protocol from the manufacturer.

Once the inserted MBP-PARP gene was confirmed, the bacmid DNA was used to transfect Sf21 insect cells using Cellfectin® II Reagent (Invitrogen). When the cells showed signs for the late stage of infection roughly 72 h after transfection, the medium was collected by centrifugation at 500 x g for 5 min. The resulting P1 viral stock was used to infect Sf21 cells grown in suspension to generate P2 viral stock.

To express the MBP-PARP protein, P2 viral stock was used to infect Sf21 insect cells grown in serum-free SF-900 II SFM medium at 27 °C with shaking at 220 rpm. At 96 h post infection, the infected insect cells were harvested by centrifugation at 4000 x g for 10 min. Cells were re-suspended and washed with PBS buffer twice. The harvested cells were stored at –80 °C until purification.

To purify PARP-1 protein, the harvested cells were thawed and re-suspended using lysis buffer containing 20 mM HEPES, 1 M NaCl, 10 mM imidazole, 1% Triton X100, 1 mM β-mercaptoethanol and 10% glycerol at pH 7.5. The cells were lyzed by sonication and the cell debris was removed by centrifugation at 20000 x g for 30 min. The subsequent purification steps for PARP-1 were similar to those previously described for the domain AB construct.

2.2.3. Preparation of DNA ligands for sedimentation velocity experiments

Single-stranded DNA primers were purchased from Integrated DNA Technologies, Inc. (IDT). Sequences of the single stranded DNA primers are listed in

Table 2-1. To generate double stranded 66-mer DNA duplex as well as the double stranded 66-mer DNA duplex with a base gap at the center (66G1), the corresponding single stranded primers were mixed, and each primer was diluted to 20 μM final concentration in annealing buffer at pH 7.5 with 100 mM sodium phosphate and 100 mM NaCl. The samples were heated to 95 °C for 5 min, and cooled slowly to 4 °C. DNA samples were stored at –20 °C until further usage.

Table 2-1. DNA primers used for sedimentation velocity experiments.

DNA duplex	DNA primers used	Primer sequence
66DS	66bpF	5'-CCAGGACCAGGGCGCAGATCACCTTGTTCTCCAGCCCACAGCAGGGTCCACAGCAGCCTTGCCCTT-3'
	66bpR	5'-AAGGGCAAGGCTGCTGTGGACCCTGCTGTGGGCTGGAGAACAAGGTGATCTGCGCCCTGGTCCTGG-3'
66G1	66bpR	5'-AAGGGCAAGGCTGCTGTGGACCCTGCTGTGGGCTGGAGAACAAGGTGATCTGCGCCCTGGTCCTGG-3'
	33bp-2	5'-GCCCACAGCAGGGTCCACAGCAGCCTTGCCCTT-3'
	32bp	5'-CCAGGACCAGGGCGCAGATCACCTTGTTCTCC-3'

2.2.4. Sedimentation velocity experiments

Sedimentation velocity (SV) experiments were carried out using a Beckman XL-A ultracentrifuge at the Core Facility of the Institute for Cellular and Molecular Biology at The University of Texas at Austin. To study the oligomerization state of PARP-1 proteins, samples of domain AB and full-length PARP-1 were dialyzed into 10 mM sodium phosphate buffer at pH 7.5 with 100 mM NaCl before data collection. Samples with 450 μL of protein analyte at different concentrations were prepared based on absorbance at 280 nm. Optimal data signals correlated with the absorbance range of 0.2 to 1.5 at 280 nm. To ensure protein was stable throughout the experiments, as judged by checking possible protein precipitation at the end of the experimental runs, data collection for domain AB was performed at 20 °C and at 4°C for PARP-1. SV

experiments were run at 42000 rpm using standard 2-channel centerpieces in an AN-60Ti rotor. Data were collected in absorbance mode with scanning at 280 nm.

For protein-DNA interaction studies, protein samples were freshly dialyzed into 100 mM sodium phosphate buffer with 300 mM NaCl at pH 7.5. DNA duplex at 1 μM was mixed with various concentrations of protein (0, 1, 2, 5 and 10 μM) in the presence of 1 mM TCEP. Samples were run under the same instrumental settings as described above. Data was collected in absorbance mode with scanning at 230, 250 or 280 nm. Criteria of selecting a given absorbance wavelength were based on maximizing the signal to noise ratio for a given experiment and maintaining the absorbance signal within the range of 0.2 to 1.5.

2.2.5. Data analyses of sedimentation velocity experiments

The sedimentation profile of samples containing only protein solutes was analyzed using c(s) analysis provided in the Sedfit program (15) to obtain sedimentation coefficients, s, for each protein species. The basic c(s) analysis requires estimation of a frictional ratio for each given data set. This makes it less ideal when a given data set corresponds to analytes with different frictional ratios due to their different shapes. When globular protein species and a linear DNA construct are both present in the solution, each individual sedimenting species would exhibit a different frictional ratio. Therefore, for protein-DNA interaction studies, the Ultrascan II program (version 9.9) was implemented for data analyses. Hydrodynamic correction for buffer conditions and the partial specific volume, $\bar{\upsilon}$, of proteins were determined using Ultrascan II. The $\bar{\upsilon}$ value of both DNA duplex was estimated to be 0.52 $mL \cdot g^{-1}$. The data was first analyzed using the enhanced van Holde-Weischet (vHW) method to characterize the distribution of sedimentation coefficients represented by a given data set (16). The observed meniscus position from

the data as well as time- and radially-invariant noise components were first extracted from a given SV data set by an initial round of two-dimensional spectrum analysis (17). The noise corrected data was then fitted again through a second 2DSA analysis. The 2DSA results were then further refined using genetic algorithm (GA) optimization. A total of 50 Monte Carlo iterations were used in the 2DSA and GA analyses to obtain 95% confidence intervals for each of the fitted parameters (17).

2.2.6. Cloning, expression and purification of the DEFΔ and PARP-1Δ mutants

To investigate the newly identified DNA binding site within domain DEF, a DEFΔ mutant which lacks amino acid residues 626–645, was constructed using the Quikchange Site-Directed Mutagenesis Kit (Stratagene). To generate the DEFΔ/MalE-pET construct by mutational PCR, 5'-CACTTCATGAAATTATATGAAGAAAA-AACCGGGAACGCTGGCCAGGATGAAGAG-3' and 5'-CTCTTCATCCTGGCCA-GCGTTCCCGGTTTTTTCTTCATATAATTTCATGAAGTG-3' were used as the primers and the DEF/MalE-pET plasmid as the template. To generate the PARP-1Δ mutant which also lacks amino acid residues 626–645, both DEFΔ/MalE-pET and PARP-1/MalE-pET plasmids were digested with PstI and XhoI restriction enzymes. The small DNA fragment was purified from the DEFΔ/MalE-pET vector digestion, and the larger DNA fragment was isolated from the digested PARP-1/MalE-pET plasmid by 0.8% agarose gel electrophoresis. The two purified DNA fragments were ligated together using T4-ligase (NEB) to generate the PARP-1Δ/MalE-pET construct. The mutation region was confirmed by sequencing carried out by the DNA Sequencing Core Facility at The University of Texas at Austin.

Expression of DEF, DEFΔ, PARP-1 and PARP-1Δ mutants was accomplished using Escherichia coli BL21 Codon-Plus (DE3)-RP competent cells (Stratagene).

Transformation, expression and purification processes were performed in manner similar to those described in Section 2.2.1.

2.2.7. Electrophoretic mobility shift assay (EMSA)

To compare the DNA binding properties of ABC, DEF and PARP-1, as well as the corresponding deletion mutants, single stranded 8-mer DNA (5'-GGAATTCC-3'), 22-mer DNA (5'-GGCTAGCTGGCCGCGACCTCGC-3') and 44-mer DNA (5'-CGGTCGA-TCGTAAGATCCACCGGCGCTGGAGCTTGCTCCAGCGC-3') were purchased from IDT. The corresponding 8-mer and 22-mer DNA duplexes, as well as 44-mer nicked dumbbell DNA was prepared based on a similar protocol as described in Section 2.2.3 using an annealing buffer containing 100 mM NaCl and 10 mM Tris-HCl at pH 7.5. To set up the assay, 150 pmol of DNA duplex was incubated with the purified protein constructs at various protein:DNA ratios in a total volume of 8 μL. The samples were then equilibrated on ice for 30 min and run on a 1.5% agarose gel. Gel visualization was done by ethidium bromide staining and UV transillumination. Images were processed using ImageJ software (NIH).

2.2.8. Automodification activity assay

To compare the automodification activities of wild type PARP-1 and PARP-1Δ mutant, a reaction mixture containing 1 μM protein, 1 μM 8-mer DNA, 5 mM NAD^+, 50 mM NaCl, 7.5 mM $MgCl_2$, in 20 mM Tris buffer at pH 7.5 (total volume: 6 uL) were prepared and incubated at room temperature. For all samples, NAD^+ was added last to initiate the reaction. The reaction was quenched at different time points using 2X SDS-PAGE loading buffer including 50 mM EDTA. As a negative control, 8-mer DNA was omitted, and the reaction mixture was quenched after 5 min of incubation. After

quenching, the automodified protein samples were analyzed by SDS-PAGE electrophoresis and visualized by staining with Coomassie Brilliant Blue.

2.3. RESULTS

2.3.1. Sedimentation velocity experiments of full-length PARP-1 and the DNA binding domain AB

To study the oligomeric state of PARP-1 and its DNA binding domain AB under native conditions, PARP-1 and domain AB were first over-expressed and purified as determined by SDS-PAGE (Figure 2-1). The oligomeric states and the potential self-association of PARP-1 and domain AB in solution under native condition were studied through sedimentation velocity (SV) experiments using different protein concentrations.

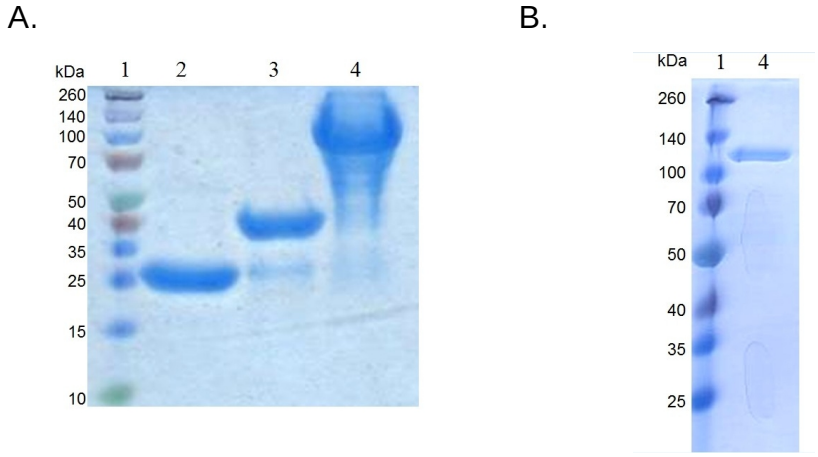

Figure 2-1. A. SDS-PAGE gel showing typical protein purities of domain AB (lane 2), ABC (lane 3) and PARP-1 (lane 4) after purification. B. SDS-PAGE gel showing protein purity of PARP-1 after Superdex 200 size-exclusion chromatography.

In an SV experiment, where rotor speeds of 40000 rpm or greater are employed, the analytes in solution will sediment toward the bottom of the centrifugation cell over the experimental time course (18). When mixtures of different biomolecules are used in

the experiments, the different components will sediment at different rates that depend both on their sizes and shapes.

The sedimentation process is governed by three forces: the gravitational force, the buoyancy, and the hydrodynamic friction. At constant velocity where the sum of all forces are equal to zero, the Svedberg equation can be derived as shown in equation (3), and the definitions of each parameter are shown in Figure 2-2 (18). Here, the sedimentation coefficient is expressed as $s = v/\omega^2$, where v is the absolute migration velocity and ω is the rotor angular velocity. The sedimentation coefficient is a molecular constant measured in units of Svedberg, S, with one Svedberg equal to 10^{-13} s. The frictional force component of the sedimentation process is expressed as $F_f = s(kT/D)\omega^2 r$, with k as the Boltzmann constant, T as the absolute temperature, D as the diffusion constant and r as the distance from the center of rotation. F_f is dependent on the absolute migration velocity as well as the translational frictional coefficient f, with f = kT/D. In practice, the translational frictional properties of a given molecule are expressed as the ratio of the frictional coefficient for that molecule versus that of a smooth sphere with the same molecular mass and density. This ratio denoted as the frictional ratio f/f_0. The value of f/f_0 provides low-resolution information on the shape and the Stoke's radii for a given molecule or complex (18).

$$\frac{s}{D} = \frac{M\left(1-\bar{\upsilon}\rho\right)}{RT} \qquad (3)$$

s: sedimentation coefficient
D: diffusion coefficient
M: protein molar mass
$\bar{\upsilon}$: effective protein partial-specific volume
ρ: solvent density

Figure 2-2. The Svedberg equation and definitions of parameters.

SV experiments generate data showing a change of concentration versus position over time. Typical raw data for a sedimentation profile of full-length PARP-1 as well as domain AB from SV experiments are shown in Figure 2-3. The concentration profiles shown here were obtained in absorbance mode for a given wavelength, and an important feature observed is the moving sedimentation boundary represented by the sigmoid-shape of the data. As shown in Figure 2-3, each data scan represents a moving boundary at a given time. A sedimentation boundary was formed between the region where solute was depleted and the region where solute was evenly distributed. The displacement of the midpoint positions of boundaries with time determines the sedimentation coefficient (s), and the change of the broadening of the curves over time is governed by the diffusion coefficient D (18). Non-interacting molecules with different sizes and shapes in solution will generate individual time-dependent concentration curves (i.e., sedimentation profile) during ultracentrifugation. Thus, SV experiments allow characterization of these molecules in terms of their sedimentation and diffusion coefficients which relate information regarding molecular size and shape.

A. Full-length PARP-1 B. Domain AB

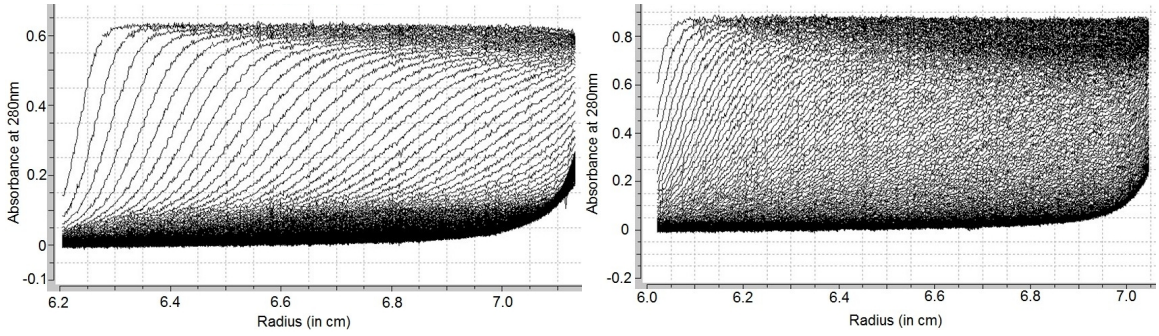

Figure 2-3. A. Typical sedimentation velocity raw data for full-length PARP-1. B. Typical sedimentation velocity raw data for DNA-binding domain AB.

To see if any self-association of PARP-1 constructs takes place, sedimentation profiles with increasing protein concentrations were generated from a series of SV experiments. The experimental design is based on the theoretical work of Tiselius characterizing how interacting solutes behave in a moving transport system such as sedimentation velocity experiments (19). When both protein monomer and dimer are present in solution, and they are in rapid equilibrium when compared with the rate of sedimentation, the sedimentation boundaries of protein monomers can not be resolved from those of protein dimers; instead, weight-average sedimentation boundaries of the two species would be observed (19). In the case of SV experiments, this would result in a concentration-dependent increase in the observed weight-average s value, s_w, for a given protein if self-association process occurs (15). Therefore, the changes in s_w values observed with increasing protein concentrations for domain AB and PARP-1 can help to determine whether self-association happens.

The weight-average sedimentation coefficient s_w was extracted from each data set using differential sedimentation coefficient distribution (i.e., c(s)) analysis by the Sedfit program (15). This analysis assumes that the change in the sedimentation boundary for a single species over time during an SV experiment using a sector-shaped ultracentrifugal cell can be modeled by the Lamm equation (4). The Lamm equation for a single solute is shown in Figure 2-4 (20), where the s and D values can be obtained directly by fitting the experimental data through solving the Lamm equation, and the molar mass M can be calculated indirectly according to the Sverberg equation using the experimental s and D values (3).

$$\frac{\partial c}{\partial t} = -\frac{1}{r}\left(\frac{\partial}{\partial r}\left(s\omega^2 r^2 c - Dr\frac{\partial c}{\partial r}\right)\right) \quad (4)$$

c: concentration function
t: time
r: radius
ω: angular velocity

Figure 2-4. The Lamm equation (4) and definitions of parameters.

When multiple non-interacting solutes are present, c(s) analysis fits the SV data containing superimposed sedimentation boundaries arising from all individual species with different s_w values (15). In addition, the c(s) analysis estimates diffusion coefficients of the individual species by assuming that all species have the same frictional ratios f/f_0, which is input by the user as a fixed parameter. The experimental data was then modeled with Lamm equations with different s values. After 100 iterations of data modeling, the c(s) analyses provides the weight-average s (s_w) and the weight-average f/f_0 for the fitted solutes. The weight-average values resulted from data fitting of the non-interacting solute alone, or between the monomeric and dimeric forms if rapid self-association occurs when compared with the experimental time scale.

Details of the fitted SV parameters are reported in Table 2-2 for full-length PARP-1 and Table 2-3 for domain AB. The values of s_w were plotted against the tested concentrations for PARP-1 and domain AB. As displayed in Figure 2-5, none of tested protein constructs showed an increasing trend among the s_w values as the loading concentration increased. This observation indicated that both PARP-1 and domain AB were present in monomeric form in solution and no self-association had occurred under the tested conditions.

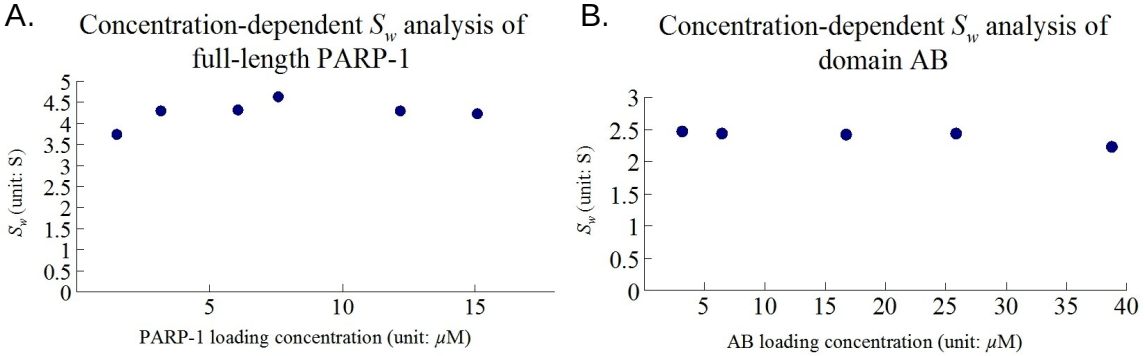

Figure 2-5. Analyses of the concentration dependency of the observed weight-average sedimentation coefficients s_w for full-length PARP-1 (A) and domain AB (B).

Table 2-2. Fitted results from full-length PARP-1 sedimentation velocity experiments

Loading Concentration (μM)	Sedimentation coefficient ($S_{20,w}$)	Weight-average sedimentation coefficient (S_w)	Frictional Ratio (f/f_o)	Experimental MW (kDa)	Oligomerization State
1.51	5.62	3.73	1.43	99.0	monomer
3.2	4.92	4.29	1.55	103.0	monomer
6.1	4.87	4.32	1.56	102.4	monomer
7.6	4.85	4.61	1.64	110.1	monomer
12.2	4.84	4.28	1.58	103.9	monomer
15.1	4.80	4.22	1.55	99.5	monomer
notes: a. Calculated MW for full length PARP-1: 113.3 kDa b. $S_{20,w}$ is an observed value that is standardized at 20 °C in water					

Table 2-3. Fitted results from domain AB sedimentation velocity experiments

Loading Concentration (μM)	Sedimentation coefficient ($S_{20,w}$)	Weight average sedimentation coefficient (S_w)	Frictional Ratio (f/f_o)	Experimental MW (kDa)	Oligomerization State
3.23	2.25	2.46	1.426	26.5	monomer
6.5	2.27	2.44	1.306	23.4	monomer
16.8	2.25	2.42	1.419	26.3	monomer
25.9	2.24	2.42	1.424	26.3	monomer
38.8	2.22	2.23	1.463	26.9	monomer
note: Calculated MW for AB: 26.2 kDa					

2.3.2. Sedimentation velocity studies of PARP-1 constructs in the presence of DNA

2.3.2.1. Enhanced van Holde-Weischet (vHW) analysis

As mentioned in Section 2.3.1, c(s) analysis requires a single f/f_o frictional ratio value for a given data set for diffusion estimation used as an input parameter and assumes that all solutes within a given data set have similar f/f_o values. This is generally true for

most proteins (21). Therefore, c(s) analysis is good for studying homogenous samples or an interacting system where the sedimenting species have similar f/f_0 values. In cases where both proteins and long DNA duplexes are present together in solution, c(s) analysis becomes less suitable, because the free protein species, the DNA molecule and the protein/DNA complex may exhibit different morphologies in solution. This results in multiple frictional ratios characterizing the same system.

Instead, the Ultrascan II program (version 9.9) was utilized to study binding stoichiometry of PARP-1 and domain AB toward different DNA lesions. A two-dimensional spectrum analysis (2DSA) provided by the program allows for heterogeneity in both s and f/f_0 parameters in a given data set. This is done by performing a two dimensional search over a certain range of s and f/f_0 that are defined by the user (17).

Data was first analyzed using the enhanced van Holde-Weischet (vHW) method in Ultrascan II in order to check for heterogeneity and get an rough estimation about s and f/f_0 ranges within a given protein-DNA sample. In this analysis, no prior knowledge of the interaction model was assumed, and the effect of diffusion was considered negligible. This is based on the fact that displacement of the sedimentation boundary due to sedimentation is linear with time, while boundary displacement due to diffusion proceeds proportionally to the square root of time (16). Therefore, as time approaches to infinity, the sedimentation boundary change due to sedimentation outweighs the change due to diffusion. (16). In the vHW analysis, the reported $s_{w,20}$ values are resulted from analyzing a specific portions of boundary fractions across different data scans, and then being extrapolated to infinite time; therefore, the effect due diffusion is minimal in the reported $s_{w,20}$ values.

Here, sedimentation boundaries are divided into multiple boundary fractions by horizontally slicing the SV raw data, as shown in Figure 2-6A; and the total boundary

fractions are plotted in percentages in the Y-axis in the final reported data, as shown in Figure 2-7. For a given boundary fraction i, the change of the intercepting radial position r_i at time t_j is compared with the reference point (i.e., solvent meniscus at radial position r_a at the beginning of the experiment (t_o), and the apparent $s^*_{i,j}$ was calculated using equations shown in Figure 2-6B. When all the calculated $s^*_{i,j}$ values are plotted against $(t_j)^{\wedge -0.5}$, the diffusion corrected $s_{w,20}$ value for a given boundary fraction i can be extrapolated as shown in Figure 2-6C. The diffusion corrected $s_{w,20}$ values for each individual boundary fractions as extrapolated in Figure 2-6C are then plotted as the boundary fraction percentage versus $s_{w,20}$ to give an integral distribution of sedimentation coefficient G(s) plot (16).

The resulting integral distribution of sedimentation coefficient G(s) plots from the analyses by the enhanced vHW method are shown in Figure 2-7. Here, the overall shape of the given G(s) plot provides information on the homogeneity and reversibility of the system (22). A nearly vertical G(s) plot indicates a homogenous, non-interacting species, as shown in the case of domain AB alone in Figure 2-7. The slight curvature of the G(s) plots in the case of DNA alone comes from the noise fluctuation within the data set. Rapid interaction kinetics compared with the experimental time scale could produce a gradual increase in $s_{w,20}$ values as the boundary fraction % increases. This results in a G(s) plot with a half-parabola shape. It is also noted that, this half- parabolic plot has a greater curvature when compared with the G(s) plot from DNA alone (22). This was observed in the cases where domain AB interacts with 66DS and 66G1 DNA (Figure 2-7 A and C). In the case where slow interaction kinetics take place or non-interacting species are present, the $s_{w,20}$ values become better separated, as shown in the case where PARP-1 interacts with 66DS and 66G1 DNA (Figure 2-7 B and D).

A.

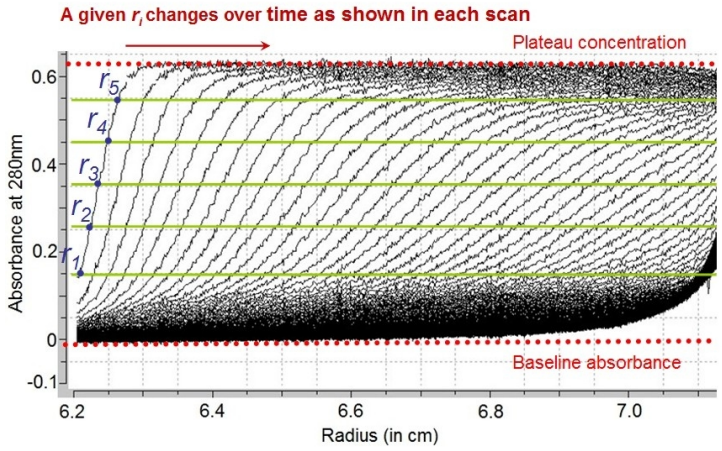

B.

$$s = \frac{v}{\omega^2 r} \quad (5)$$

$$\frac{dr}{r} = \omega^2 s\, dt \quad (6)$$

$$s^*_{i,j} = \left[\frac{r_i(t_j)}{r_a(t_o)}\right]\left[\omega^2(t_j - t_o)\right]^{-1} \quad (7)$$

$$1 \geqslant i \geqslant m, \quad 1 \geqslant j \geqslant n$$

v: absolute migration velocity
r: radius
ω: angular velocity
r_a: radius of the meniscus

r_i: the radius at the intercept of the scan and boundary fraction i
m: the number of scans with clear meniscus and stable plateau concentration
t_j: the time at which scan j was taken
n: number of equally spaces boundary fractions

C.

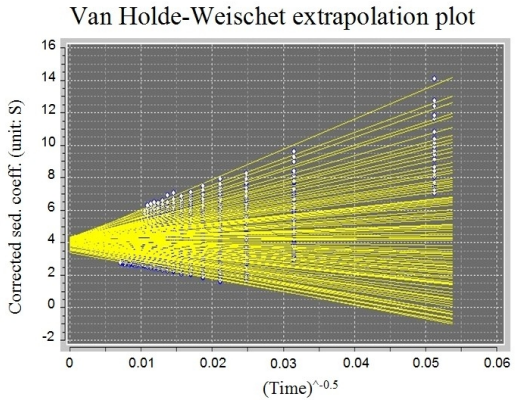

Figure 2-6. A. Demonstration of dividing SV data into a number of boundary fractions (n) that are analyzed by enhanced van Holde-Weischet (vHW) method. B. equations used to calculate the apparent sedimentation coefficient, $s^*_{i,j}$ at the intercept of boundary fraction i with data scan at time t_j (17). C. Extrapolation of the diffusion corrected $s_{w,20}$ values for all boundary fractions; this is done by plotting a collection of calculated apparent sedimentation coefficients $s^*_{i,j}$ against their corresponding time t_j in forms of $(t_j)^{\wedge -0.5}$.

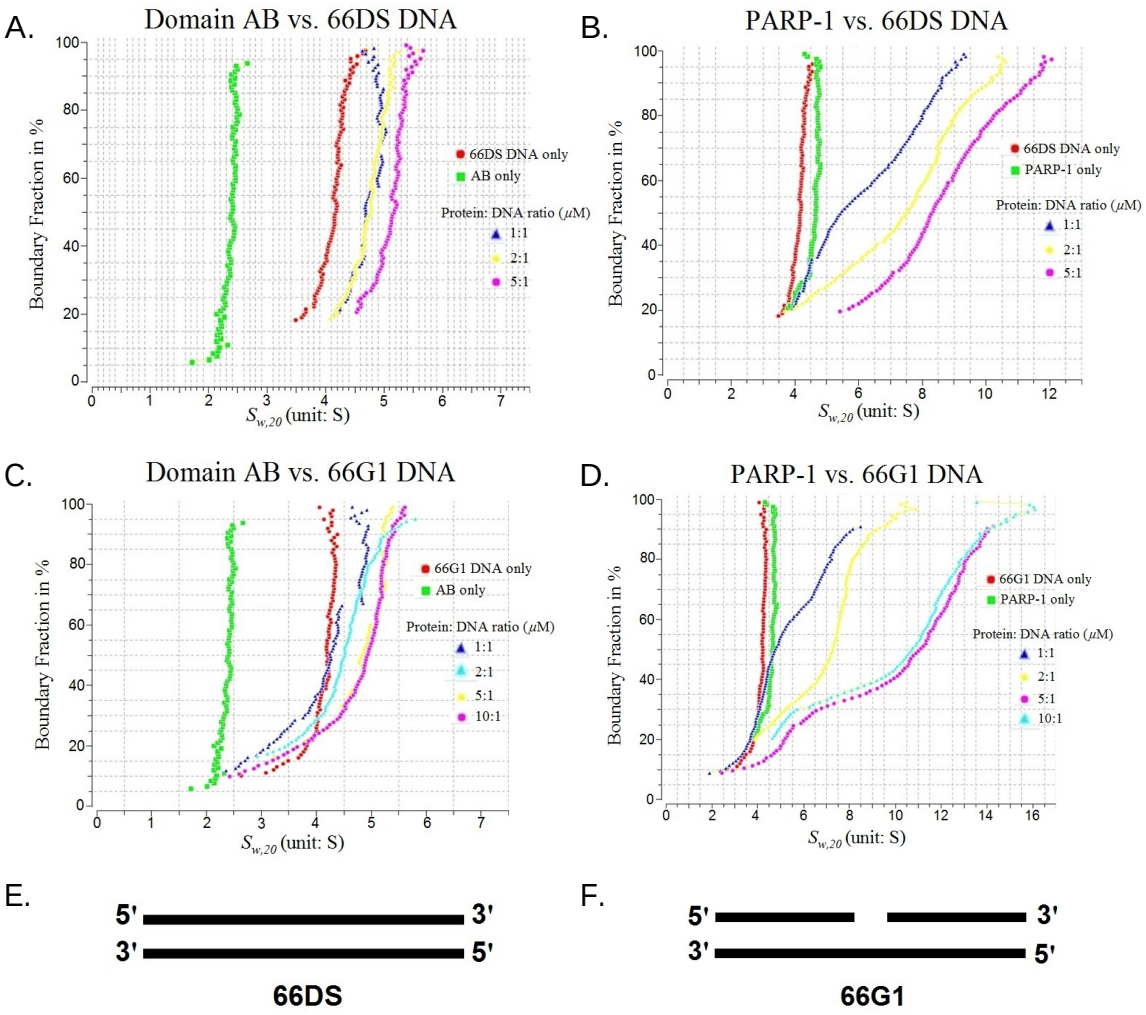

Figure 2-7. G(s) plots generated from diffusion-independent data analysis using the enhanced van Holde-Weischet (vHW) method.

The 66DS and 66G1 DNA constructs (Figure 2-7 E and F) served as mimics for double and single stranded breaks, respectively, and were used to test the binding stoichiometry of PARP-1 toward these DNA lesions. In these experiments, a fixed concentration of DNA (1 μM) was used, and either domain AB or PARP-1 was titrated in. When compared with DNA alone, increasing concentrations of domain AB or PARP-1 caused gradual increases of $s_{w,20}$ values. The observation of a increasing trend of $s_{w,20}$

values compared with DNA suggested the formation of protein-DNA complexes (Figure 2-7).

2.3.2.2. Two-dimensional spectrum analysis (2DSA)

As the diffusion corrected van Holde-Weischet (vHW) method provides a good estimate of the $s_{w,20}$ range within a given data set, it helps to set the lower and upper limiting values of $s_{w,20}$ during data fitting by two-dimensional spectrum analysis (2DSA) provided by the Ultrascan II program (17). A 2DSA analysis can help to identify the different solute species represented by a given data set that may have different sizes and shapes, because it does not post constraints on the f/f_o parameter as in the case of c(s) analysis (17). Furthermore, this method does not require a pre-established model of protein-DNA interaction, and it searches over a range of $s_{w,20}$ and f/f_o values. Therefore, a 2DSA analysis is suitable for the studies of PARP-DNA interactions where the protein, DNA, and the corresponding protein-DNA complex in the solution are expected to have different $s_{w,20}$ values and shapes as characterized by f/f_o.

Similar to the case of c(s) analysis, the 2DSA method also tries to fit the sedimentation boundaries by solving the sum of Lamm equations L through simulation. First, a two-dimensional grid of frictional ratios and sedimentation coefficients is generated based on the provided range of the two parameters from the user (Figure 2-8). As the diffusion coefficient can be parameterized in terms of f/f_o using equation (8), each grid point can be then assigned with a unique value of s and D. One grid point represents a potential solute species, and its associated s and D values are used to simulate the sedimentation velocity data by solving the Lamm equation (17). The combined simulation data generated from multiple grid points can then be used to fit the experimental data. At the same time, the total concentration of all solutes was also

determined based on the observed absorbance signal from a given data set, and assigned as 100%. The partial concentration of each fitted solute species can also be simulated in a similar manner using the observed signal intensity at a specific radial position in a given time during the sedimentation process (17). Furthermore, the program also accounts for and removes the time and radially invariant noise components from an experimental data set. Data fitting can be further optimized by genetic algorithm (GA) analysis (23). A Monte Carlo approach is implemented to characterize the confidence intervals for the determined solutes in both the 2DSA and GA analyses steps (23).

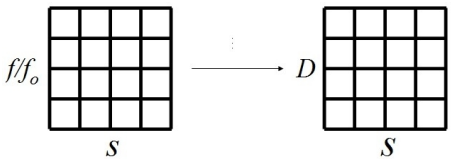

$$D = RT\left[N18\pi(k\eta)^{3/2}\left(\frac{s\bar{\upsilon}}{2(1-\bar{\upsilon}\rho)}\right)^{1/2}\right]^{-1} \quad (8)$$

R: the universal gas constant
T: temperature
N: Avogadro's number
η : viscosity
k: frictional ratio, f/f_o

Figure 2-8. Generation of two dimensional grid points with sedimentation coefficients and diffusion coefficients for data simulation in the 2DSA analysis.

The fitted $s_{w,20}$ values of the major sedimenting species identified by 2DSA analysis were plotted as shown in Figure 2-9. The fitted details for each solute are presented in Tables 2-5 to 2-9, and they are discussed further in the later sections. Here, the red dots correspond to species with the highest solute concentration percentage within a given data set. Table 2-4 provides a reference for the expected molecular weights (kDa) of the potential solute species.

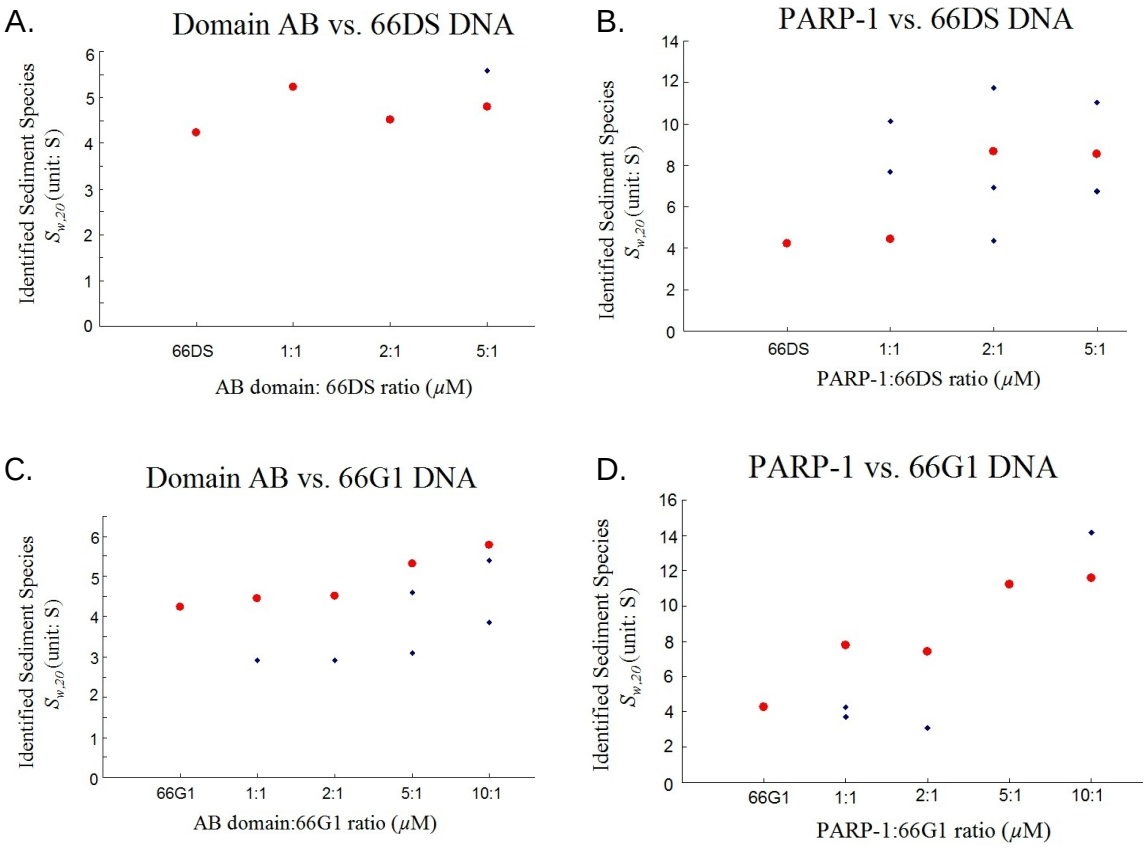

Figure 2-9. Sedimenting species identified from 2DSA analyses were plotted based on the fitted $s_{w,20}$ values for each protein-DNA ratios. Here, the red dots correspond to species with the highest solute concentration percentage within a given data set. A. domain AB vs. 66DS DNA; B. PARP-1 vs. 66DS DNA; C. domain AB vs.66G1; D. PARP-1 vs. 66G1 DNA.

Table 2-4 A-B. Tables of calculated molecular weights for the potential protein-DNA complexes identified from the SV experiments: A. 66DS DNA; B. 66G1 DNA.

A. 66DS DNA

Tested protein/DNA pair	Protein: DNA complex	Calculated Molecular Weight (kDa)
AB vs. 66DS	66DS only	40.7
	1:1	66.9
	2:1	93.1
	3:1	119.3
PARP-1 vs. 66DS	1:1	154.0
	2:1	267.3
	3:1	380.6

B. 66G1 DNA

Tested protein/DNA pair	Protein: DNA complex	Calculated Molecular Weight (kDa)
AB vs. 66G1	66G1 only	40.3
	1:1	66.5
	2:1	92.7
	3:1	118.9
PARP-1 vs. 66G1	1:1	153.6
	2:1	266.9
	3:1	380.2

For comparison, SV experiments of 66DS and 66G1 DNA alone were analyzed, and the results for the major solutes are presented in Table 2-5. While 66DS DNA contains no discontinuous region within the double helix, 66G1 DNA has a discontinuous gap at the center of the duplex, which mimicks a double stranded break. These two DNA constructs differ by a single nucleotide base. Consistent with their similar calculated molecular weights, both DNA constructs have similar sedimentation coefficients ($s_{w,20}$).

The partial concentration listed for each identified solute (i.e., average solute concentration % obtained from 50 iterations of data simulations) was used to determine whether the corresponding solute truly exists or it is due to noise or fitted errors in the SV data. This value is obtained by simulating the concentration of a given solute species that are identified from data fitting. It was first simulated in terms of absorbance and then converted to a percentage concentration. Here, the total absorbance signal within a given data set was assigned as 100%, and the percentage conversion was done by the Ultrascan II program at the end of the fitting. Generally, the percent solute concentrations should sum to 100% when all solutes present in the solution are considered; however, the fitted

result for a system containing a single solute species is usually less than 100% as shown in the case of DNA (Table 2-5). There are few factors contributing to this problem. First, the 2DSA analysis cannot account for the time- and radial- dependent noise signals in the experimental data. Second, many solutes may undergo conformational changes when they are in solution. While one conformation is dominant and the other is not, the minor conformation can also be resolved from the data set, but with less confidence due to the low absorbance signal associated with it. When a species has a solute concentration of less than 5%, it is not considered as one of the solutes in this study, because it can not be differentiated from the noise or the fitted error.

When considering the stoichiometries of the protein-DNA complexes, the reported ratios shown in Tables 2-6 to 2-9 were based on a comparison of the observed molecular weights of a given solute to the references shown in Table 2-4. In the case of PARP-1, 1:1 and 2:1 protein-DNA complexes were observed for both 66DS and 66G1 DNA constructs (Table 2-6 and Table 2-8); and the formation of the 2:1 complex was observed as protein concentration increased. In contrast, higher oligomeric states (i.e., 3:1 and 4:1 protein-DNA complexes) were observed when domain AB was tested. Using 66DS DNA as the counterpart, in addition to the 1:1 and 2:1 protein-DNA complex, a 3:1 protein-complex was observed with increasing protein concentration (Table 2-7). In the case of 66G1 DNA, a 4:1 protein-DNA complex was observed when protein concentration was in excess (Table 2-9).

Table 2-5. Fitted parameters of the SV experiments with only DNA using 2DSA analyses with 95% confidence intervals.

DNA	66DS	66G1
Fitted $s_{w,20}$ (S)	4.24 (4.21, 4.27)	4.25 (4.25, 4.25)
Fitted f/f_0	2.00 (1.99, 2.01)	1.69 (1.68, 1.69)
Experimental MW (kDa)	42.6 (42.1, 43.2)	32.4 (32.4, 32.6)
Calculated MW (kDa)	40.7	40.3
Average solute concentration %	52%	79%

Table 2-6. Fitted parameters of the SV experiments with PARP-1 and 66DS DNA using 2DSA analyses with 95% confidence intervals

Protein:DNA ratio	1:1			2:1		5:1	
$s_{w,20}$ (S)	4.44 (4.43, 4.45)	7.68 (7.66, 7.70)	10.10 (10.06,10.12)	8.69 (8.62, 8.75)	11.7 (11.7, 11.8)	8.55 (8.52, 8.59)	11.0 (10.9, 11.1)
f/f_0	1.17 (1.15, 1.19)	1.00 (1.00, 1.00)	1.00 (1.00, 1.00)	1.08 (1.07, 1.10)	1.00 (1.00, 1.00)	1.21 (1.19, 1.23)	1.00 (1.00, 1.00)
MW (kDa)	57.7 (56.2, 59.3)	103.8 (103.4, 104.2)	156.4 (155.7, 157.2)	140.5 (136.8, 144.2)	196.1 (195.5, 196.7)	162.7 (158.8, 166.7)	178.2 (176.4, 180.1)
Average solute concentration %	37%	30%	14%	28%	14%	30%	20%
Protein-DNA complex	n/a	1:1	1:1	1:1	2:1	1:1	2:1

Table 2-7. Fitted parameters of the SV experiments with domain AB and 66DS DNA using 2DSA analyses with 95% confidence intervals

Protein:DNA ratio	66DS only	1:1	2:1	5:1	
$s_{w,20}$ (S)	4.24 (4.21, 4.27)	5.22 (5.22, 5.22)	4.51 (4.49, 4.53)	4.80 (4.77, 4.83)	5.59 (5.52, 5.66)
f/f_0	2.00 (1.99, 2.01)	1.00 (1.00,1.00)	1.34 (1.33, 1.35)	1.47 (1.46, 1.48)	1.57 (1.56, 1.59)
MW (kDa)	42.6 (42.1, 43.2)	54.8 (54.8, 54.8)	68.2 (67.5, 68.9)	86.3 (84.7, 87.8)	119.7 (117.1, 122.3)
Solute concentration %	52%	20%	56%	54%	22%
Protein-DNA complex	n/a	1:1	1:1	2:1	3:1

Table 2-8. Fitted parameters of the SV experiments with PARP-1 and 66G1 DNA using 2DSA analyses with 95% confidence intervals

Protein:DNA ratio	1:1	2:1	5:1	10:1	
$s_{w,20}$ (S)	7.77 (7.76, 7.78)	7.40 (7.38, 7.42)	11.19 (11.04, 11.35)	11.65 (10.21, 13.08)	14.17 (13.69, 14.65)
f/f_0	1.23 (1.20, 1.25)	1.34 (1.32, 1.35)	1.00 (1.00, 1.00)	1.01 (0.88, 1.13)	1.00 (1.00, 1.00)
MW (kDa)	143.2 (139.1, 147.4)	151.8 (149.6, 154.0)	182.6 (178.8, 186.4)	196.1 (139.3, 253.0)	260.2 (246.8, 273.28)
Solute concentration %	28%	31%	33.4%	31%	11%
Protein-DNA complex	1:1	1:1	2:1	2:1	2:1

Table 2-9. Fitted parameters of the SV experiments with domain AB and 66G1 DNA using 2DSA analyses with 95% confidence intervals

	66G1: AB ratio				
Protein:DNA ratio	66G1 only	1:1	2:1	5:1	10:1
$s_{w,20}$ (S)	4.25 (4.25, 4.25)	4.45 (4.43, 4.46)	4.52 (4.48, 4.56)	5.31 (5.27, 5.36)	5.79 (5.75, 5.82)
f/f_0	1.69 (1.68, 1.69)	1.52 (1.51, 1.53)	1.58 (1.56, 1.60)	1.85 (1.78, 1.92)	1.67 (1.65, 1.68)
MW (kDa)	32.4 (32.4, 32.6)	80.9 (80.1, 81.7)	88.0 (85.9, 90.0)	141.7 (132.4, 151.0)	137.8 (136.6, 138.9)
Solute concentration %	79%	36%	43%	40%	22%
Protein-DNA complex	n/a	2:1	2:1	4:1	4:1

2.3.3. Characterization of a secondary DNA-binding site in PARP-1

2.3.3.1. Comparison of DNA-binding ability of truncated PARP-1 constructs ABC and DEF

Based on the structural model of PARP-1 bound with 8-mer DNA built from the small angel X-ray scattering (SAXS) and molecular dynamics studies, the WGR motif within domain E was proposed to interact with DNA. To further investigate this hypothesis, the DNA-binding ability of DEF was tested. The domain ABC served as a positive control in the electrophoretic mobility shift assays (EMSA), because it showed strong binding affinities toward different DNA lesions (24). A double stranded 22-mer

DNA served as a mimic for a double stranded break in these experiments. Likewise, DNA with a single strand nick was generated using the 44-mer dumbbell DNA.

Results from the EMSA assays were shown in Figure 2-10. Based on protein-DNA complex formation represented by retention at the top of the agarose gel, it was clear that DEF has the ability to bind DNA when either 22-mer duplex or nicked DNA is used. To estimate the dissociation constants (K_d) of ABC and DEF with different DNA constructs, the fraction of protein bound DNA was quantified and plotted against the loaded protein concentrations, as shown in Figure 2-11. The plotted data was fitted using the equation (8) with KaleidaGraph 4.0 software, and the K_d values were reported in Figure 2-11. Due to the smearing effect resulted from dissociation of the protein-DNA complex during electrophoresis, the quantification here are rough estimations only. Nevertheless, it still provides a way for comparisons under the same experimental conditions. Based on the fitted K_d values, DEF exhibited weaker binding affinities than ABC when either 22-mer DNA or nicked DNA was used.

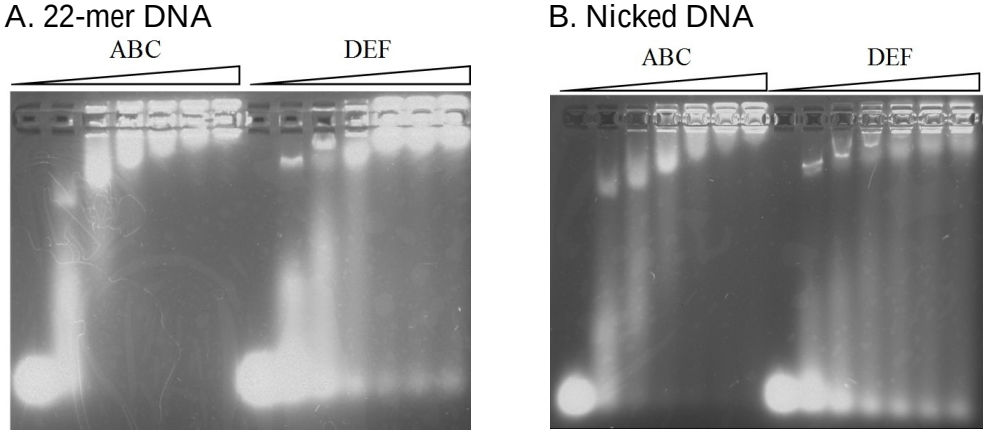

Figure 2-10. Comparison of DNA binding abilities of domain ABC and DEF based on EMSA assays, with protein-DNA loading ratios increasing from left to right (0:1, 1:1, 2:1, 3:1, 4:1, 5:1 and 6:1). A. Using a 22-mer DNA duplex. B. Using a nicked DNA construct.

A.

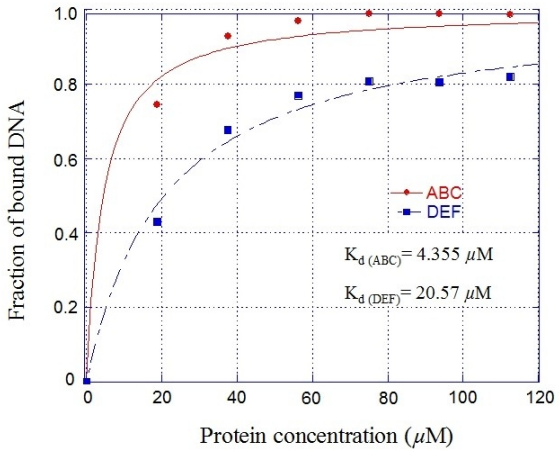

B.

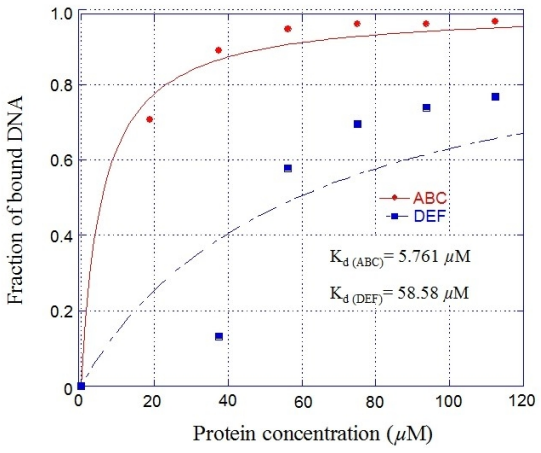

C.

Here, a simple bimolecular interaction model is assumed,

$$\text{Protein-DNA} \rightleftharpoons \text{Protein} + \text{DNA}$$

$$f = \frac{1}{1 + \left(K_d/[P]\right)} \quad (9)$$

f: fraction of protein bound DNA
$[P]$: total protein concentration used
K_d: equilibrium dissociation constant

Figure 2-11. Binding affinity comparisons of domain ABC and DEF based on EMSA results with different DNA constructs. A. Using a 22-mer DNA duplex. B. Using a nicked DNA construct. C. A simple model of protein-DNA interaction is provided together with the equation used for data fitting (25).

2.3.3.2. Characterization of the DNA-binding region within DEF

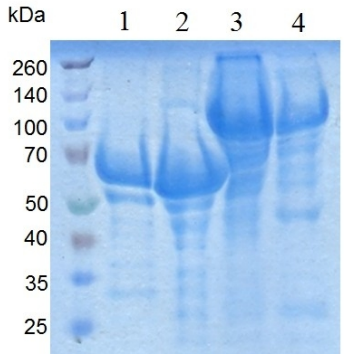

Figure 2-12. A. SDS-PAGE gel showing typical protein purities of domain DEF (lane 1), DEFΔ (lane 2), PARP-1 (lane 3) and PARP-1Δ (lane 4) in concentration of 3 mg/mL.

Based on the structural model of PARP-1 and 8-mer DNA, it was proposed that a flexible loop region within residues 626 to 645 of PARP-1 is brought into contact with 8-mer DNA. Therefore, a deletion mutant of DEF lacking this flexible loop, namely DEFΔ, was prepared (Figure 2-12, lane 2) and its DNA-binding ability was compared with wild type DEF.

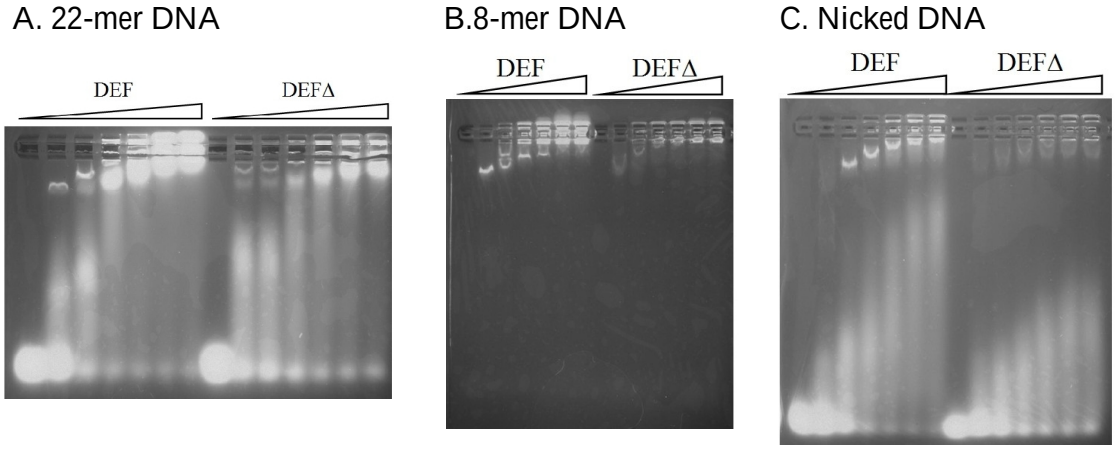

Figure 2-13. Comparison of DNA binding abilities of wild type DEF and DEFΔ mutant based on EMSA assays with protein-DNA loading ratios increasing from left to right (0:1, 1:1, 2:1, 3:1, 4:1, 5:1 and 6:1). A. Using a 22-mer DNA duplex. B. Using an 8-mer DNA duplex. C. Using a nicked DNA construct.

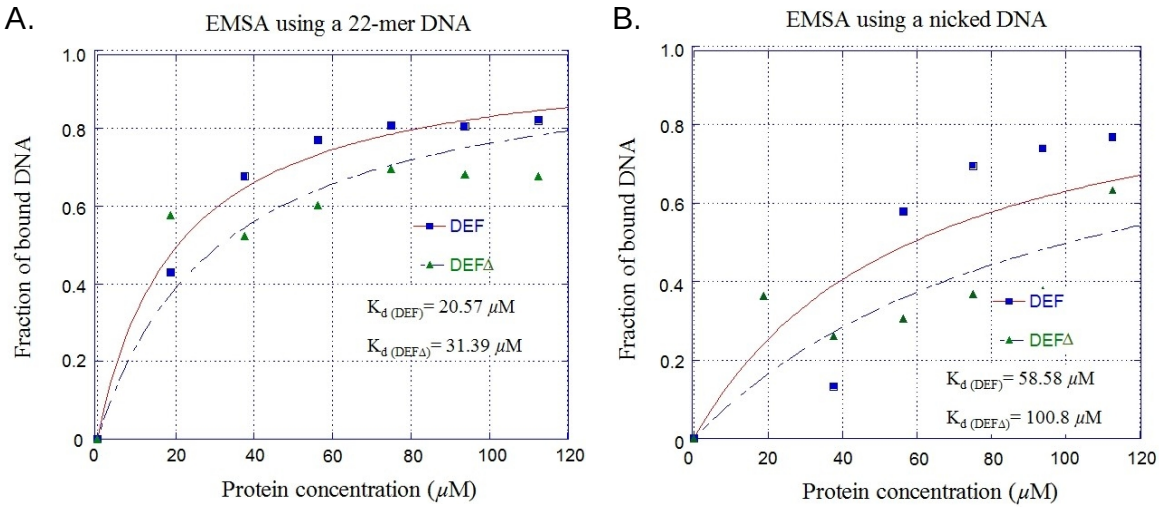

Figure 2-14. Binding affinity comparisons of DEF and DEFΔ mutant based on EMSA results with different DNA constructs. A. Using a 22-mer DNA duplex. B. Using a nicked DNA construct.

Based on the EMSA results shown in Figure 2-13, the lower UV signal intensity showing on top of the agarose gel indicated lower protein-DNA complex formation with the DEFΔ mutant when compared with wild-type DEF for both 22-mer DNA (Figure 2-13A) and the nicked DNA (Figure 2-13C) constructs. K_d values were obtained for the DEFΔ mutant both DNA constructs using equation (9), and the fitted results were shown in Figure 2-14. In both cases, DEFΔ mutant exhibited weaker DNA-binding affinities than the wild type DEF. However, the DNA-binding affinity was affected more significantly in the case of nicked DNA, as shown in Figure 2-14B; whereas in the case of 22-mer DNA, the effect of mutation was less substantial.

An EMSA assay was also performed using the 8-mer DNA duplex, because the proposed DNA interaction site in DEF was based on the structural studies of PARP-1/8-mer DNA. When the DEFΔ mutant was tested for binding with 8-mer DNA, a similar conclusion was drawn as in the case of 22-mer DNA due to the low observed intensity arising from the protein-DNA complex (Figure 2-13B). A K_d value was not obtained in

the case of 8-mer DNA due to the low signal within this data set. Based on results from the mutation studies, it was concluded that, domain DEF harbors a secondary DNA-binding site within the WGR motif, with a stronger binding influence on the single stranded DNA break.

2.3.3.3. Effect of the secondary DNA-binding site on PARP-1 activity

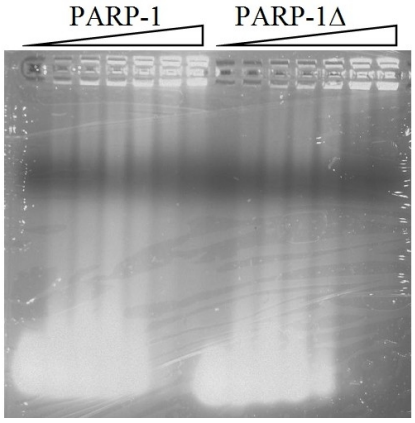

Figure 2-15. Comparison of binding ability of wild type PARP-1 and PARP-1Δ mutant toward nicked DNA. The protein:DNA loading ratios increase from left to right (0:1, 1:1, 2:1, 3:1, 4:1, 5:1 and 6:1).

To study the influence of the WGR motif on DNA-binding affinity as well as the automodification activity in the context of full-length enzyme, amino acid residues 626 to 645 were deleted from PARP-1, and the resulting PARP-1Δ mutant was isolated (Figure 2-12, lane 4). Its DNA-binding affinity was compared with that of wild type PARP-1 using the nicked DNA. The EMSA result is presented in Figure 2-15. It was observed that the PARP-1Δ mutant had a binding affinity toward the nicked DNA similar to that of wild type PARP-1. This observation indicated that deletion of the flexible loop region within WGR domain of PARP-1 has little effect on the overall DNA binding ability of

PARP-1. This observation is consistent with the results shown in Figure 2-10, where domain ABC exhibits a stronger DNA binding affinity than DEF. Taken together, these results suggest that domain ABC plays a critical role in binding DNA lesions, whereas domain DEF plays a subsidiary role in stabilizing the conformation of protein-DNA complex.

To see whether the deletion would have any effect on the automodification activity of PARP-1, a time course assay was carried out using both wild type PARP-1 and PARP-1Δ mutant in the presence of 8-mer DNA. The activity level of the enzymes was estimated by determining the amount of protein band shift toward the top of the SDS-PAGE gel, and the result is shown in Figure 2-16. Wild type PARP-1 demonstrated a protein band shift within 10 sec of adding the NAD^+ substrate, but there was no detectable band shift of the PARP-1Δ mutant even after 5 min. These results indicate that the flexible loop region of the WGR motif participates in the DNA-dependent activation of PARP-1.

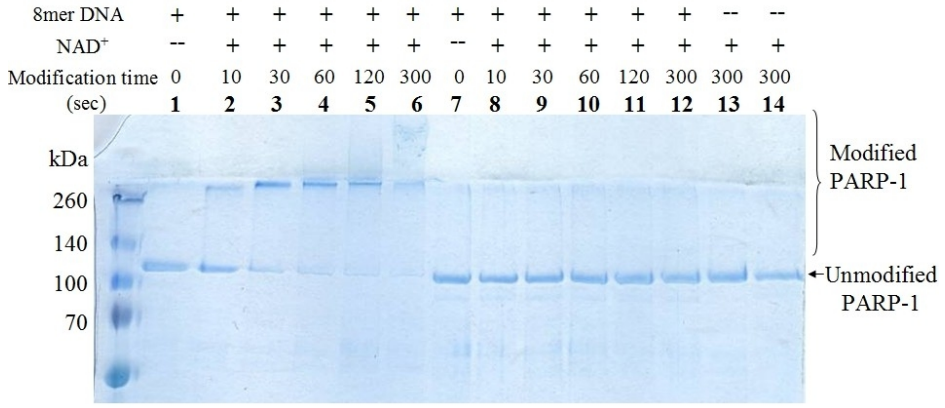

Figure 2-16. Levels of automodification activity are compared between wild type PARP-1 and PARP-1Δ mutant. Wild type PARP-1 was added in lanes 1 to 6, and lane 13; PARP-1Δ mutant was added in lanes 7-12, and lane 14.

2.4. DISCUSSION

2.4.1. Full-length PARP-1 and the DNA binding domain AB exist as monomers in solution

In the case of full-length PARP and domain AB, SV experiments were done by varying the concentration of proteins to test if reversible self-association occurs in solution. If formation of protein monomer and dimer is in rapid equilibrium as compared to the rate of sedimentation during experiments, these two species can not be resolved into two separated sedimentation boundaries (12). Instead, a weight-average sedimentation coefficient s_w of monomeric and dimeric species is obtained from the SV data. This coefficient is increased when protein loading concentration becomes higher (13). In the case where the equilibrium favors the formation of protein dimers, formation of the dimer should be well-resolved as a distinct species with a larger s_w value as compared to the monomer. Finally, when only a monomeric form is present in solution, and there is no self-association occurs, a single solute species with the same weight-average s_w value in different tested protein concentrations would be observed.

Based on the results shown in Figure 2-5, in the cases of PARP-1 and domain AB, the observed weight-average sedimentation coefficients s_w are similar under different protein loading concentrations. There is no increasing trend among the s_w values as the protein loading concentration increased. This is consistent with PARP-1 and domain AB present as monomers in solution.

Values of the frictional ratio f/f_o provide information on the molecular symmetry of an analyte. An f/f_o value of 1 suggests a symmetric, globular shape for a macromolecule (16). Since both PARP-1 and domain AB have average f/f_o values of 1.55

and 1.41, respectively, the observed values suggest that both proteins have an elongated conformation in solution.

2.4.2. Sedimentation velocity studies of DNA constructs

Prior to the protein-DNA interaction studies, SV experiments were carried out using DNA alone. It served as a reference point for comparison when proteins were titrated in. The 66DS and 66G1 DNA were used to mimick the double and single-stranded breaks, respectively (Figure 2-7 E and F). These two 66bp DNA constructs have similar molecular weights, and are only different by a single nucleotide base. In the case of 66G1, a discontinuous gap is introduced in the middle of the double helix, as shown in Figure 2-7F. Based on 2DSA analyses, 66DS DNA has a $s_{w,20}$ value of 4.24 S, and the 66G1 DNA has a $s_{w,20}$ value of 4.25 S.

While the two DNA constructs have similar observed $s_{w,20}$ values, the overall shapes of the two constructs are different (Table 2-5). In the case of 66DS, there is no discontinuous region within the double helix; therefore, the majority of the molecules is present as a long rod shape in solution as indicated by the f/f_0 value of 2.00. In comparison, 66G1 DNA has an f/f_0 value of 1.69, indicating that the overall shape is more compact when compared with 66DS. Based on these observations, it is clear that introducing a discontinuous break within a DNA duplex has an impact on its overall shape in solution.

It should be mentioned that the fitted molecular weights for both 66G1 and 66DS DNA duplexes deviated from their calculated molecular weights based on the DNA sequences. This is because SV experiments provide direct measurements through Lamm equation modeling on the sedimentation coefficients and diffusion coefficients, but not for molecular weights (Figure 2-4, equation (4)). While the experimental molecular

weights can be extracted from the fitted results of the $s_{w,20}$ and f/f_o values based on the Sverberg equation (Figure 2-2, equation (3)), it is highly dependent on the noise level of the data, the purity, and heterogeneity of a given sample. As the last two factors would cause further broadening of the sedimentation boundary in addition to diffusion, the resulted experimental molecular weights would be underestimated (20). Hence, the fitted molecular weight obtained from SV experiments are rough estimations, and it holds true for the later discussion of protein-DNA interactions where samples are highly heterogeneous.

2.4.3. Sedimentation velocity studies of PARP-1 in the presence of DNA

When PARP-1 was used for protein-DNA interaction studies, the current results suggest that PARP-1 forms a 1:1 and 2:1 protein-DNA complex when either 66DS or 66G1 DNA is used. This conclusion was drawn based on the observed G(s) plots from the enhanced van Holde-Weischet analysis in Figure 2-7 B and D, and it was further confirmed by the 2DSA analysis.

In the case of 66G1 DNA, a two step increase in the $s_{w,20}$ value was clearly observed in the G(s) plots as PARP-1 loading concentration increased, as shown in Figure 2-7D. Compared with DNA alone, when PARP-1:DNA loading ratio was 1:1, 30% of the boundary fraction was associated with the $s_{20,w}$ value near 7 S. It was well-separated from the boundary fraction at about 4 S for the DNA species. Good separation between the two species indicates the occurrence of slow dissociation kinetics (18), where formation of DNA-protein is less favored than DNA being alone when equal amounts of protein and DNA were used. As PARP-1:DNA loading ratio increased to 2:1, higher percentage of the boundary fraction was associated with 7 S. This indicated that more 1:1 protein-DNA complex was formed under this condition as compared to a 1:1

protein:DNA loading ratio. Interestingly, when PARP-1 concentration was in 5 and 10 folds excess, in addition of the observed 7 S species, a 12 S species was also observed, indicating the formation of a 2:1 PARP-1: 66G1 complex.

The conclusion drawn here was further confirmed by the 2DSA analysis for these protein-DNA pairs. The 1:1 and 2:1 protein-DNA complexes were well-resolved by data fitting. As presented in Figure 2-9 D, the 1:1 complex was observed as a major species under 1:1 and 2:1 protein: DNA loading ratios. With an $s_{20,w}$ value of 7.6 S for this complex, the observed molecular weight was in good agreement with the expected molecular weight (Table 2-8). When 10-fold excess of PARP-1 was loaded, a minor solute species was observed with an $s_{20,w}$ value of 14.17 S. This species correlated well with a 2:1 protein-DNA complex based on its observed molecular weight (Table 2-8). Furthermore, when protein concentration was in excess, a species of 11 S was also observed as the major species. This species represents a weight-average species of the 1:1 and 2:1 complex which was not well-resolved from the sedimentation boundaries due to fast kinetics. Taking all these together, the current data suggest that in the presence of 66G1 DNA, which mimicks a single stranded break, PARP-1 can form 1:1 and 2:1 protein-DNA complex depending on the protein/DNA ratio of the solution. The interconversion between the 1:1 and 2:1 complex was fast, thus resulted in a weight-average solute species of 11 S from the SV experiments.

In contrast, the 1:1 protein-DNA complexes formed by PARP-1 and 66DS DNA was less well-resolved in the G(s) plots as shown Figure 2-7B. For different PARP-1 loading concentrations, all of them showed a smooth transition over a wide range of $s_{20,w}$ values, indicative of rapid transition between complex formation and the free DNA. Increasing PARP-1 concentration caused a gradual shift of the G(s) plots toward a $s_{20,w}$ value of 8 S and stabilized at that region, indicative of the 1:1 protein-DNA complex

formation. This was further confirmed by the 2DSA analysis. As shown in Figure 2-9B and Table 2-6, a species with the $s_{20,w}$ value of 8.6 S was observed as a major species when 2 or 5-folds of PARP-1 was used. When equal amount of protein and DNA were used, instead of observing a distinct 1:1 protein-DNA complex, a weight-average species of a free DNA and the 1:1 protein-DNA complex was observed, with an $s_{20,w}$ value of 7.68 S for the 1:1 protein-DNA complex. This can be explained by the fast kinetic process for the complex formation, as indicated by the smooth curve in the G(s) plot.

The formation of a 2:1 protein-DNA complex was less apparent by solely looking at the G(s) plots in Figure 2-7B. This was due to the low percentage of boundary fraction associated with higher $s_{20,w}$ values. Nevertheless, data obtained from the 2DSA analyses also suggested a 2:1 protein-DNA complex formation. As shown in Figure 2-9B, a minor 11 S species was observed in the case of 2 and 5 folds of protein loading, indicative of a 2:1 protein-DNA complex. In addition, a solute species of 10.1 S was observed when equal concentrations of protein and DNA were used. This is likely to be the weight average species resulting from the 1:1 and 2:1 protein-DNA complex. Based on the discussions above, it is concluded that, in the presence of 66DS DNA, PARP-1 indeed forms a 1:1 and 2:1 protein-DNA complex.

While the data presented here suggest a 2:1 protein-DNA complex formation in the case of full-length PARP-1, it is not consistent with the recently published SV data reported by Langelier et. al (26), where PARP-1 forms a 1:1 complex with 8-mer DNA. The discrepancy may be explained by the differences in terms of experimental set up and data analysis methods. First, considering the DNA constructs used in these studies, both 8-mer DNA and 66DS are mimicks for double stranded breaks. In the case of 66DS DNA, the presence of the 2:1 protein-DNA complex was confirmed based on a series of protein titration experiments, and by two different data analysis methods: enhanced van

Holde-Weischet and 2DSA. In the case of 8-mer DNA SV experiment reported by Langelier et. al. (26), only 1:1 protein-DNA loading ratio was tested, and the SV data was analyzed using c(s) analysis.

As discussed in the Results section, the enhanced van Holde-Weischet (vHW) analysis minimizes the effect of diffusion and provides a range of the s values within the protein-DNA sample. The diffusion process is dependent on the f/f_0 parameter, or the shape of the molecule (Figure 2-8, equation 8). Therefore, result obtained from the vHW analysis provides information of the numbers of solute species regardless of their different shapes. In contrast, the 2DSA analysis allows data fitting in both the s and the f/f_0 dimensions and searching for solute species with different f/f_0 values. Therefore, the 2DSA accounts for the heterogeneity in terms of f/f_0 within a given data set. However, the c(s) analysis can not accurately account for the effect of species with different f/f_0 values because it requires an input of a single f/f_0 estimation by the users. Based on the discussion above, it is likely that the 2:1 protein-DNA complex is not well-resolved in the study of PARP-1 interaction with 8-mer DNA carried out by Langlier et al. (26) based on the experimental set up and the data fitting methods.

However, it should be mentioned that, when 2:1 protein-DNA complex is observed in the case of PARP-1 interacting with DNA, it is not sure which region of DNA is recognized and interacts with PARP-1. As shown in Figure 2-7 E, 66DS DNA contains two blunt ends, representing two individual double stranded break lesions. In the case of 66G1 DNA (Figure 2-7 F), in addition to the two blunt ends, 66G1 DNA also contains a gap site in the center, with a total of three lesions that can be potentially recognized by PARP-1. With DNA molecules which have more than one lesion sites, it is not certain how many PARP-1 molecules interact with a single lesion site.

Different DNA constructs harboring only one lesion site was considered when designing the experiments, these types of DNA constructs are usually large plasmids and often containing other secondary structures such as hairpin loops, which can also be recognized by PARP-1. Therefore, SV experiments with these DNA constructs were not pursued.

Finally, it was observed that PARP-1 undergoes a conformational change upon DNA binding. When only PARP-1 is present in solution, it adapts an elongated conformation, indicated by an observed f/f_o value of 1.55. When DNA is added, the observed protein-DNA complexes have f/f_o values ranging from 1.0 to 1.2, depends on the oligomeric states as well as the DNA it encounters. The observed decreases in f/f_o values suggest that the PARP-DNA complex adapts a more compact conformation.

2.4.4. Sedimentation velocity studies of domain AB in the presence of DNA

The oligomeric state of AB-DNA complex was less well defined when compared with the case of full-length PARP-1. Although higher orders of AB oligomerization were observed upon binding to DNA, this is inconsistent with the results obtained from the case of PARP-1. Discussion of the results and explanations for the discrepancies between two protein constructs will be provided in more details below.

When double stranded DNA 66DS was incubated with domain AB, there was a two step increase in the $s_{w,20}$ values as protein concentration increased, indicated by the G(s) plots (Figure 2-7A). As the protein:DNA ratios were maintained at 1:1 and 2:1, most of the boundary fractions shifted from about 4 S to 4.5 S in comparison with free DNA. When a ratio of 5:1 of protein:DNA was used, majority of the boundary fraction associated with $s_{w,20}$ values of 5 S. Furthermore, individual G(s) plot associated with different protein:DNA loading ratios showed a smooth change within a narrow range of

$s_{w,20}$ values, indicative of a rapid interconversion between protein-DNA complex and free DNA. A similar phenomenon was also observed in the G(s) plots generated from the experimental data of 66G1 DNA with domain AB (Figure 2-7C).

Two step increases of the $s_{w,20}$ values as protein loading concentration becoming higher indicated the formation of 1:1 and 2:1 protein-DNA complexes. However, the change in the $s_{w,20}$ values between different protein:DNA loading ratios was relatively small, which made it hard to conclude whether the protein-DNA complex is 1:1 or higher when solely based on the enhanced van Holde-Weischet analysis.

When domain AB versus 66DS data set was further analyzed by 2DSA analysis, a 1:1 and 2:1 AB-DNA complex was observed (Table 2-7). The 1:1 protein-DNA complex has a $s_{w,20}$ value of 4.51 S, and the 2:1 complex corresponds to the 4.80 S species. Consistent with the observation from the G(s) plots in Figure 2-7A, the difference of $s_{w,20}$ values between two protein-DNA complex is rather small.

Furthermore, when 5:1 protein:DNA ratios was used in the experiments, a third complex was formed. This complex had an experimental molecular weight that matches well with the 3:1 protein-DNA complex, with a sedimentation coefficient of 5.59 S. This is different than the case of full-length PARP-1, where no 3:1 protein-DNA complex was observed.

Considering that PARP-1 interacts with 66 DS DNA to form a 2:1 protein-DNA complex, two possible scenarios can be envisioned to account for the binding stoichiometry of PARP-1 toward each blunt end site. One possible binding mode is that one PARP-1 molecule interacts with one lesion site, and the 2:1 protein-DNA complex is resulted from the occupancy of both lesion ends in the 66DS DNA. Another possible binding mode is that two PARP-1 molecules form a dimer at a single blunt end site. As discussed in Chapter 1, there is crystallographic evidence supporting either of the two

scenarios (Figure 1-8) (8). However, the SV experiments only provide stoichiometric information of the protein-DNA complex; therefore, these results can not help to distinguish between the two possibilities. While the observed 3:1 AB-66DS complex may be due to the non-specific binding of the third protein molecule, one cannot exclude the possibility that two AB molecules bind to one lesion site, and the third protein molecule interacts with the second lesion site.

In the SV experiments of domain AB and 66G1 DNA, a 2:1 and a 4:1 protein-DNA complex were identified from 2DSA analyses (Table 2-9). This is again different from the case of PARP-1 when the same DNA construct was used. Although both PARP-1 and domain AB contain the DNA-binding zinc fingers I and II, the sizes of these two proteins are quite different. In the case where a DNA construct such as 66G1 contains both lesions, both the gap site as well as the two blunt ends may be accessible for PARP-1 binding, since PARP-1 zinc fingers are known to recognize both double and single stranded breaks (10). While a DNA construct with 66bp may not be able to accommodate large proteins like PARP-1 at all three lesion sites, small size protein like domain AB may be able to access those lesion sites in solution. This may explain why higher oligomeric states were observed when domain AB was tested in SV experiments.

2.4.5. Characterization of the secondary DNA-binding site in human PARP-1

As demonstrated by Alvarez-Gonzalez et al., PARP-1 activity can be increased over 500-fold from its basal level in the presence of damaged DNA (2). Two zinc fingers at the N-terminus are critical for both DNA recognition and PARP-1 activation. This implies that interactions with DNA at the N-terminus can be relayed to the distant catalytic site in the C-terminal domain F in some manner that may involve a

conformational change. In attempting to gain insight into the conformational state of PARP-1 upon DNA binding, a structural model of PARP-1 bound with 8-mer DNA was constructed by our previous group member Dr. Steven Mansoorabadi using SAXS and molecular dynamics. In addition to the two zinc fingers, a flexible loop region within the WGR motif in domain E was predicted to be in contact with the 8-mer DNA as shown in Figure 2-17.

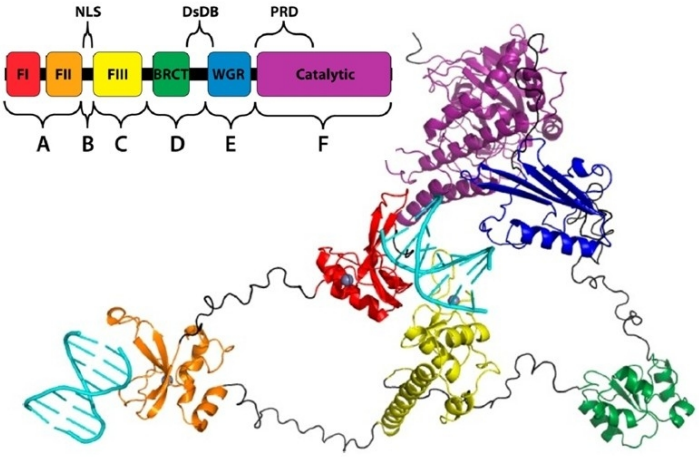

Figure 2-17. Proposed structural model of PARP-1 complexed with 8-mer DNA. Two molecules of 8mer DNA are displayed in cyan, and a color scheme for the individual domains is also provided. Adapted from Mansoorabadi et al., Biochemistry 2014, 53: 1779–1788.

To test whether the predicted secondary DNA binding site in the loop region of the WGR motif has any DNA-binding capability, a truncated protein representing domain DEF was first examined. Based on the EMSA assays shown in Figure 2-10, domain DEF was indeed capable of interacting with either double stranded blunt end DNA or a nicked DNA. When the loop region within the WGR motif was removed, the resulting DEFΔ mutant showed a lower level of protein-DNA complex formation as compared with the wild type DEF (Figure 2-13 and Figure 2-14). These results indicate that the loop region

within the domain E likely involves in DNA interactions as predicted by the structural model.

However, when compared with domain ABC, the DNA-binding affinity of DEF is relatively weak (Figure 2-11). Hence, unlike what ABC does in the process of DNA recognition, DEF is not the major determinant in sensing the DNA lesion. However, since DEF has DNA-binding capability, this weak protein-DNA interaction at the C-terminal region can help to support the active conformation of PARP-1 bound with DNA by providing further assistance to stabilize the protein-DNA complex in addition to the N-terminal domain ABC. Furthermore, as the WGR motif is located next to the C-terminal catalytic domain F, protein-DNA interaction at the WGR region brings the catalytic domain close to DNA. As a result, it relays the "DNA-activating" signal to the catalytic domain and triggers PARP-1 activity.

This hypothesis was further supported when the DNA-binding ability of this loop region was assessed in the context of full-length PARP-1. When the loop region was deleted from the full-length PARP-1, the resulting PARP-1Δ mutant showed similar extent of DNA-binding as compared with the wild type protein (Figure 2-15). This again implies that the flexible loop within the WGR motif is less critical for recognition of DNA lesion. To test whether the DNA-binding loop participates in the DNA-dependent activation process of PARP-1, automodification activity was examined in a time-dependent manner using both PARP-1 and the PARP-1Δ mutant. As shown in Figure 2-16, the PARP-1Δ mutant did not show any band shift which is indicative of automodification. Removal of the DNA-binding loop within the WGR motif apparently abolished the automodification activity of the mutant protein, suggesting a critical role in forming an activated complex between PARP-1 with DNA.

While this work was in progress, a crystal structure of near full-length PARP-1 in complex with DNA was reported by Langelier et al. (Figure 1-10) (26). By co-crystallizing zinc finger I, domain C and WGR-CAT peptides with DNA, it was shown that the WGR motif is important for establishing the active conformation of PARP-1. One side of the WGR motif interacts with DNA, zinc finger I and domain C, whereas the other side of the WGR motif is in contact with the regulatory domain PRD near domain F. Multiple sites of interaction centered about the WGR motif lead to structural compaction and result in a catalytically competent conformation of PARP-1 upon DNA binding. This is consistent with the observations from the SAXS and SV experiments discussed herein, where PARP-1 was noted to become more compact in the presence of DNA (13). Therefore, the structural model shown in Figure 2-17 correctly predicted the WGR interactions with both DNA and the regulatory region in domain F.

Interestingly, it has also been recently demonstrated that the WGR motif can interact with poly(ADP-ribose) (27). Since the automodification domain is located next to the WGR motif, poly(ADP-ribose) generated by extensive automodification may result in charge repulsion and competition with DNA for binding at the WGR motif. This may cause destabilization of the activated complex even though DNA may remain bound via the N-terminal DNA binding region and lead to inactivation of PARP-1.

2.5. REFERENCES

1. Mendoza-Alvarez, H., and Alvarez-Gonzalez, R. (1993) Poly(ADP-ribose) polymerase is a catalytic dimer and the automodification reaction is intermolecular, J. Biol. Chem. 268, 22575-22580.
2. Alvarez-Gonzalez, R., and Althaus, F.R. (1989) Poly(ADP-ribose) catabolism in mammalian cells exposed to DNA-damaging agents, Mutat. Res. 218, 67-74.

3. Kristensen, T., and Holtlund, J. (1978) Poly(ADP-ribose) polymerase from Ehrlich ascites tumor cells. Properties of the purified polymerase, Eur. J. Biochem. 88, 495-501.

4. Ohgushi, H., Yoshihara, K., and Kamiya, T. (1980) Bovine thymus poly(adenosine diphosphate ribose) polymerase. Physical properties and binding to DNA, J. Biol. Chem. 255, 6205-6211.

5. Bauer, P.I., Buki, K.G., Hakam, A., and Kun, E. (1990) Macromolecular association of ADP-ribosyltransferase and its correlation with enzymic activity, Biochem. J. 270, 17-26.

6. Buki, K.G., Bauer, P.I., Hakam, A., and Kun, E. (1995) Identification of domains of poly(ADP-ribose) polymerase for protein binding and self-association, J. Biol. Chem. 270, 3370-3377.

7. Mendoza-Alvarez, H., and Alvarez-Gonzalez, R. (2004) The 40 kDa carboxy-terminal domain of poly(ADP-ribose) polymerase-1 forms catalytically competent homo- and heterodimers in the absence of DNA, J. Mol. Biol. 336, 105-114.

8. Langelier, M.F., and Pascal, J.M. (2013) PARP-1 mechanism for coupling DNA damage detection to poly(ADP-ribose) synthesis, Curr. Opin. Struct. Biol. 23, 134-143.

9. Gradwohl, G., Ménissier, de Murcia, J.M., Molinete, M., Simonin, F., Koken, M., Hoeijmakers, J.H., and de Murcia, G. The second zinc-finger domain of poly(ADP-ribose) polymerase determines specificity for single-stranded breaks in DNA, Proc. Natl. Acad. Sci. U.S.A. 87, 2990–2994.

10. Pion, E., Bombarda, E., Stiegler, P., Ullmann, G.M., Mély, Y., de Murcia, G., and Gérard, D. Poly(ADP-ribose) polymerase-1 dimerizes at a 5' recessed DNA end in vitro: a fluorescence study, Biochemistry 42, 12409-12417.

11. Langelier, M.F., Planck, J.L., Roy, S., and Pascal, J.M. (2011) Crystal structures of poly(ADP-ribose) polymerase-1 (PARP-1) zinc fingers bound to DNA: structural and functional insights into DNA-dependent PARP-1 activity, J. Biol. Chem. 286, 10690-106701.

12. Ali, A.A., Timinszky, G., Arribas-Bosacoma, R., Kozlowski, M., Hassa, P.O., Hassler, M., Ladurner, A.G., Pearl, L.H., and Oliver, A.W. (2012) The zinc-finger domains of PARP1 cooperate to recognize DNA strand breaks, Nat. Struct. Mol. Biol. 19, 685-692.

13. Mansoorabadi, S.O., Wu, M., Tao, Z., Gao, P., Pingali, S.V., Guo, L., and Liu, H.W. (2014) Conformational activation of poly(ADP-ribose) polymerase-1 upon DNA binding revealed by small-angle X-ray scattering, Biochemistry 53, 1779–1788.

14. Tao, Z., Gao, P., Hoffman, D.W., and Liu, H.W. (2008) Domain C of human poly(ADP-ribose) polymerase-1 is important for enzyme activity and contains a novel zinc-ribbon motif, Biochemistry 47, 5804-5813.

15. Schuck P. (2003) On the analysis of protein self-association by sedimentation velocity analytical ultracentrifugation, Anal. Biochem. 320, 104-124.

16. Demeler B., and van Holde K. E. (2004) Sedimentation velocity analysis of highly heterogenous systems, Anal. Biochem. 335, 279-288.

17. Brookes E., Cao W., and Demeler B. (2009) A two-dimensional spectrum analysis for sedimentation velocity experiments of mixtures with heterogeneity in molecular weight and shape, Eur. Biophys. J. 39, 405-414.

18. Schuck P., and Scott D. J. (2005) A brief introduction to the analytical ultracentrifugation of proteins for beginners, in Analytical ultracentrifugation: techniques and methods (Scott D. J., Harding S. E., and Arthur J. R. Eds.) pp1-25, Royal Society of Chemistry Publishing, Cambridge, U.K..

19. Tiselius A. (1930) The moving-boundary method of studying the electrophoresis of proteins, Nova Acta Regiae Soc. Sci. Upsal. Ser. IV 7, 1.

20. Lamm O. (1929) Die differentialgleichung der Ultrazentrifugierung, Ark. Mat. Astr. Fyr. 21B, 1-4.

21. Schuck P. (2000) Size distribution analysis of macromolecules by sedimentation velocity ultracentrifugation and Lamm equation modelings, Biophys. J. 78, 1606-1619.

22. Demeler B., Saber H., and Hansen J. C. (1997) Identification and interpretation of complexity in sedimentation velocity boundaries, Biophys. J. 72, 397-407.

23. Demeler B., and Brookes E. (2007) Monte Carlo analysis of sedimentation experiments, Colloid Polym. Sci. 286, 129-137.

24. Zhou, Y. (August, 2009) Ph.D Thesis, University of Texas at Austin

25. Ryder S.P., Recht M. I., and Williamson J. R. (2008) Quantitative analysis of protein-DNA interactions by gel mobility shift, Methods Mol. Biol. 488, 99-115

26. Langelier, M.F., Planck, J.L., Roy, S., and Pascal, J.M. (2012) Structural basis for DNA damage-dependent poly(ADP-ribosyl)ation by human PARP-1, Science 336, 728-732.

27. Huambachano, O., Herrera, F., Rancourt, A., and Satoh, M. S. (2011) Double-stranded DNA binding domain of poly(ADP-ribose) polymerase-1 and molecular insight into the regulation of its activity, J. Biol. Chem. 286, 7149-7160.

Chapter 3. DNA Recognition of Human PARP-1

Part II: Single Molecule Fluorescence Colocalization Studies

3.1. INTRODUCTION

Protein-DNA interactions represent an important molecular process which regulates a broad range of fundamental biological functions that are critical for the survival of an organism. This type of interaction may look simple as many of the DNA-binding proteins interact with DNA molecules in a sequence specific manner. However, this is not true in many cases, especially for those enzymes which participate routinely in transcription and DNA repair pathways. In eukaryotes, to interact with the DNA promoter region during transcription initiation, RNA polymerase II forms a multi-protein complex at the promoter region, with each protein subunit (i.e., specificity factor) interacting with a specific promote element (1). Here, DNA recognition of RNA polymerase II at a given promoter region is governed by its interacting specificity factors within the complex. In the base excision repair pathway, members of the glycosylase enzyme family can recognize different types of base damages based on their chemical structures (2).

Human PARP-1 is an enzyme that interacts with different DNA molecules and involves in the processes of DNA repair and transcription regulation (3). PARP-1 interacts with DNA in a sequence independent manner. DNA binding by PARP-1 often happens when it encounters a specific structural feature within the DNA molecule. Different forms of DNA damage can be recognized by PARP-1, such as single and double stranded breaks as well as DNA overhangs (4). The binding affinity of PARP-1 towards DNA depends on the structure of the DNA lesion, with stronger affinities for the single strand nicked or blunt end DNA (4).

In addition, PARP-1 activation is stimulated by the presence of DNA. However, the induced activity levels are different depending on the type of DNA lesions it encounters. As proposed by Pion et al., the difference in enzymatic activity of PARP-1 may arise from the different binding stoichiometries of PARP-1 toward different DNA lesion structures, and has little to do with the DNA binding affinities (5). This proposal was based on a series of biochemical studies, where Pion et al. concluded that PARP-1 forms a 1:1 complex with DNA molecules containing a double stranded break or a 3'-recessed end and results in low levels of activity. In the case where DNA contains a 5'-recessed end, PARP-1 forms a 2:1 protein-DNA complex, with a comparably higher level of enzymatic activity (5). In the case of blunt end DNA, this proposal is supported by crystallographic studies of the individual PARP-1 zinc fingers bound with DNA, as discussed in Section 1.3.3 (Figure 1-7). However, when a DNA molecule with a 3'-recessed end is used for crystallization, dimer formation is observed and both zinc fingers interact directly with the lesion (Figure 1-8).

Correlation between activity level and DNA structure can also be explained by engaging different functional domains of PARP-1 in DNA binding. If different DNA structures interact with different regions of PARP-1, this may perturb the overall protein conformation in different ways. Thus, PARP-1 may be able to adopt various active conformations in a DNA-specific manner resulting in different activity levels. This hypothesis is based on the fact that several domains within PARP-1 are known to interact with DNA. As discussed in Chapter 1, the N-terminal zinc fingers I and II are the primary sites for recognition of DNA damage. In the case of a single stranded break, Ikejima et al. demonstrated that both zinc fingers I and II are needed for PARP-1 activity (6). However, when a double stranded break is present, only zinc finger I is needed for full activation of PARP-1 (6). Therefore, it seems that PARP-1 utilizes different sets of zinc fingers for

activity when encountering different types of DNA damage. Recently, a so-called double stranded DNA binding domain (DsDB) was also identified. It is located in a loop region between the BRCT and the WGR motif (7). As presented in Chapter 2, the WGR motif is also involved in DNA interactions, and the flexible loop responsible for DNA interaction is important for PARP-1 activity (8). Currently, how the DsDB and WGR motifs participate in promoting an active conformation of PARP-1 is still not well understood.

Taking all the above evidence together, the two hypotheses put forth argue that there are at least three essential factors determining the activity levels of PARP-1 upon DNA binding: 1. the specific DNA structure; 2. the protein-DNA binding stoichiometry; 3. the protein regions that are in contact with the bound DNA. While many published biochemical and structural studies discussed in this thesis provide valuable insight regarding these questions, in many cases the results are contradictory among themselves. Therefore, it is hard to draw a clear conclusion regulating the DNA-dependent PARP-1 activity.

Human PARP-1 is one of the first enzymes to recognize and localize at a site of DNA damage, and its activity is essential for the recruitment of other related DNA repair enzymes at the same site (9). This makes PARP-1 an attractive drug target for cancer therapy (10). Since PARP-1 also binds to undamaged DNA and influences other fundamental biological functions, understanding the DNA recognition process of PARP-1 and how it relates to the corresponding enzyme activity level is essential for drug development to regulate DNA repair pathways.

In order to understand how PARP-1 interacts with a specific DNA structure in details, a single molecule fluorescence colocalization technique was utilized in this protein-DNA interaction study. This single molecule platform allows direct visualization of individual protein molecule interacting with a single DNA molecule in real-time. By

collecting data over hundreds of binding events on a molecule-by-molecule basis, instead of an ensemble average from multiple protein-DNA states, the distribution of each individual protein-DNA interaction state can be identified and measured directly. Thus, potential transient intermediates in the protein-DNA interaction dynamics may be identified in this way.

Here, the protein-DNA interaction process of PARP-1 is directly visualized by the colocalization of two fluorescent signals at the same spot. These two fluorescent signals are arised from the Cy3 fluorophore labeled PARP-1 DNA-binding domain AB and the Cy5 fluorophore labeled double stranded break DNA mimic which are immobilized onto a glass surface. Upon laser excitation of Cy3 fluorophores, protein binding events can be monitored in real-time by the increase in fluorescent intensity coming from Cy3 (no FRET (Förster resonance energy transfer)) or Cy5 (high FRET transfer) fluorophore emission. Duration of the colocalized Cy3 and Cy5 fluorescent intensity signal were collected from each binding event and analyzed. Dissociation kinetic analyses revealed that there are two distinct protein-DNA binding complexes in the DNA recognition process by domain AB: a long-lived, stable binding complex and a less stable binding complex which rapidly dissociates. Furthermore, results obtained from analyses of total fluorescent intensity difference between individual protein-DNA complex, and the observation of multi-step photobleaching process in many protein binding events indicate that protein dimerization occurs in the presence of DNA having double stranded break.

Finally, the choice of Cy3 and Cy5 fluorophores here are capable of Förster resonance energy transfer (FRET) process, with Cy3-labeled domain AB being the fluorescence donor and the Cy5-labeled DNA being the energy acceptor. Since Cy3 was labeled close to the zinc finger II of domain AB, direct excitation of the Cy3 fluorophore resulted in the detection of two distinct FRET states. The observed high FRET state

reveals that zinc finger II is in close proximity to the DNA lesion; whereas the low FRET state suggests that zinc finger I binds close to the lesion site. The observation of two distinct FRET states indicates that both N-terminal zinc fingers are involved in recognizing DNA double stranded break.

Information obtained from these single molecule studies has shed light on the mechanisms by which domain AB interacts with a double stranded DNA break. Results from dissociation kinetics, protein binding stoichiometry as well as FRET state analyses lead to a mechanistic proposal in regarding how PARP-1 recognizes a double stranded break lesion.

3.2. Materials and Methods

3.2.1. Site directed mutagenesis for introduction of a genetically encoded aldehyde tag into AB constructs

A bioorthogonal method developed by Carrico et al. was applied (11) to introduce a reactive aldehyde functional group into the DNA binding domain AB. This method involves insertion of the six-amino-acid consensus sequence LCTPSR, which is known as the "aldehyde tag," at a selected site. The aldehyde tag can then be recognized by a formylglycine generating enzyme (FGE) which catalyzes oxidation of the inserted cysteine residue in the "aldehyde tag" to a formylglycine.

Using the AB/MalE-pET vector as the mutation template, an aldehyde tag was introduced according to the Quikchange site-directed mutagenesis protocol (Stratagene) to generate different site specific protein constructs. The aldehyde tag was introduced at the N-terminus of domain AB using the forward (5'-CATGAAAACCTGTATTTTCA-GGGACTGTGCACCCCGAGCCGTTCGGATAAG-3') and reverse (5'-CTTATCCGA-

ACGGCTCGGGGTGCACAGTCCCTGAAAATA-CAGGTTTTCATG-3') primers, and the resulting recombinant DNA construct was named Fgly-AB/MalE-pET. A similar insertion was introduced at the C-terminus of AB using forward (5'-GACAAGGAT-AGTCTGTGCACCCCGAGCCGTTAACTCGAGCACC-3', with the inserted sequence underlined) and reverse (5'-GGTGCTCGAGTTAACGGCTC-GGGGTGCACAG-ACTATCCTTGTC-3') primers to give the final Fgly-AB-CT/MalE-pET construct. When the aldehyde tag was positioned internally, it was introduced by substitution using the cysteine residue at position 151 of domain AB. The Fgly-150AB/MalE-pET was constructed using the forward (5'-GAAGATGGTGGACCCGGAGAAGCTGTGC-ACCCCGAGCCGTGACCGCTGGTACCATCCAGG-3') and reverse (5'-CCTGGATGGTACCAGCGGTCACGGCTCGGGGTGCACAGCTTCTCCGGGTCCA CCATCTTC-3') primers. Plasmids with the desired mutation were confirmed by sequencing carried out by the DNA Sequencing Core Facility at The University of Texas at Austin.

3.2.2. Generation of aldehyde functionalized Fgly-AB constructs in vivo by coexpression with formylglycine generating enzyme (FGE)

To convert the cysteine residue within the aldehyde tag of the FGly-AB protein construct to the formylglycine (Fgly) functional group, a modified coexpression system of FGE and the Fgly-AB protein constructs was developed based on the published protocol by Carrico et al. (11).

The coexpression system was created by cloning both FGE and the MBP-Fgly-AB constructs to a single expression vector. Specifically, the FGE gene was first obtained from a DNA plasmid containing the encoded Mycobacterium tuberculosis FGE enzyme in the pBAD/myc-his A vector (Addgene). The FGE gene, which was located between the NcoI and XhoI restriction sites, was cut out by double digestion using the

aforementioned restriction enzymes. The agarose gel purified FGE gene was then ligated into the pET-28b vector that had been treated with the same restriction enzymes to generate the His_6-FGE/pET expression vector.

The MBP-Fgly-AB gene in the construct of Fgly-AB/MalE-pET lies between the XbaI and XhoI restriction sites within the MalE-pET vector. Therefore, both the Fgly-AB/MalE-pET and His_6-FGE/pET plasmids could be treated with XbaI and XhoI restriction enzymes in order to cut and insert the MBP-Fgly-AB gene into the His_6-FGE/pET vector. However, this approach could lead to loss of the FGE gene during the restriction enzyme treatment. To keep the FGE gene in place, a SpeI digestion site was introduced between the stop codon of the FGE gene and the neighboring XhoI digestion site. As the flanking region (3'-GATC-5') generated by the SpeI restriction enzyme digestion is complementary to the flanking region (5'-CTAG-3') generated from the XbaI enzyme, this allowed the MBP-Fgly-AB gene to be cleaved out by the treatment with the XbaI and XhoI restriction enzymes, whereas the His_6-FGE/pET vector could be linearized by treatment with the SpeI and XhoI restriction enzymes without losing the FGE gene. Subsequent ligation of the MBP-FGly-AB and the linearized His_6-FGE/pET DNA fragments generated the final His_6-FGE/MBP-Fgly-AB/pET expression vector construct.

In order to insert the SpeI digestion site into the His_6-FGE/pET vector, the FGE gene was cloned from the His_6-FGE/pET vector by PCR using the forward (5'-GGAATTCCATATGCTGACCGAGTTGGTTGACC-3') and reverse (5'-CCGCTC-GAGACTAGTCTACCCGGACACCGG-3') primers, where the SpeI site within the reverse primer is shown underlined. The PCR product was subjected to NdeI and XhoI restriction enzyme digestion, and further purified by QIAprep Spin Miniprep Kit (Qiagen). The purified product was cloned into the pET/28 vector that had been

linearized by the same set of restriction enzymes. The insertion of the SpeI site within the final His_6-FGE-SpeI/pET plasmid was confirmed by sequencing.

To generate the coexpression vector, the His_6-FGE-SpeI/pET vector was linearized by first treating with SpeI and XhoI restriction enzymes followed by CIP. The high molecular weight DNA fragment was purified by 0.8% agarose gel electrophoresis. The MBP-Fgly-AB insert was obtained by treating the Fgly-AB/MalE-pET vector using XbaI and XhoI restriction enzymes, and the low molecular weight DNA fragment was purified similarly as described before. Ligation was then carried out to generate the His_6-FGE/MBP-Fgly-AB/pET vector. The same method was applied to generate the following expression constructs: His_6-FGE/MBP-Fgly-AB/pET, His_6-FGE/MBP-Fgly-AB-CT/pET and His_6-FGE/MBP-Fgly-150AB/pET.

3.2.3. Expression and purification of Fgly-tagged domain AB constructs

Coexpression and purification of the His_6-FGE and the Fgly-AB proteins was done in a manner similar to that described for the wild type PARP protein constructs in Section 2.2.1. The formyglycine within the Fgly-AB protein was formed in vivo, and the expressed His_6-FGE enzyme was readily removed during the purification process. Therefore, the resulting purified proteins were formylglycine functionalized: Fgly-AB, Fgly-AB-CT and Fgly-150AB.

3.2.4. Confirmation of the formylglycine (Fgly) functional group within the protein constructs by biotin-hydrazide labeling

The N-terminal Fgly-AB construct was used as a prototype, and the wild type AB protein was used as the negative control to confirm that the Fgly functional group was generated in vivo. In a 200 μL reaction mixture, 50 or 100 μg of protein was incubated with 300 μM of DMSO solublized biotin hydrazide (Sigma Aldrich) in 100 μM MES

buffer, pH 5.5. The reaction mixture was incubated at 37 °C for 2 h. The unreacted biotin hydrazide was removed by filtering the reaction mixture using the 10 kDa Cutoff Amicon® MLtra 0.5 mL filters (Millipore) and then washed 10 times with 300 μL of 100 mM HEPES and 10% glycerol at pH 7.5. The samples were resolved using 12% SDS-PAGE gels. Detection of the biotinylated proteins was performed using western blot with HRP-conjugated Streptavidin antibody (Pierce). Colorimetric development was done using 1-step TMB-Blotting substrate solution (Pierce).

3.2.5. Cy3-labeling of Fgly-tagged AB protein constructs

Initially, Alexa Fluor® 555 Hydrazide (Life Technologies) was chosen for protein labeling due to its commercial availability and high photostability. However, it was observed that this fluorescent probe has poor photostability under the experimental condition of single molecule studies. Later on, the choice of fluorescent dye was switched to Cy3-hydrazide (GE Healthcare), and it was used as the FRET donor fluorophore for protein labeling. Typically, 30 μM of Fgly protein was incubated with 480 μM of Cy3-hydrazide in 100 μM MES buffer at pH 5.5 (total volume: 200 μL). To stabilize the proteins, 10% glycerol was also added in the buffer, and the reaction mixture was incubated at 37 °C for 2 h. Next, the sample was dialyzed against 20 mM HEPES, 300 mM NaCl, and 10% glycerol at pH 7.5. Three changes of the 500 mL dialysis buffer were performed for each Cy3-labeled protein construct. The final concentration of both the protein and Cy3 dye was determined by UV absorbance using a nanodrop spectrophotometer (Nanodrop). A typical labeling efficiency was about 60%. The protein sample was flash frozen with liquid nitrogen and stored at –80 °C before usage.

3.2.6. Preparation of fluorescent DNA ligands

All single stranded DNA ligands were purchased from IDT. Individual sequence information is listed in Table 3-1. The complementary DNA strands were annealed under similar conditions as described in Section 2.2.7 in order to produce the single stranded break mimic, which is a DNA duplex with a gap in the middle of the sequence (66G), and the double stranded break mimic 32B. Information about the biotinylated and Cy5-labeling sites is shown in Figure 3-1.

Table 3-1. DNA primers used for fluorescence experiments.

DNA duplex	DNA primers used	Primer sequence
66G	66bpR	5'-AAGGGCAAGGCTGCTGTGGACCCTGCTGTGGGCTGGAGAACAAGGTGATCTGCGCCCTGGTCCTGG-3'
	33bp	5'-GCCCACAGCAGGGTCCACAGCAGCCTTGCCCTT-3'
	32bp	5'-CCAGGACCAGGGCGCAGATCACCTTGTTCTCC-3'
32B	32bp	5'-CCAGGACCAGGGCGCAGATCACCTTGTTCTCC-3'
	32bp-2	5'-GGAGAACAAGGTGATCTGCGCCCTGGTCCTGG-3'

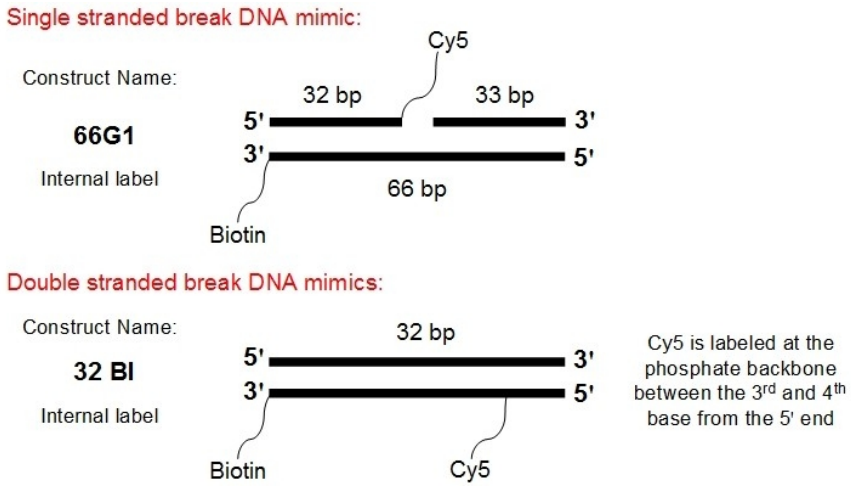

Figure 3-1. A. Nomenclature of the DNA constructs used in the fluorescence assay, with positions of biotin and Cy5 labels being specified for each tested construct.

3.2.7. Electrophoretic mobility shift assay (EMSA)

Different amounts of AB or Fgly-AB protein constructs (0 to 2.048 μM) were incubated with 4 nM of Cy5-labeled DNA duplex on ice for 20 min in 15 μL of 20 mM Tris buffer, pH 8.0, containing 150 mM KCl, 5 mM $MgCl_2$, 50 μM $ZnCl_2$, 0.1% Nonidet P40, 2 mM DTT and 10% glycerol. The samples were then mixed with 6X DNA loading buffer (0.25% bromophenol blue and 15% Ficoll 400) and subjected to electrophoresis in a dark room. An 8% native polyacrylamide gel (acrylamide/bisacrylamide ratio 75:2) was prepared with tris-glycine buffer (24.9 mM Tris/191.8 mM glycine, pH8.3) and used for the EMSA assay. The gel was pre-run at 100 V for 2 hrs at room temperature with an ice water cooling system before sample loading. After electrophoresis, the gel was visualized using a Typhoon Trio Scanner (GE Healthcare) with red laser excitation (633 nm), and the image was processed using Quantity One software (Bio-Rad).

3.2.8. Single molecule fluorescence colocalization experiments

3'-Biotinylated Cy5-DNA duplexes were immobilized onto a quartz slide surface through streptavidin conjugation. This was done by first preparing the biotinylated quartz slide through passivation with a mixture of methoxy polyethylene glycol (mPEG) and biotinylated mPEG (1-2%), which allowed streptavidin immobilization on the glass slide. A typical imaging chamber (about 0.5 cm x 1.5 cm) sealed with double-sided tape was formed between the quartz slide surface and a cover slip. Typically, a 50 μL sample of 50 pM DNA duplex in the loading buffer containing 50 mM Tris, pH 8.0 and 250 mM NaCl was loaded onto the glass surface that had been pre-treated with streptavidin. Unbound DNA was washed out using loading buffer. Various concentrations of Cy3-labeled Fgly-AB proteins in a buffer containing 50 mM Tris, pH 8.0, 25 mM NaCl, 22.5 mM DTT and 22.5 mM $MgCl_2$ was loaded onto the chamber for imaging. To slow down the photobleaching process, an oxygen scavenging system was mixed with the Cy3-labeled

proteins during imaging. The oxygen scavenging system consisted of 0.6 mM Trolox, 8% glucose, 0.05 mg/mL catalase and 0.1 mg/mL glucose oxidase. PEGylated glass slides, the oxygen scavenging system, and access to a total internal reflection (TIR) microscope platform were all provided by Prof. Rick Russell in the Institute for Cellular Molecular Biology at The University of Texas at Austin.

Protein-DNA complex formation events were imaged by mounting the imaging chamber beneath the prism-type total internal reflection (TIR) microscopy which consists of an inverted Olympus IX-71 microscope connected to an I-PentaMAX IIC CCD camera with a cooling unit (Princeton Instruments). For the colocalization experiment, the Cy3-labeled protein was directly excited with a 532 nm laser (Crystalaser). This was conducted through continuous Cy3 excitation with 10 frames/s data acquisition for 90 s, or it was done with 2 s on/2 s off pulse excitations for a total excitation time of 300 s with 1 frame/s data acquisition. At the end of each movie, the Cy5 dye was excited with a 637 nm laser (Coherent) for 10 s to locate the positions of the immobilized DNA and confirm protein colocalization with Cy5-labeled DNA. Movies were taken randomly from several fields of view for each protein concentration.

3.2.9. Single molecule fluorescence colocalization data analyses

Fluorescence signals generated from each field of view were splitted into Cy3 (donor) and Cy5 (acceptor) intensity signals by a pair of dichroic mirrors. Colocalized signals from Cy3 and Cy5 dyes were matched using an affine transformation that was based on predetermined fiducial markers using fluorescent nanobeads (12). Raw intensity time traces of the colocalized Cy3 and Cy5 signals were generated for each movie using the single molecule data analysis program written by Dr. Brian Cannon. For the pulse-excitation experiments, individual binding events were identified based on the appearance

and disappearance of the Cy3 and Cy5 signals above background threshold. For each individual binding event, the intensity changes of the Cy3 and Cy5 signals as well as the dwell time for each binding event were extracted for kinetic, total intensity and FRET analyses.

3.3. RESULTS

3.3.1. Generation of formylglycine (Fgly)-tagged AB constructs

To generate a domain AB protein construct that can be labeled with a fluorescent dye in a site specific manner for the single molecule fluorescent study, a genetically encoded formylglycine (Fgly) tag was utilized based on the method developed by Carrico, et al. (9). Specifically, the six-amino-acid sequence LCTPSR, which represents the “aldehyde” tag, was introduced into a defined region within domain AB. This short amino acid sequence can be recognized by the formylglycine generating enzyme (FGE) from Mycobacterium tuberculosis, and the cysteine residue within this aldehyde tag is converted to a formylglycine functional group by FGE. Generation of the Fgly functional group in the domain AB constructs allow modification with hydrazide functionalized probes, such as biotin hydrazide or Cy3-hydrazide (Figure 3-2).

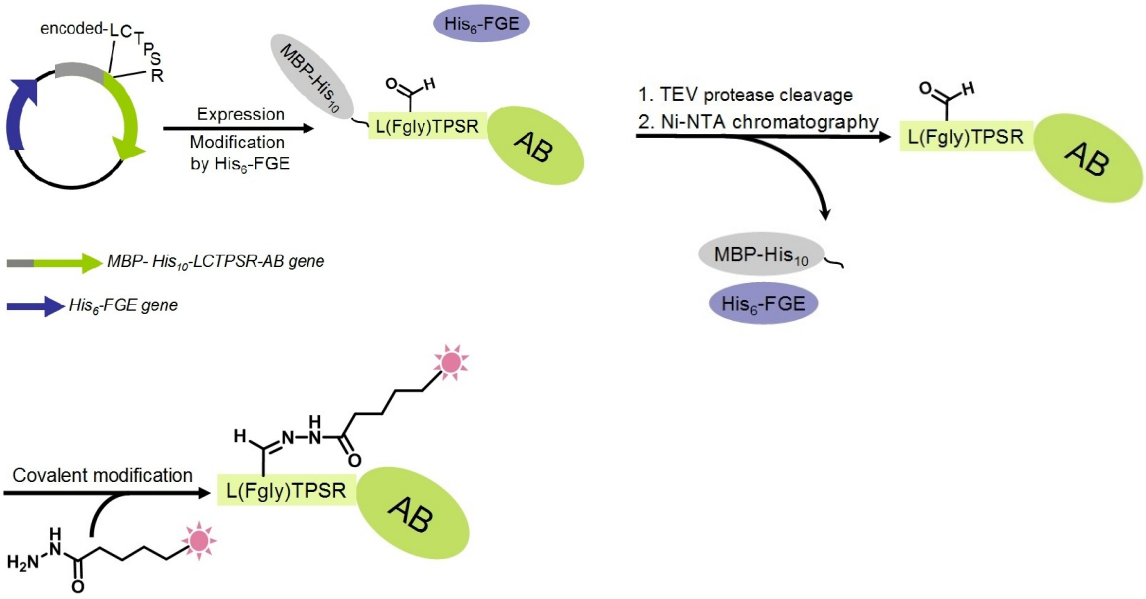

Figure 3-2. In vivo generation of the Fgly functional group within AB constructs and subsequent labeling with hydrazide functionalized fluorescent probes used in this study.

Formation of the formylglycine functional group within an Fgly-AB construct took place in vivo during coexpression of the Fgly-AB and His_6-FGE proteins. After that, the His_{10}-maltose binding protein (i.e., MBP-His_{10}) was cleaved from the MBP-Fgly-AB constructs and removed along with the His_6-FGE protein by Ni-NTA resin (Figure 3-2). The purities of the resulting Fgly-AB protein constructs are shown in Figure 3-3A.

A. B.

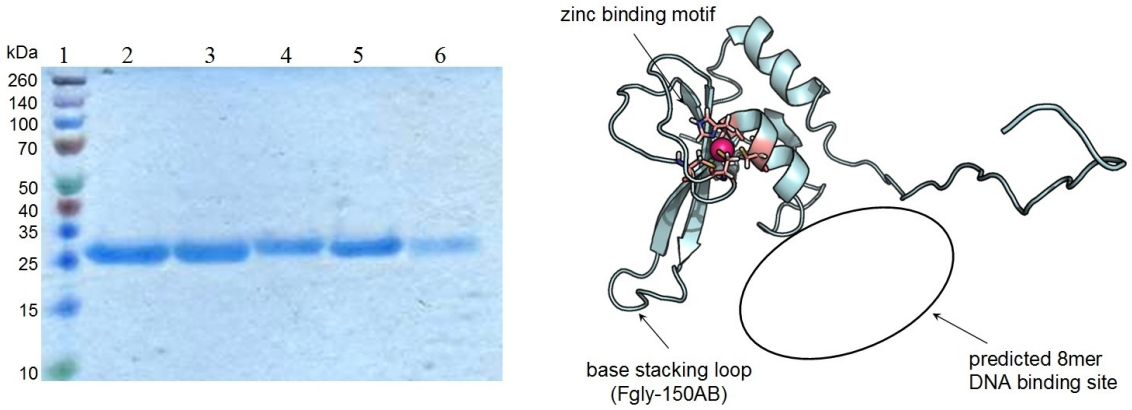

Figure 3-3. A. An SDS-PAGE gel showing typical protein purities of domain AB wild type (lane 2), Fgly-AB (lane 3), Fgly-AB-CT (lane 4), Fgly-150AB (lane 5) and Fgly-210AB (lane 6) after purification. B. Indication of the internally labeled Fgly-tag position within zinc finger II (PDB ID:2CS2).

To study the DNA recognition of PARP-1 zinc fingers toward DNA lesions by single molecule experiments, the protein-DNA pairs used were designed to exhibit Förster resonance energy transfer (FRET) once positioned in close proximity. To obtain good FRET response, the location of the fluororphore labeling sites within the protein and DNA are important. It was expected that, upon excitation of the Cy3 donor labeled domain AB which binds to the lesion site of the DNA labeled with the acceptor fluorophore Cy5, the close proximity between the Cy3 and Cy5 fluorophores should allow energy transferred from Cy3 to Cy5, producing FRET signal. The FRET signal could be detected by monitoring the increase in Cy5 fluorescent intensity. The potential

fluctuation in FRET signal would provide information of the protein-DNA interaction in terms of the proximity of protein binding relative to the lesion sites, as well as the binding kinetics for the protein-DNA complex formation.

In addition to the N- and C-terminally labeled domain AB protein constructs, a formylglycine functional group was also introduced within zinc finger II. This was done because of the strong binding affinity of zinc finger II toward DNA lesions. Its direct interaction with DNA is expected to give an easily detected signal. It should be noted that, at the beginning of this project, there was no crystallographic information available on how PARP-1 or individual domains interact with DNA lesions that can serve as guidance for the design of the fluorescent labeled protein. Therefore, the choices of formyglycine labeling positions within zinc finger II were based on the preliminary small-angel X-ray scattering data and the molecular dynamics simulations of PARP-1 and 8-mer DNA kindly provided by Dr. Steven O. Mansoorabadi. The internal labeling sites for formylglycine in zinc finger II are shown in Figure 3-3 B.

3.3.2. Confirming the presence of the formyglycine (Fgly) group within Fgly-AB

To confirm whether the Fgly functional group was generated in vivo from the coexpression system described above, a labeling test was done using the N-terminal tagged Fgly-AB construct and biotin hydrazide. After the conjugation reaction, the biotinylated protein was detected by HRP-conjugated Streptavidin antibody and western blot. As shown in Figure 3-4, lanes 8 and 9, biotin was conjugated into Fgly-AB successfully, indicating that the formylglycine functional group was present in the Fgly-AB construct. No biotin signal was detected in the case of wild type domain AB incubated with biotin hydrazide under the same condition (Figure 3-4: lanes 4-5). Based

on the observations discussed here, introduction of the formylglycine tag into domain AB was successful using the coexpression system; and the biotin labeling was specific to the Fgly-tagged domain AB.

Lane	1	2	3	4	5	6	7	8	9
Biotin hydrazide (μM)		0	0	300	300	0	0	300	300
Fgly–AB (μg)		0	0	0	0	100	100	50	100
AB (μg)		100	100	50	100	0	0	0	0

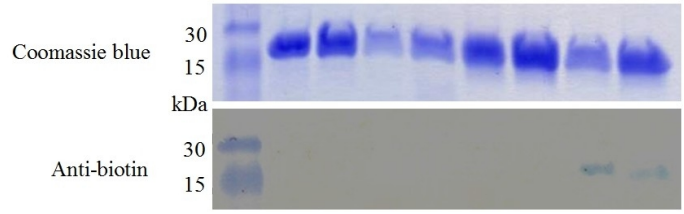

Figure 3-4. Existence of the Fgly-tag within domain AB was confirmed by biotin hydrazide labeling assay. Details of labeling conditions for each sample lane are listed. Noted that lanes 2 and 6 are protein samples taken directly from stocks. Lanes 3 and 7 are protein samples undergoing the whole labeling process to test for potential protein degradation.

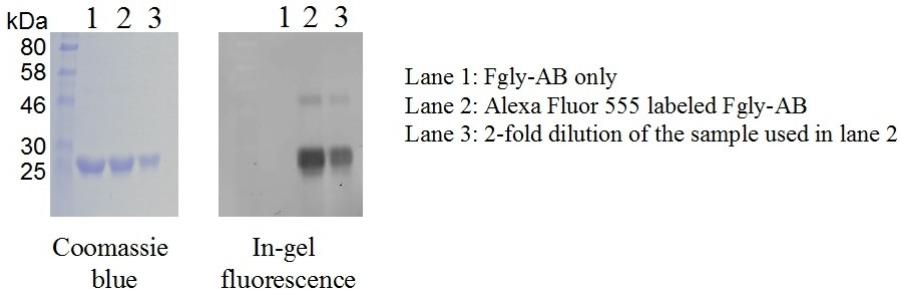

Figure 3-5. Fgly-AB protein labeled with Alexa Fluor® 555 hydrazide. Coomassie blue staining of the SDS-PAGE gel is shown on the left. Presence of the fluorescent probe in the SDS-PAGE gel was detected by a 532 nm laser excitation using a Typhoon scanner, and the resulted in-gel fluorescence is shown on the right.

Once the coexpression system proved to be working, domain ABs with Fgly-tag inserted at different positions were expressed and purified. They were then labeled with appropriate fluorescent dyes that serve as the FRET donor. Alexa Fluor® 555 hydrazide

was chosen for protein labeling here due to its commercial availability and high photostability. An example of successful fluorophore labeling of Fgly-AB is shown in Figure 3-5. To check if the protein-fluorophore linkage is covalent, proteins used for in-gel fluorescence were denatured with SDS and boiling before loading onto the gel. Association of the fluorescent signal with a correct molecular weight band of Fgly-AB suggested that the fluorophore-protein conjugation is covalent. It should be noted that there is a fluoresecent protein band likely coming from protein contaminants in the Fgly-AB samples (Figure 3-5). This band is hardly seen using Coomassie blue staining, and its identity remains elusive. While fluorescent labeling of the contamination protein band may indicate that the labeling protocol is nonspecific, it is also possible that this protein band may be a degraded fragment of the MBP-Fgly-AB construct during protein purification based on the following reasons. Before trying the coexpression system discussed above, two other methods were tried but unsuccessful in generating the formyglycine functional group within the Fgly-AB construct. One of them was in vitro generation of formylglycine by incubating the Fgly-AB construct with purified His_6-FGE enzyme. Another method was the coexpression method reported by Carrico et al. which utilized two plasmids harboring the Fgly-AB and the FGE genes separately (11). While the generation of formylglycine was not successful in these two cases, no fluoresecent labeled protein could be detected after filtering out the unreacted dyes from the reaction mixture, and the biotin hydrazide labeling tests were also failed in these two cases. Secondly, based on the biotin hydrazide labeling test shown in Figure 3-4, wild-type AB without the Fgly-tag is not labeled, suggesting that the biotin labeling is specific to the presence of the formyglycine functional group. Finally, when high concentration of this Fgly-AB construct was analyzed by SDS-PAGE and Coomassie blue staining, additional contamination bands were discernible on the gel. These were from the residual MBP-

His_{10} fusion protein that had not been completely removed by Ni-NTA resins. However, these contamination bands showed no fluoresecence in the in gel fluoresecence test. Therefore, it was suspected that the observed fluoresecently labeled contamination band is related to the degradation of the MBP-Fgly-AB construct during purification. Because this contamination problem happened occasionally, purification by size exclusion chromatography was often included as the last step in the Fgly-AB protein purification protocol.

While Alexa Fluor dye was used in the initial stage of the single molecule experiments, it was found that this fluorescent probe exhibited poor photostability under the single molecule platform used in our experiments. Therefore, the fluorescent probe was switched to the Cy3 and Cy5 FRET pair. As a fluorescent donor, Cy3-hydrazide was used to label Fgly-AB proteins for all later experiments.

3.3.3. DNA binding abilities of the Cy3-labeled Fgly-AB protein constructs

The Fgly-tag was introduced into domain AB through mutagenesis. To test whether these mutational changes had any effect on the DNA binding abilities, electrophoretic mobility shift assays (EMSA) were performed using the Cy3-labeled protein constructs and the Cy5-labeled 66G1 DNA (Figure 3-1). The EMSA results from all Fgly-AB constructs are shown in Figure 3-6, with the wild type domain AB serving as a positive control for comparison. While the unbound free DNA migrated to the bottom of the gel, distinct band shifts indicated the formation of high affinity protein-DNA complexes, and the smearing effect during electrophoresis resulted from protein-DNA complexes that are more dissociable (11). Based on the results shown in Figure 3-6, all Fgly-AB protein constructs are capable of interacting with 66G1 DNA to some extent, as indicated by the observation of similar protein-DNA band shifts as well as smearing

effects. Due to the smearing nature arised from the protein-DNA complex dissociation, it is hard to accurately quantify the fraction of DNA bound with protein in this assay. Therefore, dissociation constants (K_d) were not determined. The EMSA assays presented here serve as a qualitative assessment of the effect of mutation. In conclusion, the introduction of the Fgly-tag at different positions of domain AB does not affect its DNA-binding ability; therefore, these protein constructs are suitable for the single molecule experiments in the protein-DNA interaction studies.

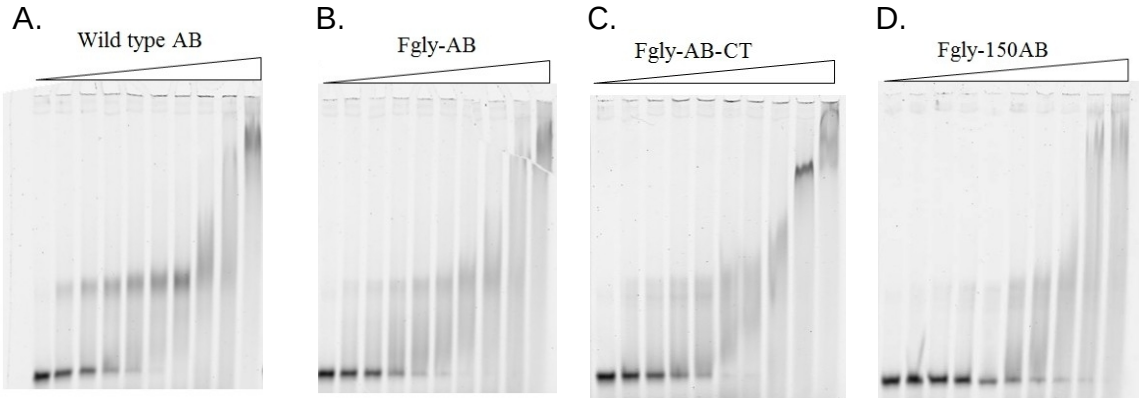

Figure 3-6. DNA-binding ability test of different Fgly-AB protein constructs using Cy5-labeled 66G1 as the DNA counterpart. DNA concentration (4 nM) stayed constant in all lanes, and the protein-DNA titration ratios increased from left to right of the gel (0:1, 2:1, 4:1, 8:1, 16:1, 32:1, 64:1, 128:1, 256:1, 512:1). A. wild type domain AB; B. Fgly-AB; C. Fgly-AB-CT; D. Fgly-150AB.

3.3.4. Fluorescence colocalization experimental set up of domain AB and DNA

To study the DNA binding process of domain AB in a single molecule platform, both protein and DNA were first labeled with different fluorescent dyes. The biotinylated Cy5-labeled DNA was then immobilized onto the glass surface through a biotin-streptavidin complex (Figure 3-7). After immobilization, Cy3-labeled AB protein was loaded onto the slide surface; and Cy3-labeled AB protein was excited by a 532 nm laser

source in a pulse manner (2 s on, 2 s off), with a total excitation time of 300 s. Positions of the Cy3-labeled AB molecules were monitored in real time, and localized fluorescent signals were recorded for both Cy3 and Cy5 channels simultaneously. After 300 s Cy3 excitation, the locations of DNA molecules were determined by Cy5 excitation with a 637 nm laser for 10 s. The latter step causes photobleaching of the Cy5 dye; this was then used to count the number of DNA molecules within a given spot for later data analyses. The colocalized Cy3 and Cy5 signals were matched based on a calibration file generated using fluorescent nanobead markers (Figure 3-7B). Once the colocalization spot was determined for each molecule, Cy3 and Cy5 fluorescent intensity trajectories can be generated for a given spot. An example is shown in Figure 3-7C.

Based on the Cy3 and Cy5 intensity trajectories, multiple pieces of information can be obtained associated with each individual binding event. Duration (t_{on}) of the protein binding event (i.e., dwell time "on") (Figure 3-7C) is defined by the appearance and disappearance of either Cy3 or Cy5 signal compared with a background signal threshold. While the appearance of Cy5 signals indicated the presence of a high FRET state, majority of the binding events showed no FRET signal, with only Cy3 signals being observed. But they were still counted as binding events. This is because the appearance of Cy3 fluorescent signal came from the Cy3-labeled protein molecule that colocalized with a single DNA molecule immobilized on the glass surface (13). For each individual binding event, the corresponding Cy3 and Cy5 intensities were obtained and used to calculate the FRET efficiency. The calculated FRET efficiency provides information on the relative distance between the Cy3 and Cy5 fluorophores. When the Cy3 labeling position of the Fgly-AB is near the zinc finger II region, the FRET efficiency thus allows identification of the interaction region between domain AB and the DNA lesion site for an individual binding event. Finally, by counting the number of photobleaching steps as

well as analyzing the change of total intensity for a given binding event, protein stoichiometry for each binding events can be extracted from the data set (13).

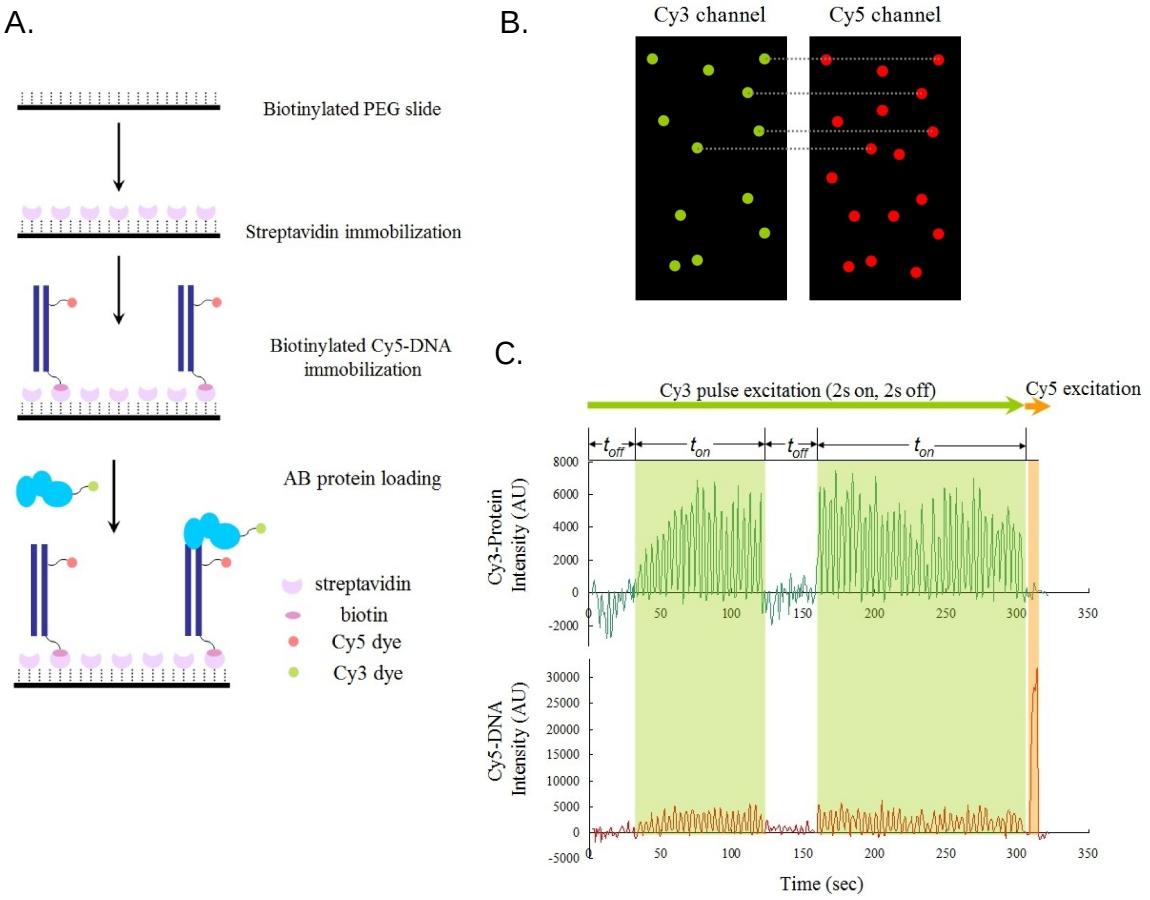

Figure 3-7. Single molecule colocalization experimental set up. A. Once the Cy5-labeled DNA was immobilized, Cy3 (or Cy5 if FRET occurs) signals would show up if domain AB binds to the DNA molecule during Cy3 pulse excitation. B. During data recording, both Cy3 and Cy5 signals were reported in a field of view and the colocalized signals between two channels were mapped (gray lines) using a calibration file. C. Cy3 and Cy5 signals associated with a given spot were extracted as intensity trajectories over time. The existence of DNA was confirmed by direct Cy5 excitation at the end of the movie.

As a selection criterion, time trajectories with no associated Cy5 signal through out the experimental time course were excluded for data analyses because no DNA

molecule was identified. Furthermore, to check whether Cy3-labeled domain AB would bind nonspecifically to the glass surface and generate artifact data, a control experiment was done by loading fluoresecently labeled AB under the same experimental condition, except that no DNA was immobilized. Movies were taken under Cy3 continuous excitation. It was noted that no Cy3 signal was localized and retained within the field of view, indicating that domain AB does not bind to the glass surface in the absence of immobilized DNA.

3.3.5. Binding kinetic studies of Cy3-AB-CT and 32BI DNA

Data present in this section was collected using an Fgly-AB-CT protein construct labeled with Cy3 at the C-terminal end (i.e., Cy3-AB-CT), and a 32-base pair blunt end DNA construct with a Cy5 fluorophore labeled internally at the phosphate backbone between the 3rd and 4th residues (i.e., Cy5-32BI) (Figure 3-8A). During the Cy3 pulse excitation experiment, binding and dissociation of Cy3-AB-CT was observed as the fluctuating of Cy3 and Cy5 signals between the elevated "on" state and the baseline "off" state (Figure 3-7C). The goal here was to see if there are multiple DNA-binding modes that are discernible from the "on" state in this data set, and if so, what mechanistic information does each binding mode reveal. From the initial screenings of all intensity trajectories, different signal response patterns could be detected (Figure 3-8B to K). It is hard to account for all these observations by a simple one- or two-step DNA-binding model. However, from all binding events identified, it was clear that some of events have high FRET signals with only Cy5 signals being detected (i.e., acceptor only, Figures 3-8J to K, and M). The rest of the binding events are associated with no FRET or low FRET signals, with an average FRET efficiency of a given binding event being less than 1 (Figures 3-8B to H, and L). For those binding events, their colocalization with DNA

molecules were confirmed by the presence of DNA molecule at the same spot through direct Cy5 excitation at the end of the movie (Figure 3-7C).

With little information regarding the details in binding mechanism of domain AB toward blunt end DNA in published literatures, it was hard to postulate how many different binding modes would be observed from the single molecule experiment. To initiate data sorting, simple criteria were set for categorizing the observed binding events from the intensity trajectories. Images shown in Figure 3-8B to M are simplified signal response patterns representing different binding events observed in the Cy3-AB-CT/Cy5-32BI data set. All binding events were separated into two groups: donor events (shaded green in Figures 3-8B to I, and L) and acceptor events (shaded red in Figures 2-8I to K, and M). In the cases of Figures 3-8G and H, there were rapid changes between high FRET and low FRET states, and they were correlated with each other. As there were no proper models proposed that can account for these observations, they were treated as donor events for the time being. In the case of Figure 3-8I, since there was no direct correlation between the low FRET and high FRET state, they were treated as individual donor only and acceptor only events. Observed binding events like in Figure 3-8I may be due to two proteins binding to the same DNA, which will be discussed in more detail in a later section. Furthermore, binding events with multiple photobleaching steps were also observed (Figure 3-8L-M). This signal response patterns indicated that there were two protein molecules binding to a single DNA strand, with one protein dissociated (or photobleached) followed by another. For simplification, they were considered as a single binding event in our analysis. It should be note that, based on this signal response pattern, it can not distinguish whether the disappearance of the fluorophore signal is due to photobleaching or protein dissociation.

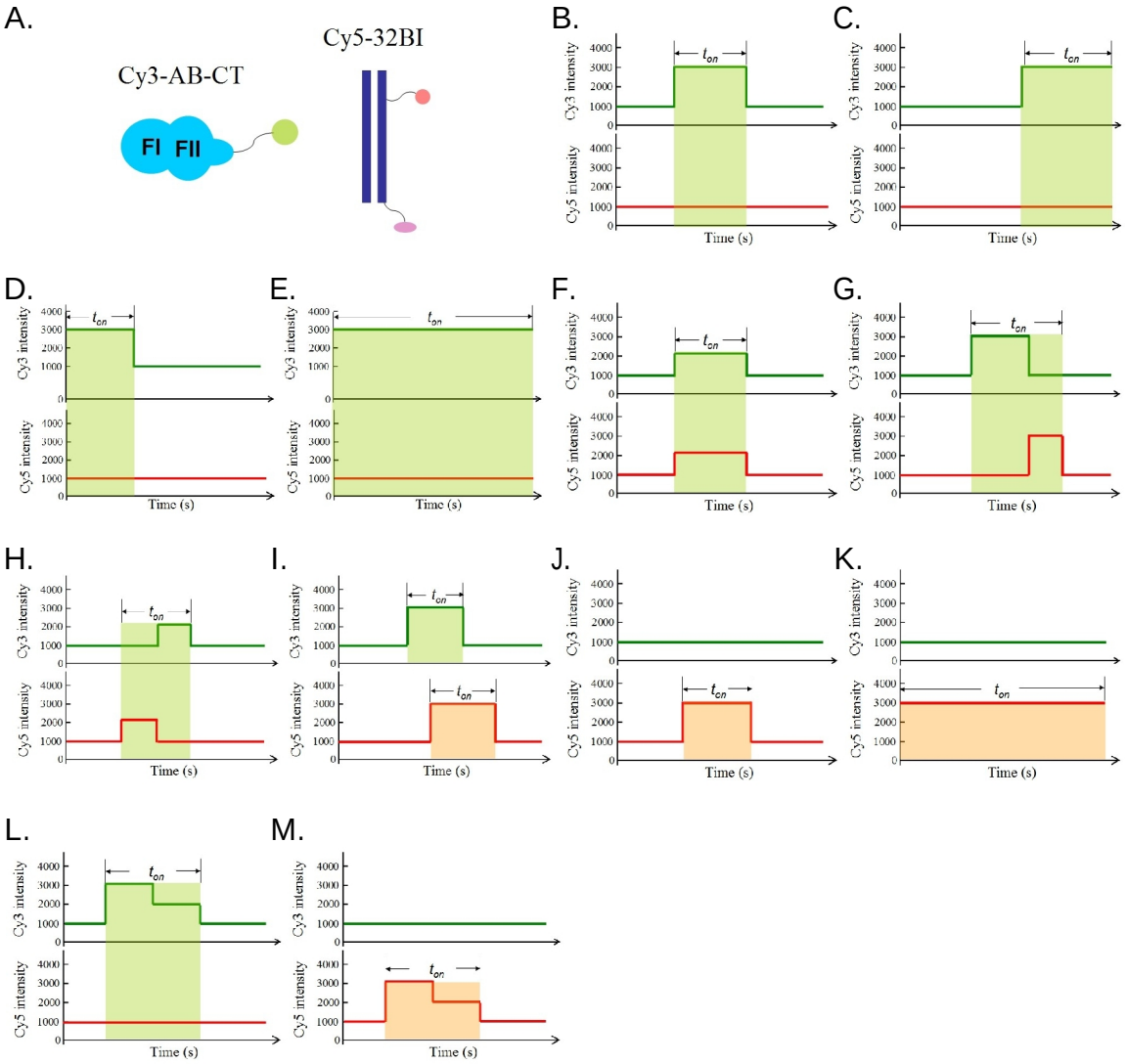

Figure 3-8. A. The Cy3-labeled AB and the Cy5-labeled DNA constructs used for this study. B to M. Cartoon representations of signal response patterns being observed in the intensity trajectories from this study, with hypothetical background intensity shown as 1000.

Following the criteria for binding event identification as described above, duration (i.e., dwelling time t_{on}) of all identified binding events were recorded, and the number of events were counted based on their corresponding dwelling time intervals. The numbers of accumulative binding events were then plotted against duration time. The accumulative dwell time distribution plot was fitted with exponential growth curves in

order to identify different modes of protein binding state. The data fitting also allows estimation of the dissociation rate constants for the identified binding modes. In this protein-DNA binding system, two different states are expected if this is a single step transition system: an off state and a single on state (Scheme 3-1). The off state was referred to the time period when no protein binding is occurred on a DNA molecule, and the on state was referred to the time when protein associates, as indicative by the appearance of Cy3 or Cy5 intensity signals in the time trajectories. Each state is characterized by the off time (t_{off}) and the on time (t_{on}), respectively (Figure 3-7C).

Based on the sedimentation velocity experiments discussed in Chapter 2, there are two protein molecules interact with a blunt end DNA. This leads to the proposal that two different binding states may exist for the on state: with one binding state having a single protein binds to the DNA, and the other binding state having two protein molecules associated with the DNA. Because it is unknown whether the second protein binding event is dependent on the DNA association with the first one, two different protein binding schemes are proposed here. Scheme 3-2 suggests that the second binding state (i.e., binding state b) depends on the existence of the first state a. Scheme 3-3 suggests that the binding state b is independent of the state a. Also, it should be noted that, for the kinetic analyses here, the numbers of AB protein molecules in binding states a or b are not known because the total Cy3 intensity of each binding event was not taken into account in this kinetic analysis.

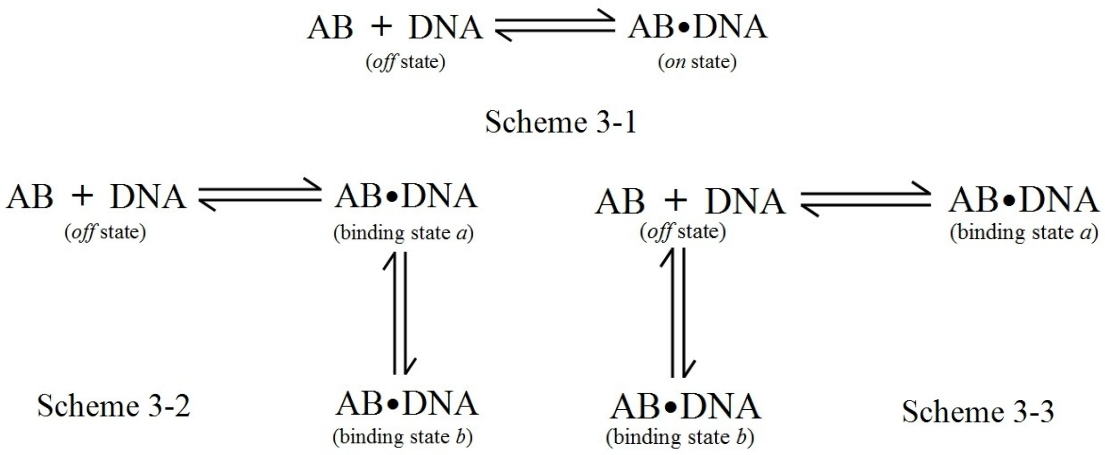

Figure 3-9. Proposed binding mechanisms of domain AB toward blunt end DNA (Cy5-32BI).

The dwell time (t_{on}) distribution analyses performed in this section may provide information that helps to distinguish the different protein binding schemes shown above. To identify the number of binding states from the collected data, dwell time (t_{on}) distribution histogram was generated using t_{on} data collected in different protein loading concentrations. Each binding state indentified is characterized by a dissociation rate constant k_{off}, and the lifetime τ of the corresponding binding state is defined as $1/k_{off}$. Based on the schemes shown in Figure 3-9, it is expected that there can be either one or two binding states. Since each protein binding happens at random, the life time of a given binding state is described by a probability distribution. The lifetime of a given binding state would follow an exponential probability distribution with a mean at $1/k_{off}$ (13). In a system having N states, the dwell time distribution is characterized by a sum of N exponentials (13). The dwell time (t_{on}) distribution was plotted, with the Y-axis representing the accumulative numbers of all binding events. Assuming there is a single binding state, the data was fitted with a single exponential growth curve. For comparison purpose, the data was also fitted with double exponential growth curves assuming the

existence of two different binding states. Single and double exponential fittings of dwell time distribution for all four Cy3-AB-CT loading concentrations are shown in Figures 3-10A to D.

As shown in Figure 3-10A to D, the dwell time (t_{on}) cumulative distributions fit better with the double exponential growth curve across different protein loading concentrations, indicative of two different protein binding states. These two binding states showed different kinetic behaviors. One of the binding state showed fast dissociation kinetics, with a dissociation rate k_{off} ranging from 0.420 s^{-1} to 0.626 s^{-1} deduced from fitting different protein concentrations. The other binding state exhibited slow dissociation kinetics, with a k_{off} value ranging from of 0.014 s^{-1} to 0.008 s^{-1} fitted from different protein concentrations. The observation of two binding states is consistent with the proposed Scheme 3-2 and Scheme 3-3.

In addition, the number of events associated with each binding state is reported as amplitude (A_1 and A_2) from the data fitting. This allows calculation of population percentage of events associated with each binding state, and can also be used to investigate how the population changes between the two states when the protein concentration is increased. As shown in Figure 3-10F, the population percentage of a binding state that exhibiting fast dissociation decreased as the protein loading concentration increased; in contrast, the binding state which dissociated slowly became predominant as protein concentration increased. These observations suggest that the occurrence of these two binding states is dependent on the protein concentration.

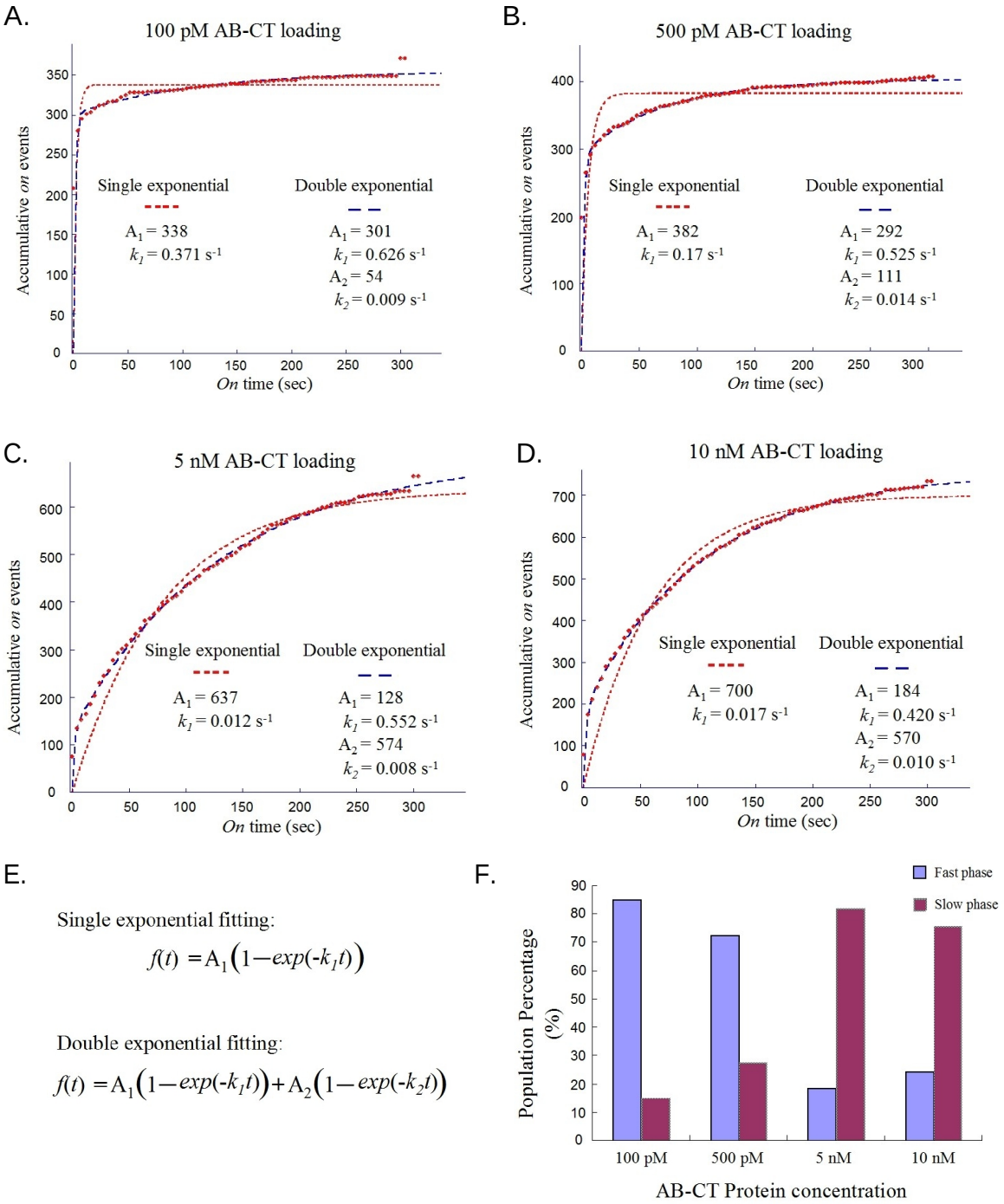

Figure 3-10. A-D. Dwell time (t_{on}) accumulative distribution fitting of different Cy3-AB-CT protein loading concentrations with single or double exponentials. Data points were shown as red dots. E. Equations used for distribution. F. Concentration-dependent occurrences of two different on states.

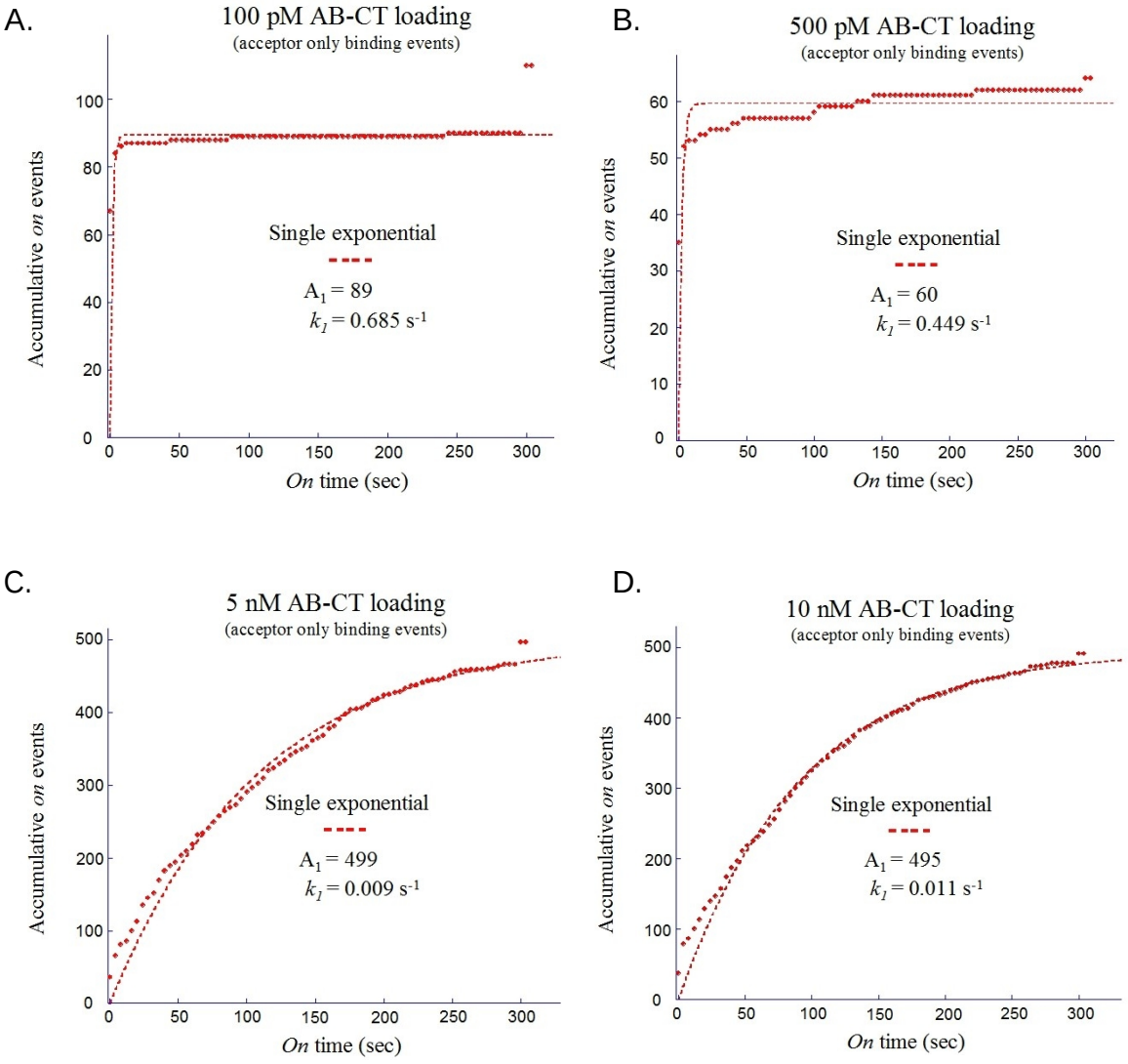

Figure 3-11. A-D. Dwell time (t_{on}) accumulative distribution fitting of acceptor binding events from different protein loading concentrations. Data points are shown as red dots, and they are fitted with single exponential equation.

Showing in Figures 3-8I to K and M, there is a significant fraction of binding events having a high FRET state (with FRET efficiency ~1). They were categorized as acceptor events because only the Cy5 acceptor signal was observed. To see if these high FRET events are associated with either fast or slow dissociating binding states, the dwell

time (t_{on}) distribution of acceptor binding events were fitted again with single or double exponentials. Interestingly, the data fit better with a single exponential in different protein concentrations (Figure 3-11), and the switch between the fast and slow dissociation phases was again dependent on the protein concentration (Figure 3-11). In low protein concentration loadings, the high FRET binding events dissociated rapidly; while protein was loaded in 5 or 10 nM concentrations, dissociation process slowed down. Taken all these observations together, the occurrence of the two different binding states is protein concentration dependent. This observation brings up a question of whether protein oligomerization happening during the DNA-binding process of domain AB.

3.3.6. Protein oligomerization analysis of Cy3-AB-CT and 32BI DNA

While the dwell time distribution analyses suggested that there are two different binding states, the protein stoichiometry associated with each state is not known since the total Cy3 donor or the Cy5 acceptor intensity were not taken into account for the analyses. The occurrence of the two states depends on the protein loading concentration, and a stable binding state (average $k_{off} = 0.010\ s^{-1}$) was dominant when protein loading concentration increases. These observations may indicate that oligomerization of protein takes place and contributes to the formation of the stable, long-live protein-DNA complex. To test this hypothesis, average Cy3 donor intensity and multi-step photobleaching analyses were carried out.

Because Cy3 hydrazide reacts specifically with the formyglycine residue within the FGly-AB-CT construct, it is expected that each protein is labeled with a single Cy3 fluorophore. For data collected under the same conditions, if a protein dimer was formed upon binding to DNA, and none of Cy3 fluorophore was photobleached during excitation, the resulting Cy3 donor intensity would be doubled when compared with the

DNA-binding event with a single protein. Therefore, if protein oligomerization happens, it would show up as a distinct population in the Cy3 intensity analysis when compared with single protein binding events. In this study, only the donor binding events were analyzed (Figures 3-8B to H, and L). Furthermore, because the Cy3 excitation was paused every two seconds during experiments, the Cy3 intensity signal was only considered when the laser excitation was turned on. With the criteria discussed above, average Cy3 intensity from each donor-only-binding-event was recorded, and the numbers of events were counted and binned in intervals of every 1000 intensity signals. The population distribution histograms are plotted as population fraction versus average Cy3 intensity shown in Figure 3-12.

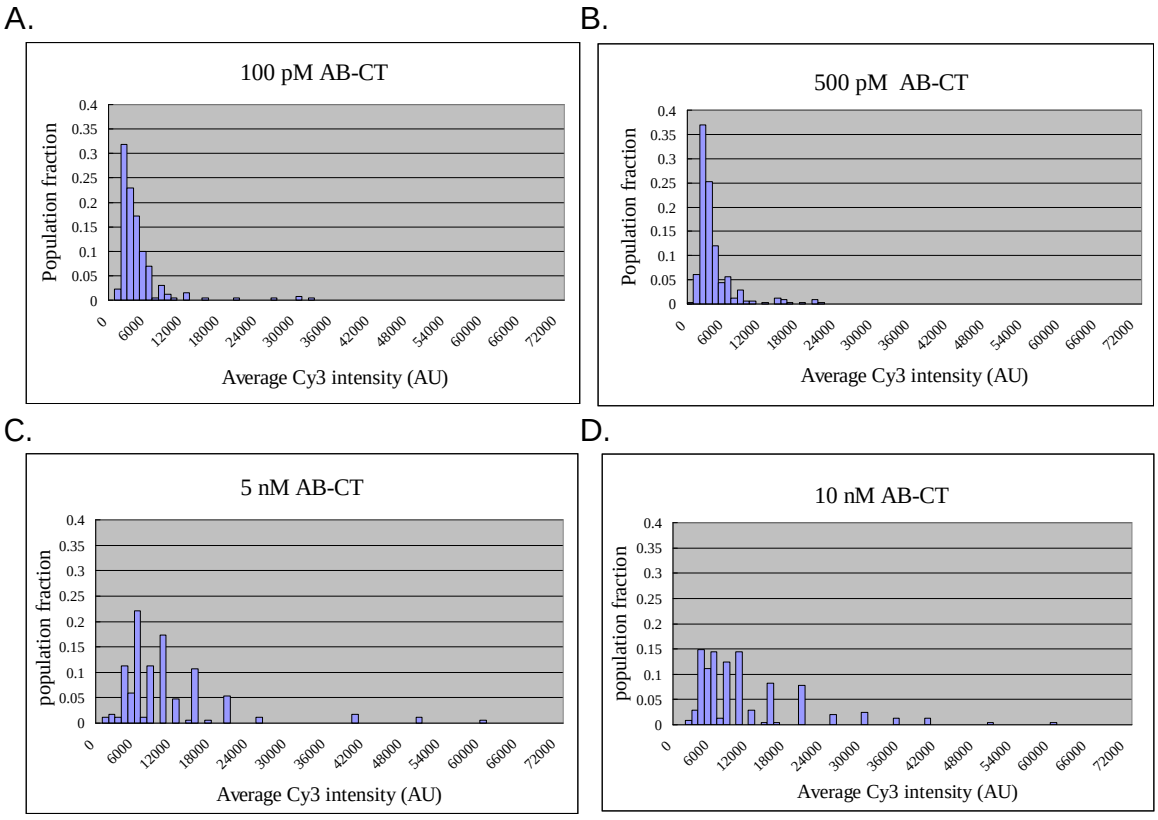

Figure 3-12. A-D. Population distribution analyses based on average Cy3 intensity for donor-only-binding-events observed in different protein concentrations.

When 100 or 500 pM of protein was loaded, majority of the binding events had the average Cy3 signal ranging from 2000 to 6000 AU. As protein loading concentration was increased to 5 and 10 nM, the population fraction of binding events became dispersed ranging from 4000 to 18000 AU. As the protein concentration increases, the average Cy3 intensity associated with the individual binding events also increases, consistent with the occurrence of protein oligomerization. The increase in average Cy3 intensity is about 2 to 3 fold, suggesting dimer or trimer formation.

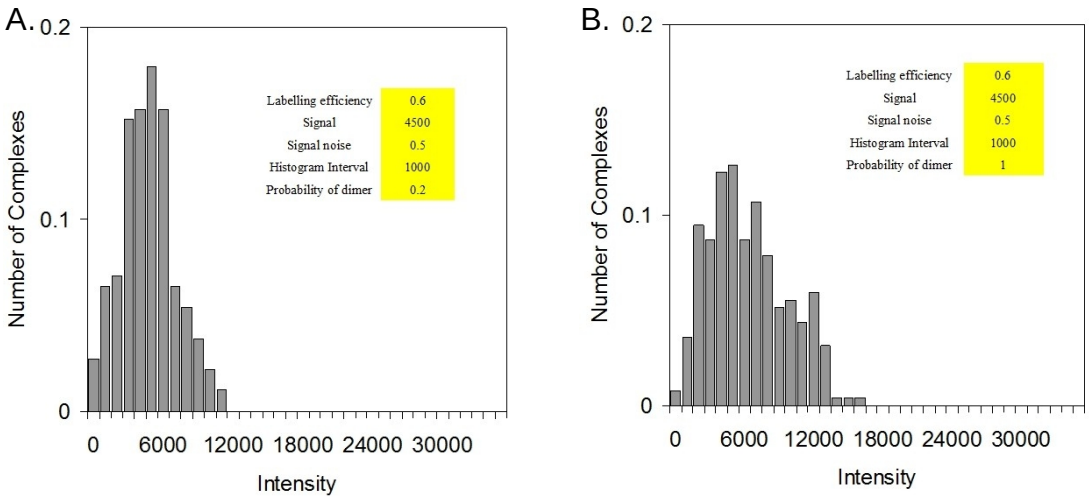

Figure 3-13. Simulations of average Cy3 intensity distribution histograms. A. Simulated histogram with probability of dimer formation setting at 0.2. B. Simulated histogram with probability of dimer formation setting at 1.

Fluctuations on the average Cy3 intensity signal associated with a given binding event are affected by the following factors: percentage of protein labeling, the noise level, and the probability of oligomer formation. To see how these factors influence the population distribution of the average Cy3 intensity and check for the likelihood of dimer formation within each protein loading concentration, data simulation was performed using a program written by Dr. Brian Cannon. Data simulation was done with a typical

protein labeling yield of 0.6. Figure 3-13 shows the simulation results for the probability of dimer formation setting at 0.2 and 1, which match quite well with the observed distribution in Figure 3-12. When the protein concentration is low (Figure 3-12A and B), the majority of the protein binding events are associated with protein monomer. When protein concentration increases (Figure 3-12C and D), a significant fraction of the binding events is associated with two protein molecules, as predicted in Figure 3-13B. Again, simulations together with the average Cy3 intensity analyses support the hypothesis that protein dimerization takes place in the DNA-binding process.

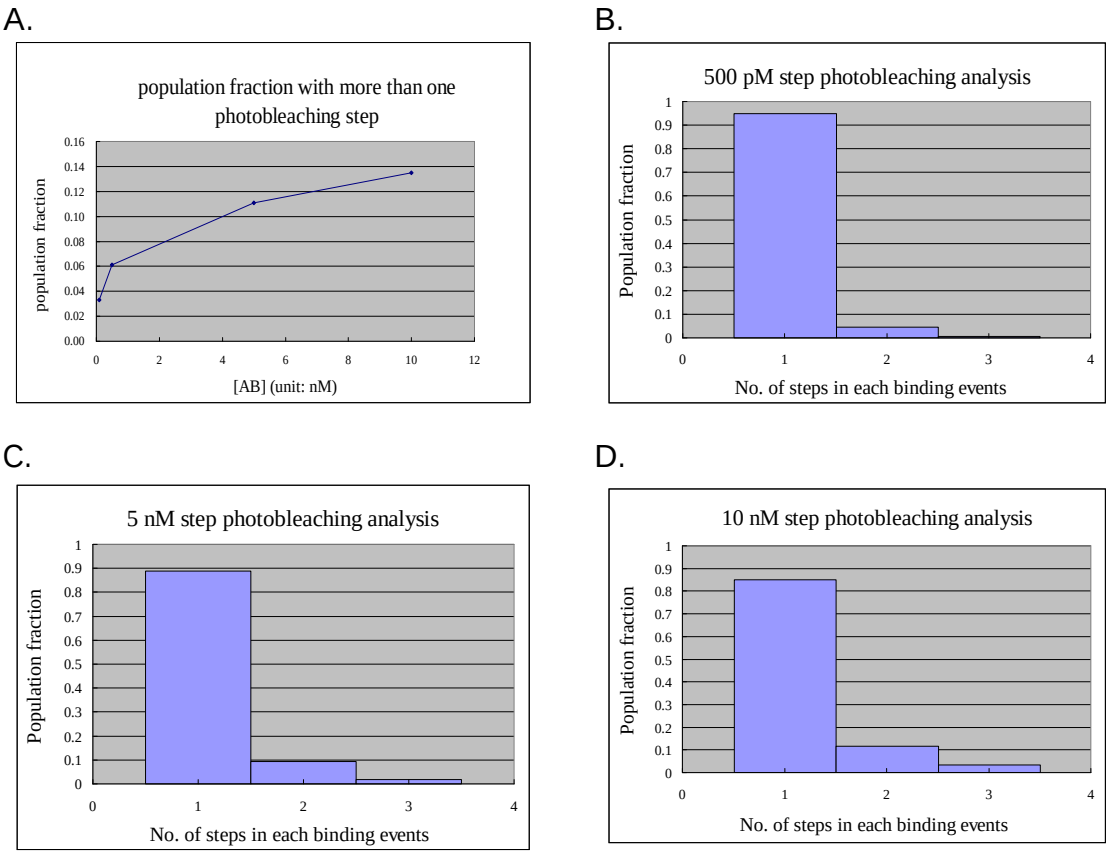

Figure 3-14. Population distribution analyses for multi-step photobleaching events. A. Quantification of the binding events for more than 1 step of photobeaching. C-D. Quantification of population fractions with different numbers of photobleaching steps.

A single-step photobleaching process is due to the dissociation of a single protein or the irreversible destruction of one fluorescent dye during Cy3 excitation (i.e., photobleaching of the fluorescent dye) (13-14). When multiple protein molecules interact with the same DNA molecule, multi-step photobleaching of Cy3 or Cy5 (in acceptor events) signal is expected as they dissociates at different time points, or one of the dyes is photobleached. Examples of signal response pattern from two-step photobeaching events are shown in Figures 3-8 L and M. To facilitate this study, the number of photobleaching steps was counted for each binding event. When there is no photobleaching happening for a given event, it is counted as one molecule binding step. Then the fraction of the event population is plotted based on the number of steps observed.

Figure 3-14 displays the multi-step photobleaching analyses of binding events collected from protein loading concentrations of 500 pM, 5 nM, and 10 nM. Data from 100 pM protein loading was not analyzed, because less than 5% of the binding events exhibited multi-step photobleaching behavior. As shown in Figure 3-14A, there are higher percentages of multi-step photobleaching observed in elevated protein concentrations. Taking a closer look, these events were mostly associated with two- or three-step photobleaching, as shown in Figures 3-14 B-D. This is consistent with the dimer and trimer formation of domain AB.

As the majority of the binding events did not photobleach during Cy3 excitation, the next question is whether the observed one-step photobleaching event arised from DNA bound with a single protein, or bound with two protein molecules without photobleaching. To answer this question, the highest Cy3 intensity of each binding event was correlated with the number of photobleaching steps for each donor-only-binding-event (i.e., 3000 in Figure 3-8B for a one-step event; 3000 in Figure 3-8L for a two-step event), and the average value of the highest Cy3 intensity was calculated for binding

events associated with one, two or three photobleaching steps, and are plotted with standard deviations, as shown in Figure 3-15.

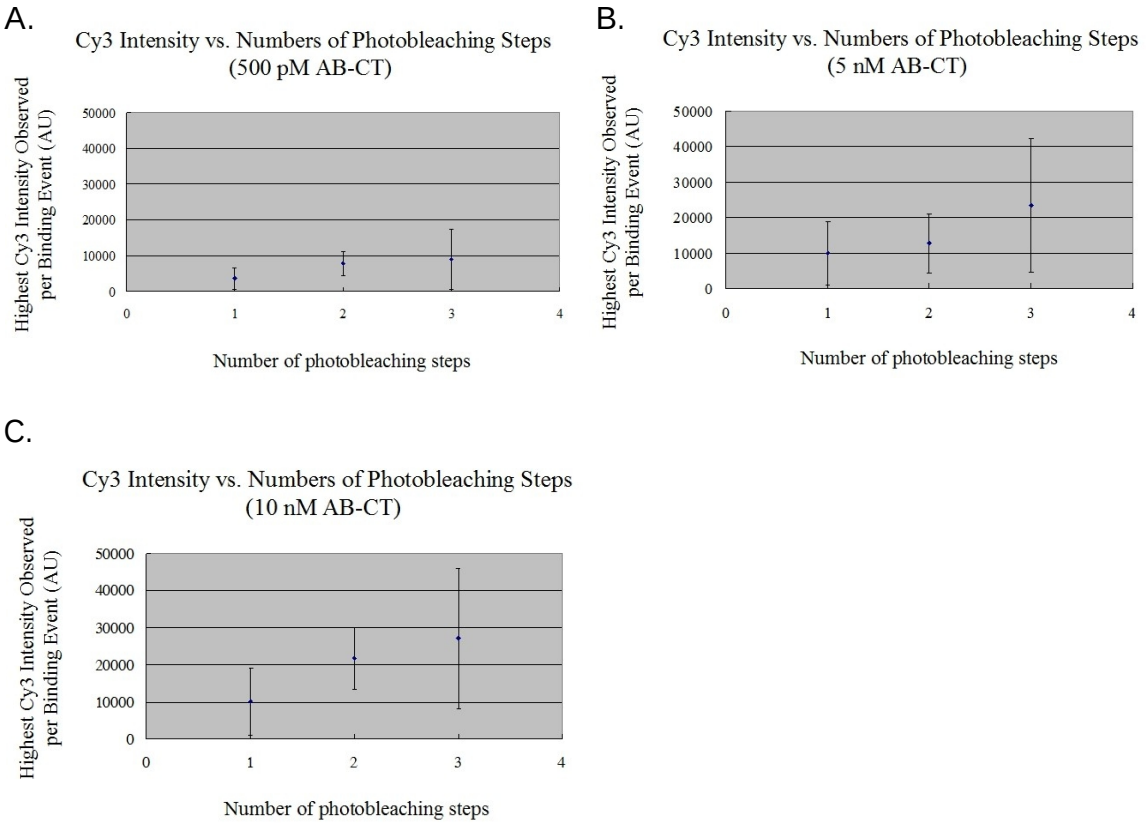

Figure 3-15. Correlation analyses of the highest Cy3 intensity and the number of photobleaching steps identified from the donor-only-binding-events. A. 500 pM AB-CT. B. 5 nM AB-CT. C. 10 nM AB-CT.

In the case of 500 pM AB-CT protein loading, one-step photobleaching events have an average intensity signal at around 3600 AU; and the two-step photobleaching events have an average intensity signal at around 7700 AU (Figure 3-15A). As the average Cy3 intensity of the two-step photobleaching events is about two-folds as the one-step photobleaching events, it is consistent with one and two protein molecules

bound with a single DNA. A similar trend was observed in the case of 10 nM AB-CT loading concentration (Figure 3-15C). The higher Cy3 intensity in the case of 10 nM AB-CT for both one and two step photobleaching events is possibly due to the increase of overall background signal coming from high concentration of protein loading. The data of the three-step photobleaching events have large standard deviations, which makes it hard to draw a clear conclusion. In the case of a 5 nM protein loading, the intensity difference between one- and two-step photobleaching is small. Here, the average Cy3 intensities of both one- and two-step photobleaching events are about 10000 to 12000 AU. This suggests that within the population of the one-step photobleaching events, some of these events actually arised from DNA with two proteins bound, but did not photobleach during the excitation process.

Finally, to make sure the observed oligomerization is not due to two DNA molecules collocated at the same spot, correlation analyses were carried out between the average Cy3 intensity and the average Cy5 intensity coming from direct Cy5 excitation at 300 s (Figure 3-7C) for each binding events. It is expected that if the projected protein dimerization is not due to two DNA molecules coexisted at the same spot, there should be no correlation between the intensity of Cy3 and Cy5 signals, because the signals are coming from two different laser excitations; and data points should be spread out in one region. However, if the projected protein dimerization is due to the presence of two DNA molecules positioned too close to each other, and not being well resolved in colocalization experiments, the Cy3 and Cy5 signals would be correlated with each other. In this case, it is expected that as Cy3 intensity gets higher, so does the Cy5 signal; and two distinct populations may result in this case. As shown in Figures 3-16 A-C, under all protein loading concentrations, most data points are found in one region of the plot, and there is no increase in the Cy5 signal as the Cy3 signal increased. Because there is no

direct correlation between the intensity of the Cy3 and Cy5 signals, the observed protein dimerization is most likely due to two protein molecules interacting with a single DNA, not due to two DNA molecules being spotted at the same position.

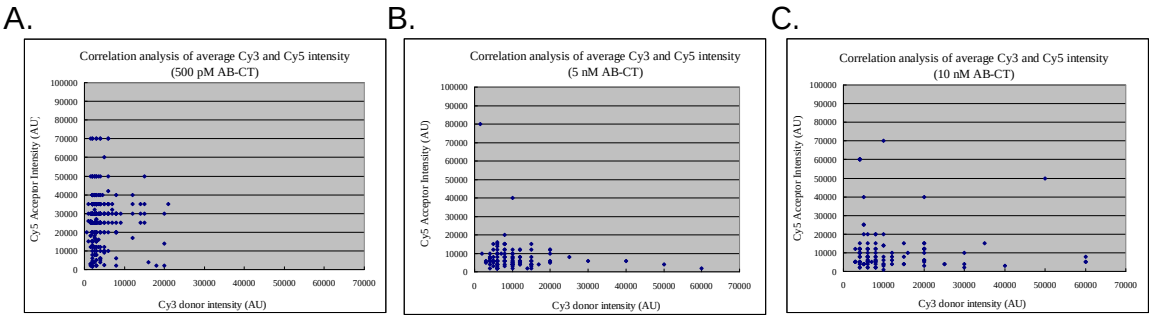

Figure 3-16. Correlation analyses of Cy3 intensity and Cy5 intensity signals. The Cy5 intensity used here was recorded from direct excitation of the Cy5-labeled DNA. A. 500 pM AB-CT. B. 5 nM AB-CT. C. 10 nM AB-CT.

3.3.7. FRET analyses of Cy3-AB-CT and 32BI DNA

As discussed in Section 3.3.5., there is a significant fraction of protein binding events that show a strong FRET signal (Figures 3-8I to K and M) as well as a medium FRET signal, with the FRET response pattern showing in Figure 3-8F. Also, some of the protein binding events show fast transition between a high FRET and a low FRET state (Figures 3-8G and H). Based on these observations, the FRET responses resulted from protein binding are highly complex. With current knowledge, it is hard to propose a protein-DNA interaction mechanism that can sufficiently account for all these different binding states. Therefore, it is unrealistic to consider all of them at the initial stage of FRET analyses. This is especially true when some of these FRET transitions are with less than 5% occurrence which may be due to artifacts (15).

To overcome this problem, and get a general idea of the true FRET states that can be identified from this protein/DNA pair, an average FRET efficiency value is calculated for each DNA molecule. Specifically, a value of FRET efficiency was first calculated for each time frame (in sec) where a protein binding event was observed, and an average FRET efficiency for each DNA molecule is obtained by summing the all the FRET efficiency values and divided by the total time of a DNA bound by proteins. This means that if multiple binding events with different FRET states are observed on a single DNA molecule during the 300 s excitation time course, the final calculated FRET efficiency is the averaged value for all these binding events, and it is weighted by the duration of the occurrence for each FRET state. In this way, the FRET responses with low occurrence may have little contribution to the average FRET efficiency per DNA molecule. By performing the data analysis discussed above, it would facilitate the identification of the most predominant FRET states, which are likely to be the true binding state. So, in turn, this allows an establishment of a minimal mechanistic model on how domain AB interacts with the double stranded break that can be tested further.

$$\text{FRET efficiency} = \frac{I_A}{I_A + I_D}$$

I_A : Cy5 acceptor intensity

I_D : Cy3 donor intensity

Two Gaussian distributions fitting:

$$f(x; a, \mu, \sigma) = a_1 \cdot exp\left(\frac{-(x-\mu_1)^2}{2\sigma_1^2}\right) + a_2 \cdot exp\left(\frac{-(x-\mu_2)^2}{2\sigma_2^2}\right)$$

x : FRET efficiency

a : amplitude

μ : mean

σ : standard deviation

Figure 3-17. Equations used for FRET efficiency calculation and the fitting of the different FRET distributions. Definitions of all parameters are shown on the right.

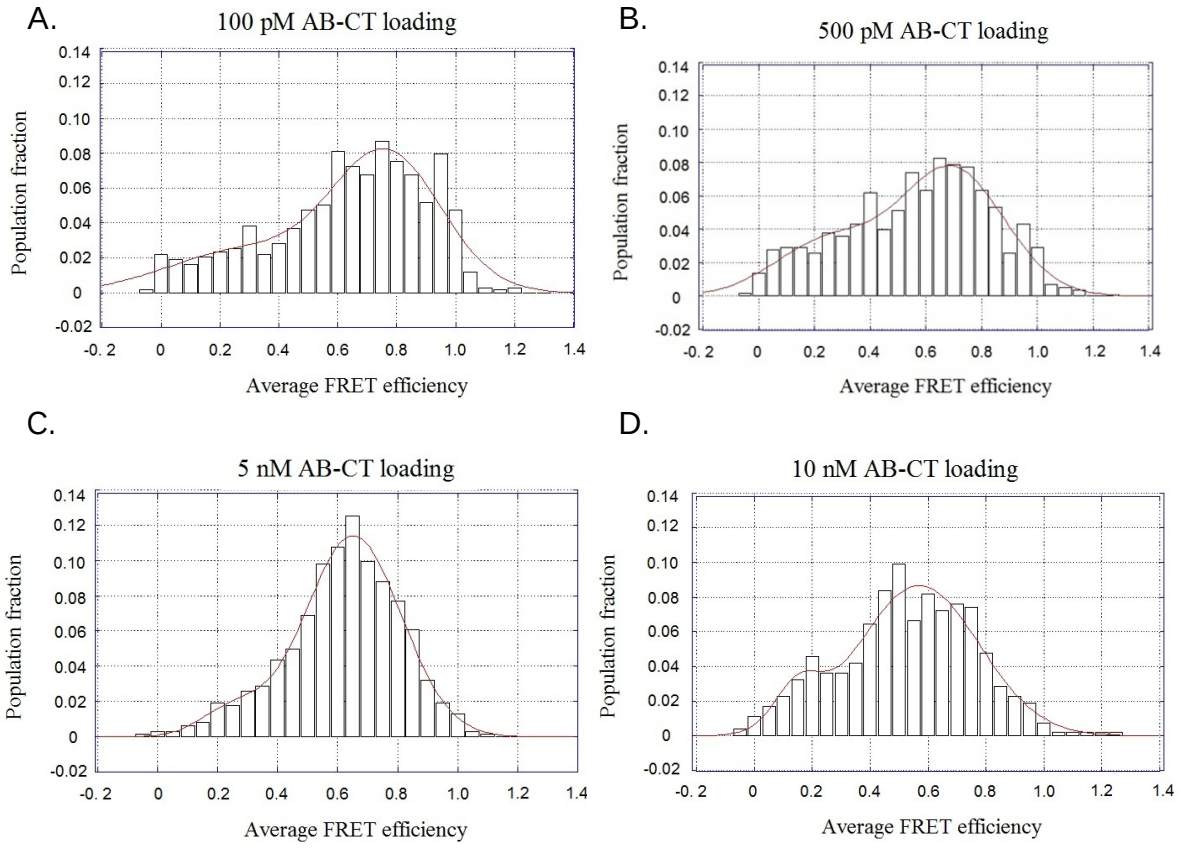

Figure 3-18. Population distributions of FRET efficiency are fitted with double Gaussian distributions.

Table 3-2. Parameters derived from double Gaussian distribution fitting shown in Figure 3-18.

AB-CT	<FRET Efficiency> μ_1	Amplitude (a_1)	σ_1^2	<FRET Efficiency> μ_2	Amplitude (a_2)	σ_2^2
100 pM	0.284	0.024	0.183	0.767	0.078	0.132
500 pM	0.248	0.033	0.136	0.695	0.076	0.132
5 nM	0.252	0.015	0.076	0.652	0.114	0.114
10 nM	0.149	0.024	0.057	0.570	0.087	0.147

Here, average FRET efficiencies are calculated based on the equation shown in Figure 3-17, and the plotted FRET distribution is fitted with double Gaussian distributions. The number of distributions is determined based on the two observed

binding states discussed in the binding kinetic studies section. Based on the fitted data shown in Figure 3-18 and Table 3-2, two distinct protein binding states could be observed with average FRET efficiencies of 0.233 and 0.671, respectively. The average FRET efficiencies are calculated using values obtained from different protein concentrations (Table 3-2).

3.4. DISCUSSION

To study the recognition mode of domain AB toward double stranded break DNA, single molecule colocalization studies were carried out using Cy3-labled domain AB and Cy5-labeled 32BI DNA (Figure 3-8A). Except to crystal structures and DNA-binding affinity studies discussed in Chapter 1, limited information is available regarding the DNA recognition mechanism of PARP-1. Work done in this chapter was intended to provide mechanistic details regarding the DNA recognition process of domain AB in real-time, which may be hard to extract from ensemble studies. The results allow the extractions of three different kinds of information: binding kinetics, protein binding stoichiometry, and the relative position between the domain AB zinc fingers and the DNA lesion site.

3.4.1. Identification of two DNA-binding states

The dwell time (t_{on}) distribution analyses reveal the presence of two different binding states of domain AB toward DNA, with one binding state that dissociates rapidly (average k_{off} = 0.51 s^{-1}) and one long-lived state which is relatively stable (average k_{off} = 0.010 s^{-1}). Compared with the k_{off} value reported by Jorgensen et al. from a SPR study using full-length PARP-1, our result is different (16). In the case of SPR measurement, a

single dissociation phase was observed, and it is more stable when compared with the two on states identified from the single molecule studies.

Table 3-3. Comparison of the dissociation kinetic results obtained from single molecule and SPR studies.

	Protein used	DNA used	Averaged dissociation constant k_{off} (s^{-1})	
SPR	Full-length PARP-1	28mer	0.0034±0.0026	
Single molecule	Domain AB	32mer	0.010±0.003	0.531±0.085
Cy3 photophysics: $k_{blink\ off}$ = 0.0096 s^{-1}				

While the difference in kinetics can be explained by the different form of PARP-1 protein used, it is also possible that there is a third binding state which is missed in the single molecule studies. Because the total observation time in the single molecule experiments is 300 s, based on the k_{off} value from the SPR measurement, it is expected that the protein molecule would stay bound for about 294 s ($\tau = 1/k_{off}$). Judging from the single molecule data, there are about 3 to 6% of the binding events staying longer than 290 s. This percentage is rather low to suggest whether this is a true binding state, or just an artifact.

When comparing the photo-physical properties of Cy3 with the dissociation rate constants obtained under the single molecule platform, the data suggests that there are only two binding states. During excitation, Cy3 dyes would occasionally undergo a reversible blinking process. This process causes the excited Cy3 dye to go to a dark state and then back to the fluorescent state. This photophysical property of Cy3 can be mis-interpreted as a unique binding state. In a control experiment, the blink off rate $k_{blink\ off}$ of Cy3 dye was measured using the immobilized Cy3-labeled DNA molecules provided by Dr. Russell's lab under the exact same experimental condition, and the value is reported in Table 3-3. This value is close to one of the reported dissociation constants (0.010 s^{-1}),

indicating that this observed binding state is likely due to the blinking of Cy3 dye. Thus, even blinking events of Cy3 were observed, domain AB remained bound to the DNA molecule without dissociation. This means that this stable binding state has a life-time longer than 105 s ($1/k_{blink\ off}$). Based on this information, it is concluded that there exist two binding states for domain AB to interact with DNA. Due to the experimental set up and the photophyical property of Cy3 dye, the long lived state is not fully captured, and only the lower limit of the dissociation rate is obtained.

In addition, the population distribution between the two binding states is dependent on the protein concentration (Figure 3-10F). This observation favors the proposed binding scheme 3-2, where the second binding state is dependent on the first. In this scenario, it is expected that when protein concentration is low, most of the binding events are in a low population fraction of binding state a. The occurrence of binding state b is less likely under such condition if this state requires protein dimerization. As protein concentration increases, majority of the protein molecules may be in binding state a by forming a 1:1 protein-DNA complex, which in turn favors the occurrence of binding state b, where dimerization of protein molecule happens on a single DNA. In scheme 3-3, the occurrence of the two binding states is expected to be less effected by the protein loading concentrations.

3.4.2. Protein dimerization on the double stranded break

The concentration dependency of the two binding states suggests that there is a possibility of protein oligomerization. The dimer formation is supported by both the average Cy3 intensity analyses as well as multi-step photobleaching analyses. The results obtained are consistent with the conclusion drawn in Chapter 2 from the sedimentation velocity experiments, where PARP-1 forms a 2:1 protein complex with double stranded

blunt end DNAs. In addition, the occurrence of protein dimerization is dependent on the protein concentration, indicating that the binding state b in Scheme 3-2 is likely a 2:1 protein-DNA complex.

3.4.3. Identification of different FRET populations

With a Cy3 FRET donor labeling at the C-terminal end of domain AB, interaction of domain AB with blunt end DNA (32BI) resulted in two distinct FRET populations, with average FRET efficiencies of 0.233 and 0.671, respectively. Here, the Cy3 dye is located close to zinc finger II, and observation of a high FRET state indicates the close proximity between the zinc finger II and the double stranded lesion site.

The low FRET state may result from the interaction of the lesion site with zinc finger I at the N-terminus. This conclusion is drawn based on the following observations. First, from the crystal structures reported by Ali et al., both zinc finger I and zinc finger II interact directly with DNA at the lesion site containing a single-base overhang, which is a mimic of the blunt end DNA structure. The two zinc fingers that interacts with the same DNA lesion site come from two separate peptides, suggesting dimer formation at the lesion site (Figure 1-8) (17). This is consistent with the two observed FRET states reported here. Secondly, as the Cy5-labeled 32BI DNA is immobilized on the glass surface (Figure 3-7A), this makes the second lesion site less accessible for protein binding. Therefore, it is unlikely that the low FRET state is due to the protein interaction to this biotinylated end.

Finally, when looking at the high FRET efficiency as protein concentration increases (Table 3-2), there is a decreasing trend in the high FRET signal. This observation may possibly result from increasing dimer formation as the protein concentration increases. When a protein dimer is formed, one of the two protein molecules shows a high FRET signal, and the other protein molecule shows a low FRET

state, the average FRET signal should be an average of the two FRET states. If this hypothesis is true, it is expected that under high protein concentration, there are three FRET states that can be identified. To test this possibility, the FRET population distribution obtained from 10 nM protein loading was fitted with three Gaussian distributions, and the result is presented in Figure 3-19 and Table 3-4. The FRET population distribution is actually fitted better with three Gaussian distributions. Here, the values of the observed high and low FRET states are similar to the reported values from other binding events obtained in different protein concentrations (Table 3-2). The additional medium FRET state has a FRET efficiency similar to the average value calculated from the high and low FRET states (average FRET efficiency = 0.445). The observation is consistent with the proposed model that, upon protein dimerization, one protein molecule results in a high FRET state, possibly through interaction with zinc finger II; and the other protein molecule results in low FRET state, possibly due to the interaction with zinc finger I.

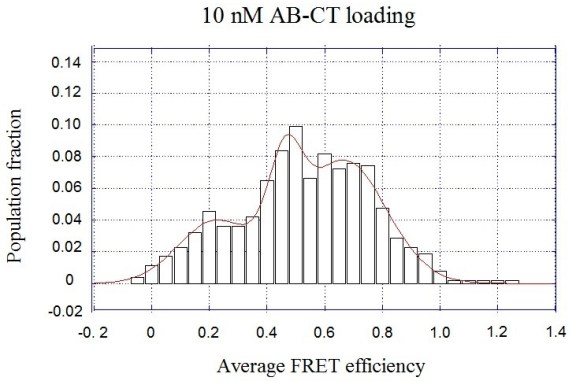

Figure 3-19. Population distribution of FRET efficiency of 10 nM AB loaded. Data was fitted with triple Gaussian distributions.

Table 3-4. Parameters derived from three Gaussian distribution fitting shown in Figure 3-19.

distribution	<FRET Efficiency> μ	Amplitude (a)	σ^2
1	0.222	0.039	0.092
2	0.463	0.057	0.041
3	0.668	0.078	0.104

3.4.4. Proposed model of DNA-recognition mechanism of domain AB

Based on the results and discussion above, a minimal model regarding how domain AB recognizing double stranded DNA break is proposed (Figure 3-20). In step 1, domain AB can interact with the double stranded break lesion either through zinc finger I or zinc finger II. This is proposed based on the observations that a fast dissociation step can be observed from both donor and acceptor binding events (Figure 3-10 and Figure 3-11). Upon dimerization, a stable long-lived protein-DNA complex was formed at the lesion site. This may result in a medium FRET state with an FRET efficiency of 0.46.

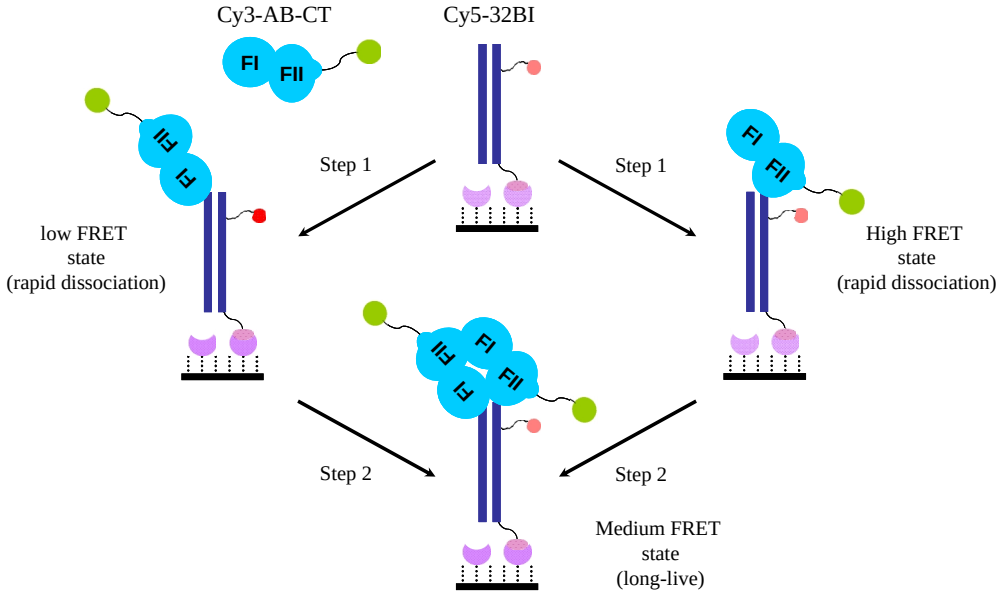

Figure 3-20. A proposed model for recognition of double stranded break DNA by domain AB.

While the data analyses done here allow the establishment of a minimal double stranded break binding model of domain AB, it should be noted that there are different signal response patterns (Figures 3-8B to M) discernible from the intensity trajectories. Based on this model, the intensity trajectories can now be further analyzed in more details based on a three binding state system shown in Figure 3-20. In addition, the FRET distribution analysis carried out here is based an average FRET efficiency from each DNA molecule. As three different FRET states are proposed according to the model shown in Figure 3-20, FRET distribution analyses can now be conducted based on individual binding events. Once the different FRET states are identified, their dwell time distribution can also be analyzed.

As a future direction, this model can be further tested using protein constructs with Cy3 labeled at different positions, such as the Fgly-AB, where Cy3 is labeled near zinc finger I, and the 150Fgly-AB with Cy3 labeled internally in zinc finger II. In addition, this model can be extended further in the context of full-length PARP-1, and provide understanding on how other DNA-interacting domains, such as WGR and DsBD domains, participate in the DNA-dependent activation process.

3.5 REFERENCES

1. Decker, K.B., and Hinton, D.M. (2013) Transcription regulation at the core: similarities among bacterial, archaeal, and eukaryotic RNA polymerases, Annu. Rev. Microbiol. 67, 113-139.
2. Germann, M.W., Johnson, C.N., and Spring, A.M. (2012) Recognition of damaged DNA: structure and dynamic markers, Med. Res. Rev. 32, 659-683.
3. D'Amours ,D., Desnoyers, S., D'Silva, I., and Poirier, G.G. (1999) Poly(ADP-ribosyl)ation reactions in the regulation of nuclear functions, Biochem. J. 342, 249-268.

4. D'Silva, I., Pelletier, J.D., Lagueux, J., D'Amours, D., Chaudhry, M.A., Weinfeld, M., Lees-Miller, S.P., and Poirier, G.G. (1999) Relative affinities of poly(ADP-ribose) polymerase and DNA-dependent protein kinase for DNA strand interruptions, Biochim. Biophys. Acta. 1430, 119-126.

5. Pion, E., Ullmann, G.M., Amé, J.C., Gérard, D., de Murcia, G., and Bombarda, E. (2005) DNA-induced dimerization of poly(ADP-ribose) polymerase-1 triggers its activation, Biochemistry 44, 14670-14681.

6. Ikejima, M., Noguchi, S., Yamashita, R., Ogura, T., Sugimura, T., Gill, D.M., and Miwa, M. (1990) The zinc fingers of human poly(ADP-ribose) polymerase are differentially required for the recognition of DNA breaks and nicks and the consequent enzyme activation. Other structures recognize intact DNA, J. Biol. Chem. 265, 21907-21913.

7. Huambachano, O., Herrera, F., Rancourt, A., and Satoh, M. S. (2011) Double-stranded DNA binding domain of poly(ADP-ribose) polymerase-1 and molecular insight into the regulation of its activity, J. Biol. Chem. 286, 7149-7160.

8. Mansoorabadi, S.O., Wu, M., Tao, Z., Gao, P., Pingali, S.V., Guo, L., and Liu, H.W. (2014) Conformational activation of poly(ADP-ribose) polymerase-1 upon DNA binding revealed by small-angle X-ray scattering, Biochemistry 53, 1779–1788.

9. Lindahl, T., Satoh, M.S., Poirier, G.G., and Klungland, A. (1995) Post-translational modification of poly(ADP-ribose) polymerase induced by DNA strand breaks, Trends. Biochem. Sci. 20, 405-411.

10. Vyas, S., and Chang, P. (2014) New PARP targets for cancer therapy, Nat. Rev. Cancer 14, 502-509.

11. Carrico, I.S., Carlson, B.L., and Bertozzi, C.R. (2007) Introducing genetically encoded aldehydes into proteins, Nat. Chem. Biol. 3, 321-322.

12. Ma, C.H., Liu, Y.T., Savva, C.G., Rowley, P.A., Cannon, B., Fan, H.F., Russell, R., Holzenburg, A., and Jayaram, M. (2014) Organization of DNA partners and strand exchange mechanisms during Flp site-specific recombination analyzed by difference topology, single molecule FRET and single molecule TPM, J. Mol. Biol. 426, 793-815.

13. Wang, Y., Guo L., Golding I., Cox E.C., and Ong N. P. (2009) Quantitative transcription factor binding kinetics at the single-molecule level, Biophy. J. 96, 609-620

14. Shu D., Zhang H., Jin J., and Guo P. (2007) Counting of six pRNAs of phi29 DNA-packaging motor with customized single-molecule dual-view system, EMBO J. 26, 527-537

15. Roy R., Hohng S. and Ha T. (2008) A practical guide to single-molecule FRET, Nat. Methods 5, 507-516

16. Jorgensen, T.J., Chen, K., Chasovskikh, S., Roy, R., Dritschilo, A., and Uren, A. (2009) Binding kinetics and activity of human poly(ADP-ribose) polymerase-1 on oligo-deoxyribonucleotide substrates, J. Mol. Recognit. 22, 446-452.

17. Ali, A.A., Timinszky, G., Arribas-Bosacoma, R., Kozlowski, M., Hassa, P.O., Hassler, M., Ladurner, A.G., Pearl, L.H., and Oliver, A.W. (2012) The zinc-finger domains of PARP1 cooperate to recognize DNA strand breaks, Nat. Struct. Mol. Biol. 19, 685-692.

Chapter 4. Mechanistic Investigation of Human PARP-1 Automodification

4.1. INTRODUCTION

As most of the PARP-1 research efforts are focusing on the aspects of its biological functions, the enzymatic reaction carried out by PARP-1 is not well-established today. Human PARP-1 can produce a nucleic acid like polymer, called poly(ADP-ribose) (i.e., PAR) through enzymatic polymerization process using NAD^+ as the ADP-ribose donor. The generated PAR polymers are covalently attached to protein substrates (i.e., heteromodification), and also PARP-1 itself (i.e., automodification). This polymerization process occurs in a single active site located at the C-terminal domain F of PARP-1, and proceeds in three distinct reaction steps: initiation, elongation and branching (Figure 1-4). The polymers being generated from these three reactions are heterogeneous in terms of chain length and branching points. The difficulty to fully characterize the reaction products generated by PARP-1 hampers the mechanistic studies of PARP-1 catalysis.

Most of the current understanding of PARP-1 reaction comes from the studies of PARP-1 automodification. It has been shown that the minimal catalytic fragment domain F alone exhibits low automodification ability in the presence of NAD^+, with less than 1% of the isolated protein being modified (1). In terms of DNA-dependent PARP-1 activation, both zinc finger I and domain C are required in addition to domain F (2-3). The majority of polymer acceptor sites in PARP-1 are located in the automodification domain D (4-5), and new acceptors sites outside domain D have also been identified recently. However, the total number of PAR acceptor sites in PARP-1 is currently uncertain (5). Finally, as discussed in Section 1.5.1, several amino acid residues within

the active site of PARP-1 have been established to be important for modulating the elongation and branching processes.

Based on the studies presented above, there is limited information regarding the regulatory elements of PARP-1 which controls its polymerization process. For the three reactions catalyzed by PARP-1, different ADP-ribose acceptor substrates are expected. During initiation, amino acid residues within a protein substrate, such as glutamate, aspartate or lysine residues serve as the substrates of PARP-1 for accepting the first ADP-ribose unit. In this process, a specific protein substrate or a domain within PARP-1 needs be recognized by the catalytic domain F. In the elongation process, a new ADP-ribose unit is added to either the initiated ADP-ribose or pre-established PAR polymers. This process can proceed through a distal or proximal mechanism (Figure 1-13). In the case of distal elongation mechanism, addition of new ADP-ribose unit happens at the terminal end of the PAR polymer, with the PAR polymer serving as the acceptor substrate. In the case of proximal elongation mechanism, addition of new ADP-ribose unit happens at the protein end of the PAR polymer, where the protein molecule serves as the acceptor substrate. Finally, for the branching reaction, one of the 2''-OH groups within the PAR polymer serves as the acceptor substrate. As these acceptor substrates are macromolecules, their recognition by PARP-1 may require large and diverse interaction surfaces. Currently, there is no satisfactory model that can account for the change of substrate specificity as the reaction progresses during PAR formation.

In an attempt to understand the structural requirements and to establish a mechanistic model for PARP-1 automodification, the truncated N- and C-terminal fragments (i.e., ABC and DEF, respectively) were tested for their activities in PAR formation using denaturing gel electrophoresis in combination with ^{32}P autoradiography. Current data suggest that DEF alone has poor initiation ability, whereas ABC together

with DNA serves as the regulatory elements for catalysis. DEF modified with different sizes of PAR polymers were also purified and tested for activity. It was observed that elongation of short PAR polymers requires ABC and DNA; however, incorporation of NAD^+ into DEF which was previously modified with larger polymers required no ABC and DNA.

Furthermore, accompanying the initiation reaction catalyzed by DEF/ABC, significant amounts of NAD^+ were hydrolyzed by water to generate ADP-ribose. This process was attenuated during the elongation reaction where modified-DEF/ABC were employed. Based on these observations as well as the crystal structure of PARP-1 domains bound with DNA solved by Langelier et al. (Figure 1-10) (6), a mechanistic model of PARP-1 automodification is proposed by our post-doctoral fellow Dr. Mark Ruszczycky.

This mechanistic model favors an intramolecular, distal elongation of PAR formation in PARP-1 automodification. As PARP-1 exhibits a flexible and elongated conformation in solution, addition of DNA causes a structural compaction of PARP-1, which brings the automodification domain D close to the active site in domain F. This structural perturbation results in formation of an active conformation, and allows PAR initiation to take place in domain D. When ABC/DEF/DNA is used in forming the active complex, even though the complex is catalytically active, the overall conformation is less confined as compared with the wild type PARP-1. Therefore, water may enter the active site and directly hydrolyze NAD^+ to generate free ADP-ribose. This observation is consistent with an intramolecular initiation process, where domain D within DEF serves as the acceptor substrate. During PAR elongation in the case of modified-DEF/ABC, the direct hydrolysis of NAD^+ slows down when compared with the rate of NAD^+ hydrolysis during initiation. This should not be observed if domain D is still the as the acceptor

substrate, as in the case of proximal elongation. However, this phenomenon can be explained by PAR polymers or a newly initiated ADP-ribose unit serving as the acceptor substrates during elongation. In this case, the less constrained conformation of ABC/DEF/DNA complex is not a serious problem as in the case of initiation, where domain D is the acceptor substrate. The fact that PAR polymers are the acceptor substrates during elongation leads to the proposal that elongation happens at the distal end.

Finally, a mechanism of forming branching polymers is also included in the proposal. Because the extensively modified-DEF (i.e., lmDEF) can incorporate ADP-ribose into PAR in the absence of ABC and DNA, the pre-established PAR polymers are likely the reactive substrates for DEF. As the PAR polymer keeps elongating, the local concentration of 2"-OH from the polymer increases near the active site in domain F. Hence, it is more likely to get into the active site, and serves as the substrate acceptor to form a branch point.

Distal elongation process is further tested by a PAR transfer assay and a pulse-chase experiment. Preliminary results are both consistent with the distal elongation mechanism. While current data supports the proposed model, additional control experiments are needed to confirm the current observation.

4.2. MATERIALS AND METHODS

4.2.1. Cloning, expression and purification of human PARP-1 protein constructs

The cloning, expression and purification of protein constructs ABC, DEF (i.e., as-purified DEF), and full-length PARP-1 used in this study had been discussed in details in Section 2.2. The C-terminal His_6-tagged version of domain ABC (i.e., C-His-ABC) was

expressed using the ABC/pET-24b(+) vector constructed by our previous group member Dr. Peng Gao. The expression and purification of this protein were similar to those used in generating the tag free ABC protein construct. After the C-His_6-ABC protein was eluted from Ni-NTA agarose resin (Qiagen) with 20 mM HEPES, 300 mM NaCl, 250 mM imidazole, 1 mM β-mercaptoethanol and 10% glycerol at pH 7.5, the eluted protein fractions were pooled and dialyzed against the dialysis buffer containing 20 mM HEPES, 300 mM NaCl, 1 mM β-mercaptoethanol and 10% glycerol at pH 7.5. The purified protein was flash frozen with liquid nitrogen and stored at -80 ^{o}C.

4.2.2. Generation of the free-DEF protein construct

It was found that the as-purified DEF produced by the E. coli overexpression system contains endogenous PAR polymers. Removal of the endogenous PAR polymers was achieved by the addition of His_6-PARG during DEF purification under mild basic condition (pH 9.5). The resulting free-DEF was devoid of endogenous PAR polymers. Here, the plasmid for His_6-PARG protein overexpression was kindly provided by our group member Dr. Yung-nan Liu. This plasmid encodes amino acid residues 448-976 of PARG, which constitute the catalytic domain of human PARG protein. MBP-DEF and His_6-PARG protein constructs were overexpressed separately in 6L LB broth based on the expression protocol described in Section 2.2.1. Cells were harvested by centrifugation at 4500 x g for 15 min, and stored at -80 ^{o}C until purification.

To prepare free-DEF, both MBP-DEF and His_6-PARG cells were thawed and resuspended in lysis buffer containing 100 mM Tris, 300 mM NaCl, 10 mM imidazole, 1 mM β-mercaptoethanol and 10% glycerol at pH 9.5. The two cell suspensions were combined, mixed, and ruptured by sonication. Cell debris was removed by centrifugation at 20000 x g for 30 min, and the resulting supernatant was incubated at 4 ^{o}C for 1 hr with

20 mL of Ni-NTA agarose resin, which had been pre-equilibrated with the lysis buffer. After that, the mixture was loaded onto a column, drained, and washed with the wash buffer containing 20 mM imidazole and 1.5 M NaCl. The MBP-DEF fusion protein and the His_6-PARG protein were coeluted with buffer containing 250 mM imidazole and 300 mM NaCl. The eluted protein fractions were pooled and dialyzed against the lysis buffer. After 2 h of dialysis, 5% (w/w) His_6-tagged TEV protease was added in, and the protein mixture was incubated for 24 hr at 4 ^oC to cleave the His_{10}-MBP tag to generate the tag-free DEF construct. The protein mixture was then incubated with 30 mL of Ni-NTA resin at 4 ^oC for 1 hr. The mixture was loaded onto a column, and the protein solution was allowed to drain slowly. The collected flow through was passed through the Ni-NTA resin slowly for a second time. The free-DEF protein recovered from the second flow through was concentrated using an Amicon ultra-15 centrifugal filter unit with a 10 kDa cut off membrane (Millipore). The concentrated free-DEF was exchanged into a storage buffer containing 20 mM HEPES, 300 mM NaCl, 1 mM β-mercaptoethanol and 10% glycerol at pH 7.5 using the same centrifugal filter. The resultant protein was flash frozen with liquid nitrogen and stored at -80 ^oC.

4.2.3. Automodification assay of the as-purified DEF

Automodification activity of the as-purified DEF was determined by measuring the amount of ^{32}P incorporation in protein using [α-^{32}P] NAD^+ (American Radiolabeled Chemicals, Inc.) as substrate. The reaction mixture (6 µL) containing 25 µM of the as-purified DEF, 100 µM NAD^+, 0.6 µCi of ^{32}P-NAD^+, 300 mM NaCl, 1 mM $MgCl_2$ in 100 mM Tris buffer at pH 7.5 was incubated at room temperature. For all samples, NAD^+ was added last to initiate the reaction; and the reaction was quenched at different time points using 2X SDS-PAGE loading buffer. After that, samples were separated using a 12%

SDS-polyacrylamide gel (16 cm x 16 cm). The gel was run at 30 mA at room temperature for 2 hrs with an ice water cooling system. After electrophoresis, the wet gel was rinsed with tap water, drained, and wrapped by saran wrap. The wrapped gel was exposed using a storage phosphor image screen (Molecular Dynamics) at 4 ^{o}C overnight. The image on screen was then visualized using a Typhoon Scanner (GE Healthcare), and the image was quantified using Quantity One software (Bio-rad).

To visualize the less abundant initiation process catalyzed by the as-purified DEF, different concentration ratios of cold: hot ^{32}P-NAD^{+} was prepared, and a final concentration of 100 μM NAD^{+} was added to each reaction sample (6 μL). The reaction samples were prepared as described previously, and they were quenched after 5 min incubation. Quenched samples were separated using a 12% SDS-polyacrylamide gel (mini gel) and were visualized in the same way as described before.

4.2.4. Automodification assay of the free-DEF

Automodification activities of the free-DEF with or without ABC were also determined by the ^{32}P incorporation assay. The experimental details including concentrations of all major components used in the reaction mixture (6 μL) were specified in the result section for each individual assay. In general, all samples were prepared in a reaction buffer containing 300 mM NaCl, 1 mM $MgCl_2$ and 100 mM Tris at pH 7.5. After 1 hr incubation at room temperature, reaction was terminated by 2X SDS-PAGE loading buffer. Samples were then separated using a 12% SDS-polyacrylamide gel (16 cm x 16 cm). Visualization of gels was carried out under the same conditions as described in Section 4.2.3.

4.2.5. Pulse-chase experiment for PAR extension

To monitor the PAR extension in the presence of free-DEF, ABC and 8-mer DNA, automodification reaction was initiated using ^{32}P NAD$^+$. After 20 min, the initially formed polymers were extended through multiple replenishments of cold NAD$^+$ chases. Concentrations for each major components as well as numbers of cold chases added are listed for each sample in Figures 4-7, 4-8 and 4-10 in Section 4.3.4. For samples that had fewer numbers of cold chases added, their volumes were adjusted by adding the reaction buffer containing 300 mM NaCl, 1 mM $MgCl_2$, and 100 mM Tris at pH 7.5. After the final chase step, all samples were quenched at the same time and analyzed by SDS-PAGE.

4.2.6. PAR polymer hydrolysis monitored by high-performance liquid chromatography

To test if the pre-established PAR polymer can be hydrolyzed by DEF, an automodication assay was set up, and the PAR hydrolysis by the modified-DEF was monitored by HPLC (i.e., high-performance liquid chromatography). First, an automodification reaction (200 µL) was set up using 12.5 µM free-DEF, 12.5 µM ABC, 25 µM 8-mer DNA, 100 µM NAD$^+$ in a reaction buffer containing 100 mM Tris at pH 7.5, 1 mM $MgCl_2$, and 300 mM NaCl. The reaction sample was incubated at room temperature for 20 min. After that, 200 µM of NAD$^+$ chase was added every 20 min. After a total of six chase steps, the reaction was stopped by filtration using 10 kDa Cutoff Amicon® MLtra 0.5 mL filters (Millipore), and washed five times with the reaction buffer. All filtrates were collected separately and stored at -80 ^{o}C freezer before HPLC analysis. The retaining portion of the modified-DEF and ABC protein was diluted to a final volume of 200 µL using the reaction buffer. This protein sample was stored at room temperature, and 50 µL of the sample was taken out after 30 min, 60 min, and overnight

incubations. The 50 µL sample was filtered using YM 10 filter, and the filtrate was stored at -80 °C freezer before HPLC analysis.

Filtrate samples collected above were analyzed by HPLC using a Dionex CarboPac PA1 anion exchange column (4 x 250 mm) coupled with UV detection at 258 nm. The solvent system used here was water (solvent A) and 1 M NH_4OAc (solvent B). The column was first pre-equilibrated with 30%B. With a flow rate of 1 mL/min, samples were eluted using a gradient method as following: the method started at 30% B; after 2 min, solvent B was increased linearly to 90% in 8 min; isocratic run with 90% B for 5 min; solvent B was brought back to 30% in 2 min. At the end, the column was re-equilibrated with 30% B for 7 min before the next run.

4.2.7. Preparation, purification and activity test of smDEF

To generate smDEF, which is the modified-DEF containing mono-ADP-ribose or short oligo- PAR polymers, modification reaction (1 mL) was set up using 12.5 µM free-DEF, 2.5 µM C-His_6-ABC, 5 µM 8-mer DNA, 5 mM NAD^+ in a reaction buffer containing 100 mM Tris at pH 7.5, 1 mM $MgCl_2$, 300 mM NaCl and 10% glycerol. The reaction sample was incubated at room temperature for 1 hr. After that, small molecules within the sample was filtered by YM 10 filtration using a 0.5 mL YM10 filter cell, and was washed five times with 300 µL of reaction buffer. After that, the reaction sample was diluted back to 1 mL volume using reaction buffer, with fresh NAD^+ added in a final concentration of 5 mM. The reaction mixture was incubated for another 1 hr and the same cleaning procedures were performed again. This NAD^+ replenishment procedure was repeated for seven times. After the last replenishment was done, the reaction mixture was exchanged to a buffer containing 10 mM imidazole, 800 mM NaCl, 100 mM potassium phosphate at pH 6.5, and 10% glycerol. This reaction mixture was then incubated with

500 µL of Ni-NTA resin that had been pre-equilibrated with the same buffer. After incubation at 4 ^{o}C for 2 hr, the mixture was loaded onto a column, and the protein solution was allowed to drain slowly. The collected flow through was passed through another column that was pre-packed with 500 µL of the Ni-NTA resin. This was done to ensure that all C-His_6-ABC protein was removed. The purified smDEF protein recovered after the second Ni-NTA column was exchanged to a storage buffer containing 100 mM Tris at pH 7.5, 300 mM NaCl and 10% glycerol. The resulting smDEF was flash frozen and stored at -80 ^{o}C. Protein concentration of smDEF was determined based on its absorbance at 280 nm (extinction coefficient for DEF= 63,940 M^{-1} cm^{-1}, obtained from Vector NTI software) using a nanodrop instrument (Nanodrop®).

To test the activity of smDEF, reaction samples were prepared and analyzed in the same way as described in Secction 4.2.4, and concentration details for each added components are listed in Figure 4-13. Samples were incubated at room temperature, and quenched after 60 min.

4.2.8. Preparation, purification and activity test of lmDEF

To generate lmDEF, a modified-DEF form containing large PAR polymers, the automodification reaction (1 mL) was carried out using 12.5 µM free-DEF, 12.5 µM C-His_6-ABC, 25 µM 8-mer DNA, 5 mM NAD^+ in a reaction buffer containing 100 mM Tris at pH 7.5, 1 mM $MgCl_2$, 300 mM NaCl, and 10% glycerol. After 1 hr incubation, the sample was cleaned up and replenished with fresh NAD^+ in the same way as described in the case of smDEF. After the last replenishment was done, the reaction mixture was exchanged to a buffer containing 10 mM imidazole, 800 mM NaCl, 100 mM potassium pyrophosphate at pH 6.5, and 10% glycerol. The subsequent removal of C-His_6-ABC protein from the reaction mixtures was conducted in the same way as described in the

case of smDEF using pyrophosphate buffer. Finally, the recovered lmDEF protein was stored in a buffer containing 100 mM Tris at pH 7.5, 300 mM NaCl, and 10% glycerol at -80 ^{o}C until future usage. Due to the high level of modification, concentration determination of lmDEF could not be done using the absorbance signal at 280 nm because it was not the absorbance maximum. Instead, concentration was determined based on quantitation of the ADP-ribose unit measured at 260 nm absorbance maximum using nanodrop (extinction coefficient for ADP-ribose = 15,400 M^{-1} cm^{-1}). For activity test of lmDEF, the experiments were done under the same condition as described in the case of smDEF.

4.2.9. Western blot analyses

To determine if protein samples containing PAR polymers or C-terminal His_6-tag, western blot analyses were carried out. After protein separations were achieved using 12% SDS-PAGE gels, the proteins were electrophoretically transferred to a nitrocellulose membrane. This transfer process was carried out with a voltage setting at 100 V for 1 hr in cold transfer buffer containing 25 mM Tris base, 192 mM glycine, and 20% ethanol at pH 8.3. After transfer blotting, the membrane was blocked with 5% nonfat dry milk in TBST buffer containing 20 mM Tris-HCl at pH 7.5, 150 mM NaCl, and 0.05% v/v Tween 20. The blocking procedure was conducted at room temperature for 1 hr, and the membrane was washed three times with TBST buffer. After that, the membrane was incubated with either anti-PAR polyclonal antibody produced in rabbit (Trevigen) for PAR polymer detection, or anti-His (C-term) antibody produced in mouse (Invitrogen) for C-terminal His-tag detection. After overnight incubation at 4 ^{o}C, the membrane was washed three times with TBST buffer. The membrane was then incubated with the secondary antibodies using either goat anti-rabbit IgG horseradish peroxidase (HRP)-

conjugate (Novex®), or goat anti-mouse IgG horseradish peroxidase (HRP)-conjugate (Novex®) for 1 hr at room temperature. After three washes with TBST buffer, antibody signal was visualized using 1-step TMB-Blotting substrate solution (Pierce). Alternatively, it could also be visualized using chemiluminescence detection system (Pierce) based on the manufacture's protocol.

4.2.10. Heteromodification of histone H1 by PARP-1

To study the heteromodification process of histone H1 catalyzed by PARP-1, a time course assay was carried out. Reaction samples were prepared in 6 µL aliquotes. Each reaction sample contained 1 µM PARP-1, 1 µM 8-mer DNA, 5 µM histone H1 (Santa Cruz Biotechnology), 5 mM NAD^+, and 0.6 µCi ^{32}P-NAD^+. The heteromodification reaction was carried out in the reaction buffer of 4 mM $MgCl_2$, 300 mM NaCl, 15% glycerol, and 50 mM Tris at pH 7.5. Addition of NAD^+ initiated the heteromodification process. After incubation at room temperature, samples were quenched at different time points using 2X SDS-PAGE loading buffer including 50 mM EDTA. For samples that underwent PARG treatment, 0.5 µL of His_6-PARG (1.5 mg/mL) was added to each sample after 60 min of heteromodification. The purified His_6-PARG used in this section was kindly provided by Dr. Yung-nan Liu. The PARG treated samples were incubated at room temperature and quenched at different time points. After reaction, the protein samples were analyzed in the same way as described in Section 4.2.3.

4.2.11. PAR transfer assay

To see if modified-PARP-1 can transfer its pre-established PAR polymers to histone H1, the modified-PARP-1 labeled with ^{32}P ADP-ribose (i.e., ^{32}P-mPARP-1) was first prepared. A reaction mixture (200 µL) of PARP-1 automodification contained 2 µM

PARP-1, 2 μM 8-mer DNA, 2 mM NAD^+, and 45 μCi ^{32}P-NAD^+ in a reaction buffer consisting of 300 mM NaCl, 4 mM $MgCl_2$, 15% glycerol, and 50 mM Tris at pH 7.5. After incubating the reaction mixture at room temperature for 1 hr, the reaction was filtered through a YM 10 filter cell and washed with the reaction buffer ten times to remove the unreacted NAD^+ and byproducts. The protein concentration of the purified ^{32}P-mPARP-1 was determined by Bradford assay.

To test the PAR transfer from ^{32}P-mPARP-1 to histone H1, a reaction sample (6 μL) containing 1 μM ^{32}P-mPARP-1 and 5 μM histone H1 was coincubated at room temperature for 1 hr with or without the addition of 3 mM cold NAD^+. For samples treated with PARG, 0.5 μL of 1.5 mg/mL His_6-PARG was added to the reaction mixture and the incubation was continued for another hr. After samples were quenched, they were separated by SDS-PAGE and analyzed in the same way as described in Section 4.2.3.

4.2.12. Pulse-chase experiment for studying distal vs. proximal elongation

To study whether the PAR elongation happens at the distal polymer end, or at the proximal protein end, a pulse-chase experiment was carried out. Before setting up the assay, 1 mM NAD^+ stocks with different ^{32}P specific activities were prepared prior to the experiments. These preparations were based on the following concentration ratios of cold: hot NAD^+: 400:1, 800:1 and 200:1. Their corresponding specific activities were denoted as α_0 (or α_1 for 400:1), α_2 (for 800:1), and α_3 (for 200:1). At the same time, 1 mM cold NAD^+ stock was also prepared and used in the experiments.

First, a ^{32}P pulse step was carried out. This was done by labeling PARP-1 with ^{32}P NAD^+ to generate PAR polymers in an automodification reaction, and the labeled PARP-1 was denoted as the pulsed product in Figure 4-17. To generate ^{32}P-mPARP-1, a reaction mixture (200 μL) containing 1 μM PARP-1, 1 μM 8mer DNA and 100 μM ^{32}P NAD^+ (α_0)

was prepared with a reaction buffer composed of 10 mM DTT, 8 mM $MgCl_2$, 300 mM NaCl, 15% glycerol, and 50 mM Tris at pH 8.0. The reaction mixture was incubated at room temperature for 30 min; after that, 50 µL of His_6-PARG (11.4 ug/uL) was added and the sample was incubated an additional 3 hrs. The reaction mixture was then cleaned up by washing with the reaction buffer eight times using YM 10 filtration. After washing, the concentration of the resulting monoADPribosylated-PARP1 (i.e., species A in Figure 4-17) was determined using Bradford assay. The final concentration of species A was corrected for the presence of His_6-PARG, which was not removed at this point.

After that, a chase step was set up using different NAD^+ stocks prepared previously. In one set of the samples (6 µL), 0.1 µM of species A and 10 µM ^{32}P NAD^+ with different α_0 values were prepared in the reaction buffer, and they were incubated at room temperature for 30 min. After that, 2 µL of His_6-PARG was added to the sample, and the PARG treatment was carried out for 60 min in order to generate species B (Figure 4-17). Finally, the reaction was quenched with 2X SDS-PAGE loading buffer including 50 mM EDTA. For another set of samples, rather than adding the PARG at the end of the chase step, 2 µL of His_6-PARG was added to the sample together with 10 µM ^{32}P NAD^+ with different α_0 values in the chase step, and the samples were quenched after incubation at room temperature for 1 hr.

After the pulse-chase experiment was done, the protein samples were separated and analyzed by SDS-PAGE under the same condition as described in Section 4.2.3.

4.3. RESULTS

4.3.1. Activity studies of as-purified domain DEF from E. coli

To study the catalytic activity of PARP-1's minimal active fragment, domain DEF was heterologously expressed and purified from E. coli. This C-terminal portion of PARP-1 protein contains the catalytic domain F and the automodification domain D that harbors acceptor sites for PAR polymers. The activity of the as-purified DEF was tested in a time course manner using ^{32}P-NAD$^+$ as the substrate. Based on the SDS-PAGE autoradiography shown in Figure 4-1A, as-purified DEF was capable of incorporating NAD$^+$, and the incorporated ^{32}P signal increased overtime. However, this catalytic activity was not very efficient, and majority of the substrate remained unreacted after reaction.

Poly(ADP-ribosyl)ation of PARP-1 is known to consist of three steps: initiation, elongation and branching reactions. First of all, if automodification of DEF is initiated and mono(ADP-ribosyl)ation takes place, it is expected that ^{32}P-signal would appear at the DEF region in the SDS-PAGE autoradiography. Secondly, when poly(ADP-ribosyl)ation takes place and forms long, branched polymers that covalently attach to protein, this would cause the protein shifting upward to be at the stacking/running gel interface and the well regions in the SDS-PAGE.

Here, there was no indication of initiation shown from the SDS-PAGE. This is based on the lack of signal shown in the DEF region even at the early reaction time points (Figure 4-1A). Instead, majority of the incorporated ^{32}P signal was detected at the gel interface region, indicative of PAR polymer formation. However, when the activity gel was stained with a highly sensitive SYRPO RUBY protein gel stain, there was no detectable protein signal in the gel interface region (Figure 4-1C). The observation here

suggested that the amount of protein associated with ^{32}P signal, if any, was very low, and it was under the detection limit.

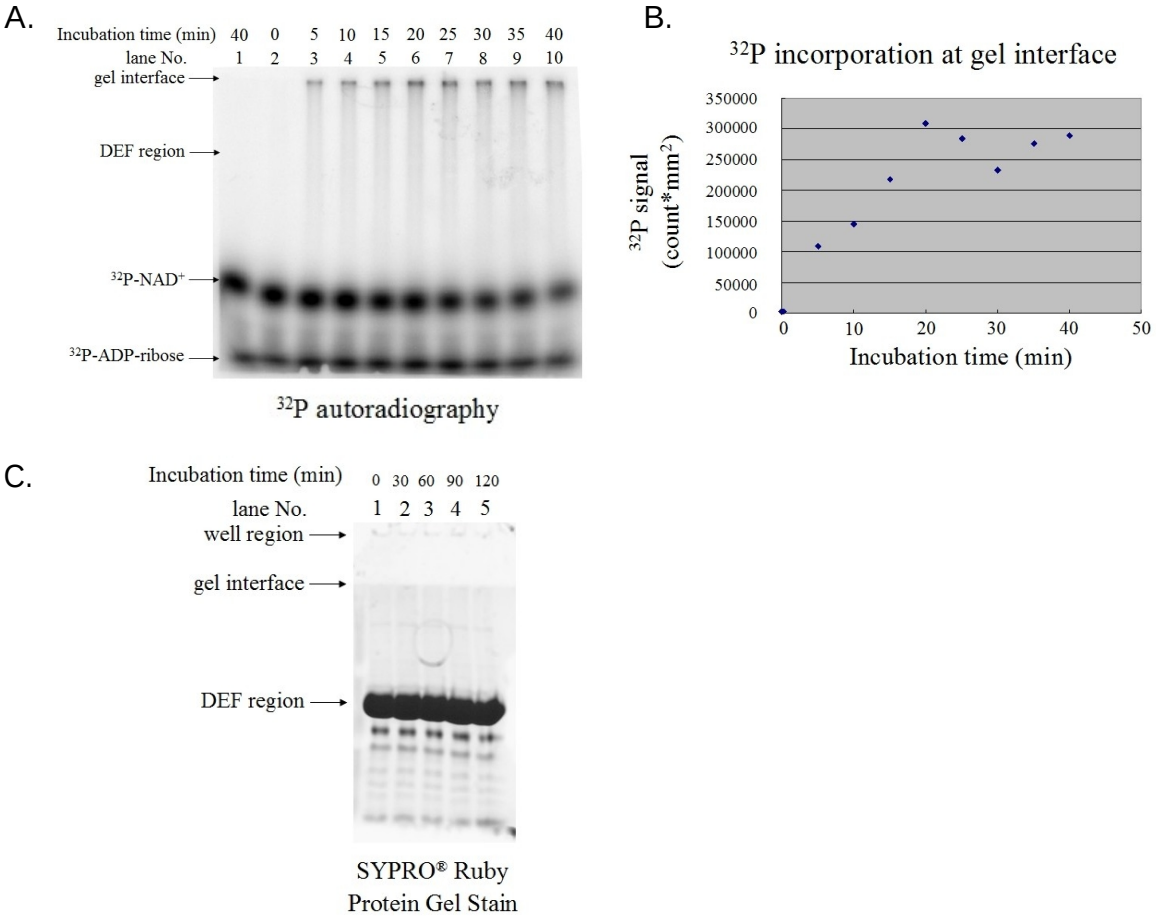

Figure 4-1. A time-course activity test of the as-purified DEF (25 µM) using ^{32}P-NAD^+ substrate (100 µM). A. Autoradiography of the activity assay. Lane 1 is a control without protein added. B. A plot of ^{32}P signal quantification at the gel interface region at different time points. The ^{32}P signal was reported as signal volume (i.e., count*mm^2). C. The extended time-course assay was done using cold NAD^+ as substrate, and it was stained with SYPRO® Ruby protein stain.

It was not clear why no initiation process was captured in the time course assay, but only formation of long PAR polymers was observed. The failure of detecting the initiation process shown in Figure 4-1 may be due to its low occurrence under the

experimental conditions, or perhaps it undergoes elongation quickly preventing accumulation of the initiation products. To test this possibility, an end point assay was carried out by varying the ^{32}P specific activity of NAD^+ used, and the samples were quenched after 5 min of reaction. It was assumed that if initiation products only accumulate at low concentration, it may become discernible when the ^{32}P specific activity of NAD^+ increases at the early reaction time points. As shown in Figure 4-2, the initiation events catalyzed by the as-purified DEF were indeed visible when ^{32}P specific activity was high enough.

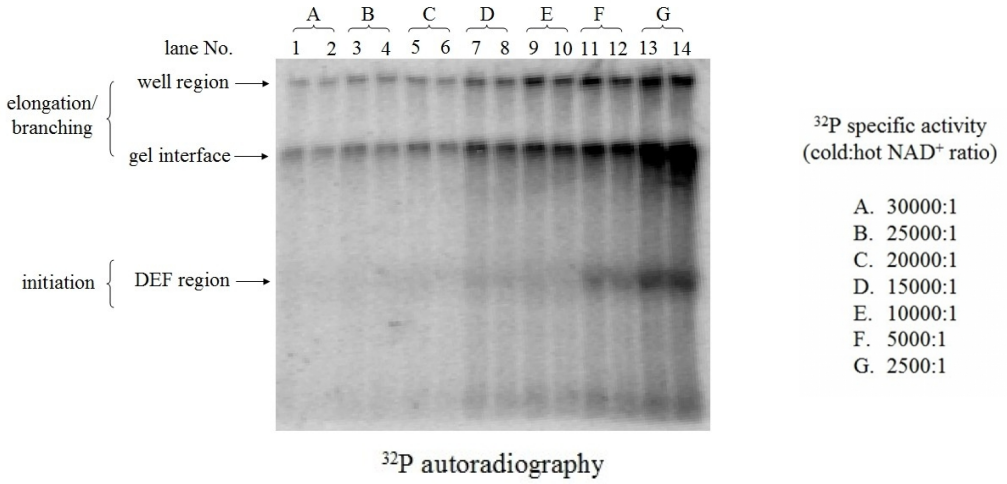

Figure 4-2. Observation of the initiation events in the DEF region is dependent on the ^{32}P specific activity of NAD^+ used. Here, sample was run in duplicate with the same concentrations of as-purified DEF (25 μM) and ^{32}P-NAD^+ substrate (100 μM) with various ^{32}P specific activities.

Furthermore, by comparing the ^{32}P signals associated with DEF, the gel interface and the well regions, it was clear that majority of the ^{32}P activities resided at the gel interface and well regions, indicating the accumulation of PAR polymers generated from elongation and branching reactions. However, since the polymer elongation and branching can only happen after the initiation step, these results raised a doubt on whether the observed ^{32}P-labeled bands on the top of the gel were really PAR related. If

the observed ^{32}P signal was due to the formation of PAR polymers, then the elongation and branching process appeared to be highly processive, and was more efficient than initiation.

To verify the identity of the ^{32}P labeled bands at the gel interface and well regions, and to determine whether its formation is truly due to the enzymatic activity of the as-purified DEF, the following assays were performed. First, by titrating increasing amounts of the ^{32}P labeled substrate NAD^+, the amounts of radioactivity incorporated at the gel and interface regions also increased (Figure 4-3A), suggesting that the incorporated ^{32}P radioactivity was derived from the as-purified DEF substrate, NAD^+. To test whether the increase in ^{32}P incorporation was due to the catalytic activity of the as-purified DEF or other protein contaminants, 3AB (i.e., 3-aminobenzamide), a competitive PARP-1 inhibitor which binds to its catalytic active site (7), was used to pre-incubate with proteins for 30 min before substrate addition. As shown in Figure 4-3B, with increasing concentrations of 3AB added, the ^{32}P incorporation at the well and interface region became less, indicative of the observed ^{32}P signals coming from the catalytic activity of as-purified DEF. Furthermore, to check if the ^{32}P incorporation was due to the formation of PAR polymers, poly(ADP-ribose) glycohydrolase (PARG) was added after the incubation of as-purified DEF with ^{32}P NAD^+ for 2 hrs. As PARG can cleave off PAR polymers, showing in Figure 4-3C, after addition of PARG, the radioactive signal diminished from the gel and interface regions. Taken all these together, the ^{32}P signal shown at the well and gel interface regions must be due to formation of PAR polymers generated by the as-purified DEF.

However, the assays shown in Figure 4-3 did not provide any clue on why only a small amount of initiation products was detected, and the subsequent elongation step appeared to be much more robust in comparison with the initiation process.

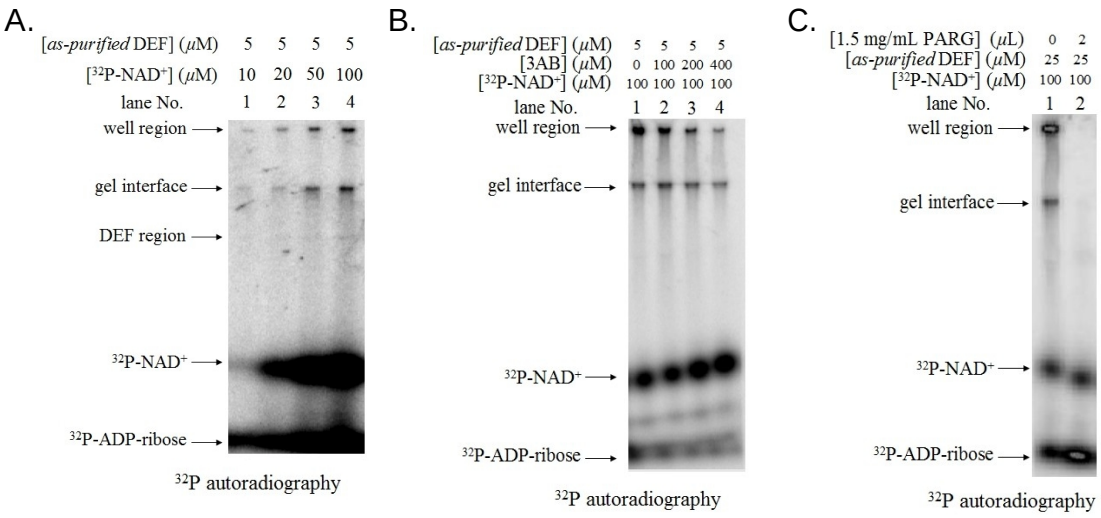

Figure 4-3. Confirmation of PAR formation at the gel and interface regions catalyzed by the as-purified DEF. A. Increase of ^{32}P NAD$^+$ concentration caused elevation of the ^{32}P radioactivity incorporation. B. Increasing amount of PARP-1 inhibitor 3AB resulted in decrease of ^{32}P incorporation. C. Addition of PARG caused disappearance of ^{32}P signal at the well and gel interface regions.

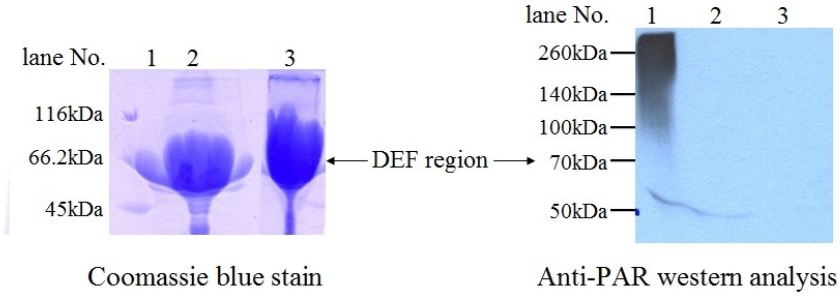

Figure 4-4. Coomassie blue staining and anti-PAR western analyses of as-purified DEF under different treatments. Lane 1. as-purified DEF with no treatment. Lane 2. as-purified DEF subjected to PARG and mild basic treatment. Lane 3. as-purified DEF under PARG treatment. The overload of protein in lanes 2 and 3 was intentional to make sure both treatments were sufficient for cleaving off PAR polymers.

Later on, it was found that the as-purified DEF protein from E. coli expression system contains endogenous PAR polymers conjugated to proteins, which could be detected by anti-PAR western blot analysis (Figure 4-4). It was also noted that even the

anti-PAR western signal was strong, the amount of protein associated with these PAR polymers was very low, because it could not be detected by the Coomassie blue staining (Figure 4-4, lane 1). The presence of endogenous PAR polymers was further confirmed by PARG treatment. PARG degrades the polymer into ADP-ribose units, leading to mono-ADPribosylated proteins, which showed no PAR signal in the anti-PAR western blot (Figure 4-4, lane 3). After that, a mild basic treatment (pH 9.5 buffer) would hydrolyze the last ADP-ribose unit off protein (Figure 4-4, lane 2).

The identification of endogenous PAR polymers conjugated to as-purified DEF proteins raised a question of whether the observation of ^{32}P signal at the well and gel interface catalyzed by as-purified DEF was due to the presence of endogenous PAR polymers. This question was based on the findings that both endogenous PAR polymers and the ^{32}P incorporation by the as-purified DEF are associated with a small amount of as-purified DEF that was invisible to Coomassie blue stain, or a more sensitive dye SYPRO® Ruby protein stain. Furthermore, the ^{32}P signal was mainly detected at the well and gel regions after incubation of the as-isolated DEF and ^{32}P NAD^+. Protein conjugated PAR polymers appeared at these regions are usually associated with large and branched PAR polymers which could not migrated into the complex gel matrix (8). While not much signal associated with initiation process was detected under the same condition, intensive ^{32}P signals at the well and gel interface can be explained by the followings hypotheses: either the elongation is a highly processive process which outcompetes the initiation process, or the elongation is due to the modification of the pre-existed PAR polymers in the as-purified DEF and requires no initiation. To test these two hypotheses, DEF with no endogenous PAR polymers attached (i.e., free-DEF) was generated and tested for activities in the following section.

4.3.2. Activity studies of free-DEF purified from E. coli

To generate the so-called the free-DEF protein that contains no endogenous PAR polymers after purifying from the E. coli expression system, the as-purified DEF was treated with His_6-PARG in pH 9.5 buffer. This treatment could remove the endogenous PAR polymers from proteins by hydrolyzing the ribose-ribose linkages of PAR polymers, and the ester linkage between the last ADP-ribose residue covalently linked to each of the carboxyl amino acid acceptor of proteins, respectively. After treatment, the His_6-PARG proteins were removed by Ni-NTA resin, and resulting free-DEF was dialyzed against HEPES buffer at pH 7.5 before activity tests. A typical Coomassie blue protein stain and anti-PAR western analysis of the resulting free-DEF protein are shown in Figure 4-4, Lane 2. Its activity was tested in comparison with as-purified DEF, and the results were shown in Figure 4-5.

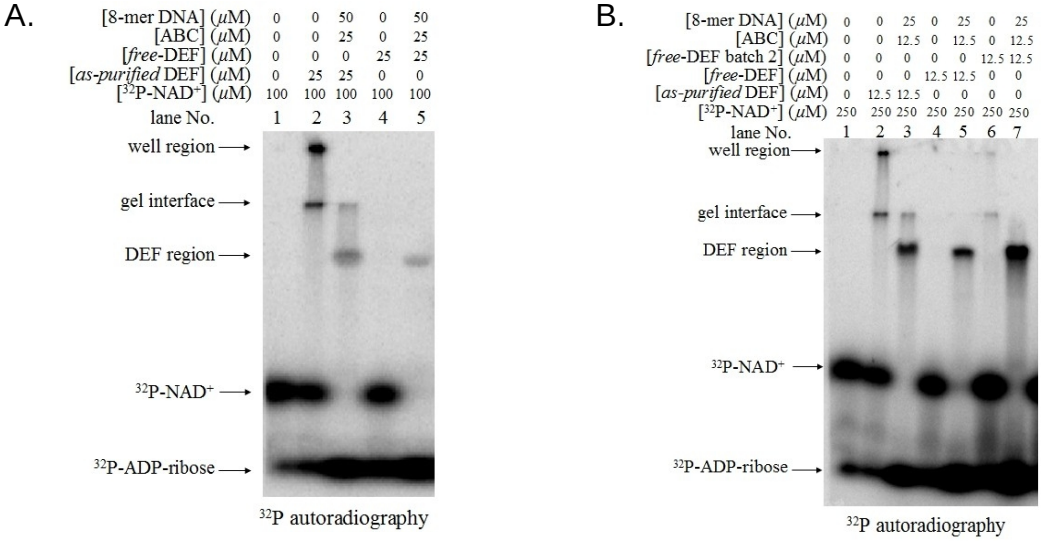

Figure 4-5. Activity assays of free-DEF and the as-purified DEF with or without addition of ABC/8-mer DNA. A. Activities was compared between free-DEF and the as-purified DEF. B. Activities was compared between free-DEF (same as in A), free-DEF (the second batch) and the as-purified DEF.

From Figure 4-5A, while the as-purified DEF showed similar activities as described before using ^{32}P labeled NAD^+ as substrates, the removal of endogenous PAR polymers from the as-purified DEF resulted in no ^{32}P signal incorporation, as shown in case of free-DEF alone (Figure 4-5A, Lane 4). This result suggested that the previous observation of ^{32}P signal at the well and interface regions when using as-purified DEF in the incubation were due to the presence of endogenous PAR polymers. While the removal of endogenous PAR polymers was incomplete (e.g., free-DEF batch 2), it still resulted in reduction of ^{32}P incorporation at the gel and well interface regions (Figure 4-5B, Lane 6) when compared with the as-purified DEF (Figure 4-5B, Lane 2). Taken together, one may conclude that the as-purified DEF incorporates ^{32}P ADP-ribose units into the endogenous PAR polymers, possibly through polymer elongation and branching reactions, giving the observed radioactive signals on top of the gel. In addition, domain DEF alone is not very efficient in carrying out initiation process in PAR formation, but it is capable of modifying the pre-existed PAR polymers, likely through elongation and branching processes.

It should be noted here that, generation of free-DEF was not always successfully, such as in the case of preparing free-DEF batch 2. The failure of producing free-DEF was due to the incomplete removal of endogenous PAR polymers during the PARG and mild-basic treatments. This was possibly ascribed to the activity variations from different batches of His_6-PARG proteins. In this study, it was later found out that, the His_6-PARG-CD (i.e., only the catalytic domain) protein constructs provided by Dr. Yung-nan Liu usually worked better than the full-length His_6-PARG protein, possibly due to higher protein stability. Accordingly, free-DEF used in assays reported in the later sections are true free-DEF whose endogenous PAR polymers had been removed completely, like the batch shown in Figure 4-5A, Lane 4.

4.3.3. PAR initiation requires the presence of ABC and DNA

As shown in Figure 4-5, robust ^{32}P labeling was observed in the DEF region only when domain ABC and 8-mer DNA were both present. Direct labeling in the DEF region was a result of initiation and oligomerization (i.e., formation of short PAR polymers). Information provided here confirmed the requirement of domain ABC and DNA for the initiation process of PAR formation. To see if DNA is needed for the initiation reaction, 8-mer DNA was omitted from the reaction mixture. As shown in Lane 3 of Figure 4-6, elimination of DNA from the reaction mixture resulted in no labeling of DEF using ^{32}P NAD^+. The above observations indicated that robust initiation of PAR formation by free-DEF requires the presence of domain ABC and 8-mer DNA.

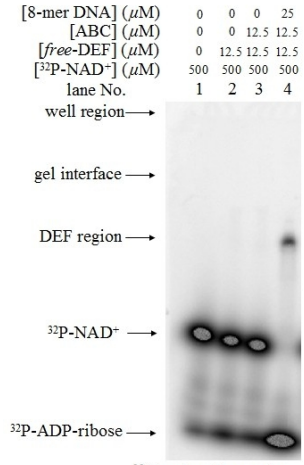

Figure 4-6. Initiation process requires the presence of 8-mer DNA.

Furthermore, in the presence of ABC and 8-mer DNA, fast hydrolysis of NAD^+ was observed to generate free ADP-ribose units. In comparison, when only as-purified DEF or free-DEF was used, this process was much slower. Based on several control experiments, PAR polymers will not be hydrolyzed during the electrophoresis process. Furthermore, DEF will not hydrolyze its conjugated PAR polymers within the experimental time scale. This will be discussed in more details in the later section.

Therefore, the above observations suggested that formation of ADP-ribose were resulted from direct hydrolysis of NAD^+, not the PAR polymers.

4.3.4. PAR polymer extension requirements in the presence of ABC/ 8-mer and free-DEF

Based on the results obtained using the as-purified DEF as catalyst described in Section 4.3.1., it was hypothesized that domain DEF alone is capable of further extending conjugated PAR polymers possibly through elongation and branching reactions. To test this hypothesis, a heavily modified DEF was needed and its elongation and branching activity could be tested for ^{32}P incorporation using ^{32}P NAD^+ without addition of ABC/8-mer DNA. If the hypothesis is true, it is expected that similar result would be obtained as in the case of the as-purified DEF alone. Therefore, using free-DEF, it was of interest in generating DEF that is heavily modified with conjugated PAR polymers large enough causing the modified DEF retained at the well and gel interface regions.

While the initiation process was observed when ABC/8-mer DNA were added to free-DEF in the presence of NAD^+, the resulting PAR units in this initiated-DEF did not get further extended under the experimental conditions shown above. This was likely due to the fast hydrolysis of NAD^+ to ADP-ribose. In order to generate the heavily modified DEF, one needed to overcome the direct hydrolysis problem. Therefore, a pulse-chase experiment was carried out to see if the initiated-DEF can get further extended in the presence of ABC/8-mer DNA by replenishing fresh NAD^+ every 10 min. Showing in Figure 4-7, the initiation process was monitored by the addition of ^{32}P labeled NAD^+ to the reaction mixture containing free-DEF and ABC/8-mer DNA (i.e., the pulse step). After 20 min, fresh cold NAD^+ (i.e., the cold chase step) was added every 10 min, and the extent of DEF modification was monitored by the ^{32}P labeled protein band upshift as more chase NAD^+ was added over time. While the modified-DEF was shifted up toward

the gel interface under consecutive chasing steps, this process was not efficient. This was indicated by the attenuation of the protein band shift, and the modified-DEF was never able to reach to the gel interface region. In attempting to solve this problem, fresh free-DEF or ABC/8-mer DNA was added during the chase, but none of them seems to help (Figure 4-8).

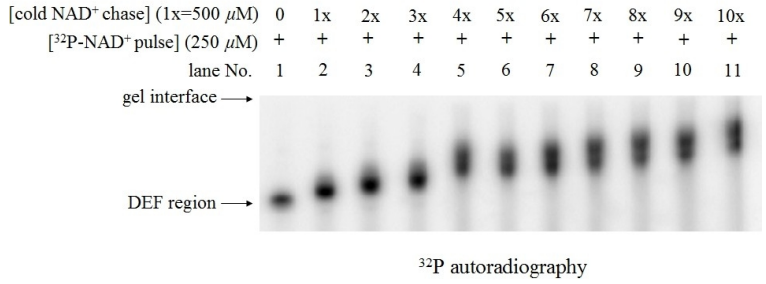

Figure 4-7. PAR polymer extension requires continuous replenishment of NAD^+. Here, reaction was initiated by adding 250 µM of ^{32}P NAD^+ into a reaction mixture containing 12.5 µM of free-DEF, 12.5 µM of ABC, and 25 µM of 8-mer DNA. After 20 min, 500 µM of cold NAD^+ (1x) was added every 10 min, and the ^{32}P labeled protein migration was monitored by SDS-PAGE.

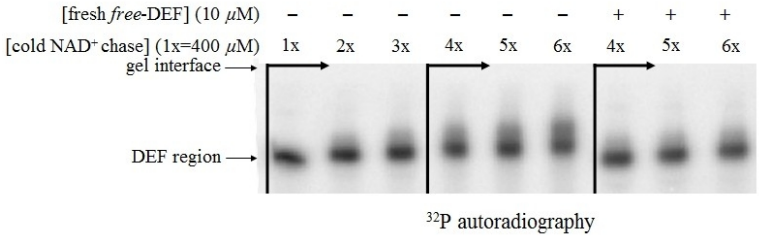

Figure 4-8. Addition of fresh free-DEF to the pulse-chase experiment did not help further PAR polymer extension. Here, reaction was initiated by adding 200 µM of ^{32}P NAD^+ into a reaction mixture containing 10 µM of free-DEF, 10 µM of ABC, and 20 µM of 8-mer DNA. After 20 min, 400 µM of cold NAD^+ (1x) was added every 10 min. After 30 min chase, fresh free-DEF was added together with the cold NAD^+, and the reaction progress was compared with the case where no free-DEF was added.

As demonstrated by a control experiment monitored by high-performance liquid chromatography (i.e., HPLC), modification attenuation of DEF was not due to the

hydrolysis of the pre-established PAR polymers. Showing in Figure 4-9, modified-DEF generated under the pulse-chase condition did not produce significant amount of ADP-ribose that was released from the pre-established PAR polymers within the experimental time scale (Figure 4-9, trace G). Small amount of ADP-ribose was detected after overnight incubation of the modified-DEF (Figure 4-9, trace H), possibly due to the degradation of the PAR polymers. Also, ADP-ribose was mainly generated during the modification process of DEF from hydrolysis of NAD^+, as shown in Figure 4-9, trace C. This is consistent with the observation from the radioactivity assays (Figure 4-5). Overall, the result suggested that DEF did not hydrolyze the pre-established PAR polymers under the experimental conditions.

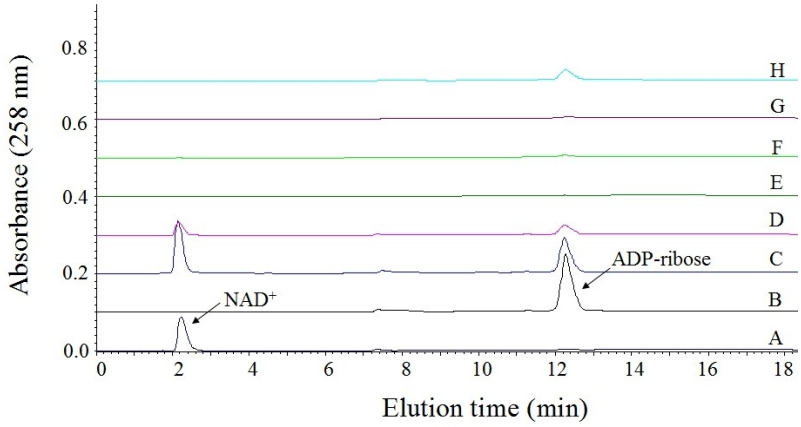

Figure 4-9. Monitor PAR polymer hydrolysis of modified-DEF. A. NAD^+ standard. B. ADP-ribose standard. C. Reaction filtrate collected from the reaction mixture of DEF modification under a pulse-chase condition. D. Modified DEF was washed with reaction buffer to remove the unreacted NAD^+ or ADP-ribose byproducts. Trace D showed the first wash of the reaction. E. The last wash of the modified-DEF. F. Pure modified-DEF incubated at room temperature for 30 min. G. Pure modified-DEF incubated at room temperature for 1 hr. H. Pure modified-DEF incubated at room temperature overnight.

Because the PARP-1 inhibitor 3AB is similar to nicotinamide, it is not surprise that nicotinamide also has inhibitory effect toward PARP-1 (7). Based on this

information, it was suspected that the built up of nicotinamide byproduct during the modification reaction may be responsible for the attenuation of generating heavily modified-DEF. To test this hypothesis, similar pulse-chase experiment was done using higher concentration of NAD^+ in each chase step to cut down the total experimental time. Furthermore, before addition of fresh NAD^+ in the chase step, the reaction sample was first subjected to buffer exchange using YM10 filter cells to remove the nicotinamide byproducts. Under this condition, the DEF conjugated PAR polymer could be extended more efficiently as the nicotinamide was excluded. This was demonstrated by the presence of modified-DEF at the gel interface region. This heavily modified-DEF was named as lmDEF, meaning that the modified-DEF was conjugated with large PAR polymers. In the case where DEF was conjugated with mono- or oligo- PARs, this form of modified-DEF was named as smDEF, meaning that DEF was decorated with small PAR polymers.

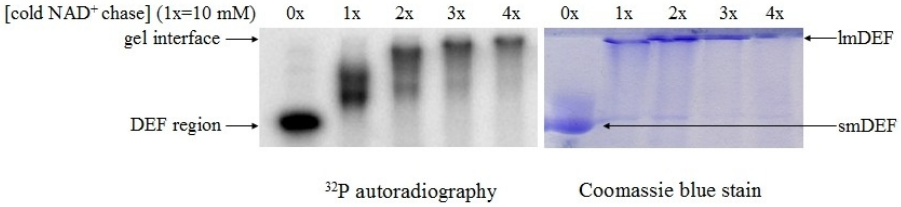

Figure 4-10. DEF conjugated PAR polymers can be extended more efficiently under the pulse-chase conditions when the nicotinamide byproducts were removed before each chase step. The experimental condition was similar to that described in the previous experiments.

4.3.5. Purification of smDEF from reaction mixture

As both smDEF and lmDEF could be generated using free-DEF incubated with ABC/8-mer DNA, the next goal of this work was to purify the two different forms of modified-DEF free of domain ABC, which could then be tested for activities. This had been a challenging task, since domain ABC was difficult to remove from the reaction mixture. MBP-His_{10}-ABC protein provided a good handle for the later removal step; however, the activity of this protein construct was pretty low. Therefore, a C-terminal His_6-ABC protein construct (i.e., C-His-ABC) was used in our experiments. Showing in Figure 4-11A, the modification level of DEF was less when using C-His-ABC in comparison with wild type ABC. Nevertheless, it showed reasonable activity level that allowed generation of smDEF. Furthermore, in our attempt to remove C-His-ABC from the modified-DEF, it was observed that C-His-ABC has strong affinity toward the modified-DEF, possibly through interaction with the conjugated PAR polymers (9). Therefore, free DEF: C-His-ABC ratio of 5:1 was used to generate the smDEF. As shown in Figure 4-11B, under the pulse-chase condition, the modified-DEF was not shifted toward the gel interface, suggesting that the majority of the modified-DEF was in the smDEF form. After the pulse-chase experiment, C-His-ABC was removed by Ni-NTA resin using potassium phosphate buffer. The recovered smDEF was confirmed by anti-PAR western analysis to show the presence of conjugated PAR polymers (Figure 4-11D). The low intensity signal of the western blot was possibly due to repetitive uses of the same anti-PAR antibody solution in this case. The complete removal of C-His-ABC from the recovered smDEF was confirmed by Coomassie blue stain as well as anti C-terminal His-tag western blot (Figure 4-11 B and C, Lane 4). Based on the assays done here, smDEF was prepared successfully in our experiments.

It should be noted that, while C-His-ABC could be completely removed from the smDEF, unreacted free-DEF was not removed from smDEF in this case. However, according to the observed activity level of C-His-ABC/8-mer and free-DEF (Figure 4-11A, Lane 3), seven rounds of 5 mM NAD^+ chases would have converted the majority of the protein to the smDEF form (Figure 4-11B, Lane 4). In addition, the recovered smDEF protein was not pure because two contamination protein bands were observed (Figure 4-11B). These two contamination bands have lower molecular mass comparing with free-DEF or lmDEF, and they are possibly resulted from degradation of DEF. This conclusion was drawn because these two proteins were discernible when high concentration of free-DEF is loaded (Figure 4-12A, Lane 7), and their intensities increased after reaction and purification (Figure 4-11B). Degradation of DEF may be caused by the prolong processing of the pulse-chase experiments and C-His-ABC removal.

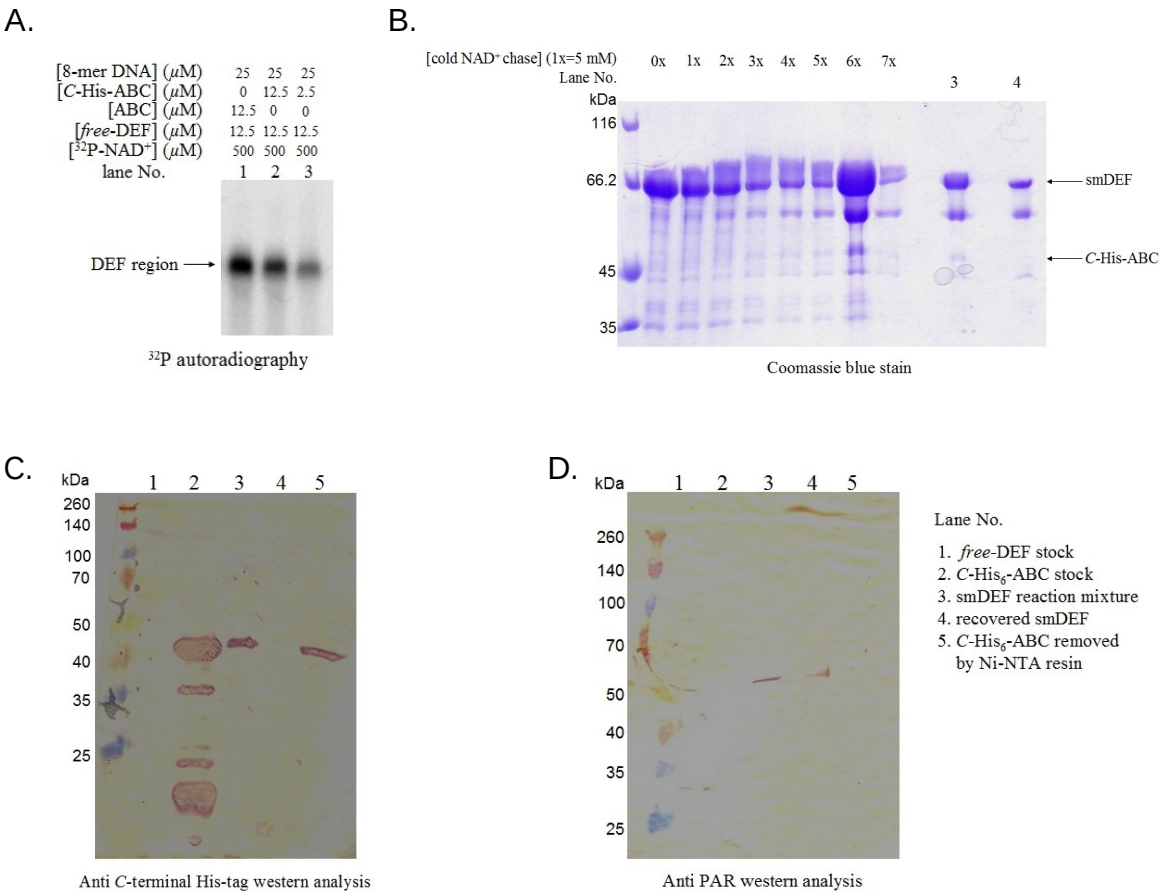

Figure 4-11. A. Comparison of the modification level of DEF using wild type ABC and different amounts of C-His-ABC. B. A pulse-chase experiment to generate smDEF. Here, the pulse step was done under the same condition as shown in A, Lane 3. The amount of cold NAD^+ and the number of chase steps were indicated for each lane. The sample labeled Lane 3 is the smDEF reaction mixture, and the sample labeled Lane 4 is the recovered smDEF after removal of C-His-ABC. C. Complete removal of C-His-ABC from recovered smDEF was confirmed by anti C-terminal His-tag western analysis. D. The presence of PAR polymers within smDEF was confirmed by anti PAR western analysis. For both C and D, the identities samples loaded in each lane were shown on the right.

4.3.6. Purification of lmDEF from reaction mixture

To generate the lmDEF, free-DEF and C-His-ABC in 1:1 ratio were used in the pulse step (Figure 4-11A, Lane 2). After that, six rounds of NAD^+ chase steps were carried out to generate lmDEF (Figure 4-12A, Lane1). The removal of C-His-ABC using Ni-NTA resin was achieved using potassium pyrophosphate buffer. The successful generation of lmDEF and its purity was verified by Coomassie blue stain, anti C-terminal His-tag and anti PAR western analyses.

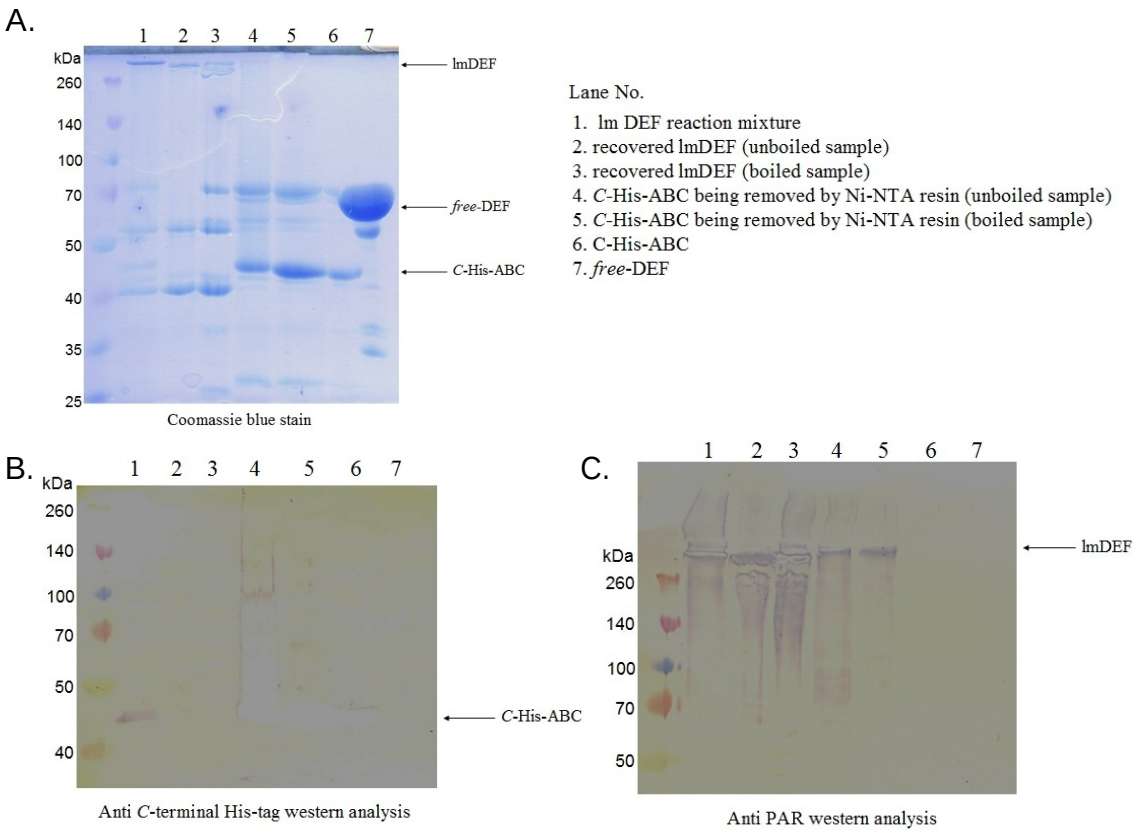

Figure 4-12. A. Coomassie blue stained SDS-PAGE showing the generation of lmDEF and its subsequent purification steps. Here, the pulse step was done under the same condition as shown in Lane 2 of Figure 4-11, and the chase step was done similarly as in the case of smDEF generation. B. Complete removal of C-His-ABC from the recovered lmDEF was confirmed by anti C-terminal His-tag western analysis. C. The presence of PAR polymers within lmDEF was confirmed by anti PAR western analysis.

4.3.7. Activity test of the purified smDEF

The purified smDEF is the modified-DEF form which contains mono-ADP-ribose or short oligomers of PAR. Its structure is supported by the observation that PAR signal could be detected on the protein sample, and the corresponding protein band shift in the SDS-PAGE gel was moderate. A set of assays were carried out using smDEF to address the following question: after DEF gets initiated, does further elongation of the initiated unit require the presence of domain ABC and 8-mer DNA?

As shown in Figure 4-13 Lane 1, smDEF itself exhibited low activity, similar as what had been seen in the case of as-purified DEF. The small amount of ^{32}P incorporation at the well and gel interface regions may be resulted from further extension of the short PAR polymers in smDEF. Addition of free-DEF did not help to enhance the ^{32}P incorporation process (Figure 4-13, Lane 2). Interestingly, when domain ABC was incubated together with smDEF, the DEF region showed ^{32}P signal incorporation, as shown in Figure 4-13, Lane 3. It was also observed that, when smDEF was used instead of free-DEF, the direct hydrolysis of NAD^+ slowed down when ABC was present. Here, ABC formed an active complex with smDEF, which in turn caused further modification of smDEF, possibly through extension of the short PAR polymers or of the initiated units. It is also possible that this active complex carried out initiation. However, the observation of slow NAD^+ hydrolysis in Lane 3 when compared with as-purified DEF incubated with ABC/8-mer DNA (Figure 4-6, Lane 4), was more consistent with the involvement of ABC/smDEF in elongation process, where slow hydrolysis was observed (Figure 4-5, Lane 2). Addition of ABC/8-mer DNA had stronger influence than ABC alone. Comparing Lane 3 and Lane 6 in Figure 4-13, it was clear that higher amount of radioactive signal was incorporated when 8-mer DNA was included. In addition, the smDEF band shifted slightly upward in Lane 6, indicating that the short PAR polymers

on smDEF were extended. Based on the above observations, the results demonstrated that further extension of the short PAR polymers conjugated with DEF requires the presence of domain ABC and 8-mer DNA to form the active complex.

Furthermore, when free-DEF was added to the smDEF/ABC/8-mer DNA reaction mixture (Figure 4-13, Lane 7) Direct hydrolysis of NAD^+ became more pronounced. Similar results were also observed in the initiation reaction of free-DEF with ABC/8-mer DNA (Figure 4-6, Lane 4). Unlike the case where free-DEF was absent (Figure 4-13, Lane 6), the ^{32}P labeled DEF band did not shift upward. Furthermore, significant amount of ^{32}P radioactivity was shown at the well and gel interface regions, similar to what had been observed when only smDEF was tested (Figure 4-13, Lane 1). These results suggested that three active protein complexes were formed. One of them is smDEF itself, which contributes to the signal observed at the well and gel interface regions, the second one is the free-DEF/ABC/8-mer DNA active complex, which contributes to the ^{32}P signal appearing at the DEF region, as well as the fast NAD^+ hydrolysis to generate ADP-ribose. The third one is the smDEF/ABC/8-mer DNA complex, which causes further modification of smDEF. However, because this is a competition process between smDEF and free-DEF for the complex formation with ABC/8-mer DNA, the protein band shift is less apparent in this case.

As ^{32}P signals associated with these three different forms of active complex can be identified in Lane 7 of Figure 4-13, the result shown here is consistent with an intramolecular elongation process of DEF. This conclusion was drawn because if the short PAR polymers conjugated to the smDEF can be modified by the free-DEF/ABC/8-mer DNA complex intermolecularly, it is expected that the ^{32}P signal at the DEF region would appear as a smear due to different sizes of PAR polymers generated at that region. Instead, signal shown in Lane 7 is more like a superposition of Lane 1, Lane 5 and Lane

6. Within each of these three lanes, different forms of active complexes described above are expected to be visible. Therefore, data obtained from smDEF activity supports a hypothesis that modification of DEF happens intramolecularly.

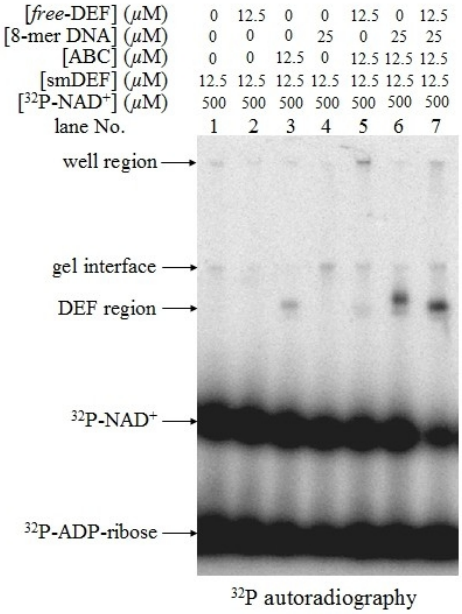

Figure 4-13. Activity test of smDEF. Reaction conditions are listed for each sample lanes.

4.3.8. Activity test of the purified lmDEF

Once lmDEF was generated in Section 4.3.6, its activity was tested. It should be mentioned that because of large amounts of PAR are conjugated to lmDEF, concentration determination by nanodrop measuring absorbance at 280 nm is not accurate. This is because the absorbance signal of proteins overlapped with the absorbance maxima at 260 nm arising from ADP-ribose. Furthermore, as shown in Lane 2 of Figure 4-12A, the lmDEF sample contains other protein contamination which could not be removed based on the current purification protocol. Due to the reasons cited above, lmDEF concentration was determined based on the concentration of ADP-ribose units. When testing lmDEF

activity, 200 µM of lmDEF was used. This means that lmDEF containing 200 µM of ADP-ribose units was employed, and the total protein concentration was about 32 µM. As the protein purity was nearly 40% based on the gel shown in Figure 4-12A, pure modified-DEF protein was about 12.8 µM, which was roughly similar to the amount of smDEF (12.5 µM) being used. The results of lmDEF activity tests are shown in Figure 4-14.

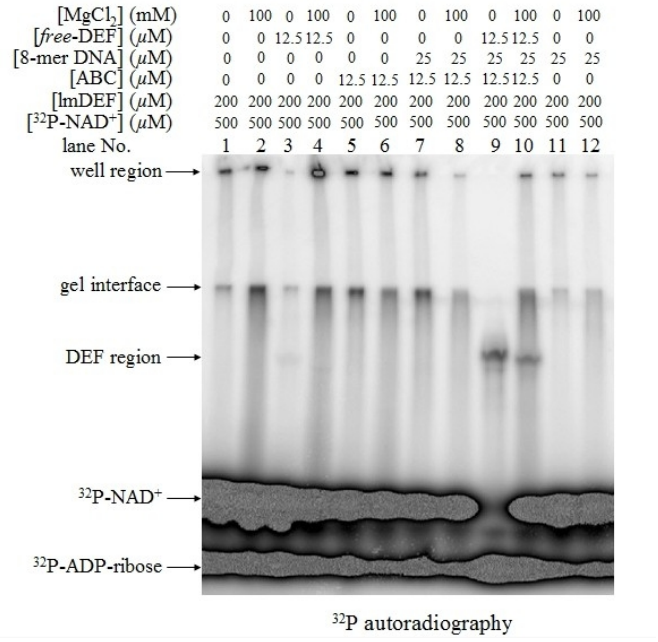

Figure 4-14. Activity test of lmDEF. Reaction condition was listed for each sample lanes.

Shown in Lane 1 of Figure 4-14, lmDEF itself is capable of incorporating ^{32}P signal at the well and gel interface regions, like the case of as-purified DEF. Since lmDEF is mainly conjugated with large PAR polymers (Figure 4-12A, Lane 2), this observation suggested that DEF itself is capable of further modifying large PAR polymers. Addition of ABC (Lane 5) or 8-mer DNA (Lane 11) had little effect on the ^{32}P

incorporation into lmDEF. Addition of ABC/8-mer DNA (Lane 7) also showed no strong influence of ^{32}P incorporation at the well region; however, signal at the gel interface region was increased in this case. Again, this observation is consistent with the previous conclusion drawn with smDEF, where ABC and 8-mer DNA are needed in extending short PAR polymers. When polymers become significantly large and retain at the well region, the participation of ABC/8-mer DNA is not required for PAR polymer extension.

Furthermore, when free-DEF was added to lmDEF, an inhibitory effect was observed in this case (Figure 4-14, Lane 1 versus Lane 3). This observation is not consistent with an intermolecular modification process, where addition of active DEF should accelerate the ^{32}P incorporation. Instead, the result indicated free-DEF is not capable of extending PAR polymers that are conjugated to another protein molecule. Finally, when free-DEF/ABC/8-mer DNA was added to lmDEF (Figure 4-14, Lane 9), initiation took place on the newly added free-DEF followed by fast NAD^+ hydrolysis. Here, modification of lmDEF with signal shown at the well and gel interface regions was not observed. These observations suggest that the major active complex is the DEF/ABC/8-mer DNA complex.

Another interesting piece of information obtained in this study is the effect of Mg^{2+}. For conventional assays done in this section, 1 mM of $MgCl_2$ was always added to all reaction samples. In this study, the effect of Mg^{2+} was examined by adding additional 100 mM of $MgCl_2$ in the reaction mixture. As shown in Lane 2, Lane 4 and Lane 10 of Figure 4-14, supplementation of Mg^{2+} caused increase of ^{32}P incorporation at the well and gel interface regions. This observation suggests that addition of Mg^{2+} ions can stimulate the elongation process of large PAR polymers.

4.3.9. PAR transfer assay

Based on the biochemical studies presented in the previous sections, a mechanistic model of PARP-1 automodification can be proposed, and details are provided in the Discussion section in this chapter. According to the proposed model, PARP-1 catalyzes PAR polymer elongation through distal addition, meaning that the new ADP-ribose unit of PAR is added to the polymer terminal that is not attached to the protein. In another possible scenario, the new ADP-ribose unit is added to the protein end during PAR elongation. The latter is called proximal addition. For the proximal elongation model, at least two amino acid residues in the active site of protein may involve as ADP-ribose/PAR acceptors, so the ADP-ribose unit can be added on one site and the PAR polymer grown on another site is then transferred to where the newly added ADP-ribose unit resides during the elongation process. This process is called the PAR transfer process. Therefore, if elongation of PAR polymers happens distally, no PAR transfer is expected; in contrast, when elongation of PAR happens through proximal addition, the PAR transfer process is expected to occur and may be observed.

Detection of the potential PAR transfer process was carried out using modified-PARP-1 and histone H1. The basic experimental design is to generate modified-PARP-1 using ^{32}P NAD^{+}. Then, the ^{32}P labeled modified-PARP-1 (i.e., ^{32}P-mPARP) is incubated with histone H1, which is a heterosubstrate of PARP-1. The process of PAR transfer is then monitored by the relocation of ^{32}P signal from PARP-1 to histone H1. Since these two proteins have different molecular mass, it can be analyzed by SDS-PAGE electrophoresis. While modification of histone H1 is a heteromodification process catalyzed by PARP-1, one assumption made here is that, the mechanism of PAR elongation carried out by PARP-1 is the same for automodification and heteromodification.

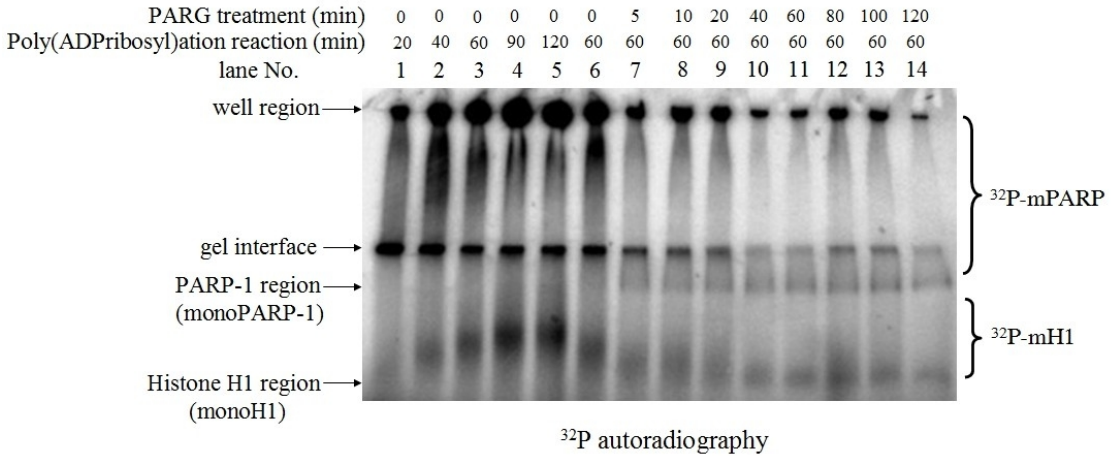

Figure 4-15. A control experiment demonstrating ^{32}P labeling of modified-PARP-1 and modified-histone H1. Here, heteromodification of histone H1 was carried out using 1 µM PARP-1, 5 µM histone H1, 1 µM 8-mer DNA and 5 mM ^{32}P-NAD^{+}. The heteromodification was monitored by a time course assay (Lane 1 to Lane 5). After 60 min of heteromodification, 0.5 µL of 1.5 mg/mL of PARG was added and formation of monoPARP-1 and monoH1 were also monitored by a time course assay (Lane 6 to Lane 14).

Before carrying out the group transfer experiment, a control assay was done to see if the ^{32}P-mPARP and ^{32}P labeled modified-histone H1 (i.e., ^{32}P-mH1) can be clearly differentiated from each other. Based on the results shown in Figure 4-15, PARG treatment was required after the PAR transfer assay to show clear ^{32}P labeled protein bands for the mono-ADP-ribosylated PARP-1 (i.e., monoPARP-1) and mono-ADP-ribosylated histone H1 (i.e., monoH1) that can be resolved by the SDS-PAGE. This was done because when the protein conjugated PAR polymers are large and branched, they tend to retain at the well and gel interface regions. In this case, modified PARP-1 and modified histone H1 can not be differentiated from each other. Therefore, PARG treatment is necessary to show the modified protein band with expected molecular mass for both PARP-1 and histone H1. As shown in the control experiment (Figure 4-15), the PARG treatment did not go to completion after 2 hr incubation because some PAR

conjugated protein was shown in the well region. However, it does not affect the result in this assay because the ^{32}P labeled protein bands showed up at the PARP-1 and histone H1 regions, indicating both PARP-1 and histone H1 was modified.

An unexpected phenomenon observed here is that there was a time delay between the PARP-1 automodification process and the heteromodication process. Showing in Figure 4-15 Lane 1 to Lane 5, it is clear that automodification was predominant at the early time, and getting saturated at around 40 min. It was also found that histone H1 heteromdification occurred in a slower rate when compared with the automodification reaction. As automodification level started to get saturated, histone H1 modification continued, as shown by the mH1 protein band shifting upward. The time difference between first occurrence of automodification and heteromodification raised an interesting question of whether automodification of PARP-1 is a pre-requisite for heteromodification to take place.

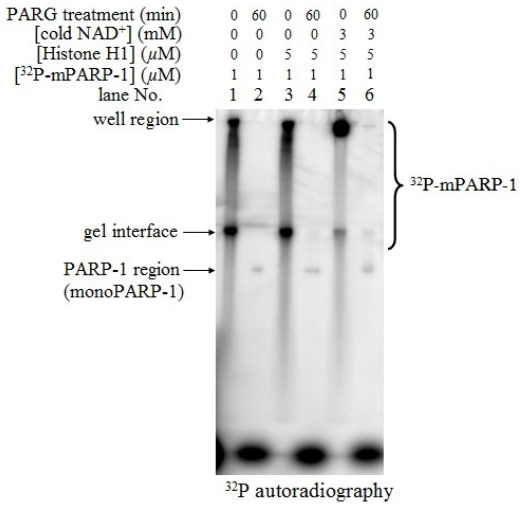

Figure 4-16. PAR transfer from the ^{32}P labeled modified-PARP-1 was tested using histone H1 as the polymer acceptor substrate. PAR conjugation to the target proteins was confirmed by PARG treatment (0.5 µL of 1.5 mg/mL stock).

Based on the information shown in Figure 4-15, a PAR transfer assay was designed as followed. First, PARP-1 automodification was carried out and the unreacted ^{32}P-NAD^{+} was washed off through YM10 filtration. The purified ^{32}P-mPARP-1 was then incubated with histone H1 under various conditions for 1 hr. After incubation, the samples were treated with PARG for another hour, and the protein samples were separated by SDS-PAGE electrophoresis (Figure 4-16).

As shown in Lane 3 of Figure 4-16, histone H1 incubated with modified-PARP-1 (^{32}P-mPARP-1) did not show any detectable ^{32}P signal below the PARP-1 region, where the modified histone H1 would be located. This was further confirmed by the same sample after PARG treatment, there was no monoADP-ribosylated histone H1 detected in this case (Figure 4-16, Lane 4). Addition of cold NAD^{+} to the reaction mixture helped to further elongate the pre-existed PAR polymers associated with PARP-1, but did not facilitate PAR transfer from ^{32}P-mPARP-1 to histone H1 (Figure 4-16, Lane 5 and Lane 6). Based on the results shown above, it was concluded that no PAR transfer occurred. If PARP-1 catalyzes PAR elongation using the same mechanism for both automodification and heteromodification, the current result is consistent with the distal elongation process of PAR, where no PAR transfer is required.

4.3.10. Proximal vs. distal elongation: pulse-chase experiment

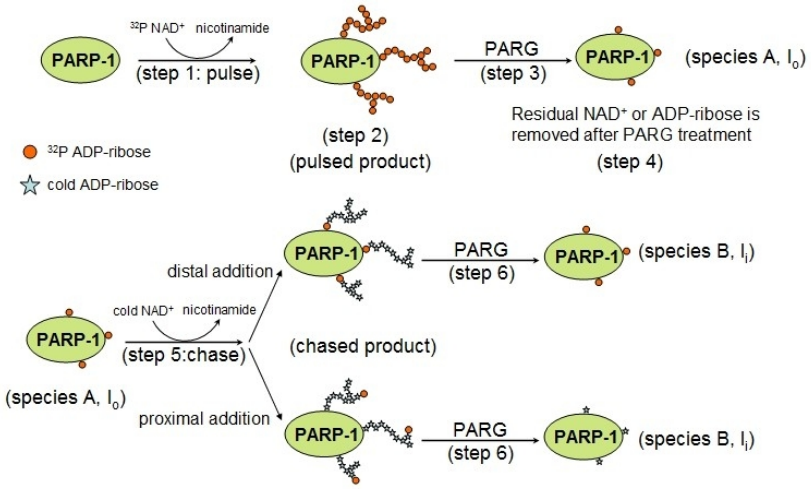

Figure 4-17. A general experimental set up for the pulse-chase experiment. Species being quantified are denoted as species A and species B.

A more straight forward way to test whether PAR polymer elongation happens at the distal end of the polymer terminus (i.e., distal addition) or at the protein ends (i.e., proximal addition) is a pulse-chase experiment where different substrate forms are added during the reaction process. The basic experimental plan is shown in Figure 4-17, and the quantitative theory discussed below was developed by our post-doctoral fellow Dr. Mark Ruszczycky. This quantitative theory accounts for the numbers of new initiation sites during the chase step and the fraction of initiated sites during the pulse step which will get further elongated during the chase step.

In the pulse step, PARP-1 was first modified by excess ^{32}P NAD$^+$ with a known amount of specific activity denoted as α_o. This pulse condition allows generation of large PAR polymers, and also have one or more than one initiation site per protein molecule (i.e., $E(N_o) \geqslant 1$, with $E(N_o)$ denoted as numbers of initiation site per PARP-1 molecule). Then this modified-PARP-1 (i.e., pulsed product in Figure 4-17) was treated with PARG. As PARG hydrolyzes PAR polymers, and leaves only one ADP-ribose unit attached to

protein, this would yield a mono-ADPribosylated-PARP-1 (i.e., species A in Figure 4-17). This species A has an E(n) value equals to 1, where E(n) denoted as the average number of ADP-ribose units per PAR polymer chain. After pulse and PARG treatment steps, the species A would have radioactivity intensity denoted as I_o which can be quantified from the ^{32}P autoradiography. The intensity I_o of species A depends on the concentration of PARP-1, the specific activity used during the pulse step as well as numbers of initiation sites. The overall dependence is described by equation (10).

$$I_0 = c_p \gamma \alpha_o E(N_o) \qquad (10)$$

I_0 : ^{32}P intensity of species A
c_p : concentration of PARP-1
γ : a conversion coefficient that accounts for differences in sample volume loaded onto gel lanes
α_o : specific activity of the hot NAD^+ used in the pulse step
$E(N_o)$: number of initiation site per PARP-1 in species A

After cold NAD^+ chase (or any NAD^+ chases with known specific activities) and PARG treatment (step 5 and step 6 in Figure 4-17), the resulting species B would have ^{32}P intensity of I_1 given by equation 11.

$$I_1 = c_p \gamma \left((1-q)\alpha_o E(N_o) + q\,\alpha'_1 E(N_o) + \alpha_1 \Delta E(N_o)\right) \quad (11)$$

α'_1 : a specific activity that depends on whether elongation is proximal ($\alpha'_1 = \alpha_1$) or distal ($\alpha'_1 = \alpha_0$)
α_1 : specific activity of NAD^+ used in the cold chase step
q : the fraction of polymer produced during pulse step would get further elongated during the chase step
$\Delta E(N_o)$: average number of new initiation sites per protein

In equation 11, the $(1-q)\alpha_0 E(N_0)$ term reflects the initiated sites which does not get further elongated during the pulse step; the $q\alpha'_1 E(N_0)$ terms reflects the initiated sites which gets further elongated during the pulse step; and the $\alpha_1 \Delta E(N_0)$ reflects new

initiation site during the chase step. Under this case, the radioactive signal of species A and species B can be compared and resulted in $R_I = I_1/I_0$.

Here, if elongation happens through distal addition, the resulting R_I is defined by equation (12). If elongation happens through proximal addition, the resulting R_I is defined by equation (13).

$$R_I = \frac{I_i}{I_o} = 1 + \frac{\alpha_i}{\alpha_o}\ \Delta E(N_o)/\ E(N_o) \quad (12)$$

I_i: ^{32}P intensity of species B when specific activity α_i was used in the chase step

α_i: specific activity of the NAD$^+$ used in the chase step

$$R_I = \frac{I_i}{I_o} = 1 - q\left(1 - \frac{\alpha_i}{\alpha_o}\right) + \frac{\alpha_i}{\alpha_o}\ \Delta E(N_o)/\ E(N_o) \quad (13)$$

During this pulse-chase experiment, different specific activity of ^{32}P NAD$^+$ was used in the chase step, such that α_i/α_0= 0, 0.5, 1 and 2 for this experiment. For this experimental trial, it was assumed that all initiated sites in the pulse step would get further elongated during the chase step, where q≈1. Based on this assumption, the equations can be re-arranged as followed. For a distal elongation process, equation (14) will be applied, and for a proximal elongation process, equation (15) will be applied. In both cases, the observable R_I -1 would be linear.

$$R_I - 1 = \frac{I_i}{I_o} - 1 = \frac{\alpha_i}{\alpha_o}\ \Delta E(N_o)/\ E(N_o) \quad (14)$$

$$\text{Y-intercept} = 0$$
$$\text{slope} = \Delta E(N_o)/\ E(N_o)$$

$$R_I - 1 = \frac{I_i}{I_o} - 1 = \frac{\alpha_i}{\alpha_o}(1 + \Delta E(N_o)/\ E(N_o)) - 1 \quad (15)$$

$$\text{Y-intercept} = -1$$
$$\text{slope} = \Delta E(N_o)/\ E(N_o) + 1$$

Based on the quantitative theory discussed above, a pulse-chase experiment was carried out using specific activity ratios (α_i/α_o) of 0, 0.5, 1 and 2. Intensity values I_0 of species A and I_i of species B were obtained and the corresponding R_I -1 values were plotted against its α_i/α_o ratio. Results are presented in Figure 4-18 and 4-19.

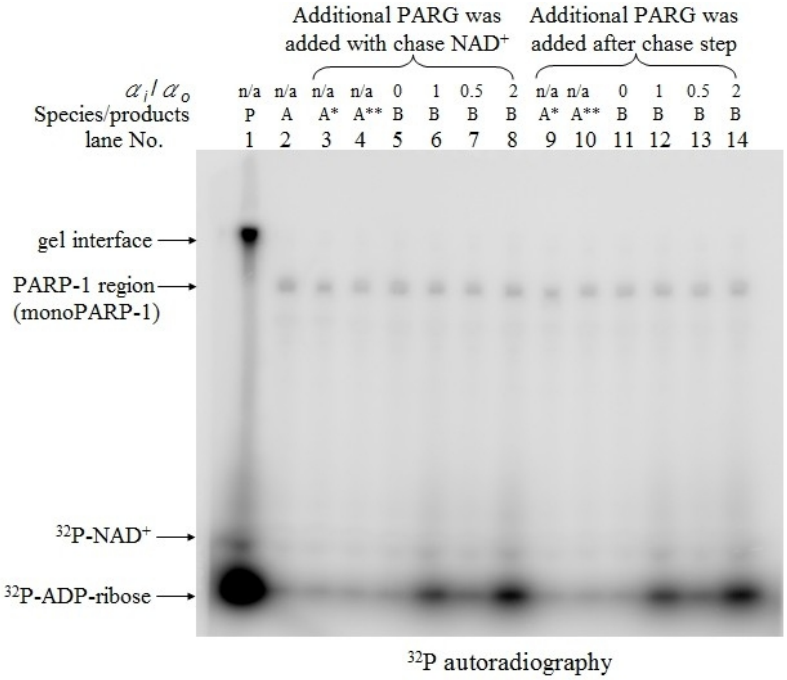

Figure 4-18. A ^{32}P autoradiography was used for quantification of the pulse-chase experiment. Here, the pulse step (denoted as P in the gel) was carried out using 1 µM of PARP-1, 1 µM of 8-mer DNA and 100 µM of hot NAD^+ with specific activity of α_o. For the chase step carrying out in Lane 3 to Lane 8, 0.1 µM of species A (denoted as A in the gel) was incubated with 10 µM of NAD^+ with specific activity of α_i for 60 min, 2 µL of PARG was also added during the chase step, and the resulting species B was denoted as B in the gel. For the chase step carrying out in Lane 9 to Lane 14, 0.1 µM of species A was incubated with 10 µM of NAD^+ with specific activity of α_i for 30 min, and then 2 µL of PARG was added and incubated for another 60 min to generate species B. Here, A* and A** were control samples of species A that went through the same treatments in the chase step, except that no chase NAD^+ was added.

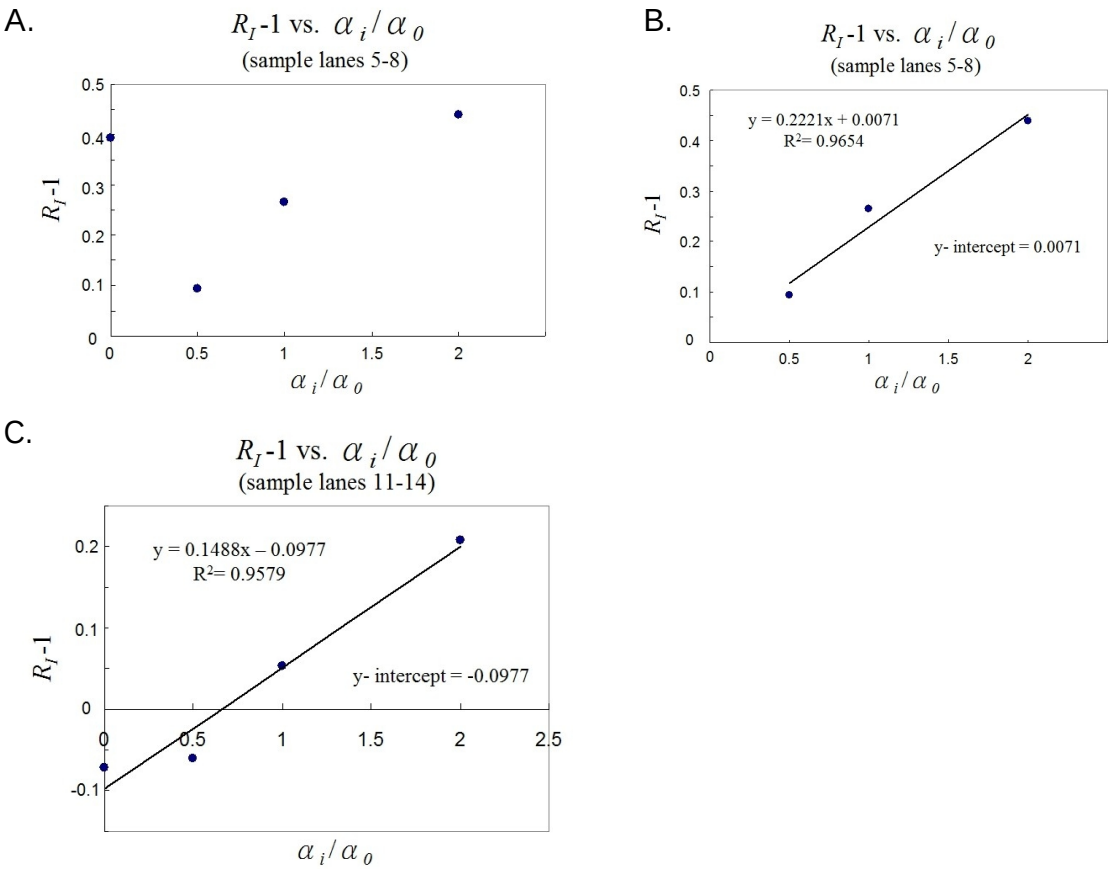

Figure 4-19. Plots of R_I -1 versus α_i/α_0 for the pulse chase experiments. A. Data points are plotted for Lanes 5-8. B. Data obtained from Lanes 5-8 are fitted linearly, and one outlier data point was excluded from the fit. C. Data points obtained from Lanes 11- 14 are plotted and fitted linearly.

Based on the 32P autoradiography shown in Figure 4-18, the pulse condition was sufficient to generate large PAR polymers, as indicated by the protein band shift (Figure 4-18, Lane 1). While it was not done in this preliminary study, a complete protein band shift needs to be confirmed by Coomassie blue stain to ensure E(No)$\geqslant$1. Here, PARG used after the pulse step was not removed. Based on previous trials of pulse-chase experiments, the removal of PARG was found to be difficult and caused large protein loss. Reported in the literature, the presence of PARG does not inhibit PARP-1 activity (10). As PARP-1 continued to generate PAR polymers, the presence of PARG would

hydrolyze these newly generated PAR polymers at the same time. To see if the presence of PARG would have any effect on the outcome of this experiment, the second PARG treatment (step 6) was combined with the chase step (step 5), by adding PARG during the chase step (Lane 3 to Lane 8 in Figure 4-18).

Lanes 5-8 in Figure 4-18 are the chase results using different α_i values of NAD^+ in the chase in the presence of extra PARG. In the case where $\alpha_i=\alpha_o$, $R_I - 1 = \Delta E(N_0)/E(N_0)$, which reflects the fraction increase of the new initiation sites during the chase step. For Lanes 5-8, when $\alpha_i=\alpha_o$, and $R_I - 1 = 0.27$. This indicated that there was about 27% increase of new initiation during chase. A plot of R_I -1 vs. α_i/α_o for Lanes 5-8 is shown in Figure 4-19A. There is a point where $\alpha_i/\alpha_o = 0$ appeared to be an outlier. When the rest of the data points are fitted linearly (Figure 4-19B), it has a y-intercept of 0.0071, and a slope of 0.2221. This result is consistent with what is expected for the distal addition.

Lanes 11-14 in Figure 4-18 are the chase results using different α_i values of NAD^+ in the chase where extra PARG was added after the chase step. In the case where $\alpha_i=\alpha_o$, $R_I - 1 = 0.05$, suggesting that about 5% increase of the new initiation sites during the chase step. When the data points of $R_I - 1$ vs. α_i/α_o is fitted linearly (Figure 4-19C), it had a y-intercept of -0.0977, and a slope of 0.1488. This result is again consistent with the expectation of a distal addition process.

4.4. DISCUSSION

4.4.1. Domain ABC and DNA serve as initiation regulators for PAR formation

To investigate the catalytic activity of PARP-1, a minimal C-terminal catalytic fragment, domain DEF of PARP-1, was first prepared. Consistent with the results reported by Mendoza-Alvarez et al. (1, 11), the as-purified DEF showed low ^{32}P NAD^+

incorporation in the absence of DNA (Figure 4-1A). Interestingly, the majority of the ^{32}P labeled species appeared at the well and gel interface regions, and little initiation products were detected unless NAD^+ with high ^{32}P specific activity was used (Figure 4-2). These observations suggested that the as-purified DEF is not efficient in catalyzing initiation reaction by itself. When the N-terminal fragment of PARP-1, the domain ABC was added together with 8-mer DNA to the incubation mixture, the initiation process was clearly observed to occur on the as-purified DEF (Figure 4-5). Similar results were also obtained when ABC/8-mer DNA were incubated with free-DEF (Figure 4-5). These findings demonstrate that, domain ABC and 8-mer DNA serve as induction elements which directly affect the initiation process of PAR formation.

In addition to promoting the initiation process, fast NAD^+ hydrolysis to generate ADP-ribose was also observed in the presence of ABC and 8-mer DNA. A control experiment showed that formation of ADP-ribose in this process is not due to the cleavage of pre-established PAR polymers (Figure 4-9). While this hydrolysis phenomenon is also observed for the wild type PARP-1, the effect is less pronounced for the wild type enzyme when compared with the ABC and DEF complex (12). This observation can be explained by the protein conformational change during DNA-dependent activation proposed by Langelier et al. (6). Specifically, PARP-1 may adapt a compact active conformation upon binding to DNA, where the BRCT domain (i.e., automodification domain) is positioned closed to the active site in domain F. This compact conformation of PARP-1/DNA active complex is achieved through multiple sites of interaction centered about the WGR motif within domain DEF (Figure 1-10). Because DEF/ABC/8-mer DNA complex is catalytically active, it may exhibits similar conformation as the PARP-1/DNA complex. However, as ABC/DEF represents a truncated construct of PARP-1, its conformation may be less confined than the wild type

PARP-1, and allows easy access of water to the active site, and thus fast hydrolysis of NAD^+.

4.4.2. Catalytic activities of DEF

As discussed before, DEF itself is not efficient in catalyzing the initiation reaction of PAR formation. However, the as-purified DEF is capable of incorporating ^{32}P signal and the modified DEF appears at the well and gel regions, where the large PAR polymers conjugated to protein are typically reside. Later, it was found that the as-purified DEF obtained from the E. coli expression system contains endogenous PAR polymers (Figure 4-4); however, their origins remain elusive at this point. Based on a series of control experiments, ^{32}P incorporation into the PAR polymers was shown to be catalyzed by the as-purified DEF (Figure 4-3). This led to a proposal that DEF is capable of catalyzing the extension of large PAR polymers in the absence of ABC/8-mer DNA. To test this hypothesis, lmDEF, a modified-DEF conjugated with large PAR polymers was generated from free-DEF, and its catalytic activity was tested. Consistent with the hypothesis, lmDEF was shown to be able to increase ^{32}P incorporation at the well and gel-interface regions, similar to in the case of as-purified DEF (Figure 4-14). This result suggested that, as a PAR polymer reaches to a certain length, it can serve as a substrate of DEF, and this catalysis is not regulated by domain ABC and 8-mer DNA. However, this catalysis is not very efficient either, possibly due to the negative charges built up during PAR polymer formation. As the size of a PAR polymer gets larger, the overall negative charges also increase. This may cause repulsion of PAR polymers from the active site in domain F. Consistent with this thought, addition of Mg^{2+} stimulates ^{32}P incorporation of lmDEF (Figure 4-14). Therefore, Mg^{2+} may serve as counter ions of the phosphate groups

of PAR polymers, which in turn reduces the overall net charge of PAR, rendering it a better substrate for DEF.

4.4.3. Domain requirements for PAR extension

As initiation of PAR formation on DEF requires ABC/8-mer DNA, short PAR polymer elongation also requires the presence of ABC and 8-mer DNA. This was demonstrated by the smDEF activity test. This modified-DEF form contains mono-ADP-ribose or short PAR oligomers (Figure 4-11 and Figure 4-13). Polymers conjugated to smDEF are expected to be short because smDEF appears at the same position as DEF on the SDS-PAGE gel. The presence of PAR polymers on smDEF was confirmed by anti-PAR western analysis (Figure 4-11). Therefore, it is expected that the polymers on smDEF are relatively short comparing with the polymers conjugated with lmDEF. However, for both smDEF and lmDEF, the exact polymer size distributions are not known at this point. It requires further analysis to learn the PAR polymer distribution of these two different modified-DEF forms in future studies.

4.4.4. Proposed model for modification of PARP-1 automodification

As the catalytic activity of DEF/ABC/DNA is similar to that of the wild type PARP-1/DNA, based on the biochemical studies discussed above, and the crystal structure of PARP-1 complexed with DNA (Figure 1-10) (6), a mechanistic model of PARP-1 automodification is proposed by Dr. Mark Ruszczycky.

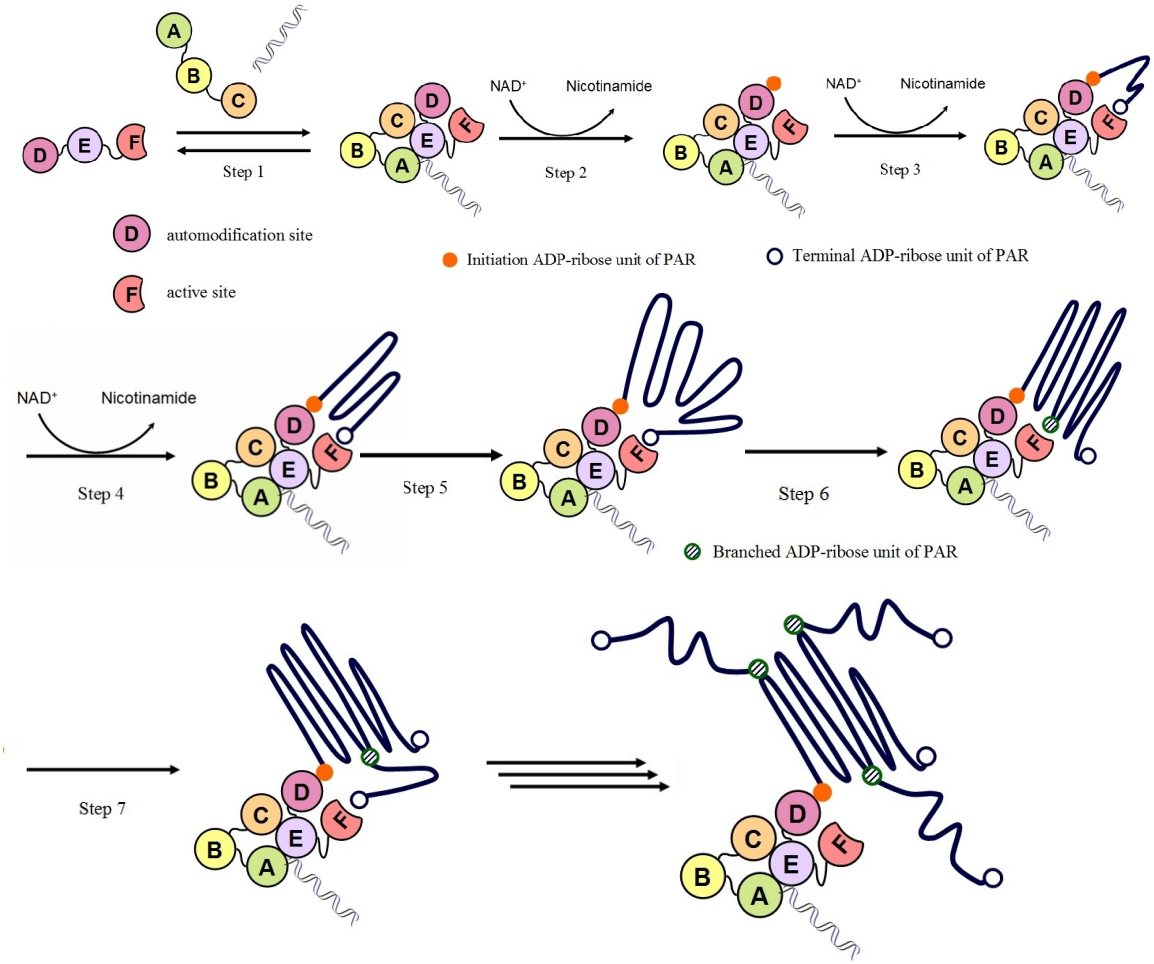

Figure 4-20. A proposed model of PARP-1 automodification.

According to the proposed model, the active conformation of PARP-1 is formed in the presence of DNA. The locations and the interaction surfaces between individual domain and DNA are postulated based on the crystal structure of PARP-1 domains complexed with DNA (6). Upon formation of the active conformation, the automodification domain D is positioned near domain F. This allows initiation of PAR formation to occur at domain D. As illustrated by step 2 and step 3, initiation and elongation of PAR polymers happen intramolecularly. This explains why free-DEF alone shows low initiation ability. Without ABC and 8-mer DNA, domain DEF may exist in a

flexible conformation, just like PARP-1 (6). In this case, the automodification domain D is not positioned closely to the active site in domain F, making initiation difficult to take place. Furthermore, addition of fresh DEF to smDEF and lmDEF does not stimulate additional ^{32}P incorporation (Figures 4-13 and 4-14). If elongation/ branching are intermolecular processes, it is expected that addition of fresh DEF would help to incorporate more ^{32}P signal as the active enzyme concentration increases.

Another key point of this proposed mechanism is that PAR elongation happens in a distal fashion. Showing in steps 3-5, the terminal unit of the PAR polymer is bound to the active site, and serves as the acceptor site for the incoming ADP-ribose during PAR elongation process. This is proposed based on the observed difference in the rates of NAD^+ hydrolysis during initiation and elongation. As discussed previously, during initiation process, direct NAD^+ hydrolysis is fast in the case of DEF/ABC/8-mer DNA when compared with the wild type PARP-1. This can be explained by the suboptimal conformation when truncated protein (i.e., ABC and DEF) is used in the incubation. During initiation, domain D serves as the ADP-ribose acceptor substrate in PAR formation catalyzed by domain DEF. While ABC and DEF can form an active complex with DNA, this complex is less stable than the full-length PARP-1, which may allow water to get into the active site and cause hydrolysis of NAD^+ to generate ADP-ribose. This effect would be more pronounced in the case where a protein is the substrate in PAR formation. However, when lmDEF or as-purified DEF alone is tested for its capability to extend the pre-established PAR polymers, the direct hydrolysis of NAD^+ slows down significantly (Figure 4-1 and Figure 4-14). If a protein molecule serves as an acceptor substrate in the elongation process, the same hydrolytic rate is expected to observe in these cases; however, this is not what was observed. While proximal elongation of PAR uses a protein as the acceptor substrate for the incoming ADP-ribose unit, distal

elongation uses a pre-established PAR polymer as the substrate, which is independent of the conformation of the protein being modified. The slower hydrolytic rate of NAD^+ during polymer elongation when compared with the initiation process indicates that the reactive substrate is switched from a protein acceptor to a polymer acceptor, consistent with the distal elongation mechanism.

In steps 6-7, a mechanism for forming a branched PAR polymer is proposed. In the case of lmDEF, which is the modified-DEF decorated with large PAR polymers, the lmDEF itself is capable of incorporating ^{32}P signal during elongation/branching reactions. This process does not require ABC and DNA (Figure 4-14). Furthermore, when the endogenous PAR polymers are removed from the as-purified DEF, the extent of ^{32}P incorporation during the elongation/branching reactions decreases (Figure 4-5B). All these observations indicate that PAR polymers are the reactive substrates for DEF. This leads to another proposal suggesting that DEF catalyzes the branching reaction as polymers getting larger. It is well known that the 2''-OH groups within PAR polymers function as the nucleophiles in the branching reactions. As the polymer grows larger, the local concentration of 2''-OH from the conjugated polymer increases near the active site. Consequently, they may become acceptor sites for the incoming ADP-ribose unit. Once a branch point is formed, it can be elongated in a similar fashion as described before.

4.4.5. Proximal versus distal PAR elongation

Based on the proposed mechanism discussed in Section 4.4.4, a distal elongation mechanism of PAR formation is proposed. To test whether PAR elongation happens distally or proximally, two different assays were carried out.

For a proximal elongation mechanism, at least two amino acid residues are required to serve as acceptor sites for the pre-established PAR polymer and the incoming ADP-ribose unit. As the incoming ADP-ribose is attached to one of the amino acid residues, the 2'-OH group of this ADP-ribose unit can serve as a nucleophile to attack the ester linkage between the pre-established PAR polymer attaching to protein. This ester bond cleavage reaction transfers the pre-established PAR polymer to the newly initiated ADP-ribose unit. Namely, the new ADP-ribose unit is added to the polymer from the protein end. Hence, in the case of proximal elongation mechanism, PAR transfer is expected. However, based on the study done using modified-PARP-1 incubated with its heterosubstrate histone H1, no PAR transfer was observed (Figure 4-16). This result is more consistent with a distal elongation mechanism, where no PAR transfer is required.

As an alternative approach to study distal versus proximal elongation process, a pulse-chase experiment was carried out, and a quantitative theory was developed for data analysis in this assay. Discussed in Section 4.3.10., current result is consistent with the distal elongation mechanism. However, it is assumed that all initiation sites generated during the pulse step would get further elongated during the chase step, with $q \approx 1$. In reality, this may not be true. Therefore, a control experiment is needed to get an estimation of the q value in this case.

4.4.6. Automodification versus heteromodification

In a time course study of PARP-1 heteromodification using histone H1 as the substrate, it is observed that there is a delay of occurrence between the automodification of PARP-1 and the heteromodification of histone H1 (Figure 4-15). This raises several interesting questions of whether automodification of PARP-1 is a pre-requisite step for

heteromodification. As histone H1 is known to interact with PAR polymers (13), it would be interesting to study whether the pre-established PAR polymers on PARP-1 helps to bring in the heterosubstrate close to the active site in domain F.

4.5 REFERENCES

1. Simonin, F., Ménissier-de Murcia, J., Poch, O., Muller, S., Gradwohl, G., Molinete, M., Penning, C., Keith, G., and de Murcia, G. (1990) Expression and site-directed mutagenesis of the catalytic domain of human poly(ADP-ribose)polymerase in Escherichia coli. Lysine 893 is critical for activity, J. Biol. Chem. 265, 19249-19256.
2. Ikejima, M., Noguchi, S., Yamashita, R., Ogura, T., Sugimura, T., Gill, D.M., and Miwa, M. (1990) The zinc fingers of human poly(ADP-ribose) polymerase are differentially required for the recognition of DNA breaks and nicks and the consequent enzyme activation. Other structures recognize intact DNA, J. Biol. Chem. 265, 21907-21913.
3. Tao, Z., Gao, P., Hoffman, D.W., and Liu, H.W. (2008) Domain C of human poly(ADP-ribose) polymerase-1 is important for enzyme activity and contains a novel zinc-ribbon motif, Biochemistry 47, 5804-5813.
4. Tao, Z., Gao, P., and Liu, H,W. (2009) Identification of the ADP-ribosylation sites in the PARP-1 automodification domain: analysis and implications, J. Am. Chem. Soc. 131, 14258-14260.
5. Chapman ,J.D., Gagné, J.P., Poirier, G.G., and Goodlett, D.R. (2013) Mapping PARP-1 auto-ADP-ribosylation sites by liquid chromatography-tandem mass spectrometry, J. Proteome Res. 12, 1868-1880.
6. Langelier, M.F., Planck, J.L., Roy, S., and Pascal, J.M. (2012) Structural basis for DNA damage-dependent poly(ADP-ribosyl)ation by human PARP-1, Science 336, 728-732.
7. Pandya, K.G., Patel, M.R., and Lau-Cam, C.A. (2010) Comparative study of the binding characteristics to and inhibitory potencies towards PARP and in vivo antidiabetogenic potencies of taurine, 3-aminobenzamide and nicotinamide, J. Biomed. Sci. 17, S16.

8. Hayashi, K., Tanaka, M., Shimada, T., Miwa, M., and Sugimura, T. (1983) Size and shape of poly(ADP-ribose): Examination by gel filtration, gel electrophoresis and electron microscopy, Biochem. Biophys. Res. Commun. 112, 102-107.

9. Huambachano, O., Herrera, F., Rancourt, A., and Satoh, M. S. (2011) Double-stranded DNA binding domain of poly(ADP-ribose) polymerase-1 and molecular insight into the regulation of its activity, J. Biol. Chem. 286, 7149-7160.

10. Lagueux, J., Ménard, L., Candas, B., Brochu, G., Potvin, F., Verreault, A., Cook , P.F., and Poirier, G.G. (1995) Equilibrium model in an in vitro poly(ADP-ribose) turnover system, Biochim. Biophys. Acta. 1264, 201-208.

11. Mendoza-Alvarez, H., and Alvarez-Gonzalez, R. (2004) The 40 kDa carboxy-terminal domain of poly(ADP-ribose) polymerase-1 forms catalytically competent homo- and heterodimers in the absence of DNA, J. Mol. Biol. 336, 105-114.

12. Jiang, H., Kim, J.H., Frizzell, K.M., Kraus, W.L., and Lin, H. (2010) Clickable NAD analogues for labeling substrate proteins of poly(ADP-ribose) polymerases, J. Am. Chem. Soc. 132, 9363-9372.

13. Kim, M.Y., Zhang, T., and Kraus, W.L. (2005) Poly(ADP-ribosyl)ation by PARP-1: 'PAR-laying' NAD+ into a nuclear signal, Genes Dev. 19, 1951-1967.

Bibliography

1. Chambon, P., Weill, J. D., and Mandel, P. (1963) Nicotinamide mononucleotide activation of new DNA-dependent polyadenylic acid synthesizing nuclear enzyme, Biochem. Biophys. Commun. 11, 39-43.

2. Fujimura, S., Sugimura, T., Okabe, K., and Yoshida, T. (1965) NMN-activated poly(A) polymerase in nuclei from rat liver and hepatoma cells. Proc. Annu. Meeting Jpn. Biochem. Soc. 38, 591 (In Japanese).

3. Chambon, P., Weill J. D., Strosser, M. T., and Mandel, P. (1966) On the formation of a novel adenylic compound by enzymatic extracts of liver nuclei, Biochem. Biophys. Commun. 25, 638-643.

4. Nishizuka, Y., Ueda, K., Nakazawa, K., and Hayaishi, O. (1967) Studies on the polymer of adenosine diphosphate ribose. I. Enzymatic formation from nicotinamide adenine dinucleotide in mammalian Nuclei. J. Biol. Chem. 242, 3164-3171.

5. Reeder R. H., Ueda K., Honjo, T., Nishizuka Y., and Hayaishi, O. (1967) Studies on the polymer of adenosine diphosphate ribose. II. Characterization of the polymer. J. Biol. Chem. 242, 3172-3179.

6. Fujimura, S., Hasegawa, S., Shimizu, Y., and Sugimura, T. (1967) Polymerization of the adenosine 5'-diphosphate-ribose moiety of nicotinamide-adenine dinucleotide by nuclear enzyme. I. Enzymatic reactions, Biochim. Biophys. Acta. 145, 247-259.

7. Futai, M., Mizuno, D., and Sugimura, T. (1967) Hydrolysis of the polymer formed from NAD with rat liver phosphodiesterase yielding nucleoside 5'-monophosphate, Biochem. Biophys. Res. Commun. 28, 395-399.

8. Miwa M., Saitô H., Sakura H., Saikawa N., Watanabe F., Matsushima T., and Sugimura T. (1977) A ^{13}C NMR study of poly(adenosine diphosphate ribose) and its monomers: evidence of alpha-(1'' leads to 2') ribofuranosy1 ribofuranoside residue, Nucleic Acid Res. 4, 3997-4005.

9. Ferro, A. M., and Oppenheimer N. J. (1978) Structure of a poly (adenosine diphosphoribose) monomer: 2'-(5"-hosphoribosyl)-5'-adenosine monophosphate, Proc. Natl. Acad. Sci. U.S.A. 75, 809-813.

10. Hayaishi, O., and Ueda, K. (1977) Poly(ADP-ribose) and ADP-ribosylation of proteins, Ann. Rev. Biochem. 46, 95-116.

11. Tanaka, M., Miwa, M., Hayashi, K., Kubota, K., and Matsushima, T. (1977) Separation of oligo(adenosine diphosphate ribose) fractions with various chain lengths and terminal structures, Biochemistry 16, 1485-1489.

12. Tanaka, M., Hayashi, K., Sakura, H., Miwa, M., Matsushima, T., and Sugimura, T. (1978) Demonstration of high molecular weight poly (adenosine diphosphate ribose), Nucleic Acid Res. 5, 3183-3194.

13. Miwa, M., Saikawa, N., Yamaizumi, Z., Nishimura, S., and Sugimura ,T. (1979) Structure of poly(adenosine diphosphate ribose): identification of 2'-[1''-ribosyl-2''-(or 3''-)(1'''-ribosyl)]adenosine-5',5'',5'''-tris(phosphate) as a branch linkage, Proc. Natl. Acad. Sci. U.S.A. 76, 595-599.

14. Miwa, M., Ishihara, M., Takishima, S., Takasuka, N., Maeda, M., Yamaizumi, Z., Sugimura, T., Yokoyama, S., and Miyazawa T. (1981) The branching and linear portions of poly(adenosine diphosphate ribose) have the same alpha(1 leads to 2) ribose-ribose linkage, J. Biol. Chem. 256, 2916-2921.

15. Hayashi, K., Tanaka, M., Shimada, T., Miwa, M., and Sugimura, T. (1983) Size and shape of poly(ADP-ribose): examination by gel filtration, gel electrophoresis and electron microscopy, Biochem. Biophys. Res. Commun. 112, 102-107.

16. Alvarez-Gonzalez, R., and Jacobson, M. K. (1987) Characterization of polymers of adenosine diphosphate ribose generated in vitro and in vivo, Biochemistry 26, 3218-3224.

17. Nishizuka, Y., Ueda, K., Honjo, T., and Hayaishi, O. (1968) Enzymic adenosine diphosphate ribosylation of histone and poly adenosine diphosphate ribose synthesis in rat liver nuclei, J. Biol. Chem. 243, 3765-3767.

18. Nishizuka, Y., Ueda, K., Yoshihara, K., Yamamura, H., Takeda, M., and Hayaishi, O. (1969) Enzymic adenosine diphosphoribosylation of nuclear proteins, Cold Spring Harb. Symp. Quant. Biol. 34, 781-786.

19. Otake, H., Miwa, M., Fujimura, S., and Sugimura, T. (1969) Binding of ADP-ribose polymer with histone, J. Biochem. 65, 145-146.

20. Ueda, K., Omachi, A., Kawaichi, M., and Hayaishi, O. (1975) Natural occurrence of poly(ADP-ribosyl) histones in rat liver, Proc. Natl. Acad. Sci. U.S.A. 72, 205-209.

21. Tao, Z., Gao, P., and Liu, H.W. (2009) Studies of the expression of human poly(ADP-ribose) polymerase-1 in Saccharomyces cerevisiae and identification of PARP-1 substrates by yeast proteome microarray screening, Biochemistry 48, 11745-11754.

22. Davidovic, L., Vodenicharov, M., Affar, E.B., and Poirier, G.G. (2001) Importance of poly(ADP-ribose) glycohydrolase in the control of poly(ADP-ribose) metabolism, Exp. Cell. Res. 268, 7-13.

23. Nguewa, P.A., Fuertes, M.A., Valladares, B., Alonso, C., and Pérez, J.M. (2005) Poly(ADP-ribose) polymerases: homology, structural domains and functions. Novel therapeutical applications, Prog. Biophys. Mol. Biol. 88, 143-72.

24. D'Amours ,D., Desnoyers, S., D'Silva, I., and Poirier, G.G. (1999) Poly(ADP-ribosyl)ation reactions in the regulation of nuclear functions, Biochem. J. 342, 249-268.

25. Messner, S., Altmeyer, M., Zhao, H., Pozivil, A., Roschitzki, B., Gehrig, P., Rutishauser, D., Huang, D., Caflisch, A., Hottiger, M.O. (2010) PARP1 ADP-ribosylates lysine residues of the core histone tails, Nucleic Acids Res. 38,6350-6362.

26. Alvarez-Gonzalez, R., and Althaus, F.R. (1989) Poly(ADP-ribose) catabolism in mammalian cells exposed to DNA-damaging agents, Mutat. Res. 218, 67-74.

27. Gibson, B.A., and Kraus, W.L. (2012) New insights into the molecular and cellular functions of poly(ADP-ribose) and PARPs, Nat. Rev. Mol. Cell Biol. 13, 411-424.

28. Nguewa, P.A., Fuertes, M.A., Valladares, B., Alonso, C., Pérez, J.M. (2005) Poly(ADP-ribose) polymerases: homology, structural domains and functions. Novel therapeutical applications, Prog. Biophys. Mol. Biol. 88, 143-172.

29. Miwa, M., Tanaka, M., Matsushima, T., and Sugimura, T. (1974) Purification and properties of glycohydrolase from calf thymus splitting ribose-ribose linkages of poly(adenosine diphosphate ribose), J. Biol. Chem. 249, 3475-3482.

30. Ikejima, M., and Gill, D.M. (1988) Poly(ADP-ribose) degradation by glycol-hydrolase starts with an endonucleolytic incision, J. Biol. Chem. 263, 11037-11040.

31. Sharifi, R., Morra, R., Appel, C.D., Tallis, M., Chioza, B., Jankevicius, G., Simpson, M.A., Matic, I., Ozkan, E., Golia, B., Schellenberg, M.J., Weston, R., Williams, J.G., Rossi, M.N., Galehdari, H., Krahn, J., Wan, A., Trembath, R.C., Crosby, A.H., Ahel, D., Hay, R., Ladurner, A.G., Timinszky, G., Williams, R.S., and Ahel I. (2013) Deficiency of terminal ADP-ribose protein glycohydrolase TARG1/C6orf130 in neurodegenerative disease, EMBO J. 32, 1225-1237.

32. Poirier, G. G., de Murcia, G., Jongstra-Bilen, J., Niedergang, C., and Mandel, P. (1982) Poly(ADP-ribosyl)ation of polynucleosomes causes relaxation of chromatin structure, Proc. Natl. Acad. Sci. U.S.A. 79, 3423-3427.

33. Realini, C. A., and Althaus, F. R. (1992) Histone shuttling by poly(ADP-ribosylation), J. Biol. Chem. 267, 18858-18865.

34. Masson, M., Niedergang, C., Schreiber, V., Muller, S., Menissier-de Murcia, J., and de Murcia, G. (1998) XRCC1 is specifically associated with poly(ADP-ribose) polymerase and negatively regulates its activity following DNA damage, Mol. Cell. Biol. 18, 3563-3571.

35. Audebert, M., Salles, B. and Calsou, P. (2004) Involvement of poly(ADP-ribose) polymerase-1 and XRCC1/DNA ligase III in an alternative route for DNA double-strand breaks rejoining, J. Biol. Chem. 279, 55117-55126.

36. Caldecott, K.W., Aoufouchi, S., Johnson, P., and Shall, S. (1996) XRCC1 polypeptide interacts with DNA polymerase beta and possibly poly (ADP-ribose) polymerase, and DNA ligase III is a novel molecular 'nick-sensor' in vitro, Nucleic Acids Res.,24, 4387-4394.

37. Weinfeld, M., Chaudhry, M.A., D'Amours, D., Pelletier, J.D,, Poirier, G.G., Povirk, L.F., and Lees-Miller, S.P. (1997) Interaction of DNA-dependent protein kinase and poly(ADP-ribose) polymerase with radiation-induced DNA strand breaks, Radiat. Res. 148, 22-28.

38. D'Silva, I., Pelletier, J.D., Lagueux, J., D'Amours, D., Chaudhry, M.A., Weinfeld, M., Lees-Miller, S.P., and Poirier, G.G. (1999) Relative affinities of poly(ADP-ribose) polymerase and DNA-dependent protein kinase for DNA strand interruptions, Biochim. Biophys. Acta. 1430, 119-126.

39. Clancy, S. (2008) DNA Damage & Repair: Mechanisms for Maintaining DNA Integrity, Nature Education 1, 103

40. Rouleau, M., Patel, A., Hendzel, M.J., Kaufmann, S.H., and Poirier, G.G. (2010) PARP inhibition: PARP1 and beyond, Nat. Rev. Cancer 10, 293-301.

41. Wielckens, K., Schmidt, A., George, E., Bredehorst, R., and Hilz, H. (1982) DNA fragmentation and NAD depletion. Their relation to the turnover of endogenous mono(ADP-ribosyl) and poly(ADP-ribosyl) proteins, J. Biol. Chem. 257, 12872–12877.

42. Jacobson, E.L., Lange, R.A., and Jacobson, M.K. (1979) Pyridine nucleotide synthesis in 3T3 cells, J. Cell Physiol. 99, 417-425.

43. Bernofsky, C. (1980) Physiology aspects of pyridine nucleotide regulation in mammals, Mol. Cell. Biochem. 33, 135-143.

44. Goodwin, P.M., Lewis, P.J., Davies, M.I., Skidmore, C.J., and Shall, S. (1978) The effect of gamma radiation and neocarzinostatin on NAD and ATP levels in mouse leukaemia cells, Biochim. Biophys. Acta. 543, 576-582.

45. Skidmore, C.J., Davies, M.I., Goodwin, P.M., Halldorsson, H., Lewis, P.J., Shall, S., and Zia'ee, A.A. (1979) The involvement of poly(ADP-ribose) polymerase in the degradation of NAD caused by gamma-radiation and N-methyl-N-nitrosourea, Eur. J. Biochem. 101, 135-142.

46. Rouleau, M., Aubin, R.A., and Poirier, G.G. (2004) Poly(ADP-ribosyl)ated chromatin domains: access granted, J. Cell. Sci. 117, 815-825.

47. Oei, S.L., Keil, C., and Ziegler, M. (2005) Poly(ADP-ribosylation) and genomic stability, Biochem. Cell Biol. 83, 263-269.

48. Bürkle, A., and Virág, L. (2013) Poly(ADP-ribose): PARadigms and PARadoxes, Mol. Aspects Med. 34, 1046-1065.

49. Bai, P., and Cantó, C. (2012) The role of PARP-1 and PARP-2 enzymes in metabolic regulation and disease, Cell Metab. 16, 290-295

50. de Murcia, G., and Ménissier-de Murcia, J. (1994) Poly(ADP-ribose) polymerase: a molecular nick-sensor, Trends Biochem. Sci. 19, 172-176.

51. Gradwohl, G., Menissier de Murcia, J. M., Molinete, M., Simonin, F., Koken, M., Hoeijmakers, J. H., and de Murcia, G. (1990) The second zinc-finger domain of poly(ADP-ribose) polymerase determines specificity for single-stranded breaks in DNA, Proc. Natl. Acad. Sci. U.S.A. 87, 2990-2994.

52. Lonskaya, I., Potaman, V.N., Shlyakhtenko, L.S., Oussatcheva, E.A., Lyubchenko, Y,L,, and Soldatenkov, V.A. (2005) Regulation of poly(ADP-ribose) polymerase-1 by DNA structure-specific binding, J. Biol. Chem. 280, 17076-17083.

53. Altmeyer, M., Messner, S., Hassa, P.O., Fey, M, and Hottiger, M,O. (2009) Molecular mechanism of poly(ADP-ribosyl)ation by PARP1 and identification of lysine residues as ADP-ribose acceptor sites, Nucleic Acids Res. 37, 3723-3738.

54. Schreiber, V., Molinete, M,, Boeuf, H,, de Murcia, G,, and Ménissier-de Murcia, J. (1992) The human poly(ADP-ribose) polymerase nuclear localization signal is a bipartite element functionally separate from DNA binding and catalytic activity, EMBO J. 11, 3263-3269.

55. Kaufmann, S.H., Desnoyers, S., Ottaviano, Y., Davidson, N.E., and Poirier, G.G. Specific proteolytic cleavage of poly(ADP-ribose) polymerase: an early marker of chemotherapy-induced apoptosis, Cancer Res. 53, 3976-3985.

56. Tao, Z., Gao, P., Hoffman, D.W., and Liu, H.W. (2008) Domain C of human poly(ADP-ribose) polymerase-1 is important for enzyme activity and contains a novel zinc-ribbon motif, Biochemistry 47, 5804-5813.

57. Trucco, C., Flatter, E., Fribourg, S., de Murcia, G., and Ménissier-de Murcia J. (1996) Mutations in the amino-terminal domain of the human poly(ADP-ribose) polymerase that affect its catalytic activity but not its DNA binding capacity, FEBS Lett. 399, 313-316.

58. Langelier, M.F., Servent, K.M., Rogers, E.E., and Pascal, J.M. (2008) A third zinc-binding domain of human poly(ADP-ribose) polymerase-1 coordinates DNA-dependent enzyme activation, J. Biol. Chem., 283, 4105-4114.

59. Cherney, B.W., McBride, O.W., Chen, D.F., Alkhatib, H., Bhatia, K., Hensley, P., and Smulson, M.E. (1987) cDNA sequence, protein structure, and chromosomal location of the human gene for poly(ADP-ribose) polymerase, Proc. Natl. Acad. Sci. U.S.A. 84, 8370-8374.

60. Uchida, K., Morita, T., Sato,T., Ogura, T., Yamashita, R., Noguchi, S., Suzuki, H., Nyunoya, H., Miwa, M., and Sugimura, T. (1987) Nucleotide sequence of a full-length cDNA for human fibroblast poly(ADP-ribose) polymerase, Biochem. Biophys. Res. Commun. 148,617-622.

61. Kawaichi, M., Ueda, K., and Hayaishi, O. (1981) Multiple autopoly(ADP-ribosyl)ation of rat liver poly(ADP-ribose) synthetase. Mode of modification and properties of automodified synthetase, J. Biol. Chem. 256, 9483-9489.

62. Tao, Z., Gao, P., and Liu, H,W. (2009) Identification of the ADP-ribosylation sites in the PARP-1 automodification domain: analysis and implications, J. Am. Chem. Soc. 131, 14258-14260.

63. Chapman ,J.D., Gagné, J.P., Poirier, G.G., and Goodlett, D.R. (2013) Mapping PARP-1 auto-ADP-ribosylation sites by liquid chromatography-tandem mass spectrometry, J. Proteome Res. 12, 1868-1880.

64. Bork, P., Hofmann, K., Bucher, P., Neuwald, A. F., Altschul, S. F., and Koonin, E. V. (1997) A superfamily of conserved domains in DNA damage-responsive cell cycle checkpoint proteins, FASEB J. 11, 68-76.

65. Hassa, P.O., Haenni, S.S., Elser, M., and Hottiger, M.O. (2006) Nuclear ADP-ribosylation reactions in mammalian cells: where are we today and where are we going, Microbiol. Mol. Biol. Rev. 70, 789-829.

66. Huambachano, O., Herrera, F., Rancourt, A., and Satoh, M. S. (2011) Double-stranded DNA binding domain of poly(ADP-ribose) polymerase-1 and molecular insight into the regulation of its activity, J. Biol. Chem. 286, 7149-7160.

67. Ruf, A., Mennissier-de Murcia, J., de Murcia, G., and Schulz, G.E. (1996) Structure of the catalytic fragment of poly(AD-ribose) polymerase from chicken, Proc. Natl. Acad. Sci. U.S.A. 93, 7481-7485.

68. Simonin, F., Höfferer, L., Panzeter, P. L., Muller, S., de Murcia, G., and Althaus, F. R. (1993) The carboxyl-terminal domain of human poly(ADP-ribose) polymerase. Overproduction in Escherichia coli, large scale purification, and characterization, J. Biol. Chem. 268, 13454-13461.

69. Ruf, A., de Murcia, G., and Schulz, G. E. (1998) Inhibitor and NAD^+ binding to poly(ADP-ribose) polymerase as derived from crystal structures and homology modeling, Biochemistry 37, 3893-3900.

70. Hassler, M., and Ladurner, A.G. (2012) Towards a structural understanding of PARP1 activation and related signalling ADP-ribosyl-transferases, Curr. Opin. Struct. Biol. 22, 721-729.

71. Schreiber, V., Dantzer, F., Ame, J.C., and de Murcia, G. (2006) Poly(ADP-ribose): novel functions for an old molecule, Nat. Rev. Mol. Cell Biol. 7, 517-528.

72. Amé, J.C., Rolli, V., Schreiber, V., Niedergang, C., Apiou, F., Decker, P., Muller, S., Höger, T., Ménissier-de Murcia, J., and de Murcia, G. (1999) PARP-2, A novel mammalian DNA damage-dependent poly(ADP-ribose) polymerase, J. Biol. Chem. 274, 17860-17868.

73. Rippmann, J.F., Damm, K., and Schnapp, A. (2002) Functional characterization of the poly(ADP-ribose) polymerase activity of tankyrase 1, a potential regulator of telomere length, J. Mol. Biol. 323, 217-224.

74. Sbodio, J.I., Lodish, H.F., and Chi, N.W. (2002) Tankyrase-2 oligomerizes with tankyrase-1 and binds to both TRF1 (telomere-repeat-binding factor 1) and IRAP (insulin-responsive aminopeptidase), Biochem. J. 361, 451-459.

75. Hottiger, M.O., Hassa, P.O., Lüscher, B., Schüler, H., and Koch-Nolte, F. (2010) Toward a unified nomenclature for mammalian ADP-ribosyltransferases, Trends Biochem. Sci. 35, 208-219.

76. Marsischky, G.T., Wilson, B.A., and Collier, R.J. (1995) Role of glutamic acid 988 of human poly-ADP-ribose polymerase in polymer formation. Evidence for active site similarities to the ADP-ribosylating toxins, J. Biol. Chem. 270, 3247-3254.

77. Caldecott, K.W., Aoufouchi, S., Johnson, P., and Shall, S. (1996) XRCC1 polypeptide interacts with DNA polymerase beta and possibly poly (ADP-ribose) polymerase, and DNA ligase III is a novel molecular 'nick-sensor' in vitro, Nucleic Acids Res. 24, 4387-4394.

78. Petrucco, S. (2003) Sensing DNA damage by PARP-like fingers, Nucleic Acids Res. 31, 6689-6699.

79. Ikejima, M., Noguchi, S., Yamashita, R., Ogura, T., Sugimura, T., Gill, D.M., and Miwa, M. (1990) The zinc fingers of human poly(ADP-ribose) polymerase are differentially required for the recognition of DNA breaks and nicks and the consequent enzyme activation. Other structures recognize intact DNA, J. Biol. Chem. 265, 21907-21913.

80. Huambachano, O., Herrera, F., Rancourt, A., and Satoh, M.S. (2010) Double-stranded DNA binding domain of poly(ADP-ribose) polymerase-1 and molecular insight into the regulation of its activity, J. Biol. Chem. 286, 7149-7160.

81. Clark, N.J., Kramer, M., Muthurajan, U.M., and Luger K. (2012) Alternative modes of binding of poly(ADP-ribose) polymerase 1 to free DNA and nucleosomes, J. Biol. Chem. 287, 32430-32439.

82. D'Silva, I., Pelletier, J.D., Lagueux, J., D'Amours, D., Chaudhry, M.A., Weinfeld, M., Lees-Miller, S.P., and Poirier, G.G. (1999) Relative affinities of poly(ADP-ribose) polymerase and DNA-dependent protein kinase for DNA strand interruptions, Biochim. Biophys. Acta. 1430, 119-126.

83. Pion, E., Ullmann, G.M., Amé, J.C., Gérard, D., de Murcia, G., and Bombarda, E. (2005) DNA-induced dimerization of poly(ADP-ribose) polymerase-1 triggers its activation, Biochemistry 44, 14670-14681.

84. Sambrook, J., Fritsch, E. F., and Maniatis, T. (1989) Molecular Cloning, Vol. 2, Cold Spring Harbor Laboratory Press, Cold Spring Harbor, NY.

85. Zhang, C.X., Chang, P.V., and Lippard, S.J. (2004) Identification of nuclear proteins that interact with platinum-modified DNA by photoaffinity labeling, J. Am. Chem. Soc. 126, 6536-6537.

86. Langelier, M.F., Planck, J.L., Roy, S., and Pascal, J.M. (2011) Crystal structures of poly(ADP-ribose) polymerase-1 (PARP-1) zinc fingers bound to DNA: structural and functional insights into DNA-dependent PARP-1 activity, J. Biol. Chem. 286, 10690-106701.

87. Ali, A.A., Timinszky, G., Arribas-Bosacoma, R., Kozlowski, M., Hassa, P.O., Hassler, M., Ladurner, A.G., Pearl, L.H., and Oliver, A.W. (2012) The zinc-finger domains of PARP1 cooperate to recognize DNA strand breaks, Nat. Struct. Mol. Biol. 19, 685-692.

88. Langelier, M.F., Planck, J.L., Roy, S., and Pascal, J.M. (2012) Structural basis for DNA damage-dependent poly(ADP-ribosyl)ation by human PARP-1, Science 336, 728-732.

89. Langelier, M.F., and Pascal, J.M. (2013) PARP-1 mechanism for coupling DNA damage detection to poly(ADP-ribose) synthesis, Curr. Opin. Struct. Biol. 23, 134-143.

90. Loseva, O., Jemth, A.S., Bryant, H.E., Schüler, H., Lehtiö, L., Karlberg, T., and Helleday, T. (2010) PARP-3 is a mono-ADP-ribosylase that activates PARP-1 in the absence of DNA, J. Biol. Chem. 285, 8054-8060.

91. Cohen-Armon, M., Visochek, L., Rozensal, D., Kalal, A., Geistrikh, I., Klein, R., Bendetz-Nezer, S., Yao, Z., and Seger, R. (2007) DNA-independent PARP-1 activation by phosphorylated ERK2 increases Elk1 activity: a link to histone acetylation, Mol. Cell 25, 297-308.

92. Kauppinen, T.M., Chan, W.Y., Suh, S.W., Wiggins, A.K., Huang, E.J., Swanson, R.A. (2006) Direct phosphorylation and regulation of poly(ADP-ribose) polymerase-1 by extracellular signal-regulated kinases 1/2, Proc. Natl. Acad. Sci. U.S.A 103, 7136-7141.

93. Alvarez-Gonzalez, R., Pacheco-Rodriguez, G., and Mendoza-Alvarez, H. (1994) Enzymology of ADP-ribose polymer synthesis, Mol. Cell. Biochem. 138, 33-37.

94. Bellocchi, D., Costantino, G., Pellicciari, R., Re, N., Marrone, A., and Coletti, C. (2006) Poly(ADP-ribose)-polymerase-catalyzed hydrolysis of NAD+: QM/MM simulation of the enzyme reaction, ChemMedChem 1, 533-539.

95. Ruf, A., Rolli,V., de Murcia, G., and Schulz, G.E. (1998) The mechanism of the elongation and branching reaction of poly(ADP-ribose) polymerase as derived from crystal structures and mutagenesis, J. Mol. Biol. 278, 57-65.

96. Rolli, V., O'Farrell, M., Ménissier-de Murcia, J., and de Murcia, G. (1997) Random mutagenesis of the poly(ADP-ribose) polymerase catalytic domain reveals amino acids involved in polymer branching, Biochemistry 36, 12147-12154.

97. Mendoza-Alvarez, H., and Alvarez-Gonzalez, R. (1993) Poly(ADP-ribose) polymerase is a catalytic dimer and the automodification reaction is intermolecular, J. Biol. Chem. 268, 22575-22580.

98. Ueda, K., Kawaichi, M., Okayama, H., and Hayaishi, O. (1979) Poly(ADP-ribosy)ation of nuclear proteins. Enzymatic elongation of chemically synthesized ADP-ribose-histone adducts, J. Biol. Chem. 254, 679-687.

99. Taniguchi, T. (1987) Reaction mechanism for automodification of poly(ADP-ribose) synthetase, Biochem. Biophys. Res. Commun. 147, 1008-1012.

100. Ikejima, M., Marsischky, G., and Gill, D.M. (1987) Direction of elongation of poly(ADP-ribose) chains. Addition of residues at the polymerase-proximal terminus, J. Biol. Chem. 262, 17641-17650.

101. Alvarez-Gonzalez, R. (1988) 3'-Deoxy-NAD^+ as a substrate for poly(ADP-ribose)polymerase and the reaction mechanism of poly(ADP-ribose) elongation, J. Biol. Chem. 263, 17690-17696.

102. Naegeli, H., and Althaus, F.R. (1991) Regulation of poly(ADP-ribose) polymerase. Histone-specific adaptations of reaction products, J. Biol. Chem. 266, 10596-105601.

103. Panzeter, P.L., Realini, C.A., and Althaus, F.R. (1992) Noncovalent interactions of poly(adenosine diphosphate ribose) with histones, Biochemistry 31, 1379-1385.

104. Ménard, L., Thibault, L., and Poirier, G.G. (1990) Reconstitution of an in vitro poly(ADP-ribose) turnover system, Biochim. Biophys. Acta. 1049, 45-58.

105. Zahradka, P., and Ebisuzaki, K. (1982) A shuttle mechanism for DNA-protein interactions. The regulation of poly(ADP-ribose) polymerase, Eur. J. Biochem. 127, 579-585.

106. Kristensen, T., and Holtlund, J. (1978) Poly(ADP-ribose) polymerase from Ehrlich ascites tumor cells. Properties of the purified polymerase, Eur. J. Biochem. 88, 495-501.

107. Ohgushi, H., Yoshihara, K., and Kamiya, T. (1980) Bovine thymus poly(adenosine diphosphate ribose) polymerase. Physical properties and binding to DNA, J. Biol. Chem. 255, 6205-6211.

108. Bauer, P.I., Buki, K.G., Hakam, A., and Kun, E. (1990) Macromolecular association of ADP-ribosyltransferase and its correlation with enzymic activity, Biochem. J. 270, 17-26.

109. Buki, K.G., Bauer, P.I., Hakam, A., and Kun, E. (1995) Identification of domains of poly(ADP-ribose) polymerase for protein binding and self-association, J. Biol. Chem. 270, 3370-3377.

110. Mendoza-Alvarez, H., and Alvarez-Gonzalez, R. (2004) The 40 kDa carboxy-terminal domain of poly(ADP-ribose) polymerase-1 forms catalytically competent homo- and heterodimers in the absence of DNA, J. Mol. Biol. 336, 105-114.

111. Mansoorabadi, S.O., Wu, M., Tao, Z., Gao, P., Pingali, S.V., Guo, L., and Liu, H.W. (2014) Conformational activation of poly(ADP-ribose) polymerase-1 upon DNA binding revealed by small-angle X-ray scattering, Biochemistry 53, 1779–1788.

112. Schuck P. (2003) On the analysis of protein self-association by sedimentation velocity analytical ultracentrifugation, Anal. Biochem. 320, 104-124.

113. Demeler B., and van Holde K. E. (2004) Sedimentation velocity analysis of highly heterogenous systems, Anal. Biochem. 335, 279-288.

114. Brookes E., Cao W., and Demeler B. (2009) A two-dimensional spectrum analysis for sedimentation velocity experiments of mixtures with heterogeneity in molecular weight and shape, Eur. Biophys. J. 39, 405-414.

115. Schuck P., and Scott D. J. (2005) A brief introduction to the analytical ultracentrifugation of proteins for beginners, in Analytical ultracentrifugation: techniques and methods (Scott D. J., Harding S. E., and Arthur J. R. Eds.) pp1-25, Royal Society of Chemistry Publishing, Cambridge, U.K..

116. Tiselius A. (1930) The moving-boundary method of studying the electrophoresis of proteins, Nova Acta Regiae Soc. Sci. Upsal. Ser. IV 7, 1.

117. Lamm O. (1929) Die differentialgleichung der Ultrazentrifugierung, Ark. Mat. Astr. Fyr. 21B, 1-4.

118. Schuck P. (2000) Size distribution analysis of macromolecules by sedimentation velocity ultracentrifugation and Lamm equation modelings, Biophys. J. 78, 1606-1619.

119. Demeler B., Saber H., and Hansen J. C. (1997) Identification and interpretation of complexity in sedimentation velocity boundaries, Biophys. J. 72, 397-407.

120. Demeler B., and Brookes E. (2007) Monte Carlo analysis of sedimentation experiments, Colloid Polym. Sci. 286, 129-137.

121. Zhou, Y. (August, 2009) Ph.D Thesis, University of Texas at Austin

122. Ryder S.P., Recht M. I., and Williamson J. R. (2008) Quantitative analysis of protein-DNA interactions by gel mobility shift, Methods Mol. Biol. 488, 99-115

123. Decker, K.B., and Hinton, D.M. (2013) Transcription regulation at the core: similarities among bacterial, archaeal, and eukaryotic RNA polymerases, Annu. Rev. Microbiol. 67, 113-139.

124. Germann, M.W., Johnson, C.N., and Spring, A.M. (2012) Recognition of damaged DNA: structure and dynamic markers, Med. Res. Rev. 32, 659-683.

125. Lindahl, T., Satoh, M.S., Poirier, G.G., and Klungland, A. (1995) Post-translational modification of poly(ADP-ribose) polymerase induced by DNA strand breaks, Trends. Biochem. Sci. 20, 405-411.

126. Vyas, S., and Chang, P. (2014) New PARP targets for cancer therapy, Nat. Rev. Cancer 14, 502-509.

127. Carrico, I.S., Carlson, B.L., and Bertozzi, C.R. (2007) Introducing genetically encoded aldehydes into proteins, Nat. Chem. Biol. 3, 321-322.

128. Ma, C.H., Liu, Y.T., Savva, C.G., Rowley, P.A., Cannon, B., Fan, H.F., Russell, R., Holzenburg, A., and Jayaram, M. (2014) Organization of DNA partners and strand exchange mechanisms during Flp site-specific recombination analyzed by difference topology, single molecule FRET and single molecule TPM, J. Mol. Biol. 426, 793-815.

129. Wang, Y., Guo L., Golding I., Cox E.C., and Ong N. P. (2009) Quantitative transcription factor binding kinetics at the single-molecule level, Biophy. J. 96, 609-620

130. Shu D., Zhang H., Jin J., and Guo P. (2007) Counting of six pRNAs of phi29 DNA-packaging motor with customized single-molecule dual-view system, EMBO J. 26, 527-537

131. Roy R., Hohng S. and Ha T. (2008) A practical guide to single-molecule FRET, Nat. Methods 5, 507-516

132. Jorgensen, T.J., Chen, K., Chasovskikh, S., Roy, R., Dritschilo, A., and Uren, A. (2009) Binding kinetics and activity of human poly(ADP-ribose) polymerase-1 on oligo-deoxyribonucleotide substrates, J. Mol. Recognit. 22, 446-452.

133. Simonin, F., Ménissier-de Murcia, J., Poch, O., Muller, S., Gradwohl, G., Molinete, M., Penning, C., Keith, G., and de Murcia, G. (1990) Expression and site-directed mutagenesis of the catalytic domain of human poly(ADP-ribose)polymerase in Escherichia coli. Lysine 893 is critical for activity, J. Biol. Chem. 265, 19249-19256.

134. Pandya, K.G., Patel, M.R., and Lau-Cam, C.A. (2010) Comparative study of the binding characteristics to and inhibitory potencies towards PARP and in vivo

antidiabetogenic potencies of taurine, 3-aminobenzamide and nicotinamide, J. Biomed. Sci. 17, S16.

135. Lagueux, J., Ménard, L., Candas, B., Brochu, G., Potvin, F., Verreault, A., Cook , P.F., and Poirier, G.G. (1995) Equilibrium model in an in vitro poly(ADP-ribose) turnover system, Biochim. Biophys. Acta. 1264, 201-208.

136. Jiang, H., Kim, J.H., Frizzell, K.M., Kraus, W.L., and Lin, H. (2010) Clickable NAD analogues for labeling substrate proteins of poly(ADP-ribose) polymerases, J. Am. Chem. Soc. 132, 9363-9372.

137. Kim, M.Y., Zhang, T., and Kraus, W.L. (2005) Poly(ADP-ribosyl)ation by PARP-1: 'PAR-laying' NAD+ into a nuclear signal, Genes Dev. 19, 1951-1967.